

**MOLECULAR DETERMINANTS OF HUMAN
ADIPOSE FUNCTION AND THEIR ROLE IN THE
PATHOGENESIS OF OBESITY AND DIABETES**

Madhur Agrawal

(M.Sc. Medical Biochemistry)

**A THESIS SUBMITTED
FOR THE DEGREE OF DOCTOR OF
PHILOSOPHY
DEPARTMENT OF MEDICINE
YONG LOO LIN SCHOOL OF MEDICINE
NATIONAL UNIVERSITY OF SINGAPORE
2016**

DECLARATION

I hereby declare that this thesis is my original work and it has been written by me in its entirety. I have duly acknowledged all the sources of information which have been used in the thesis.

This thesis has also not been submitted for any degree in any university previously.

Madhur Agrawal

21st January 2016

Acknowledgements

I would like to thank each and everyone who was a part of my PhD life of 4 years. Firstly I would like to express my sincere gratitude to Dr Sue Anne Toh, my supervisor who was patient, understanding and inspiring throughout my candidature. She has been an extraordinary guide, helping me every time I was confused or held; she has been a source of immense knowledge and learning experience for me. I would like to show my deepest sincerity to Dr. Tai E Shyong for his mentorship and guidance during my research projects.

I was supported by each and everyone in the metabolic medicine lab (Cheryl, Tammy, Sonia, Ehsan, Shabeer, Vanna, Edmund, Yvonne, Sunny, Audrey and Jocelyn); we have worked together for past few years and I have learned so much from each one of you.

I would like to convey my deepest acknowledgment to my Thesis Advisory Committee, Dr. Shigeki Sugii and Dr. David Silver. I thank our collaborator Dr. Shawn Hoon from A-star and Dr. Mei Hui from Food Science and Technology department for helping through sequencing experiments and Dr. Eshter Woon from Pharmacy for providing us FTO inhibitors. Thank you for all the suggestions, guidance and motivation.

A big shout to my family and friends, you were supportive and kind. I cannot thank you enough.

Contents

Acknowledgements	II
Publications	X
Abstract.....	XII
List of tables.....	XIV
List of figures.....	XVI
List of abbreviations	XXI
Chapter 1: Introduction	1
1.1 Type 2 diabetes and obesity	2
1.2 Functional categories of adipocytes and anatomical distribution of adipose tissue	4
1.3 Main functions of adipose tissue.....	6
1.4 Adipose tissue expandability hypothesis	8
1.4.1 Mechanisms involved in healthy adipose tissue expansion or adipose tissue remodelling during obesity	9
1.4.1.1 Hypertrophy and hyperplasia	10
1.4.1.2 Extracellular matrix components and angiogenesis.....	10
1.4.1.3 Lipid mobilization into lipid droplets	12
1.5 Mechanisms involved in adipose tissue dysfunction during obesity	13
1.5.1 Accumulation of pathogenic lipid species	13
1.5.2 Inflammation.....	15
1.5.3 Unfolded protein response (UPR).....	17
1.6 Adipocyte models used for studying adipose tissue function	20
1.7 FIT2: lipid storage promoting GWAS identified T2DM candidate.....	21
1.8 FTO: mitochondrial function prompting GWAS identified obesity candidate	22
1.9 Aims and hypothesis of the study	24

1.9.1 Specific objectives were to:	26
Chapter 2: General Materials and Methods	28
2.1 Procedure for RNA isolation	29
2.1.1 Protocol for RNA isolation from adipocytes and other adherent cells	29
2.1.2 Protocol for RNA isolation from adipose tissue samples	30
2.2 Relative quantification of gene expression	31
2.2.1 cDNA synthesis protocol	31
2.2.2 Real-time qPCR protocol.....	31
2.2.3 Protocol for isolation of genomic DNA and relative quantification of mitochondrial DNA content.....	32
2.2.4 Relative quantification of mitochondrial DNA content.....	33
2.3 Western blot protocol.....	34
2.3.1 Preparation of protein lysate from adherent cells	34
2.3.2 Preparation of protein lysates from adipose tissue	35
2.3.3 Protein quantification using Bradford protein assay.....	36
2.3.4 Protocol for SDS Polyacrylamide Gel Electrophoresis (SDS-PAGE)	36
2.3.4.1 Stock buffers and reagents	36
2.3.4.2 Working buffers and solutions.....	37
2.3.4.3 Other materials.....	37
2.3.4.4 Electrophoresis.....	38
2.3.4.5 Transfer	38
2.3.4.6 Immunoblotting.....	39
2.4 Protocols for cell culture	39
2.4.1 Isolation, culture and differentiation of adipocytes	39
2.4.1.1 Protocol for tissue digestion.....	39

2.4.1.2 Differentiation of primary adipocytes derived from adipose tissue	41
2.4.2 SGBS cell culture and differentiation	41
2.4.3 Preparation of BSA: palmitic acid conjugate.....	42
2.4.4 Treatment with palmitic acid and insulin stimulation in cell culture	43
2.4.5 Protocol for quantification of triglyceride accumulation.....	43
2.5 Protocol for knock-down of proteins using siRNA	44
2.6 Protocol for radioactive glucose uptake assay	45
2.7 Protocol for RNA sequencing.....	46
2.8 Protocol for measuring mitochondrial function of adipocytes	48
Chapter 3: Re-evaluating the use of SGBS adipocytes as a representative model of human adipocytes, by comparison with primary human subcutaneous adipocytes	51
3.1 Introduction.....	52
3.2 Materials and methods	53
3.2.1 Subject recruitment and cell culture	53
3.2.2 RNAseq experiment and analysis	54
3.2.3 Real-time quantitative PCR and mitochondrial DNA content.....	55
3.2.4 Western blotting.....	56
3.2.5 Mitochondrial respiration analysis.....	56
3.2.6 Lipid accumulation and radioactive glucose uptake assay	56
3.3 Results.....	57
3.3.1 Fully differentiated SGBS and SC adipocytes display distinct transcriptomic profiles	57
3.3.2 Differentially enriched metabolic pathways in SGBS adipocytes compared to SC adipocytes.....	66

3.3.2.1 Significantly up and downregulated metabolic pathways in SGBS adipocytes compared to SC adipocytes.....	70
3.3.3 Adipogenic and metabolic gene profiling of SGBS and SC adipocytes	72
3.3.4 SGBS adipocytes have energy dissipating browning phenotype....	76
3.3.5 Lipid accumulation and glucose uptake in SGBS adipocytes compared to SC adipocytes.....	78
3.3.6 Adipocyte lineage markers in SGBS and SC adipocytes.....	79
3.4 Discussion	82
3.5 Conclusion	85
Chapter 4: Partial deficiency of FIT2 protein impairs triglyceride storage and insulin signaling in human adipocytes.....	86
4.1 Introduction.....	87
4.2 Materials and Methods.....	91
4.2.1 Research design	91
4.2.2 Isolation and culture of adipocytes	91
4.2.3 Free fatty acid preparation and treatment	92
4.2.4 FIT2 protein knockdown.....	92
4.2.5 TAG accumulation and lipid droplet size	93
4.2.6 RNA isolation and Real time PCR.....	93
4.2.7 Protein isolation and western blot.....	94
4.2.8 Insulin stimulated glucose uptake assay	94
4.2.9 Statistical analysis	95
4.3 Results.....	95
4.3.1 FIT2 protein expression in adipose tissue is higher in obese non- diabetics when compared to obese diabetics	95
4.3.2 FIT2 protein expression is higher in omental adipocytes from non- diabetics as compared to diabetics	97

4.3.3 TAG accumulation after FIT2 knockdown using siRNA.....	98
4.3.4 Effect of palmitic acid on inflammation and ER stress in FIT2 KD adipocyte.....	100
4.3.5 Effect of palmitic acid on insulin signaling pathway proteins and glucose uptake in FIT2 knockdown adipocytes.....	105
4.4 Discussion.....	107
4.5 Conclusion.....	110
Chapter 5: FTO protein knockdown or chemical inhibition of FTO can increase energy expenditure in human adipocytes	111
5.1 Introduction.....	112
5.2 Materials and methods.....	114
5.2.1 Cell culture and differentiation and drug treatment of SGBS adipocytes	114
5.2.2 Protein knockdown using FTO specific siRNA.....	114
5.2.3 Preparation of protein lysates and western blotting.....	114
5.2.4 RNA isolation and mRNA expression analysis.....	115
5.2.5 Measurement of mitochondrial respiration.....	115
5.3 Results.....	115
5.3.1 FTO knockdown and inhibition increased mRNA expression of PGC1 α and UCP1 in SGBS adipocytes.....	115
5.3.2 FTO inhibition using drug CA potentiated spare respiratory capacity and maximal respiration rate.....	117
5.3.3 FTO knockdown and inhibition increased AMPK α phosphorylation	120
5.4 Discussion.....	120
5.5 Conclusion.....	122
Chapter 6: Transcriptomic analysis reveals a role for extracellular matrix and fibrosis pathways in maintaining healthy human adipose tissue function in obese non-diabetics.....	123

6.1 Introduction.....	124
6.2 Materials and methods	126
6.2.1 Characteristics of subject	126
6.2.2 Tissue RNA isolation.....	126
6.2.3 RNA sequencing and data analysis.....	127
6.3 Results.....	128
6.3.1 Depot specific and disease specific differences in transcriptomes.....	128
6.3.1.1 Sample – to – sample distance	128
6.3.1.2 Up and downregulated genes	131
6.3.2 Enriched KEGG biological pathways in OM depot compared to SC depot.....	133
6.3.2.1 PI3K-Akt signaling pathway.....	135
6.3.2.2 ECM receptor interaction pathway	138
6.3.3 Enriched cellular components in OM depot compared to SC depot	140
6.3.4 Enriched KEGG pathways in T2DM compared to NT2DM	150
6.3.5.1 ECM and fibrosis components.....	155
6.4 Discussion	159
6.5 Conclusion	164
7. Summary and future work.....	165
8. References	170
9. Appendix.....	183
I. List of SYBR green primers used for real-time qPCR.	183
2. List of primers and probes used for quantification of mitochondrial DNA content.....	185
3. Table of KEGG biological pathways enriched in SC depot from diabetics compared to SC depot from non-diabetics.....	186

4. Table of KEGG biological pathways enriched in OM depot from diabetics compared to OM depot from non-diabetics.	189
5. Table of GO_cellular components enriched in SC depot from diabetics compared to SC depot from non-diabetics.....	191
6. Table of GO_cellular components enriched in OM depot from diabetics compared to OM depot from non-diabetics.	193

Publications

Manuscripts in preparation

1. Re-evaluating the use of SGBS adipocytes as a representative model of human adipocytes, by comparison with primary human subcutaneous adipocytes

Chia Rou Yeo*¹, Madhur Agrawal*¹, Asim Shabbir², Manu Shrivastava³, Chin Meng Khoo¹, Muhammad Shabeer¹, E Shyong Tai¹, Sue Anne Toh¹

¹Department of Medicine, National University of Singapore, ²Department of Surgery, National University Hospital, Singapore, ³Jesus College, Cambridge University, England.

Partial deficiency of FIT2 protein impairs triglyceride storage and insulin signaling in human adipocytes

Madhur Agrawal*¹, Chia Rou Yeo*¹, Asim Shabbir², Chin Meng Khoo¹, Muhammad Shabeer¹, E Shyong Tai¹, Sue Anne Toh¹

¹Department of Medicine, National University of Singapore, ²Department of Surgery, National University Hospital, Singapore.

2. Characterization of fat mass and obesity associated (FTO) gene in skeletal muscle and adipose tissue energy and nutrient metabolism and its epigenetic link to obesity

Tammy Song Lin Lin*¹, Madhur Agrawal*², Esther Woon³, Mei Hui Liu⁴, E Shyong Tai¹, Sue Anne Toh¹

¹National Cancer Centre Singapore, Singapore, ²Department of Medicine, National University of Singapore, ³Department of Pharmacy, National University of Singapore, ⁴Food Science and Technology, National University of Singapore, Singapore.

Transcriptomic analysis reveals a role for extracellular matrix and fibrosis pathways in maintaining healthy human adipose tissue function in obese non-diabetics

Madhur Agrawal*¹, Chia Rou Yeo*¹, Shawn Hoon², Vanna Chhay¹, Jonathan Caleb You Xing Quek¹, Asim Shabbir³, Muhammad Shabeer¹, E Shyong Tai¹, Chin Meng Khoo¹, Jimmy Bok Yan So³, Davide Lomanto³, Sue-Anne Ee Shiow Toh¹

¹Department of Medicine, National University of Singapore, ²Molecular Engineering Lab, Biomedical Sciences Institutes, ³Department of Surgery, National University Hospital, Singapore.

Posters presented

1. Role of fat storage inducing transmembrane protein 2 (FIT2) in regulating human adipocyte function

(74th Scientific Sessions, American Diabetes Association, 2014)

Madhur Agrawal, Chia Rou Yeo, Asim Shabbir, Jimmy So Bok Yan, Chin Meng Khoo, E Shyong Tai, Sue Anne Ee Shioh Toh, Singapore, Singapore.

2. Metabolic profiles differ in human adipose tissue and primary adipocytes derived from different adipose depots and in diabetic versus non-diabetic individuals

(10th International Diabetes Federation West Pacific Region Congress, 2014)

Chia Rou Yeo, Madhur Agrawal, Asim Shabbir, Chin Meng Khoo, Muhammad Shabeer, Mei Hui Liu, E Shyong Tai, Sue Anne Toh, Singapore, Singapore.

Posters submitted

1. Transcriptomic analysis reveals a role for extracellular matrix and fibrosis in maintaining human adipose tissue function

(76th Scientific Sessions, American Diabetes Association, 2016)

Chia Rou Yeo, Madhur Agrawal, Shawn Hoon, Vanna Chhay, Jonathan Caleb You Xing Quek, Asim Shabbir, Muhammad Shabeer, E Shyong Tai, Chin Meng Khoo, Jimmy Bok Yan So, Davide Lomanto, Sue-Anne Ee Shioh Toh, Singapore, Singapore.

Abstract

Adipose tissue (AT) functions as an active endocrine organ and an energy reserve compartment for storing lipids. It's now well accepted that adipose tissue expandability, remodelling and effective storage of excess lipids in the form of triglycerides (TAGs) play an important role in maintaining metabolic homeostasis. To understand healthy AT expansion and function, we used human derived in-vitro adipocyte models to interrogate pathways of interest, as well as Next Generation Sequencing methods. We first sought to validate and functionally characterize two GWAS candidate genes involved in lipid metabolism and expressed in adipose; FIT2 (Fat Storage Inducing Transmembrane Protein 2) and FTO (Fat Mass and Obesity Associated). The FIT2 gene is associated with type 2 diabetes in the East Asian population and plays a role in transporting TAGs from ER to lipid droplets. On the other hand, FTO is an obesity associated gene in multiple ethnicities and regulates mitochondrial energy expenditure through central and peripheral mechanisms. Our observations suggest that improved TAG storage via FIT2 protein as well as improved mitochondrial oxidative capacity via FTO protein can promote insulin sensitivity in primary human adipocytes. Next, using RNA sequencing data from AT, we observed positive enrichment in the extracellular matrix (ECM) and fibrosis components in omental AT depots from T2DM when compared to NT2DM subjects. Excessive ECM and fibrosis components have been shown to inhibit obesity associated adipose tissue expansion and inflammation in the obese, but the differences identified in the OM depot among obese T2DM and obese NT2DM subjects are novel. Overall, our work contributes insights into the molecular and transcriptomic determinants of

adipocyte and adipose tissue function as well as their potential role in health and disease.

List of tables

Table 1: ER stress proteins involved in various metabolism related disorders.....	20
Table 2: Adipocyte models used for research.....	21
Table 3: Preparation of master mix for cDNA synthesis.	31
Table 4: Cycling conditions for cDNA synthesis.....	31
Table 5: Preparation of master mix for qPCR reaction for gene expression.	32
Table 6: Cycling conditions for qPCR reaction for gene expression.	32
Table 7: Preparation of master mix for quantification of mitochondrial DNA content.	34
Table 8: Cycling conditions for quantification of mitochondrial DNA. ...	34
Table 9: Differentiation and maintenance medium for SGBS adipocytes.	42
Table 10: Preparation of transfection cocktail for introduction of siRNA.	44
Table 11: Preparation of start solution for glucose uptake assay.	45
Table 12: Top KEGG biological pathways significantly enriched in SGBS vs SC control adipocytes.....	67
Table 13: Metabolic pathways significantly enriched in SGBS adipocytes compared to SC adipocytes.....	71
Table 14: Lineage specific markers in adipocytes and their expression in SGBS and SC control adipocytes. NA: Genes with FPKM < 1 and thus excluded from further analysis. P value < 0.05 and FDR < 0.05 were used as thresholds to select significant genes.	82

Table 15: Characteristics of obese diabetic and obese non-diabetic subjects from whom adipose tissue was derived for FIT2 expression analysis.....	91
Table 16: Characteristics of obese diabetic and obese non-diabetic subjects from which adipose tissue was derived for RNA sequencing analysis....	126
Table 17: Significantly enriched biological pathways in NT2DM and T2DM subjects (OM vs SC).....	134
Table 18: Enriched GO_CC in OM depot compared to SC depot in both NT2DM and T2DM subjects.....	142
Table 19: List of SYBR green primers for Real-time qPCR.	185
Table 20: List of primers and TaqMan probes for quantification of mitochondrial DNA.....	185
Table 21: KEGG biological pathways enriched in SC depot from diabetics when compared to SC depot form non-diabetics.....	188
Table 22: KEGG biological pathways enriched in OM depot from diabetics when compared to OM depot form non-diabetics.....	190
Table 23: GO_cellular components enriched in SC depot from diabetics when compared to SC depot form non-diabetics.....	192
Table 24: GO_cellular components enriched in OM depot from diabetics when compared to OM depot form non-diabetics.....	194

List of figures

Figure 1: Diabetes burden in Singapore and United States of America (USA).	3
Figure 2: Prevalence of obesity and overweight adults in Singapore and USA.	4
Figure 3: Types of adipocytes in mammals.	5
Figure 4: Illustration of functions of adipose tissue.	7
Figure 5: Basic components of ECM.	11
Figure 6: Mechanism of lipid induced insulin resistance.	14
Figure 7: Progression of inflammatory response in adipose tissue and inhibition of insulin signaling.	15
Figure 8: Modulation of adipose tissue inflammation during weight gain or metabolic dysfunction.	16
Figure 9: Canonical unfolded protein response pathway.	18
Figure 10: The unfolded protein response, nutrient sensing and inflammation.	19
Figure 11: GWAS candidates overlapping between obesity and T2DM. ..	23
Figure 12: Arrangement of PVDF membrane and SDS-PAGE gel during transfer.	38
Figure 13: Isolation of ASCs from adipose tissue digest.	40
Figure 14: Work flow of RNA-SEQ data analysis for comparing SGBS versus SC control adipocytes.	55
Figure 15: Global transcriptome profiling of SGBS and SC adipocytes (volcano plot).	57

Figure 16: Transcriptome profiling of top 1000 differentially expressed genes in SGBS adipocytes.	58
Figure 17: Fully differentiated SGBS and SC adipocytes display distinct ontology clustering.	65
Figure 18: Representation of fold changes in ECM-receptor interaction pathway (SGBS vs SC adipocytes).	68
Figure 19: Representation of fold changes in fatty acid metabolism pathway (SGBS vs SC adipocytes).	70
Figure 20: Up and downregulated genes in ECM-receptor interaction pathway (SGBS vs SC adipocytes).	70
Figure 21: SGBS adipocytes have distinct expression pattern of (A) adipogenic and (B) lipid storage and metabolism genes during adipogenesis	73
Figure 22: SGBS adipocytes have distinct expression pattern of (A) inflammatory and (B) browning genes during adipogenesis.	75
Figure 23: Gene expression data from RNAseq significantly correlated with qPCR data.	76
Figure 24: SGBS and its browning phenotype.	77
Figure 25: lipid accumulation and insulin-stimulated glucose uptake assay in SGBS vs SC adipocytes.	79
Figure 26: Lipid storage genes in NT2DM and T2DM subjects.	88
Figure 27: Expression pattern of FIT1 and FIT2 protein.	89
Figure 28: Schematic representation of FIT1 and FIT2 protein structure.	89

Figure 29: Key time points within protocol for siRNA transfection in primary human adipocytes.	93
Figure 30: FIT2 protein expression in adipose tissue is higher in non-diabetics when compared to diabetics.	96
Figure 31: FIT2 protein expression is higher in omental adipocytes from non-diabetics as compared to diabetics.	98
Figure 32: TAG accumulation is reduced after siRNA mediated knockdown of FIT2 protein	100
Figure 33: Effect of palmitic acid on inflammation related genes in FIT2 knockdown adipocytes.	102
Figure 34: Effect of palmitic acid on ER stress related genes and proteins in FIT2 knockdown adipocytes.	104
Figure 35: Effect of palmitic acid on adipogenesis related genes in FIT2 knockdown adipocytes.	105
Figure 36: Effect of palmitic acid on insulin signaling pathway proteins and glucose uptake in FIT2 knockdown adipocytes.	107
Figure 37: Effect of FTO knockdown and drug inhibition on browning genes in SGBS and 3T3-L1 adipocytes.	116
Figure 38: Effects of FTO drug inhibition on mitochondrial respiration and function in SGBS adipocytes.	119
Figure 39: Effect of FTO knockdown and drug inhibition on AMPKα phosphorylation in SGBS adipocytes.	120
Figure 40: Workflow for RNA-SEQ data analysis for comparing adipose tissue depots.	128

Figure 41: Euclidean distance (sample – to – sample distance) heatmap of all tissue RNA-SEQ data.	129
Figure 42: Principle component analysis of RNA-SEQ data.	131
Figure 43: Illustration of the number of differentially expressed genes by depot specific comparisons.	132
Figure 44: Illustration of the number of differentially expressed genes by disease specific comparisons.	133
Figure 45: Top 10 up and downregulated genes in PI3K-Akt signaling pathway in T2DM subjects (OM vs SC).	136
Figure 46: Representation of fold change of genes in PI3K-Akt signaling pathway in T2DM subjects.	138
Figure 47: ECM receptor interaction pathway genes in NT2DM and T2DM subjects.	139
Figure 48: Positively enriched cellular components in NT2DM (OM vs SC).	144
Figure 49: Negatively enriched cellular components in NT2DM (OM vs SC).	146
Figure 50: Positively enriched cellular components in T2DM (OM vs SC).	147
Figure 51: Negatively enriched cellular components in T2DM (OM vs SC).	150
Figure 52: KEGG pathway enrichment and their interaction map illustrating transcriptomic signatures in T2DM compared to NT2DM subjects.	152

Figure 53: GO cellular component enrichment and their interaction map illustrating transcriptomic signatures in T2DM compared to NT2DM subjects.....	154
Figure 54: Heat map and enrichment plots of ECM genes in OM depot (T2DM vs NT2DM).....	157
Figure 55: Enrichment analysis of fibrosis genes in T2DM compared to NT2DM (SC and OM depots).....	159

List of abbreviations

ACTB/BA	Actin, Beta
ADIPOQ/ADIPONECTIN	adiponectin, C1Q and collagen domain containing
AGRN	agrin
ALDH1A1	aldehyde dehydrogenase 1 family, member A1
ALDH3B2	aldehyde dehydrogenase 3 family, member B2
AMPKA/PRKAA1	Protein Kinase, AMP-Activated, Alpha 1 Catalytic Subunit
ANGPT4	angiopoietin 4
APOB	apolipoprotein B (including Ag(x) antigen)
ASC1/SLC7A10	Solute Carrier Family 7 (Neutral Amino Acid Transporter Light Chain, Asc System), Member 10
ASCs	Adipose derived stem cells
ASK1/MAP3K5	Mitogen-Activated Protein Kinase Kinase Kinase 5
ATF4	activating transcription factor 4
ATF6	activating transcription factor 6
ATGL/PNPLA2	Patatin-Like Phospholipase Domain Containing 2
BAT	brown adipose tissue
BCAA	branched chain amino acids
BIP/HSPA5	Heat Shock 70kDa Protein 5
BMI	body mass index
BP	biological process
BSA	bovine serum albumin
BSCL2	Bernardinelli-Seip congenital lipodystrophy 2 (seipin)
C3	similar to Complement C3 precursor; complement component 3
CAV1	caveolin 1, caveolae protein, 22kDa
CC	cellular component
CCND1	cyclin D1
CD11C/ITGAX	Integrin, Alpha X (Complement Component 3 Receptor 4 Subunit)
CD206/MRC1	Mannose Receptor, C Type 1
CD301/CLEC10A	C-Type Lectin Domain Family 10, Member A

CD36	CD36 molecule (thrombospondin receptor)
CD44	CD44 molecule (Indian blood group)
cDNA	complementary DNA
CEBPα	CCAAT/enhancer binding protein (C/EBP), alpha
CHOP/DDIT3	DNA-Damage-Inducible Transcript 3
CIDEA	cell death-inducing DFFA-like effector a
CITED1	Cbp/p300-interacting transactivator, with Glu/Asp-rich carboxy-terminal domain, 1
COL11A1	collagen, type XI, alpha 1
COL1A1	collagen, type I, alpha 1
COL1A2	collagen, type I, alpha 2
COL24A1	collagen, type XXIV, alpha 1
COL27A1	collagen, type XXVII, alpha 1
COL3A1	collagen, type III, alpha 1
COL4A1	collagen, type IV, alpha 1
COL4A2	collagen, type IV, alpha 2
COL4A3	collagen, type IV, alpha 3
COL4A4	collagen, type IV, alpha 4
COL4A5	collagen, type IV, alpha 5
COL4A6	collagen, type IV, alpha 6
COL5A1	collagen, type V, alpha 1
COL5A2	collagen, type V, alpha 2
COL5A3	collagen, type V, alpha 3
COL6A1	collagen, type VI, alpha 1
COL6A2	collagen, type VI, alpha 2
COL6A3	collagen, type VI, alpha 3
COL6A6	collagen type VI alpha 6
COMP	cartilage oligomeric matrix protein
CSF3	colony stimulating factor 3 (granulocyte)
CYP19A1	cytochrome P450, family 19, subfamily A, polypeptide 1
DAG	diglyceride
DAVID	Database for Annotation, Visualization and Integrated Discovery

DGAT1	diacylglycerol O-acyltransferase homolog 1
DGAT2	diacylglycerol O-acyltransferase homolog 2
DIO2	deiodinase, iodothyronine, type II
DMEM	Dulbecco's Modified Eagle Medium
DMEM-F12	Dulbecco's Modified Eagle Medium: Nutrient Mixture F-12
DMSO	dimethyl sulfoxide
DNA	deoxy ribonucleic acid
ECM	extracellular matrix
ENPP1	ectonucleotide pyrophosphatase/phosphodiesterase 1
ER	endoplasmic reticulum
ERAD	endoplasmic reticulum associated protein degradation
EWAT	epididymal white adipose tissue
FABP4	fatty acid binding protein 4, adipocyte
FBS	fetal bovine serum
FCCP	Carbonyl cyanide 4-(trifluoromethoxy) phenylhydrazone
FDR	false discovery rate
FFA	free fatty acid
FGF1	fibroblast growth factor 1 (acidic)
FGF9	fibroblast growth factor 9
FGF21	fibroblast growth factor 21
FITM2	fat storage-inducing transmembrane protein 2
FN1	fibronectin 1
FPKM	Fragments Per Kilo base of transcript per Million mapped reads
FTO	fat mass and obesity associated
GAPDH	glyceraldehyde-3-phosphate dehydrogenase
GLUT4/SLC2A4	Solute Carrier Family 2 (Facilitated Glucose Transporter), Member 4
GM2A	GM2 ganglioside activator
GO	gene ontology
GPC3	glypican 3
GSEA	gene set enrichment analysis

GST	Glutathione S-transferase
GWAS	genome wide association studies
GYS2	glycogen synthase 2 (liver)
HBBS	Hank's Balanced Salt Solution
HEK-293T	human Embryonic Kidney 293
HEPES	4-(2-hydroxyethyl)-1-piperazineethanesulfonic acid
HFD	high fat diet
HIF1α	hypoxia inducible factor 1, alpha subunit (basic helix-loop-helix transcription factor)
HMOX1	heme oxygenase (decycling) 1
HO1	Heme Oxygenase 1
HRP	horse radish peroxidase
HSPG2	heparan sulfate proteoglycan 2
IBMX	3-isobutyl-1-methylxanthine
IκKB/IKBKB	Inhibitor Of Kappa Light Polypeptide Gene Enhancer In B-Cells, Kinase Beta
IL18	interleukin 18 (interferon-gamma-inducing factor)
IL1β	interleukin 1, beta
IL6	interleukin 6 (interferon, beta 2)
IRE1α/ERN1	Endoplasmic Reticulum To Nucleus Signaling 1
IRS1	insulin receptor substrate 1
ITGA1	integrin, alpha 1
ITGA10	integrin, alpha 10
ITGA11	integrin, alpha 11
ITGA2	integrin, alpha 2 (CD49B, alpha 2 subunit of VLA-2 receptor)
ITGA3	integrin, alpha 3 (antigen CD49C, alpha 3 subunit of VLA-3 receptor)
ITGA4	integrin, alpha 4 (antigen CD49D, alpha 4 subunit of VLA-4 receptor)
ITGA7	integrin, alpha 7
ITGB1	integrin, beta 1 (fibronectin receptor, beta polypeptide, antigen CD29 includes MDF2, MSK12)

ITGB3	integrin, beta 3 (platelet glycoprotein IIIa, antigen CD61)
ITGB4	integrin, beta 4
ITGB5	integrin, beta 5
ITGB8	integrin, beta 8
JNK	C-Jun N-Terminal Kinase 1
KEGG	Kyoto Encyclopedia of Genes and Genomes
LAMA2	laminin, alpha 2
LAMA3	laminin, alpha 3
LAMB1	laminin, beta 1
LAMB2	laminin, beta 2 (laminin S)
LAMB3	laminin, beta 3
LAMC2	laminin, gamma 2
LPL	lipoprotein lipase
MCP1	monocyte Chemotactic Protein 1
MET	met proto-oncogene (hepatocyte growth factor receptor)
MHO	metabolically healthy obese
MMP	Matrix Metallopeptidase
mRNA	messenger RNA
MSR1	macrophage scavenger receptor 1
mTOR	mechanistic target of rapamycin (serine/threonine kinase)
MTUS1	mitochondrial tumor suppressor 1
MYF5	myogenic factor 5
NADH	nicotinamide adenine dinucleotide
NEAA	non-essential amino acids
NFκB1	Nuclear Factor Of Kappa Light Polypeptide Gene Enhancer In B-Cells 1
NR1H3	nuclear receptor subfamily 1, group H, member 3
NRF2/NFE2L2	Nuclear Factor, Erythroid 2-Like 2
NRIP1	nuclear receptor interacting protein 1
NT2DM	non type 2 diabetes or non-type 2 diabetics
OCR	oxygen consumption rate
OFD1	oral-facial-digital syndrome 1
OM	omental

OSBPL11	oxysterol binding protein-like 11
PAX7	paired box 7
PBS	phosphate buffered saline
PDGFRα	platelet-derived growth factor receptor, alpha polypeptide
PERK/EIF2AK3	Eukaryotic Translation Initiation Factor 2-Alpha Kinase 3
PGC1α/PPARGC1A	Peroxisome Proliferator-Activated Receptor Gamma, Coactivator 1 Alpha
PKA/PRKACA	Protein Kinase, CAMP-Dependent, Catalytic, Alpha
PLIN1	perilipin
PLIN2	adipose differentiation-related protein
PLIN4	KIAA1881
PLIN5	lipid storage droplet protein 5
PNPLA2	patatin-like phospholipase domain containing 2
PPARα	peroxisome proliferator-activated receptor alpha
PPARγ	peroxisome proliferator-activated receptor gamma
PPP2R2C	protein phosphatase 2 (formerly 2A), regulatory subunit B, gamma isoform
PRDM16	PR domain containing 16
PTPN2	protein tyrosine phosphatase, non-receptor type 2
PVDF	polyvinylidene fluoride
RBP4	retinol binding protein 4, plasma
RELN	reelin
RNA	ribonucleic acid
ROS	reactive oxygen species
SAT	subcutaneous adipose tissue
SC	subcutaneous
SCARB1	scavenger receptor class B, member 1
SDC4	syndecan 4
SDS	sodium dodecyl sulfate
SGBS	Simpson Golabi Behmel Syndrome
siRNA	small interfering RNA
SNP	single nucleotide polymorphism
SPP1	secreted phosphoprotein 1

SV2B	synaptic vesicle glycoprotein 2B; hypothetical protein LOC100128403
SVF	stromal vascular fraction
T2DM	type 2 diabetes or type 2 diabetics
T3	triiodothyronine
TAG	triglyceride
TBS	tris buffered saline
TCA	tricarboxylic acid (TCA)
TGF	transforming growth factor
THBS1	thrombospondin 1
THBS2	thrombospondin 2
THBS3	thrombospondin 3
THBS4	thrombospondin 4
TIP47/PLIN3	Perilipin 3
TLR4	toll-like receptor 4
TNC	tenascin C
TNF	Tumor Necrosis Factor
TNN	tenascin N
TNXB	tenascin XB; tenascin XA pseudogene
UCP1	uncoupling protein 1 (mitochondrial, proton carrier)
UPR	unfolded protein response
VAT	visceral adipose tissue
VEGF	Vascular Endothelial Growth Factor
VWF	Von Willebrand factor
WAT	white adipose tissue
XBP1	X-Box Binding Protein 1

Chapter 1:

Introduction

1.1 Type 2 diabetes and obesity

Diabetes mellitus is a group of metabolic diseases in which there is hyperglycemia, due to either the pancreas not producing enough insulin (insulin deficiency) or the cells of the body not responding properly to the insulin produced (insulin resistance), or both [1]. If left untreated, diabetes can cause many complications, including cardiovascular disease, stroke, chronic kidney failure, foot ulcers, and damage to the eyes [2].

Type 2 diabetes mellitus (T2DM) is the most common form of adult onset (observed usually at age of 40 years and above) diabetes in the world with strong genetic, ethnic and environmental influence. Owing to polygenic nature and involvement of multiple tissues and proteins in its pathogenesis, diabetes has no cure yet and a major focus in metabolism research has been towards better management and longer healthy lifespan of the patients. Currently, T2DM affects almost 387 million (8.3% of total population) people worldwide, and this figure is expected to increase to 592 million by the year 2035 with approximately 46.3% of patients remaining undiagnosed. T2DM as a disease also levies huge financial burden (612 billion USD in 2014) on the patients and thus there is a constant requirement for better research, healthcare management guidelines and strategies for early diagnosis of T2DM [3]. Worldwide demographics show that the Western Pacific region has the highest number of diabetic individuals (138 million) followed by Southeast Asian population which includes approximately 70 million diabetic adults. Within Singapore, 12.3% of the total population (18-69 years old) is diabetic (increased from 4.7% in the year 1984, figure 1).

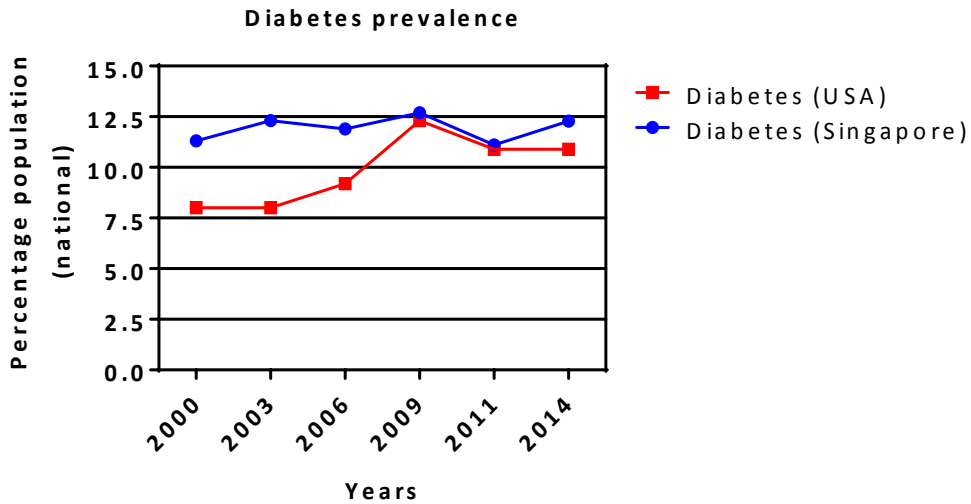


Figure 1: Diabetes burden in Singapore and United States of America (USA).

Adapted from Diabetes Atlas, International Diabetes Federation (edition 1-6). Dots and squares represent the percentage of diabetic individuals calculated based on the national population.

Ethnic Asians are predisposed to cardio-metabolic disorders at an earlier age as well as lower Body Mass Index (BMI) [4], primarily due to the differences in their body fat distribution [5]. Epidemiology studies indicate that at a given BMI, Asians tend to accumulate greater amounts of central or abdominal fat when compared to western population which accelerates the development of insulin resistance and associated complications [5, 6]. This phenomenon is exemplified in the Singaporean population (figure 1 and 2) as they have a similar prevalence of diabetes when compared to United States of America (USA), even though the percentage of the obese and overweight population is lower than that of USA. Hence, there exists a discordance between obesity or amount of adipose tissue depot and incidence of insulin resistance or diabetes in various ethnic groups. Thus, studying adipose tissue depots in adult humans might provide clues for understanding the reasons behind variances in the manifestation of insulin resistance and T2DM.

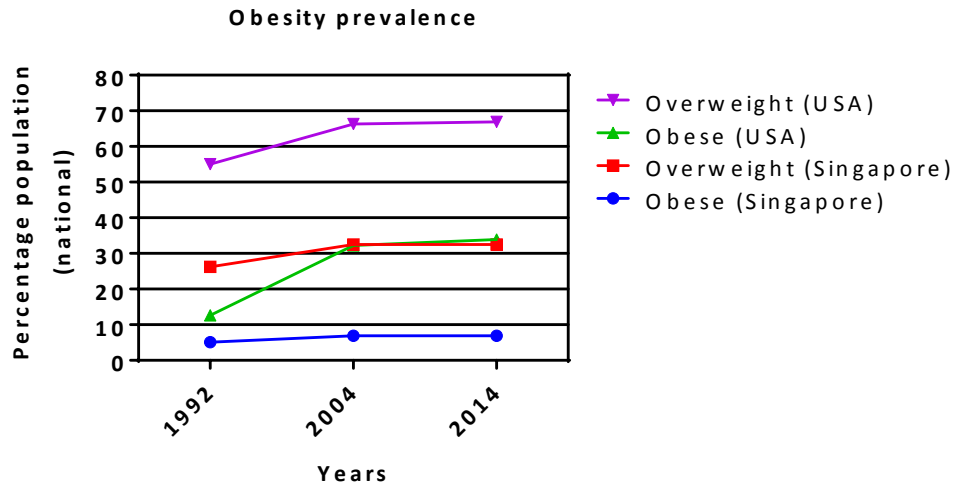


Figure 2: Prevalence of obesity and overweight adults in Singapore and USA.

Bars represent the percentage of obese and overweight people calculated based on national population. Data adapted from WHO Global Database for Body Mass Index. Overweight and obesity were defined as $BMI \geq 25.0$ and $BMI \geq 30$ respectively. Obesity percentage in Singapore increases to 23% if $BMI \geq 27.5$ is used for defining obesity (Asian cut-off).

1.2 Functional categories of adipocytes and anatomical distribution of adipose tissue

In adult humans, white adipose tissue (WAT) forms majority of adipose and is important in maintaining metabolic homeostasis along with brown adipose tissue (BAT). Adipocytes are functional lipid storing cells inside adipose tissue and three types of functionally different adipocytes found in humans are white, brown and beige [7, 8] (figure 3). Depending on anatomical location, mammalian white adipocytes are typically distributed into subcutaneous (SAT or SC) and omental (OM) or visceral adipose tissue depots (VAT). SAT lies underneath the skin performing a more protective and thermoregulatory function whereas VAT is located inside the abdominal cavity, enveloping the abdominal organs. Additionally, BAT is involved in heat production via mitochondrial uncoupling and was known to predominantly exist only in intrascapular region of neonates and infants. However, recently Kirsi A et al

used positron emission tomography and observed UCP1 expressing functional brown adipose tissue in the paracervical and supraclavicular region of adult humans [9]. Functionally, brown adipocytes actively express UCP1 protein and have a large number of mitochondria and smaller lipid droplets compared to white adipocytes [8]. Beige adipocytes are embedded in white adipose tissue (WAT) of adult humans and possess inducible browning phenotype [10]; an ability to transform from white adipocyte to brown adipocyte upon stimulation with cold, β 3-adrenergic receptor agonist, PPAR γ agonist, FGF21 and irisin.

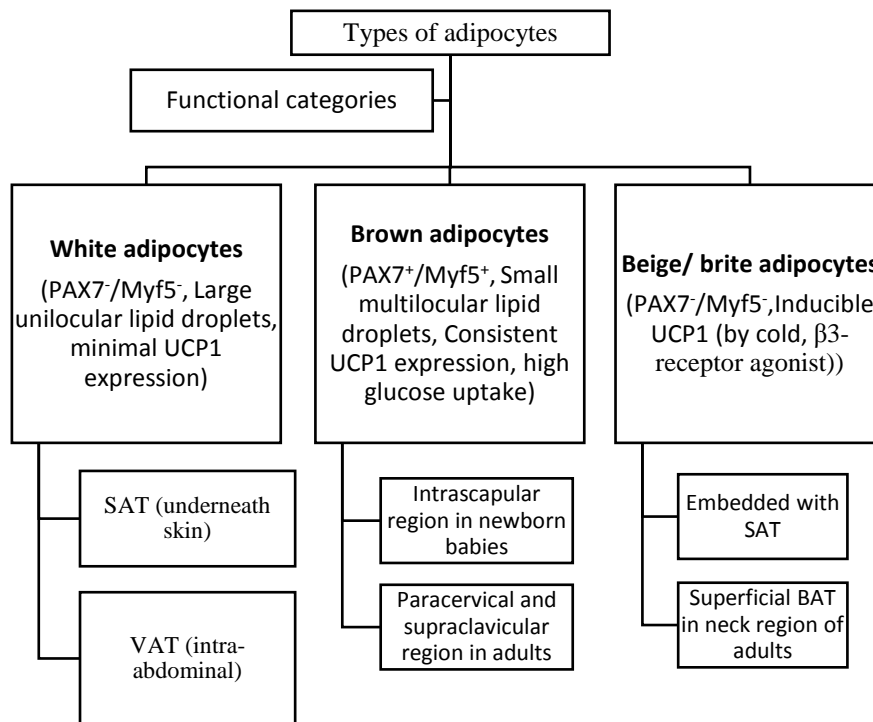


Figure 3: Types of adipocytes in mammals.

Adipocytes are classified as either white, brown or beige depending on their phenotype and functions. Brown and beige adipocytes differentiate from PAX7⁺/Myf5⁺ and PAX7⁻/Myf5⁺ precursors respectively, whereas white adipocytes differentiate from PAX7⁻/Myf5⁻ lineage.

Adipose tissue depots are known to have distinct characteristics in terms of metabolism and endocrine capacity. Between SAT and VAT, the latter correlates better with the onset of cardio-metabolic disorders in humans and its

removal also proved to have more beneficial effects in terms of metabolic markers when compared to removal of subcutaneous fat [11, 12]. Interestingly, adipocytes isolated from respective depots and cultured *in vitro* maintain their phenotype to an extent and hence used as valid experimental models. For instance, upon stimulation with rosiglitazone and insulin, OM adipocytes isolated from adipose tissue secrete less adiponectin compared to SC adipocytes [13] which is a characteristic feature of OM adipose tissue [14].

1.3 Main functions of adipose tissue

Conventionally, adipose tissue was considered as merely a storage organ for excess nutrients in the form of lipid droplets which could be utilized during periods of fasting/starvation via lipolysis. Over the years, more complex functions of fat (mentioned below) were slowly understood. Figure 4 summarizes known functions of adipose tissue. Adipose tissue functions include:

1. Endocrine function: secretion of hormones such as leptin [15, 16] and adiponectin [17] which regulate food intake and fuel utilization.
2. Regulation of angiogenesis to support adipocyte growth within the tissue [18].
3. Regulation of inflammation and macrophage infiltration [19].
4. Metabolic functions including lipogenesis, lipid storage and lipolysis.

In healthy individuals, the degree of lipid storage or breakdown is controlled primarily by insulin and glucagon hormones. During the fed state, insulin promotes the storage of dietary lipids in adipose tissue. Free fatty acids after being absorbed are converted to TAGs (triacylglycerol/triglycerides) in the liver

and transported to the adipose tissue after being packaged inside lipoproteins. Inside adipose, lipase enzyme in the plasma membrane of adipocytes breaks these TAGs to free fatty acids which eventually enter inside ER as fatty acyl-CoA. In ER, these fatty acyl-CoA are converted back to TAGs (re-esterification) and stored in lipid droplets. Adipocytes also synthesize free fatty acids such as palmitic acid from acetyl-CoA by the process of de novo lipogenesis. During fasting state, glucagon hormone is secreted from pancreatic alpha cells, which in turn activates lipolysis of stored TAGs in adipocytes. Free fatty acids released upon lipolysis are distributed to energy deficient tissues such as skeletal muscle. Here, these free fatty acids are oxidized into acetyl-CoA in mitochondria via β -oxidation pathway to generate energy in the form of ATP.

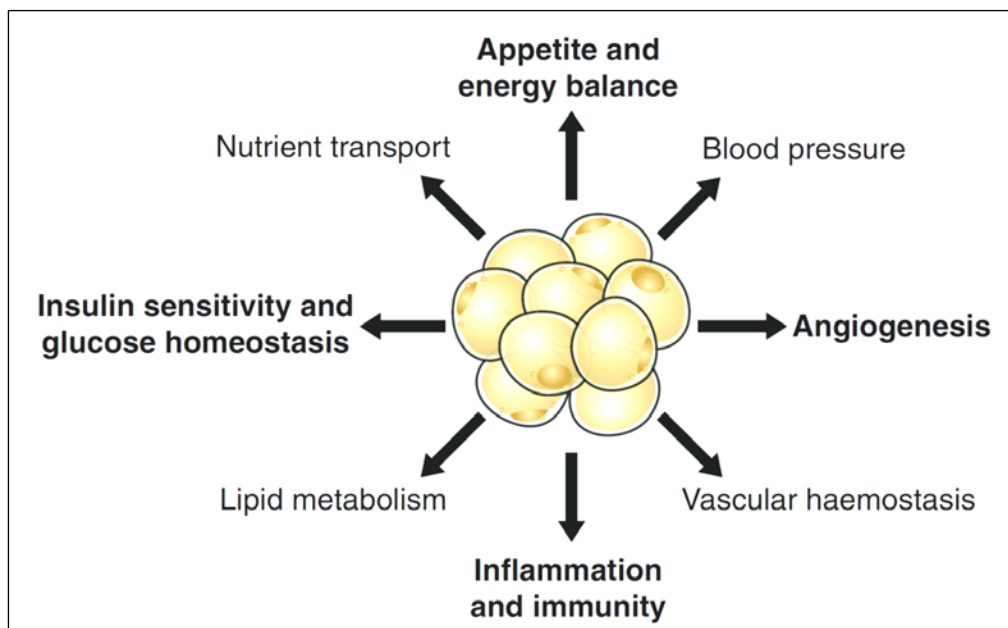


Figure 4: Illustration of functions of adipose tissue.

Adipocytes actively store lipids in form of triglycerides or TAGs (lipogenesis) inside stable lipid droplets which are catabolized by lipolysis. In healthy adipose tissue, insulin switches the adipocytes from lipolytic to lipogenic to promote fuel storage. Adiponectin and leptin regulate appetite and energy balance via central and peripheral mechanisms. Adopted from Trayhurn, Paul et al, 2013 [20].

1.4 Adipose tissue expandability hypothesis

“The adipose tissue expandability hypothesis states that the capacity of an individual to expand their fat mass to store lipid is a more important determinant of obesity-associated metabolic problems than the absolute amount of adipose tissue an individual possesses” [21, 22]. In a situation where an individual fails to maintain adipose tissue functions due to impaired expansion, usually due to excessive obesity, ectopic lipids begin to accumulate in tissues such as liver, heart and skeletal muscle which accelerates development of metabolic syndrome.

Obesity and insulin resistance were always believed to exist hand in hand, but multiple clinical and animal model observations now establish that link between obesity and insulin resistance is not directly proportional. In humans, it is well recognised that metabolically healthy obese (MHO) are protected from insulin resistance and its complications, even though they are extremely obese [23, 24]. Conversely, some individuals with lipodystrophy syndrome who are unable to store lipids properly in adipose tissue, suffer from insulin resistance, dyslipidaemia and other metabolic complications [25]. Moreover, TZDs (thiazolidinediones), a class of antidiabetic drugs are known to increase body weight and improve insulin sensitivity simultaneously [26].

Animal model studies support this hypothesis as well. Adiponectin is an insulin sensitizing, anti-inflammatory adipokine which exerts favourable effects on lipid and glucose homeostasis via multiple mechanisms [27]. Mice with adiponectin overexpression (AdTG-ob/ob) do not exhibit ectopic lipid deposition or insulin resistance even with 50% extra body weight compared to ob/ob mice who extremely overweight and become diabetic at an early age [28].

These mice have increased SC and reduced OM adipose tissue depots with smaller adipocytes when compared to ob/ob mice. Similar phenomenon is observed in MHO individuals, who have increased circulating adiponectin [24] and maintain metabolic homeostasis and even in humans, expansion of SC depot decreases odds of insulin resistance whereas expansion of OM depot increases odds of insulin resistance [29]. Additional evidence comes from adipose tissue transplantation studies. Reversal of hyperglycaemia, insulin deficiency as well as insulin resistance is seen in lipoatrophic diabetic mice (ZIP/F-1) on being transplanted with healthy adipose tissue from wild type mice [30].

1.4.1 Mechanisms involved in healthy adipose tissue expansion or adipose tissue remodelling during obesity

Massive non-neoplastic expansion of adipose tissue with increasing weight is one of its exceptional ability [31]. Several interlinked properties of adipose tissue biology confer this unique ability and determine the metabolic outcome.

They are:

1. Hypertrophy (increase in size) and hyperplasia (increase in number) of adipocytes.
2. Modifications in ECM to support growing adipocytes.
3. Angiogenesis
4. Macrophage mobilization to remove excess lipids and dead cells (discussed in section 1.5.2).
5. Lipid mobilization into lipid droplets.
6. Adipokine secretion.

1.4.1.1 Hypertrophy and hyperplasia

Weight gain and weight loss have distinct effects on adipocyte phenotype. As an individual becomes obese, adipocytes or fat cells increase in size to accommodate extra nutrients and upon reaching a threshold, they start dividing to proliferate in number [32]. Hypertrophy has a greater pathogenic effect than hyperplasia [33] and different adipose depots may react differently in response to obesity environment. In *ad libitum* fed male wistar rats, intra-abdominal adipose tissue growth is due to hypertrophy whereas retroperitoneal and inguinal adipose depot grow by hyperplasia [34]. Studies also support the idea that total number of preadipocytes are fixed after birth, but the percentage of adipocytes maturing from these depend on obesity [35]. Similarly, weight loss affects adipocyte size as well. Subjects with hyperplastic obesity who undergo jejunum-ileostomy for weight loss have smaller adipocytes after 21 months of surgery with no change in number of adipocytes [36].

1.4.1.2 Extracellular matrix components and angiogenesis

In addition to adipocyte size and number, vasculature and ECM components are equally crucial for healthy adipose tissue [37, 38]. ECM (figure 5) is a mesh like structure enveloping and supporting all the cells within. Primary functions of ECM include adhesion (during cell migration), providing tensile strength, comprehensive strength, elasticity, supporting angiogenesis as well as binding and signalling of growth factors, hormones, cytokines etc. [39]. Angiogenesis is a process of formation of new blood vessels from existing ones harbored in ECM and its significance in maintaining healthy adipose tissue have been confirmed in adipose tissue from *ob/ob* mice as well as human subjects [40]. Obese insulin resistant individuals tend to have a reduced number of capillaries

and larger blood vessels when compared to lean subjects and these differences in angiogenesis were attributed to differences in ECM [41].

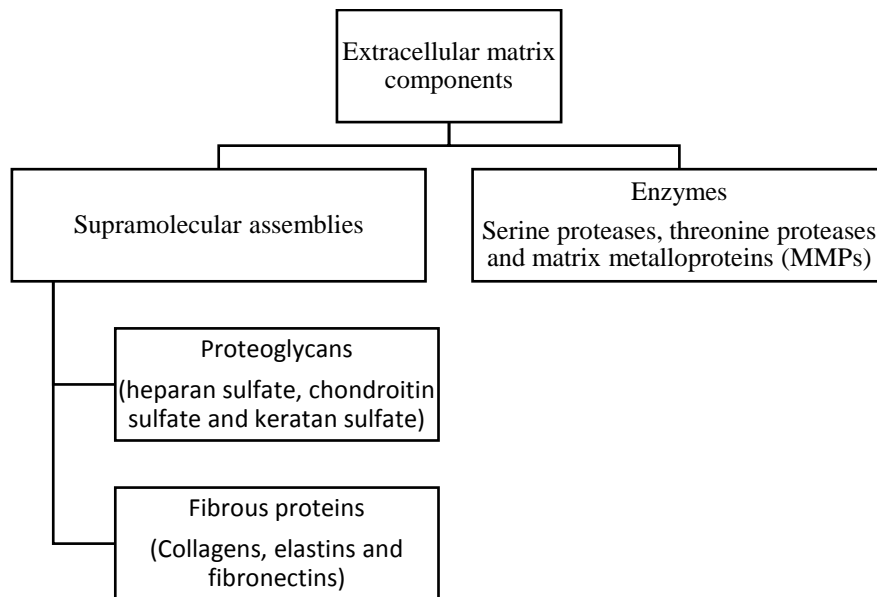


Figure 5: Basic components of ECM.

ECM composition is tissue specific and varies with obesity and age in adipose tissue. Macromolecules including fibrous proteins and proteoglycans support internal cellular components and enzymes such as MMPs which are usually involved in degeneration of ECM, particularly important for a process like bone resorption, migration and tissue remodeling.

Maria A. Rupnick et al [18] treated *ob/ob* mice with anti-angiogenic agents and observed dose dependent reduction in weight and adipose tissue mass along with increased apoptosis, vascular abnormalities and shift from carbohydrate utilization to fatty acid utilization indicating adipose tissue dysfunction. In *db/db* mice, administration of antibodies against vascular endothelial growth factor (VEGF) lead to a reduction in angiogenic/adipogenic clusters or in other words adipogenesis [42]. Sufficient vasculature is key to prevent hypoxia or lack of oxygen; which is a common observation in obese individuals [43] due to an imbalance between increasing adipose tissue mass and insufficient growth in the vasculature. Hypoxia-inducible factor 1 α (HIF1 α) gets activated due to hypoxia and a constitutive overexpression of HIF1 α directs adipose tissue

towards fibrosis (possibly by activation of lysyl oxidase and subsequent crosslinking of collagen I and collagen III to form fibrillary collagen) with increased local inflammation [39, 44]. Fibrosis inhibits healthy expansion of adipose tissue and accelerates obesity associated metabolic disorders [20, 45].

1.4.1.3 Lipid mobilization into lipid droplets

Formation of lipid droplets occurs since most primitive species and is important for survival during fasting and starvation. From an evolutionary perspective, they are highly conserved in their constitution and mechanism of formation from invertebrates to animals. In mammals, although adipocytes are primary site for lipid storage, they are present in all metabolically active tissues such as skeletal muscle, adipose tissue and liver.

Lipid droplets store triglycerides (TAGs), retinyl esters and cholesteryl esters surrounded by a phospholipid monolayer and almost 90% of them are found in the proximity of endoplasmic reticulum (ER). Three mechanisms primarily involved in lipid droplet biology include; (I) transfer of newly formed TAG in ER and other constituents into lipid droplets, (II) transfer of lipids from small to large droplets (III) fusion of smaller droplets to form bigger droplets. Particularly, members of perilipin family, i.e. PLIN2 (adipophilin, ADRP), PLIN1 (perilipin), TIP-47 (PLIN3), S3-12 (PLIN4) and PLIN5 are actively involved in regulation of lipid droplets [46]. Additionally, several proteins present at the junction of ER and lipid droplet mediate the transport of new synthesized TAGs into lipid droplets. Seipin and FIT1/2 are two such proteins responsible for the formation of bigger sized lipid droplets [47-50] and failure to partition triglycerides effectively is thought to be detrimental to adipose tissue health [48, 51, 52]. Knockdown of seipin in 3T3-L1 adipocytes leads to

increased oleate accumulation and clustering of smaller lipid droplets into bigger ones accompanied by insulin resistance [49]. Furthermore, Berardinelli-Seip Congenital Lipodystrophy 2 (BSCL2)/Seipin mutants in humans are lipodystrophic with fatty liver and severe insulin resistance along with complete loss of adipose tissue [50, 53]. The role of lipid droplet proteins in maintaining adipose tissue health is now increasingly appreciated and studied in the context of adipose tissue expandability.

1.5 Mechanisms involved in adipose tissue dysfunction during obesity

Mechanisms involved adipose tissue dysfunction are:

1. Accumulation of pathogenic lipid species.
2. Production of reactive oxygen species (ROS).
3. Activation of inflammatory pathways.
4. Upregulation of unfolded protein response (UPR).

These are highly interconnected pathways responsible for the development of insulin resistance and other complications in T2DM. Mechanism which is induced at first during overfeeding and obesity was a long standing debate. But, very recently a study involving overfeeding of individuals with approximately 6000 Kilo-calorie/day for a week observed significant upregulation of ROS production in their subcutaneous adipose tissue even when inflammation or ER stress was not observed [54], suggesting ROS production to be the first pathogenic mechanism.

1.5.1 Accumulation of pathogenic lipid species

Diacylglycerols (DAGs), ceramides and sphingolipids are lipid intermediates [55, 56] elevated during free fatty acid excess and are known to be pathogenic

in nature. Free fatty acids lead to increased ROS production, ER stress and inflammation in 3T3-L1 adipocytes as well as mice [57]. Excessive DAGs result in insulin resistance by activating protein kinase C θ which phosphorylates IRS-1 protein at serine residue and in turn inhibit insulin mediated tyrosine phosphorylation of IRS proteins (figure 6). The importance of regulating the amount of DAG formation have been worked out in several studies.

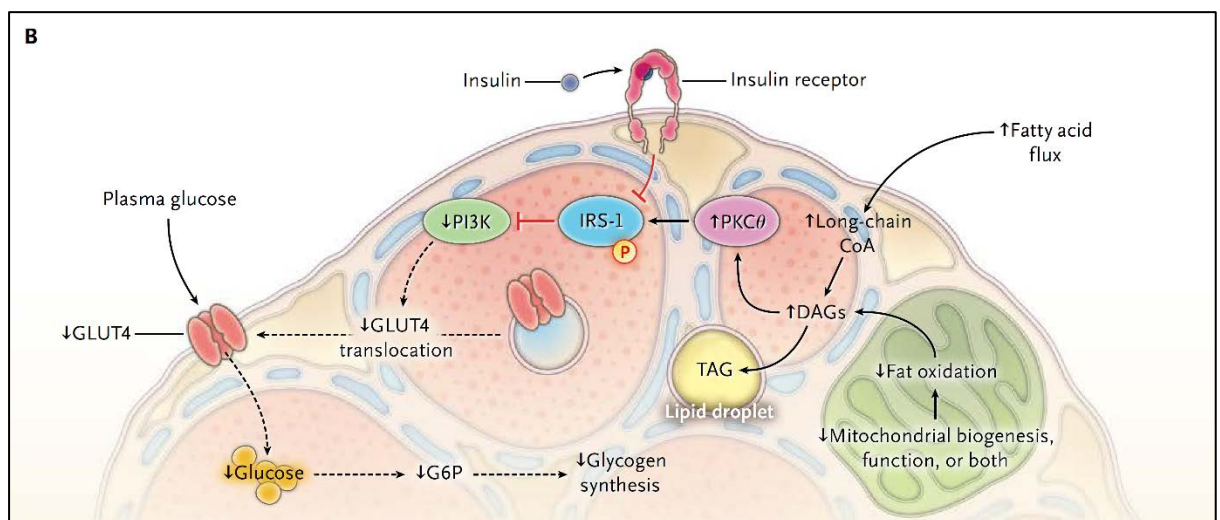


Figure 6: Mechanism of lipid induced insulin resistance.

Elevated DAGs and free fatty acids activate PKC θ (protein kinase C θ) which blocks IRS1 signaling by serine phosphorylation of IRS1. Eventually, insulin stimulated GLUT4 translocation is compromised. Adopted from Shulman et al [58].

DGAT1 and DGAT2 (Acyl-CoA: diacylglycerol acyltransferase) are ER resident enzymes synthesizing TAGs from DAGs by the addition of fatty acyl-CoA moiety. Mice with DGAT overexpression (hence reduced quantity of DAGs) are protected from lipid induced insulin resistance even though they have increased triglyceride accumulation in liver [59]. Conversely, reduced expression of DGAT2 in adipose tissue and liver reverses diet induced hepatic insulin resistance by reducing lipogenesis. Similar effects of DGAT enzyme were also observed in muscle cells derived from mice and human skeletal muscle [60-62].

1.5.2 Inflammation

Metabolic disorders are often a result of prolonged uncontrolled inflammation. Induction of inflammation is body's defense mechanisms against external pathogens and important to maintain health. Inflammation induced due to metabolic intermediates is also termed as 'meta-flammation' [63]. Extensive research has brought forward mechanistic association between chronic low grade inflammation and metabolic diseases such as obesity and T2DM. Figure 7 represents a pathway of progression from induction of inflammation due to metabolites and downstream impairment in insulin signaling in adipose tissue.

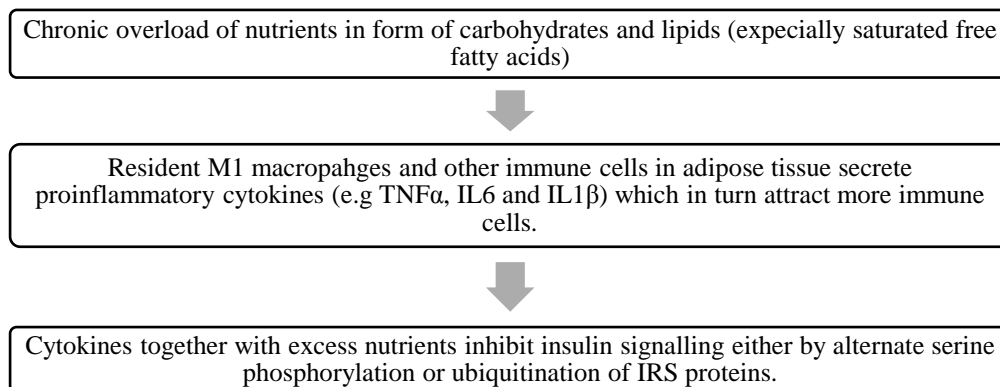


Figure 7: Progression of inflammatory response in adipose tissue and inhibition of insulin signaling.

Obesity and excess nutrients induce inflammation in all metabolically active tissues. In adipocytes, TLR4 receptors present in cell surface are activated by excess free fatty acids and induce inflammatory pathways inside the cell [64, 65]. Presence of immune cells in adipose tissue is known for decades [66], but obesity induced increment in TNF α (secreted by macrophages) was observed in obese mice recently [19]. Being one of the earliest discovered inflammation induced cytokine, IL6 is well studied and is known to phosphorylate insulin receptor substrate (IRS) at serine residue and thus impair tyrosine phosphorylation in IRS proteins [67].

Unhealthy adipocytes are prone to attract macrophages. This process is clearly demonstrated in FAT-ATTAC mice, where apoptosis can be induced in adipose tissue by activation of caspase-8 and increased apoptosis leads to macrophage infiltration along with downregulation in adipokine secretion [68]. Phenotypically, macrophages are now categorized as either M1 or M2 and their ratio is crucial to maintain adipose tissue health. M2 macrophages (expressing CD206 or CD301 surface marker) are protective or anti-inflammatory, whereas M1 macrophages (expressing CD11c surface marker) are pro-inflammatory and secrete IL6, TNF α and IL1 β cytokines. Obesity leads to increased infiltration of M1 macrophages in adipose tissue which leads to insulin resistance [69-71]. Figure 8 depicts changes in expression pattern of macrophages and adipokines from anti-inflammatory in the lean state to pro-inflammatory in obese state.

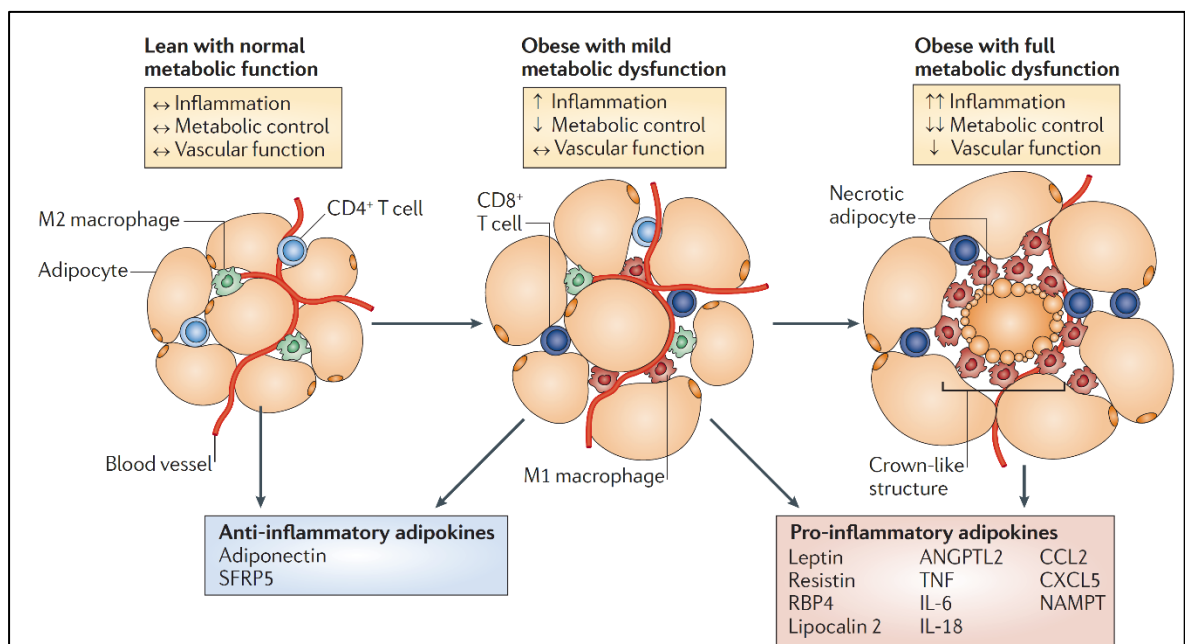


Figure 8: Modulation of adipose tissue inflammation during weight gain or metabolic dysfunction.

An imbalance between inflammation, metabolic control and vascular function occurs in obese individuals. Along with increasing inflammation, adipocytes secrete pro-inflammatory adipokines such as leptin, resistin and RBP4 in increasing amounts. Macrophage phenotype changes from M2 to M1, which further contributes to inflammation. Adopted from Ouchi, N. et al [72].

Nevertheless, beneficial effects of inflammation in maintaining health cannot be negated. Local inhibition of inflammation in adipocytes results in systemic inflammation, ectopic lipid accumulation and glucose intolerance [73]. Likewise, inflammation and impaired insulin signaling is usually accompanied with anti-TNF α treatment against rheumatoid arthritis [74, 75]. Interestingly, upregulation of M2 type macrophages is also observed during cold induced browning of adipose tissue [76]. Thus, a delicate balance between beneficial and pathogenic inflammation exists and more research is needed to understand the switch between the two phenotypes.

1.5.3 Unfolded protein response (UPR)

Early studies observed induction of ER stress and apoptosis in MIN6 beta cells treated with nitric oxide (NO), a compound which has been implicated in cytokine induced beta cell dysregulation in type I diabetes [77]. Figure 9 illustrates a typical ER stress response in a cell. ER stress induction have been linked to excess nutrients and obesity in different experimental models [78-80]. Figure 10 illustrates nutrient induced ER stress mechanisms. Chronic hyperglycemia (mainly through PERK pathway), free fatty acids and certain amino acids (via mTOR pathway) induce UPR as a counteractive mechanism which ultimately leads to ER stress, cytotoxicity and cell death if uncontrolled.

In human subcutaneous adipose tissue, ER stress markers have a direct positive correlation to increasing BMI [81, 82] and elevated UPR proteins (calnexin and phospho-JNK1) and genes (XBP1s) are often observed in obese insulin resistant individuals [83]. UPR induction has been reported not only in nutrient excess, but in hyperinsulinemic conditions as well, which is a common prediabetic stage. Boden et al. observed UPR induction in 3T3-L1 adipocytes and human

subcutaneous adipose tissue from obese non-diabetic individuals after insulin treatment *in vitro* and during hyperinsulinemic clamps respectively [84]. Being an anabolic hormone, insulin upregulates protein synthesis and accumulation of misfolded proteins; eventually leading to UPR. Interestingly, there is also a decrease in ER stress markers in liver and adipose tissue from obese patients after they undergo marked weight loss [85].

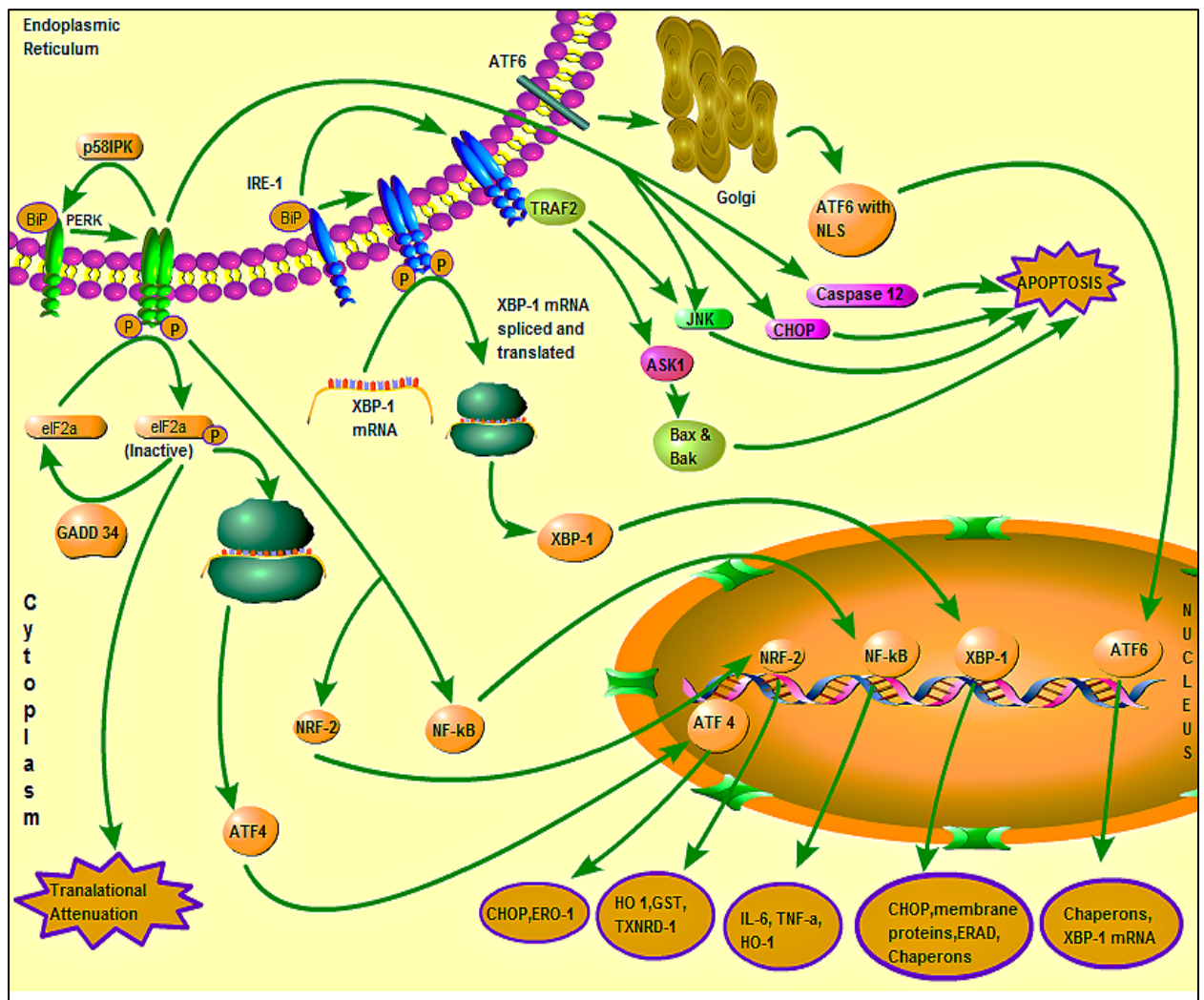


Figure 9: Canonical unfolded protein response pathway.

UPR pathways are activated by stressful conditions such as depletion of Ca^{2+} , oxidative stress, inflammatory stress etc. This may result in increased accumulation of unfolded and misfolded proteins. UPR is like a chain reaction with the initiators being PERK, ATF6 and IRE1a proteins. The main motive of this type of response is to alleviate the cellular stress. It does so by increasing ER chaperones, decreasing protein synthesis and by induction of ER associated protein degradation (ERAD). When all these measures are not able to help, the

cell undergoes autophagy and apoptosis. PERK leads to translational attenuation that reduces load on ER protein folding machinery. Activation of transcription factors ATF6 and IRE1a results in increased amount of ER chaperons and ERAD components. Activated IRE1a causes nonconventional splicing of XBP1 forming XBP1s which is important in eliciting the effect of IRE1a. In case of insufficient ERAD, cells proceed to apoptosis. All three, PERK, ATF6 and IRE1a pathways cause apoptosis via ATF4, XBP1s and ATF6 respectively. They induce increased expression of pro-apoptotic factors such as CHOP. PERK and IRE1a also directly activates JNK, ASK1 and CHOP proteins which leads to apoptosis. Another important response is anti-oxidant response resulting from PERK pathway. PERK mediates this through the transcription factors NRF-2 and NFκB, resulting in increased expression of HO1, GST and IL6 respectively to combat oxidative stress. Figure developed in Pathway Builder, based on literature review.

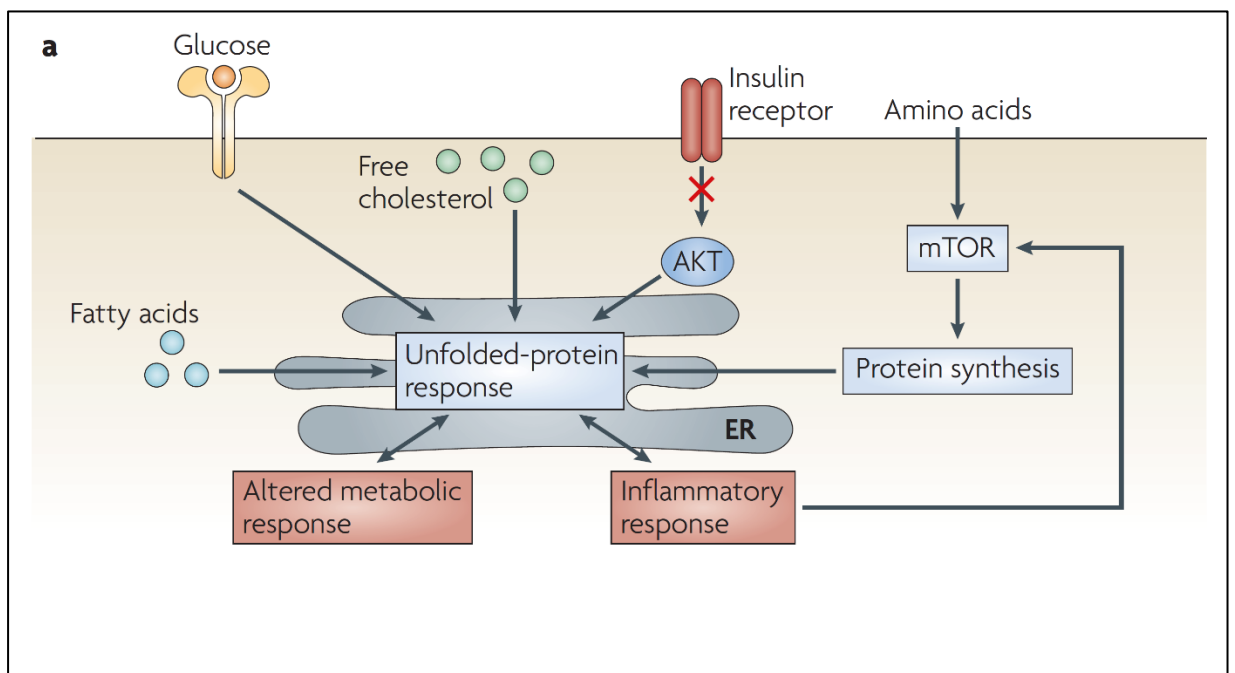


Figure 10: The unfolded protein response, nutrient sensing and inflammation.

UPR is induced in response to ER stress inducers and can result in altered metabolic and inflammatory responses and thus metabolic disease. Adopted from Hotamisligil, G.S. et al [86].

Mice studies suggest that during initial stages of obesity, UPR is an adaptive response. For example, a heterozygous deletion of GRP78, an upstream controller of ER stress response leads to an adaptive activation of CHOP and XBP1s proteins, better adipogenesis, increased energy expenditure and in turn protection from diet induced hepatic steatosis and insulin resistance particularly

in white adipose tissue [87]. Currently, the research community is persistently gaining deeper insights in contributions of ER stress pathway in the pathogenesis of metabolic syndrome. Table 1 summarizes involvement of some ER stress proteins in different metabolism related disorders.

Proteins involved	Related syndrome/ condition	Role of ER stress	References
XBP-1 and ASK1	Heart disorders	Cardiomyocytes gets degraded by ER stress due to ischemia. Myocardial infarction also induces ER stress	[88]
IRE1	Atherosclerosis	Excess cholesterol leads to ER stress in macrophages and also excess oxidized lipids induce ER stress in vascular cells and metabolic disturbances	[89]
XBP-1, JNK	Type 2 Diabetes	Obesity leads to ER stress which further causes insulin resistance and this diabetes	[90, 91]
CHOP (Pro-apoptotic protein)	Type 2 Diabetes	Free fatty acids like palmitic acid in beta cells leads to ER stress and causes diabetes via beta cell death	[92-95]
PERK, eIF2α	Type I diabetes (Wolcott Rallison syndrome)	PERK pathway is impaired in these individuals and leads to ER stress and subsequent development of diabetes	[96]
IRE1, ATF6 and PERK	Inflammation	UPR caused increased synthesis of inflammatory cytokines such as IL6, IL8 and CRP. Inflammation further leads to complications such as diabetes, atherosclerosis etc	[97-100]
NFκB- IKKβ	Leptin resistance/Obesity	ER stress causes impaired signaling. Homocysteine and high fat diet also cause ER Leptin resistance.	[85]

Table 1: ER stress proteins involved in various metabolism related disorders.

1.6 Adipocyte models used for studying adipose tissue function

Obesity research has advanced significantly during last few decades, primarily due to the availability of appropriate animal models, cell culture models and advanced protocols for culture and differentiation of adipocytes *in vitro*. Some of the commonly used adipocyte models are enlisted in table 2. Owing to its robust growth and proliferation potential, SGBS adipocytes is currently a widely used non-transformed primary human adipocyte model used for research [101]. Previous reports suggest that primary human subcutaneous adipocytes

and SGBS adipocytes have similar trends in differentiation and gene expression of PPAR γ and FABP4 [102], and recently it was found to possess a transient brown adipocyte like phenotype [103] which has increased research interest in SGBS adipocyte biology.

Cell line/model	Origin	Reference
Adipocytes from rodent models		
3T3-L1 adipocytes	Mouse 3T3-L1 fibroblasts	[104, 105]
3T3-F442A adipocytes	Mouse 3T3-L1 fibroblasts	[105]
Ob17 adipocytes	Epididymal fat pad of C57BL/6J ob/ob mouse	[106]
Adipocytes from human derived adipose depot		
Human or animal preadipocytes	Mature adipocytes from adipose tissue depot from humans or rats – also called ceiling culture	[107]
Simpson-Golabi Behmel Syndrome or SGBS adipocytes	3 month old infant suffering from SGBS	[101]

Table 2: Adipocyte models used for research.

1.7 FIT2: lipid storage promoting GWAS identified T2DM candidate

Adipose tissue expandability hypothesis emphasizes on healthy lipid storage inside lipid droplets in the form of TAGs. In East Asian population, meta-analysis found SNP (rs6017317) in FIT2-R2HDML-HNF4 α locus to be significantly associated with onset of T2DM (odds ratio =1.09 (1.07 – 1.12), P = 1.12E-11) [108]. FIT2 protein is an ER membrane associated lipid droplet protein actively involved in partitioning newly synthesized TAGs from ER to lipid droplets. Data from 3T3-L1 adipocytes and animal model indicate its role in maintaining adipose tissue function via TAG accumulation [48, 51]. Mice with adipose tissue specific FIT2 knockout are lipodystrophic and insulin intolerant accompanied by increased macrophage infiltration and inflammation.

Moreover, FIT2 overexpression in mice skeletal muscle (CFK2 mice) results in increased lipid droplets in muscle tissue, reduced body weight, fat mass and lean mass at 6 weeks of age along with increased oxygen consumption, glucose excursion rate, energy expenditure and complete protection from diet induced obesity [52]. These observations suggest a rather vital role of FIT2 mediated lipid storage in adipose tissue and make it an interesting target for obesity research.

1.8 FTO: mitochondrial function prompting GWAS identified obesity candidate

Response to “obesigenic” environment such as life style and diet varies in individual, often influenced by genetic components. Twin studies in monozygotic and dizygotic twins show greater inter-pair than an intra-pair alteration in weight loss, suggesting adiposity as a highly heritable trait with the estimated genetic contribution up to 40 – 70% of the difference in weight gain [109, 110]. Recognition of possible genetic influence on obesity has led to a search for causal genes which might assist us in containing obesity epidemic. Currently, 76 and 185 loci have been linked to T2DM and obesity respectively, with 17 overlapping loci among them (figure 11), FTO being the strongest association with obesity. SNPs in the first intron of FTO (Fat Mass and Obesity Associated) gene were strongly associated with obesity and T2DM [111, 112]. However, upon adjustment with BMI, association to T2DM was lost suggesting an indirect influence on T2DM, likely via obesity or increased BMI. Association of FTO SNPs with obesity has been validated across multiple ethnicities [113-115] and the presence of a minor risk allele leads to increase in BMI by 0.39 kg/m² [116]. In mice, FTO deletion leads to reduced body weight and protection

from diet induced obesity [117]. The leanness of FTO-deficient mice is implicated to increased energy expenditure and systemic sympathetic activation, despite decreased spontaneous locomotor activity and relative hyperphagia. Overall, these observations suggest FTO SNPs to be valid targets to studying human obesity.

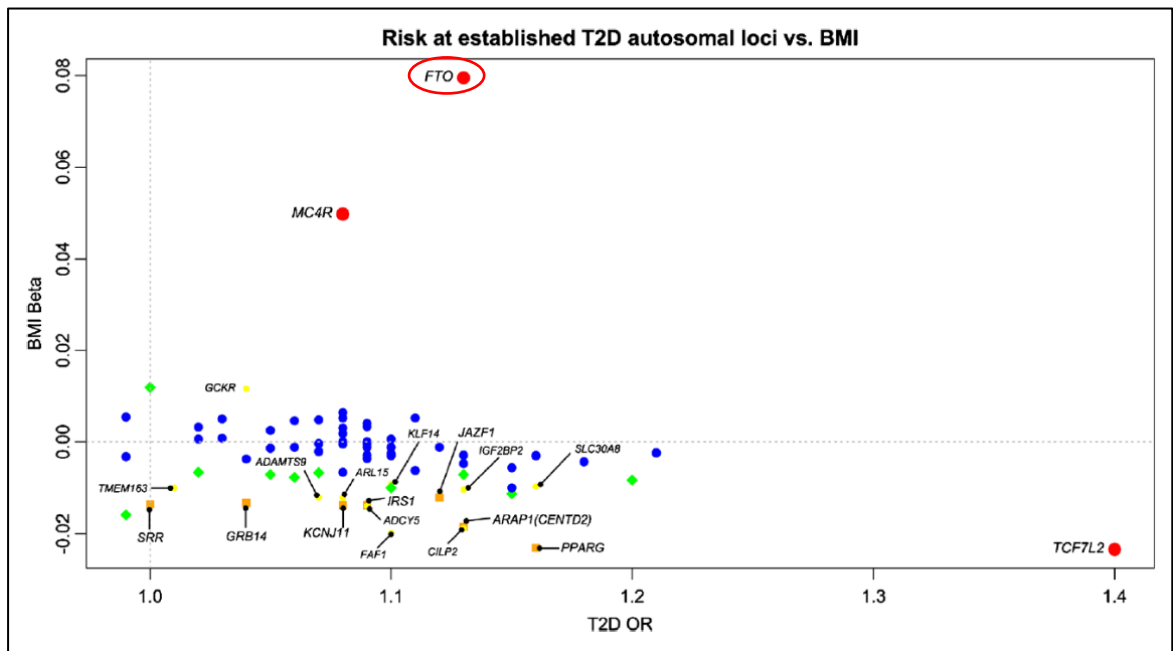


Figure 11: GWAS candidates overlapping between obesity and T2DM.

P value thresholds for association with BMI (y-axis) are $P < 5 \times 10^{-8}$ (red), $5 \times 10^{-8} \leq P < 10^{-4}$ (orange), $10^{-4} \leq P < 0.01$ (yellow), $0.01 \leq P < 0.05$ (green) and $P \geq 0.05$ (blue). Red, orange and yellow associations are labeled with corresponding gene names. Adopted from Karaderi et al, 2015 [118].

1.9 Aims and hypothesis of the study

In the studies presented here, we have leveraged on current knowledge on adipose tissue expandability hypothesis [3], with the aim of furthering insights into novel adipose tissue related mechanisms leading to the development of insulin resistance or T2DM.

In order to understand the biological role of specific GWAS genes of interest expressed in human adipose, we first sought to characterize human adipocyte cell models, to better understand the strengths and limitations of the SGBS human adipocyte cell line. SGBS adipocytes were derived from a child with an overgrowth syndrome [2, 5] and are widely used as a representative human adipocyte syndrome. Since isolation from SC adipose tissue depot from an infant, SGBS have been perceived and observed to have gene expression and adipogenic pattern similar to primary human adipocytes from adults. But recently SGBS were observed to retain a transient browning phenotype mid-way during their course of differentiation [6]. However, transcriptome and functional differences between SGBS and primary human subcutaneous adipocytes emphasizing on their unique phenotype have not been described yet and we have addressed this question here. We hypothesized that while there are overlapping phenotypic similarities, there would be distinct metabolic signatures involving adipogenesis, lipid metabolism, browning and mitochondrial capacity between the two cell types, understanding which would assist in their appropriate usage in our studies or other studies in future.

Following this, we used these adipocytes and investigated the role of two GWAS gene candidates expressed in adipose and associated with type 2 diabetes and obesity; FIT2 and FTO. Both these proteins are involved in lipid

metabolism in adipocytes. FIT2 is an ER membrane associated lipid droplet protein, responsible for transferring newly synthesized TAGs into lipid droplets and a GWAS gene candidate for T2DM among East Asian population [7]. Adipose tissue specific FIT2 protein knockout mice show a lipodystrophic phenotype with smaller adipose tissue depots accompanied by peripheral insulin resistance [8]. The Role of FIT2 protein in human derived adipocytes or adipose tissue is not established yet, and we used subcutaneous adipocytes to study FIT2 protein biology. We hypothesized that Partial deficiency of FIT2 protein would lead to reduced triglyceride storage, accumulation of free fatty acids and defective insulin signalling in the adipocytes.

In contrast to lipid storage function of FIT2 protein, data from human adipocytes and animal models suggest a role of FTO protein in regulating energy expenditure through central and peripheral mechanisms [9-11]. Along with FTO protein knockdown, we tested the effects of a novel chemical inhibitor of dioxygenase activity of FTO protein in SGBS adipocytes [12]. We hypothesized that chemical inhibition of FTO protein would mimic increase in mitochondrial energy expenditure as observed after FTO protein knockdown in SGBS adipocytes [13] and thus may potentially be developed as an anti-obesity drug. Since FTO protein influences mitochondrial energy expenditure and SGBS adipocytes showed higher mitochondrial oxidative capacity in our initial experiments, SGBS were initially used for studies related to FTO protein.

Next chapter focusses on studying transcriptomic signatures different amongst obese diabetics and obese non-diabetics. We aimed to identify adipose tissue components preventing the development of insulin resistance in obese non-diabetics. Contributions of ECM components in obesity and inflammation

associated adipose tissue dysfunction has been suggested widely [14], but differences amongst obese diabetics and obese non-diabetics are not fully understood. We compared transcriptomes of subcutaneous and omental adipose tissue from obese diabetics and obese non-diabetics to address the question whether ECM components are involved in adipose tissue dysfunction in obese diabetics.

1.9.1 Specific objectives were to:

1. Evaluate the differences among SGBS and primary human adipocytes differentiated from stromal vascular fraction from subcutaneous adipose tissue. We sought to explore their
 - a. Transcriptome differences using RNA sequencing.
 - b. Adipogenic capacity using real-time qPCR.
 - c. Mitochondrial function or energy expenditure using Seahorse mitochondrial flux analyzer.
 - d. Brown and beige adipocyte markers using real-time qPCR and UCP1 protein expression by western blot.
 - e. Triglyceride storage and glucose uptake.
2. Characterize the role of FIT2 protein in regulating lipid storage and maintaining adipocyte health. We studied:
 - a. mRNA and protein expression pattern in human adipose tissue from obese diabetics compared to obese non-diabetics.
 - b. mRNA and protein expression pattern in subcutaneous and omental adipocytes derived from adipose tissue.
 - c. Adipocyte phenotype in the context of triglyceride accumulation, inflammation, ER stress and insulin signaling

- after siRNA mediated FIT2 protein knockdown and addition of palmitic acid to the mimic high fat challenge.
3. Examine the effects of chemical inhibition of FTO demethylase activity in SGBS adipocytes when compared to SGBS with siRNA mediated FTO knockdown. We investigated the phenotype as:
 - a. PGC1 α and UCP1 gene expression pattern using real-time qPCR.
 - b. Mitochondrial respiration capacity using Seahorse mitochondrial flux analyzer.
 - c. AMPK pathway using western blot.
 4. Analyze transcriptome wide differences among subcutaneous and omental adipose tissue derived from obese diabetics compared to obese non-diabetics. We studied:
 - a. The Number of differentially up and downregulated genes.
 - b. Enriched biological pathways and cellular components (gene ontology) in omental compared to the subcutaneous depot.
 - c. Enriched biological pathways and cellular components (gene ontology) in T2DM compared to NT2DM subjects.
 - d. Positive and negative enrichment in extracellular matrix and fibrosis genes in T2DM compared to NT2DM subjects.

Chapter 2:

General Materials and Methods

2.1 Procedure for RNA isolation

Qiagen RNeasy plus kit was used for RNA isolation from both adipocytes or other adherent cells and adipose tissue.

2.1.1 Protocol for RNA isolation from adipocytes and other adherent cells

1. Cell-culture medium was aspirated completely and cells were lysed directly in the cell-culture vessel by adding 350 μ l of buffer RLT. The lysate was homogenized with the help of a cell scraper and collected in a microfuge tube.
2. The tube was vortexed for about a minute to ensure no cellular clumps were remaining and the lysate was passed through QIAshredder homogenizer (spin at maximum rpm for 2 min) placed in 2 ml collection tube.
3. Flow-through was added to gDNA (genomic DNA) removal columns and centrifuged at maximum rpm for one minute.
4. One volume of 70% ethanol was added to the flow-through and mixed with a pipet or by vortexing.
5. Finally, a maximum of 700 μ l of lysate mixed with ethanol was added to RNeasy spin column placed in a 2 ml collection tube. Tube was centrifuged at 10,000 rpm for 30 sec and flow-through was discarded. Any remaining lysate from step 4 can be added to RNeasy spin column again with repeated centrifugation to collect all RNA in RNeasy spin column.
6. 700 μ l Buffer RW1 was added to the RNeasy spin column and centrifuged at 10,000 rpm for 15 sec to wash the spin column membrane. Flow-through was discarded.

7. 500 μ l Buffer RPE was added to the RNeasy spin column and centrifuged at 10,000 rpm for 15 sec and flow-through was discarded. The column was washed with RPE buffer again with centrifugation for 2 min. Care was taken that no ethanol was carried over in column during washing and discarding processes.
8. RNeasy spin column was transferred to a new 1.5 ml collection tube and 30-50 μ l of nuclease free water (depending on expected yield) was added directly onto column for RNA elution. The column was centrifuged at 10,000 rpm for 2 min to ensure complete elution. If lower yields were expected, the eluate was added to column and centrifugation step was repeated.
9. The RNeasy spin column was discarded and RNA was quantified using NanoDrop spectrophotometer (Thermo Scientific)

2.1.2 Protocol for RNA isolation from adipose tissue samples

1. Frozen adipose tissue samples (about 250 mg) were used for homogenization using Qiagen TissueLyser LT. Samples were added directly into TissueLyser homogenization tubes with 500 μ l TRIzol reagent (Thermo Scientific) and homogenized at 50 hertz for 10 min or until no tissue clumps were observed.
2. Tubes were kept at room temperature for 5 min and 300 μ l of chloroform was added to tubes and mixed by shaking for 15-20 sec. Tubes were incubated at room temperature for 5 min and centrifuged at 15,000 rpm for 20 min at 4°C. The clear upper layer containing RNA was transferred to new 1.5 ml microfuge tube and an equal volume of 70% ethanol was added and mixed by vortexing.

3. This mixture was processed downstream similar to cell culture RNA (step 5 onwards).

2.2 Relative quantification of gene expression

2.2.1 cDNA synthesis protocol

Isolated RNA was converted to cDNA with the help of High-Capacity cDNA Reverse Transcription Kit (Thermo Scientific). 500-1000 ng of RNA was made to a final volume of 10 μ l with nuclease free water and was added to 10 μ l master mix prepared from individual components as

Component	Volume/Reaction (μ l) per reaction
10 \times RT Buffer	2.0
25 \times dNTP Mix (100 mM)	0.8
10 \times RT Random Primers	2.0
MultiScribe™ Reverse Transcriptase	1.0
Nuclease-free water	4.2
Total per Reaction	10

Table 3: Preparation of master mix for cDNA synthesis.

Final reaction mixtures were converted to cDNA using following cycling conditions

	Step 1	Step 2	Step 3	Step 4
Temperature ($^{\circ}$C)	25	37	85	4
Time	10 min	120 min	5 min	∞

Table 4: Cycling conditions for cDNA synthesis.

2.2.2 Real-time qPCR protocol

For qPCR, primers were designed using Primer Express 3.0 (Thermo Scientific) and QuantiFast SYBR Green PCR Kit (Qiagen) was used to prepare reaction mix as follows

Component	Volume/reaction (384 well block)	Final concentration
2X QuantiFast SYBR Green PCR Master Mix	5 µl	1X
Forward Primer	0.1 µl	1 µM
Reverse Primer	0.1 µl	1 µM
Template cDNA	2 µl	15ng per reaction
RNase-free water	2.8 µl	
Total reaction volume	10 µl	

Table 5: Preparation of master mix for qPCR reaction for gene expression.

384 well plate was used in ViiA™ 7 Real-Time PCR System (Thermo Scientific) with below mentioned protocol.

Step	Time	Temperature
PCR initial activation step	5 min	95°C
Two-step cycling		
Denaturation	10 sec	95°C
Combined annealing/ extension	30 sec	60°C
Number of cycles	40	

Table 6: Cycling conditions for qPCR reaction for gene expression.

Threshold cycle (Ct) values were obtained and $\Delta \Delta C_t$ method was used to calculate relative expression using GAPDH as internal control throughout.

2.2.3 Protocol for isolation of genomic DNA and relative quantification of mitochondrial DNA content

Genomic DNA was isolated using traditional phenol: chloroform method.

1. Cell culture medium was completely removed, the monolayer was washed with 1X ice cold PBS and 500 µl of DNA extraction buffer (0.1 M NaCl, 10 mM Tris pH 8.0, 1 mM EDTA pH 8.0, 1% SDS) was added. With freshly added Proteinase K (0.2 µg/µl).
2. Monolayers were scrapped and contents collected in microfuge tubes and incubated at 50°C overnight. One volume of Phenol Chloroform

Iso-amyl alcohol (PCI, Sigma) was added to the digested sample and tubes were shaken vigorously for 10-15 sec.

3. Tubes were centrifuged at 15,000 rpm for 10 min and the upper layer was carefully transferred to new microfuge tubes.
4. 500 μ l (or equal to DNA extraction buffer used) of chloroform was added and tubes were shaken vigorously for 10 min. Tubes were centrifuged at 15,000 rpm for 10 min and upper aqueous phase and transferred to new tube.
5. 1/10th volume of sodium acetate (3 M, Sigma) and two volumes of 100% ethanol was added, vortexed and incubated overnight at -20°C.
6. Tubes were centrifuged at 15,000 rpm for 10 min and supernatant was discarded. DNA pellet was usually visible at this stage.
7. Pellet was washed with 70% ethanol and centrifuged at 15,000 rpm for 10 min. Supernatant was carefully removed with help of a pipet and pellet was allowed to air dry for 10-15 min till pellet was translucent.
8. The pellet was dissolved in 20-30 μ l nuclease free water, quantified using NanoDrop spectrophotometer and stored at -20°C till further analysis.

2.2.4 Relative quantification of mitochondrial DNA content

Protocol was adopted from [119] and used with DNA extracted from adipocytes. 2 ng of total DNA was used for running qPCR with below mentioned reaction setup.

Component	Volume/reaction (384 well block)	Final concentration
TaqMan Universal PCR	5 μ l	1X
Forward Primer	0.05 μ l	500 nM
Reverse Primer	0.05 μ l	500 nM
TaqMan probe	0.02 μ l	200 nM
Template cDNA	2 μ l	2 ng per reaction
RNase-free water	2.88 μ l	
Total reaction volume	10 μ l	

Table 7: Preparation of master mix for quantification of mitochondrial DNA content.

Step	Time	Temperature
uracil-N-glycosylase (UNG) activation	2 min	50°C
PCR initial activation step	10 min	95°C
Two-step cycling		
Denaturation	15 s	95°C
Combined annealing/ extension	60 s	60°C
Number of cycles	40	

Table 8: Cycling conditions for quantification of mitochondrial DNA.

2.3 Western blot protocol

2.3.1 Preparation of protein lysate from adherent cells

1. Adipocytes or other adherent cells were grown in 6 well plates and used for protein lysate preparation for protein studies.
2. All plates were removed from incubator and immediately placed on ice. Cell culture medium was removed from wells and were thoroughly washed with ice cold PBS. 100 μ l of RIPA buffer (Thermo Scientific) supplemented with protease and phosphatase inhibitor cocktail (Halt™ Protease and Phosphatase Inhibitor Cocktail, Thermo Scientific) was used to digest cell membrane and prepare cell lysate.

3. All contents of the well were pooled with help of a cell scrapper and transferred to a new microfuge tubes prechilled on ice. Lysates were incubated here for about 45 min with vortexing every ten min.
4. Finally, the tubes were centrifuged at 15,000 rpm for 30 min at 4°C and clear supernatants were collected in new microfuge tubes and quantified using Bradford protein assay.

2.3.2 Preparation of protein lysates from adipose tissue

1. Frozen adipose tissue samples (about 100 mg) were used for homogenization using Qiagen TissueLyser LT. Samples were added directly into TissueLyser homogenization tubes with 600 µl RIPA buffer (Thermo Scientific) supplemented with protease and phosphatase inhibitor cocktail (Halt™ Protease and Phosphatase Inhibitor Cocktail, Thermo Scientific) and homogenized at 50 hertz for 10 min or until no tissue clumps were observed.
2. Homogenate was centrifuged at 15,000 rpm at 4°C for 45 min. Typically, three layers are formed which includes debris at bottom, protein lysates in middle and deep yellow colored oily layer on the top. Red to beige colored middle layer containing protein lysate was carefully transferred to a new 1.5 ml microfuge tube and centrifuged at 15,000 rpm at 4°C for 15 min and subsequently transferred to new tubes to remove excess lipids.
3. Lysates were then snap frozen-thawed for 5 times with help of liquid nitrogen and protein quantification was done using Bradford protein assay.

2.3.3 Protein quantification using Bradford protein assay

Bradford protein assay was performed in 96 well plates.

1. Standard curve was made using 10 concentrations of BSA (Bio-Rad, 2 mg/ml) ranging from 0.05 mg/ml to 0.5 mg/ml in distilled water. Final volume was made to 10 μ l for all.
2. Cell culture protein lysates were then diluted either 10-20 times with distilled water depending on expected yield. Adipose tissue protein lysates were diluted 50-100 times with distilled water.
3. 10 μ l of each standard and unknown protein lysate was pipetted in 96 well plate compatible with plate reader and 200 μ l of diluted Bradford reagent was added to the wells. Bradford reagent was bought from Bio-Rad as 4X concentrate and it was diluted to 1X, allowed to warm to room temperature and filter with 0.22 μ m filter to remove any debris as it might interfere with optical density (OD).
4. Plate was shaken carefully and incubated at room temperature for 5-10 min (not more than 1 h) and read at 595nm in plate reader (VarioSkan from Thermo Scientific). OD obtained was used to draw standard graph and calculate concentration of protein lysates.

2.3.4 Protocol for SDS Polyacrylamide Gel Electrophoresis (SDS-PAGE)

2.3.4.1 Stock buffers and reagents

1. 4X loading buffer (Laemmli buffer, Bio-Rad).
2. 10X Tris-glycine SDS running buffer (Bio-Rad): To prepare 1L 1X running buffer: add 100 ml 10X running buffer to 900 ml distilled H₂O.

3. 10X Tris-glycine transfer buffer (Bio-Rad): To prepare 1L 1X transfer buffer: add 100 ml 10X transfer buffer to 200 ml methanol + 700 ml distilled H₂O.
4. 10X Tris buffered saline (TBS) (Bio-Rad): To prepare 1L 1X TBS: add 100 ml 10X TBS to 900 ml distilled H₂O.
5. Nonfat dry milk
6. Bovine Serum Albumin (BSA, Sigma)
7. Beta-mercaptoethanol (Bio-Rad)

2.3.4.2 Working buffers and solutions

1. Wash buffer: 1X TBST (1L of TBS + 1 ml Tween-20)
2. Blocking buffer: 1X TBST with 5% w/v nonfat dry milk
3. Primary antibody dilution buffer: 1X TBST with 5% BSA or 5% nonfat dry milk as indicated on primary antibody datasheet

2.3.4.3 Other materials

1. Prestained protein marker: Prism ultra-protein ladder (10-245 kDa) (Abcam)
2. Blotting membrane and filter paper (Bio-Rad)
3. Secondary antibody conjugated to HRP: anti-rabbit and anti-mouse (Bio-Rad)
4. Detection reagent: Luminata crescendo western HRP substrate (Merck Millipore)
5. X-ray film: X-ray film for western blot detection (Thermo Scientific)

2.3.4.4 Electrophoresis

1. 10% acrylamide gels were used for all proteins in our studies unless indicated.
2. All protein samples were made to closest equal volumes with distilled water and one-third volume of 4X laemmli sample buffer (supplemented with beta-mercaptoethanol) was added, vortexed gently to mix and boiled in water bath for 5 min.
3. Samples were loaded in the gel and run till the dye front migrates about 2mm from the bottom of the gel. Gels were then transferred to PVDF membrane.

2.3.4.5 Transfer

1. PVDF membrane was immersed in methanol for 2-3 min and then transferred to ice cold transfer buffer along with filter papers and transfer sponges. Gel was arranged in the following order and a clean plastic tube was used to roll air bubbles out (crucial step).
2. Setup was organized in the cassette and transfer was carried for 2 h at 100V (Bio-Rad apparatus)

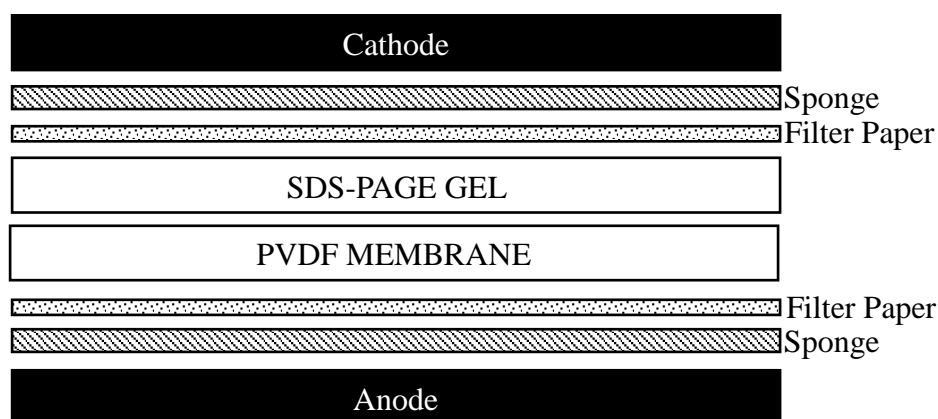


Figure 12: Arrangement of PVDF membrane and SDS-PAGE gel during transfer.

2.3.4.6 Immunoblotting

1. After transfer, membranes were blocked with 5% milk in TBST (blocking buffer) for 45 min and then washed with TBST for 45 min with three buffer changes.
2. Membranes were either cut or incubated with primary antibody overnight in 5% BSA or 5% milk as suggested by the protocol. They were then washed with TBST (15 min X 3 times) and incubated with respective secondary antibody in 5% milk in TBST for 2 h and washed again with TBST (15 min X 3 times).
3. Blots were then incubated with HRP substrate for 5 min, excess substrate was drained and blots were packed in plastic sheets.
4. X-ray films were exposed on the membrane and developed in dark room using x-ray film developer (Konica Minolta).

2.4 Protocols for cell culture

2.4.1 Isolation, culture and differentiation of adipocytes

We have used two different adipocyte models in our study. (1) Human adipose tissue derived adipocytes and (2) Simpson-Golabi-Behmel syndrome (SGBS) adipocytes. Both are obtained as preadipocytes and differentiated to mature adipocytes using specific medium.

2.4.1.1 Protocol for tissue digestion

1. The tissue sample was immediately immersed in Hank's Balanced Salt Solution (HBSS, Thermo Scientific) and transferred to lab.

2. Digestion medium (1 mg/ml collagenase in 2% BSA in DMEM) was prepared fresh and filtered. Tissue specimens were then transferred to digestion medium (10 ml digestion medium/gram tissue).
3. Using scissors, tissue was cut into small pieces (as long as no specimens can be picked up by the scissors, the tissues are considered apt for digestion).
4. Tubes were incubated at 37°C for one hour for collagenase digestion and then filtered through 100µm cell strainer.
5. Filtrate was then Centrifuge at 400g for 1 minute. Two layers were obtained after this. Top lipid rich fraction containing mature adipocytes was used as ceiling culture if required. Infranatant was centrifuged at 400g for 5min after which the pellet of stromal vascular fraction (SVF) was obtained (usually SVF contains ASC, fibroblasts, vascular endothelial cells and some immune cells).
6. Pellet was resuspended in 10 ml HBSS and Centrifuged at 400g for 5 min. The step was repeated 3 times with change to a new tube after resuspending the pellet to avoid oily layer sticking to sides of the tube.

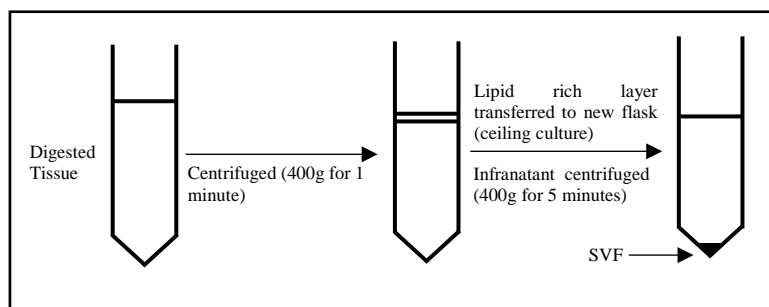


Figure 13: Isolation of ASCs from adipose tissue digest.

7. Pellet was resuspended in 10 ml growth medium (DMEM high glucose, 15% fetal bovine serum (FBS), 1% non-essential amino acids (NEAA), 1% penicillin-streptomycin (pen-strep) and 5 ng/ml fibroblast growth

factor) plated in bacterial dish and incubated in 37°C incubator for 1 h. This step allows monocytes and macrophages to attach to bacterial plate and gives purer ASC population.

8. The supernatant was carefully transferred (red blood cells also float in the medium) to the new T75 flask with growth medium. At this stage, cells have small circular morphology which changes to fibroblastic once they become adherent and grow. Medium was replaced with new growth medium once most of the cells were adhering to the flask.
9. Cells adhering as fibroblasts are typically adipocyte specific stem cells, which undergo differentiation to preadipocytes at confluence and can be differentiated to mature adipocytes.

2.4.1.2 Differentiation of primary adipocytes derived from adipose tissue

1. Differentiation medium (Preadipocyte basal medium 2, PBM-2) was purchased from Lonza and their recommended protocol was followed.
2. Typically, Differentiation medium was reconstituted from individual components (Preadipocyte growth medium -2 bulletkit, PGM-2) and used within 2 weeks. Both PBM-2 and PGM-2 are proprietary of Lonza and concentration of individual components is unknown although it is acknowledged that final reconstituted medium contains FBS, L-glutamine, GA-1000, human insulin, dexamethasone, 3-Isobutyl-1-methylxanthine (IBMX) and indomethacin.

2.4.2 SGBS cell culture and differentiation

1. SGBS cells were grown and multiplied in their growth medium (DMEM-F12 (Thermo Scientific), 10% FBS and 1% pen-strep).

- Once they were ready for differentiation, cells were incubated in differentiation medium for 4 days and then maintenance medium for another 4 to 6 days till they were fully mature or differentiated (as judged by lipid accumulation). Protocol was followed as published [120].

Component	Differentiation	Maintenance
Rosiglitazone (Sigma)	2 μ M	Not added
Dexamethasone	25 nM	
IBMX	0.5 mM	
Cortisol	0.1 μ M	0.1 μ M
Transferrin	0.01 mg/ml	0.01 mg/ml
Triiodothyronine	0.2 nM	0.2 nM
Human insulin	20 nM	20 nM

Table 9: Differentiation and maintenance medium for SGBS adipocytes.

2.4.3 Preparation of BSA: palmitic acid conjugate

Fatty acids are not soluble in water and thus have to be conjugated to BSA for addition in cell culture. Protocol was adapted from [121] and final concentration of palmitic acid obtained was 10 mM.

- 20% fatty acid free BSA (Sigma) was prepared by adding 2 g of BSA to 8 ml distilled water and made to 10 ml final volume once BSA is fully solubilized. Typically, overnight incubation results in maximum solubility.
- 56 mg sodium palmitate (Sigma) was added to 10 ml of 0.01 N NaOH (sodium hydroxide) and incubated at 70°C water bath. Palmitic acid gets partially dissolved at this stage. Maintaining in water bath, 200 μ L of 1N NaOH was added to above solution which results in clear fully dissolved palmitic acid.
- Finally, 10 ml of solubilized palmitate was added to 8 ml of 20% BSA outside the water bath (BSA will precipitate if subjected to 70°C) which

gives a clear solution of palmitic acid conjugated to BSA. The solution was cooled down to room temperature and filtered using 0.22 μm filter, aliquoted and stored at -20°C . Precipitation at room temperature would indicate improper conjugation of palmitic acid with BSA. Palmitic acid was used within 6 months.

2.4.4 Treatment with palmitic acid and insulin stimulation in cell culture

Free fatty acid challenge was performed in mature adipocytes (at day 8 or day 9 of differentiation). Differentiation medium was replaced with respective growth medium for 24 h after which medium was changed to DMEM supplemented with 2% FBS and 1% pen-strep. Using lower percentage FBS medium is suggested as (1) conjugated palmitic acid also introduces protein in form of BSA (2) effect of palmitic acid is partially masked by presence of 10% FBS and (3) FBS also contains free fatty acids which might interfere with externally added palmitic acid. Cells were then treated with 500 μM palmitic acid for 24 h and subsequently medium was replaced with serum free DMEM for 2-3 h for serum starvation. 100nm insulin was added in respective wells for 30 min before any further studies.

2.4.5 Protocol for quantification of triglyceride accumulation

Triglyceride accumulation was read fluorometrically after staining neutral lipids with Nile Red dye. Protocol was followed as recommended (AdipoRed Assay Reagent, Lonza). Assay was performed in 6 well cell culture plates.

1. Medium in adipocyte culture was removed and cells were washed with PBS. Next, 2 ml of fresh PBS was added in wells followed by 140 μl of assay reagent. Plates were swirled and contents were mixed gently.

2. Volume in each well was made up to 5 ml with help of PBS and incubated in dark for 30 min at room temperature.
3. Plate reader (Varioscan, Thermo Scientific) was set as excitation at 485 nm and emission at 572 nm and plates were read.
4. Results were reported as fluorescence units.

2.5 Protocol for knock-down of proteins using siRNA

In our studies, we used siRNA against FIT2 and FTO in primary human adipocytes obtained from adipose tissue and SGBS. Protocol was adapted from datasheets and optimized to our cell culture conditions and adipocyte requirements.

1. Adipocytes (primary human or SGBS) were seeded at about 60% confluence. At about 80% confluence, siRNA was introduced in them with the help of siTran 1.0 (OriGene, USA) transfection reagent. FIT2 and FTO siRNA were purchased from Qiagen and OriGene respectively along with their scrambled negative control siRNAs. Transfection cocktail was optimized as

Components	Volume in μL per well
Opti-MEM (Thermo Scientific)	120
siRNA (5 μM stock)	2
siTran reagent	4.5
Final volume added per well	120 for 5 nm concentration siRNA

Table 10: Preparation of transfection cocktail for introduction of siRNA.

2. On the day of transfection, growth medium was replaced by serum free, pen-strep free DMEM and transfection cocktail was introduced for 6 h after which medium was replaced by growth medium.

3. Cells were allowed to grow for next 24 h till they reach 90-100 confluence and then growth medium was replaced by differentiation medium. After 4 days, the transfection was repeated in serum free, pen-strep free medium and finally replaced by differentiation medium.
4. On day 6 or 7 of differentiation, cells were ready for further studies which included addition of FTO inhibitors or palmitic acid for respective studies.

2.6 Protocol for radioactive glucose uptake assay

Glucose uptake assay is an essential tool to study insulin sensitivity or insulin resistance at a functional level. We used mature adipocytes to study glucose uptake in various conditions. Each condition was tested as 2 biological replicates with each of them having 3 experimental and 2 technical replicates.

Protocol for a 6 well plate is as follows

1. Medium for cells was replaced with serum free DMEM supplemented with pen-strep and 0.2% BSA for 4-5 h to allow them to undergo a serum free stepdown.
2. Next, cells were thoroughly washed twice with PBS and subsequently 900 μ l of PBS supplemented with 0.2% BSA was added to wells (1 ml for 6 well plate) for 30 min (glucose free stepdown).

Component	Stock concentration	Volume (in μl) to be added per well
Deoxyglucose	10 mM	10
[³ H]2-deoxyglucose	1 mCi (millicurie)	0.5
PBS (with 0.2%)	10X	90

Table 11: Preparation of start solution for glucose uptake assay.

3. Next, 100 μ l of 10X start solution was added to all the wells. Composition of start solution is elaborated in table 11.
4. Cells were allowed to uptake radioactive glucose for 20 min after which they were immediately placed on ice and maintained.
5. Cells were washed twice with ice cold PBS and finally 500 μ l of RIPA buffer was added to all the wells and contents were collected in prechilled microfuge tubes with the help of a scrapper.
6. Tubes were incubated in ice for 30 min after which 200 μ l of each of the lysate was added to 3.5 ml of Liquid Scintillation Cocktail (PerkinElmer) placed in 4 ml vials for measuring radioactivity. Each tube was prepared in technical duplicates at this stage. All the vials were capped tightly and mixed by inverting 4-5 times. Beta counts were measured as counts per minute using MicroBeta2 counter (PerkinElmer).

2.7 Protocol for RNA sequencing

RNA-SEQ was used to study transcriptome wide differences within following groups of interest. (1) Obese diabetics compared to obese non-diabetics (omental vs subcutaneous adipose tissue) and (2) SGBS compared to primary human subcutaneous adipocytes. Protocol used is as follows.

1. Total RNA was extracted from either primary human adipocytes, SGBS or adipose tissue for respective experiments. Poly-A mRNA was then enriched with oligodT beads (Life Technologies) from approximately 5 μ g of total RNA. 100 ng of poly-A mRNA recovered was used to construct multiplexed strand-specific RNA-seq libraries as per

manufacturer's instruction (NEXTflex™ Rapid Directional RNA-SEQ Kit (dUTP-Based) v2).

2. Individual library quality was assessed with an Agilent 2100 Bioanalyzer and quantified with a QuBit 2.0 fluorometer before pooling for sequencing on a HiSeq 2000 (1x101 bp read). The pooled libraries were quantified using the KAPA quantification kit (KAPA Biosystems) prior to cluster formation. Fastq formatted reads were processed with Trimmomatic to remove adapter sequences and trim low quality bases (LEADING:3 TRAILING:3 SLIDINGWINDOW:4:15 MINLEN:36). Reads were aligned to the human genome (hg19) using Tophat version 2 (settings--no-coverage-search--library-type=fr-firststrand). Feature read counts were generated using htseq-count (Python package HTSeq default union-counting mode, strand=reverse).
3. Differential Expression analysis was performed using the edgeR package in both 'classic' and generalized linear model (glm) modes to contrast groups of interest. This generated a list of approximately 15,000 genes.
4. A false discovery rate (FDR) ≤ 0.05 and a fold change (FC) ≥ 1.5 were used to call significance in the input list of genes for further analysis.
5. iPathwayGuide (Advaita bioinformatics), a web-based pathway analysis tool was used to identify the top biological pathways and biological processes different among groups (significance pegged at $P \leq 0.05$, with Bonferroni correction) [122, 123]. iPathwayGuide uses two step approach to compute significantly different pathways; (1) over-representation of differentially expressed genes and (2) the perturbation

of that pathway computed by propagating the measured expression changes across the pathway topology. This allows both upregulated and downregulated genes to be input together while computing enriched pathways and processes.

6. We used DAVID [124, 125] for certain pathway analysis, especially for reporting enriched pathways in genes either upregulated or downregulated among groups.

2.8 Protocol for measuring mitochondrial function of adipocytes

XF Cell Mito Stress test kit (Seahorse Bioscience) was used to measure mitochondrial function in adipocytes in a 24 well plate format. Data were reported as pmoles of oxygen consumed per minute or oxygen consumption rate. Cellular respiration parameters calculated are basal respiration, ATP production, proton leak, maximal respiration and spare respiratory capacity. As suggested by the manufacturer, 5 replicates of control, treatment conditions and negative controls were used. Oligomycin inhibits ATP synthase (complex V) and the decrease in OCR following injection of oligomycin correlates to the mitochondrial respiration associated with cellular ATP production. Carbonyl cyanide-4 (trifluoromethoxy) phenylhydrazone (FCCP) is an uncoupling agent that collapses the proton gradient and disrupts the mitochondrial membrane potential. As a result, electron flow through the ETC is uninhibited and oxygen is maximally consumed by complex IV. The FCCP-stimulated OCR can then be used to calculate spare respiratory capacity, defined as the difference between maximal respiration and basal respiration. Spare respiratory capacity is a measure of the ability of the cell to respond to increased energy demand. The third injection is a mix of rotenone, a complex I inhibitor, and antimycin A,

a complex III inhibitor. This combination shuts down mitochondrial respiration and enables the calculation of non-mitochondrial respiration driven by processes outside the mitochondria. Detailed protocol can be found at manufacturer's website.

1. SGBS adipocyte were seeded (density of 40,000 cells per well) in a XF²⁴-well cell culture microplate and differentiated as per protocol mentioned before (2.4.2).
2. On day 6 of differentiation, FTO inhibitor CA (50 μ M and 100 μ M) or DMSO (2 μ l) were added in respective wells. DMSO served as a vehicle control for drug CA.
3. XF²⁴ sensor cartridge was put to 24 h hydration in CO₂ free incubator on day 7 by adding 1 ml of XF calibrant in each well of the utility plate and placing hydro-booster plate and sensor cartridge over it. All sensors must be submerged in calibrant fluid and cover lid should be placed in position.
4. On day 8, XF test medium was prepared by adding glucose, sodium pyruvate and L-glutamine to XF basal medium as suggested by the manufacturer. Cells were then washed twice with XF test medium and finally 475 μ l of XF test medium was added to all the wells. The plate was incubated in CO₂ free incubator at 37°C for 1 h.
5. During this incubation, sensor cartridges were removed from the incubator and it's respective wells were filled up with XF test medium containing oligomycin (2 μ M), FCCP (1 μ M) and Rotenone+antimycin A (1 μ M each).

6. Next, flux analyzer instrument (switched on from previous day to equilibrate at 37°C) was programmed for a particular experiment and run was finally executed by first calibrating it with sensor cartridge plate and finally replacing the utility plate with cell culture plate containing SGBS.
7. Readings were obtained as pmole of oxygen consumed per minute in various conditions and Seahorse Bioscience tools were used to compute individual components such as ATP production, proton leak etc.

Chapter 3:

Re-evaluating the use of SGBS adipocytes as a representative model of human adipocytes, by comparison with primary human subcutaneous adipocytes

3.1 Introduction

Primary human adipocytes are essential cell model for metabolic research, particularly for mechanistic studies requiring knockdown, overexpression and editing of specific RNAs or proteins. But, adipocyte precursors or preadipocytes isolated from human adipose tissue are limited by the ability to grow and differentiate after few passages [101]. In 2001, investigators isolated preadipocytes from an infant derived adipose tissue [101] which could grow up to 50 passages while maintaining growth and differentiation capacity. SGBS adipocytes were derived from a 3 year old infant suffering from Simpson Golabi Behmel syndrome or SGBS. Since isolation, they have been widely distributed around the world and reported as a representative adipocyte model for primary human adipocytes. SGBS syndrome was first described in 1975 and is a rare X-linked recessive disorder characterized by pre- and post-natal overgrowth (visceral and skeletal abnormalities). The majority of the SGBS patients are type 1, triggered by deletions or point mutations in glypican 3 (GPC3) gene. A loss-of-function mutation in GPC3 gene is thought to inhibit Hedgehog signaling [126-130]. Type 2 SGBS is a more severe variant due to mutations in oral-facial-digital syndrome (OFD1) gene. As a result of these mutations, there is unregulated growth of many neonatal tissues, including mesenchyme and progenitors of adipose tissue. However, a GPC3 defect was not described in the formative paper [101] and the precise mutation in the SGBS adipocytes has not yet been characterized.

Previous reports suggest that primary human subcutaneous adipocytes and SGBS adipocytes have similar trends in the expression of FABP4 and PPAR γ mRNA as well as secretion of FABP4 during differentiation [102]. Another

study comparing SGBS adipocytes with primary human omental adipocytes derived from obese and non-obese individuals found similarity in morphology, induction of adipocyte-specific gene expression and GAPDH activity [131]. Although adult human adipose tissue and adipocytes have a minimal UCP1 expression, SGBS adipocytes have been shown to possess nominal browning capacity in a study [132, 133]. Additionally, SGBS adipocytes were recently reported to display a rather versatile, inducible browning phenotype, with transient expression of UCP1 and PPAR γ peaking at day 14 and declining by day 28 during differentiation [103]. But, inherent differences between metabolic profiles of SGBS adipocytes and primary human adipocytes remain inconclusive. Therefore, we hypothesized that while there are overlapping similarities; distinct metabolic and adipogenic signatures exist between SGBS and primary human adipocytes, understanding which will contribute to the knowledge and appropriate usage of relevant cell culture model in future metabolic research.

3.2 Materials and methods

3.2.1 Subject recruitment and cell culture

All subjects recruited were patients at the National University Health System (NUHS, Singapore) undergoing bariatric surgery and had body mass index (BMI) ≥ 35 kg/m². Nature, purpose and risks involved in the study were explained to subjects and written consent was obtained. Ethics approval was directed by the National Healthcare Group Domain Specific Review Board (reference number 2014/00396). Adipose tissue samples were obtained from the abdominal region during the surgery and primary human subcutaneous (SC)

preadipocytes (n=4 donors) were isolated by collagenase digestion. SGBS adipocytes were a kind donation from Dr. David Silver, DUKE-NUS, Singapore. Isolation, growth and differentiation of primary human adipocytes and SGBS adipocytes are discussed in section 2.4.

3.2.2 RNAseq experiment and analysis

Total RNA was extracted from SGBS (n=2) and SC control adipocytes (n=4) using Qiagen RNeasy plus mini kit (section 2.1.1). Protocol for RNA sequencing is described in section 2.7. Figure 14 represents work flow for RNA-SEQ data analysis. We used two different methods for enrichment analysis of gene ontologies and KEGG biological pathways. “R” package was used to generate heatmap and clustering genes. GSEA (Gene Set Enrichment Analysis, Broad Institute) [134] and enrichment map creator (Cytoscape Plugin) [135] was used to analyze enriched gene ontologies and visualize interactions between them. Gene Set Enrichment Analysis (GSEA) uses a ranking system to distribute FPKM values across all the samples and classify ontologies into positively and negatively enriched ontologies. KEGG biological pathway enrichment analysis was done using iPathwayGuide [122, 136]. Impact analysis used by iPathwayGuide provides a systems biology approach to pathway analysis. It takes into consideration the role, type, position, function and interactions of genes in each pathway and measures the impact by propagating the signals through the pathway topology. The advantage of this approach is that it not only avoids false positive results, but it also identifies truly significant pathways.

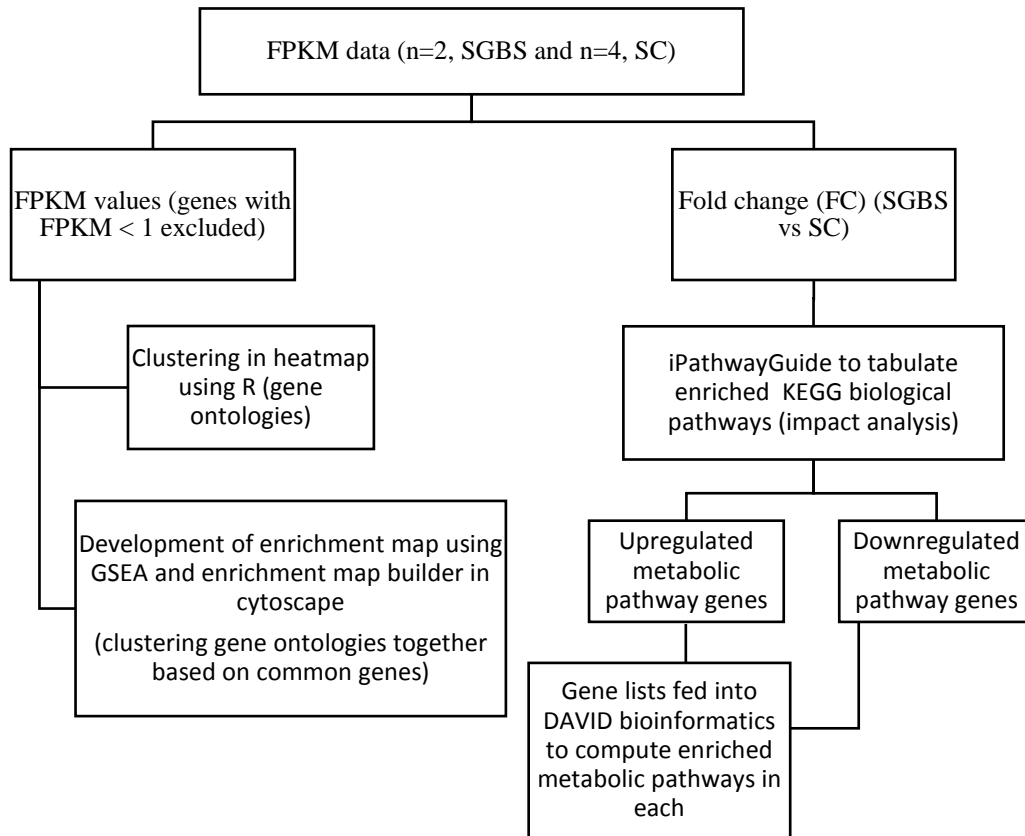


Figure 14: Work flow of RNA-SEQ data analysis for comparing SGBS versus SC control adipocytes.

FPKM values were used either in “R” package or enrichment map creator to visualize positively and negatively enriched gene ontologies including biological processes (BP), cellular components (CC) and molecular functions (MF). For tabulation of KEGG biological pathways, fold changes ($\log FC \geq \pm 0.5$, $FDR < 0.05$) were analyzed in iPathwayGuide and pathways enriched with the highest impact were enlisted. Metabolic pathway genes obtained from iPathwayGuide were further distributed as up and downregulated genes, and DAVID bioinformatics was used to compute enriched KEGG biological pathways in both sets of genes.

3.2.3 Real-time quantitative PCR and mitochondrial DNA content

Total RNA was isolated using Qiagen RNeasy plus kit and quantified using NanoDrop spectrophotometer. cDNA was synthesized from 800 ng of total RNA using ABI high capacity cDNA synthesis kit (Thermo Scientific) according to protocol described in section 2.2.1. Quantitative PCR reactions were setup and run according to protocol suggested (section 2.2.2). Genes involved in different pathways such as adipogenesis ($PPAR\gamma$, $PPAR\alpha$, $CEBP\alpha$,

adiponectin and leptin), lipid metabolism (FABP4, DGAT1, FTO, and FIT2), inflammation (IL18, IL1 β , NFK β 1, TLR4, and TNF α) and browning (UCP1, PRDM16, PGC1 α , and DIO2) were probed. ABI primer express 3.0 was used to design primer sequences. Mitochondrial DNA content in SGBS and SC controls was quantified as described in section 2.2.4.

3.2.4 Western blotting

Cell lysates were prepared using RIPA buffer (Thermo Scientific) supplemented with protease and phosphatase inhibitors. 30 μ g of total protein was separated using 10% acrylamide gel, transferred to PVDF membrane, blocked using 5% milk in TBS (with 0.1% Tween 20), and incubated overnight with UCP1 (Thermo Scientific) and GAPDH (Cell Signaling, MA, USA) antibodies at 4°C. Following this, blots were incubated with HRP-conjugated secondary antibody for 2 h and exposed using x-ray films. Detailed protocol in section 2.3.

3.2.5 Mitochondrial respiration analysis

Seahorse XF²⁴ Analyzer (Seahorse Biosciences, MA, USA) was used to measure mitochondrial respiration in adipocytes. Protocol described in section 2.8 was followed.

3.2.6 Lipid accumulation and radioactive glucose uptake assay

Adipocytes were washed with sterile PBS and stained with AdipoRed (Lonza) according to the manufacturer's protocol (section 2.4.5). After 30 min incubation, fluorescence was read at 485 nm excitation and emission at 572 nm. Protocol for insulin-stimulated glucose uptake assay was followed as described in section 2.6.

3.3 Results

3.3.1 Fully differentiated SGBS and SC adipocytes display distinct transcriptomic profiles

RNAseq analysis showed numerous differences in transcriptomes of SGBS and SC adipocytes. Red dots in volcano plot (figure 15) represent differentially expressed genes (inclusion was capped at $FC \geq \pm 0.6$, $FDR \leq 0.05$). 1667 genes were upregulated and 2050 genes were downregulated in SGBS adipocytes when compared to SC controls. Disease association between SGBS adipocyte transcriptome and SGBS syndrome was established by GPC3 ($FC = 0.181$, $FDR = 4.62E-06$) and OFD1 ($FC = 0.299$, $FDR = 0.00394$) genes.

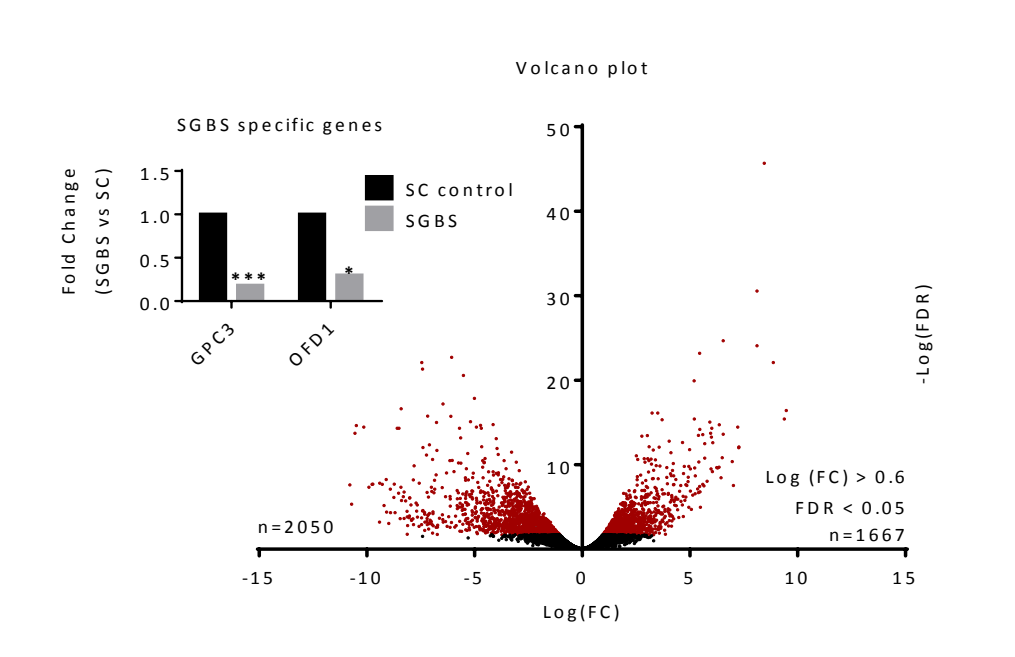


Figure 15: Global transcriptome profiling of SGBS and SC adipocytes (volcano plot).

Volcano plots displaying number of differentially expressed genes in SGBS adipocytes compared to SC adipocytes. Red dots denote statistically significant genes. Genes with $FDR < 0.05$ and $\log(FC) > 0.60$ were included. For the experiments involving SC adipocytes, experiments were performed in cells derived from 4 different donors (SC_1 to SC_4). For SGBS adipocytes, experiments were performed in duplicates (SGBS_1 and SGBS_2) from the same SGBS adipocyte.

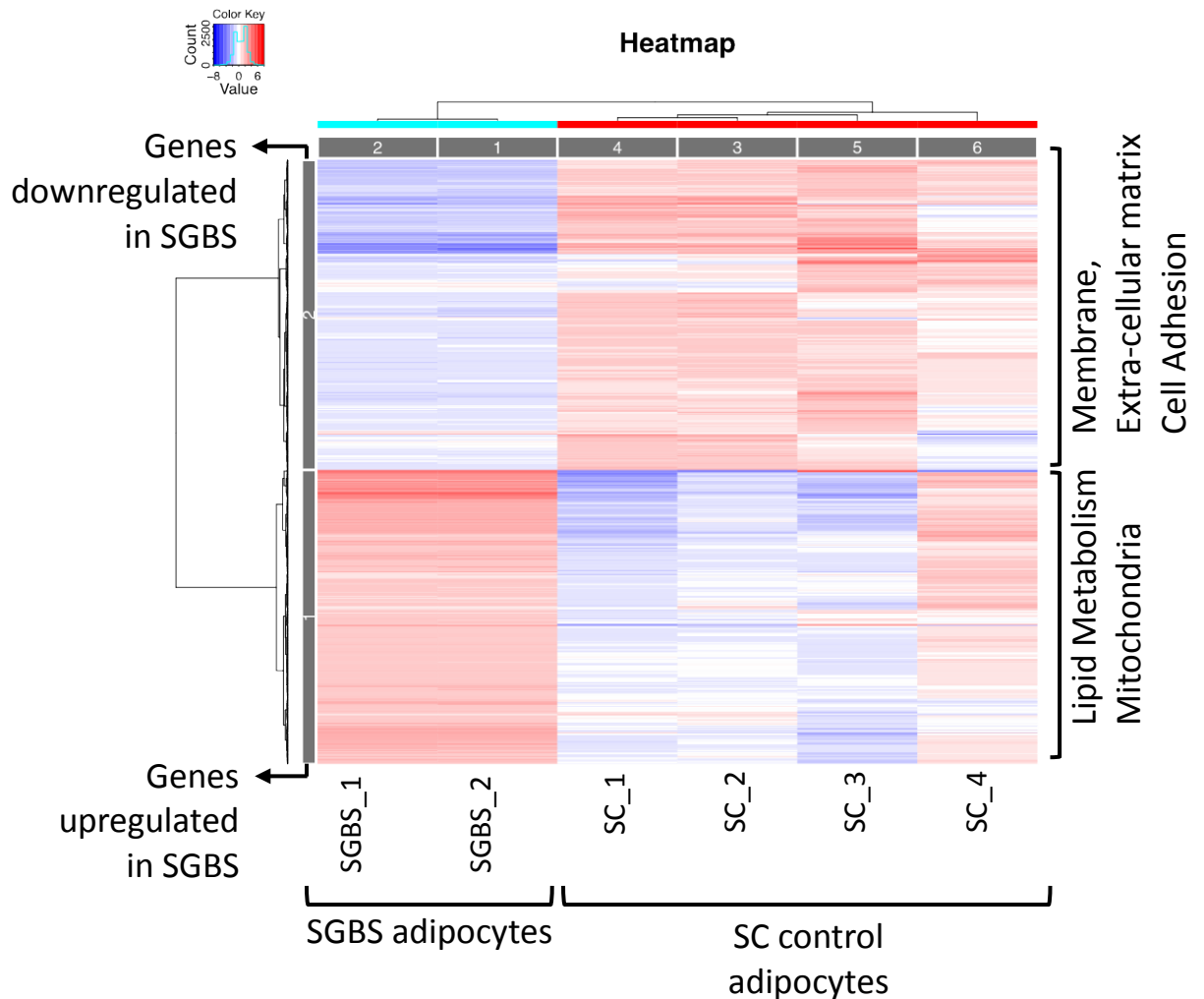


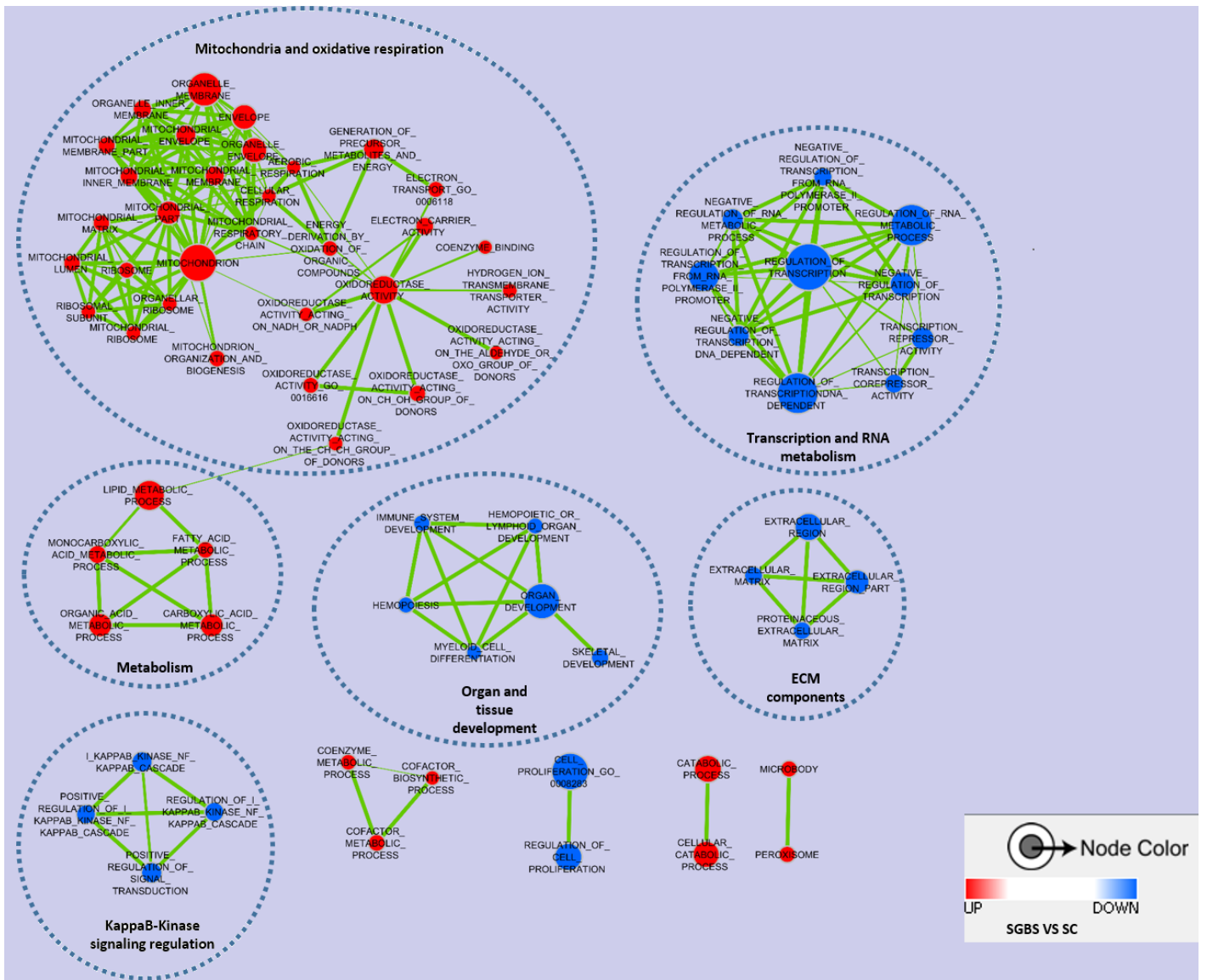
Figure 16: Transcriptome profiling of top 1000 differentially expressed genes in SGBS adipocytes.

Heat map clustering (unsupervised) top 1000 significantly upregulated (red) or downregulated (blue) genes in SGBS ($n = 2$) when compared to SC ($n = 4$) adipocytes. Enriched genes ontologies in up (lipid metabolism) or downregulated (membrane, extra-cellular matrix) set of genes in SGBS adipocytes are denoted on the right side of the figure. For the experiments involving SC adipocytes, experiments were performed in cells derived from 4 different donors (SC_1 to SC_4). For SGBS adipocytes, experiments were performed in duplicates (SGBS_1 and SGBS_2) from the same SGBS adipocyte.

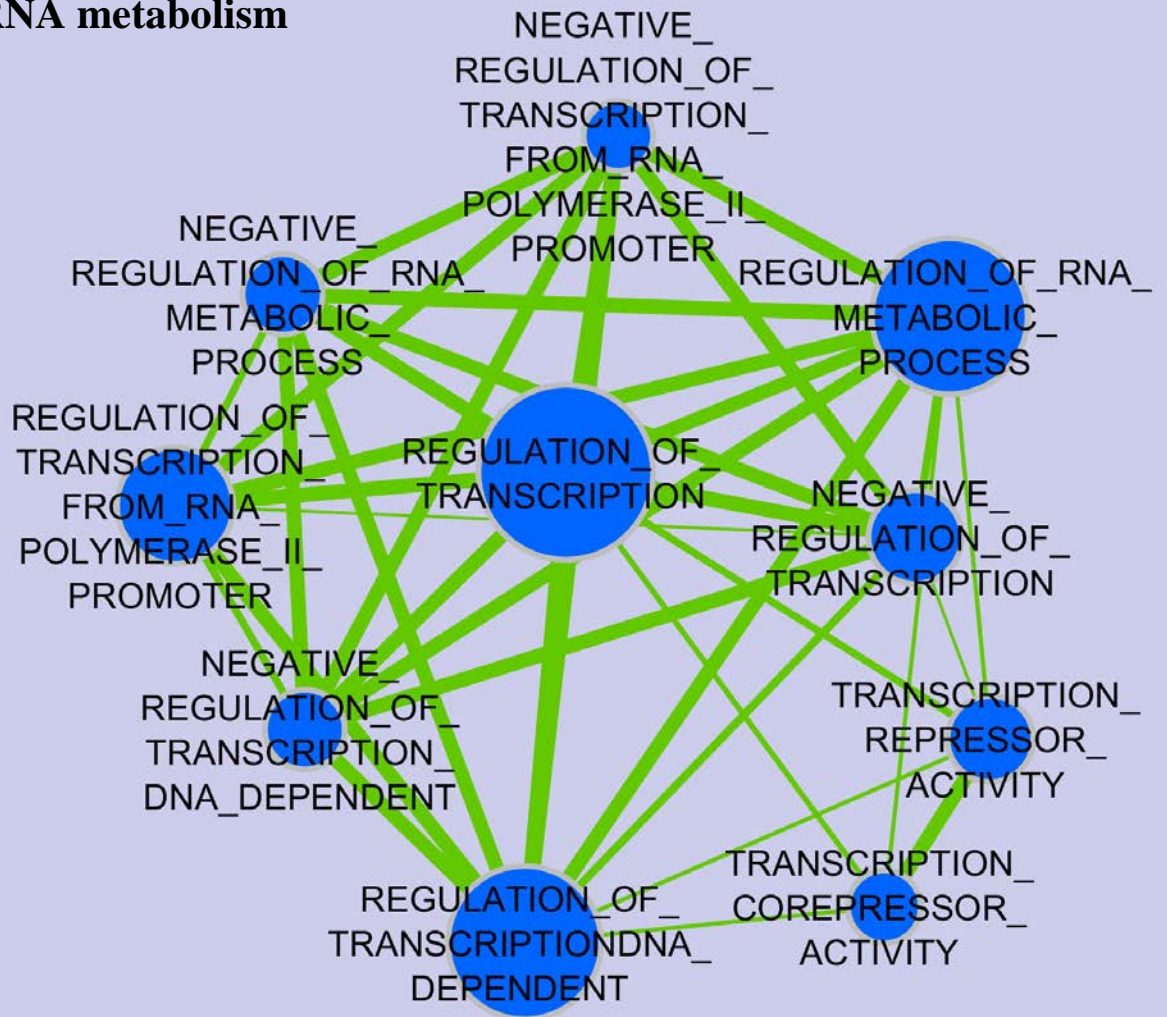
Heatmap (figure 16) was generated to cluster all six adipocyte samples and enriched biological processes (GO_BP) and cellular components (GO_CC) were analyzed in parallel. SGBS and SC adipocyte samples clustered distinctly from each other and all four SC adipocyte samples (except SC_025_1 or sample 6) had comparable gene expression pattern. Cluster 1 (represented by red

colored brackets) included genes upregulated in SGBS adipocytes and was significantly enriched in lipid metabolism (BP) and mitochondria (CC) ontologies. Cluster 2 (represented by blue colored brackets) included genes downregulated in SGBS and was significantly enriched in membrane (CC), extracellular matrix (CC) and cell adhesion (BP) ontologies.

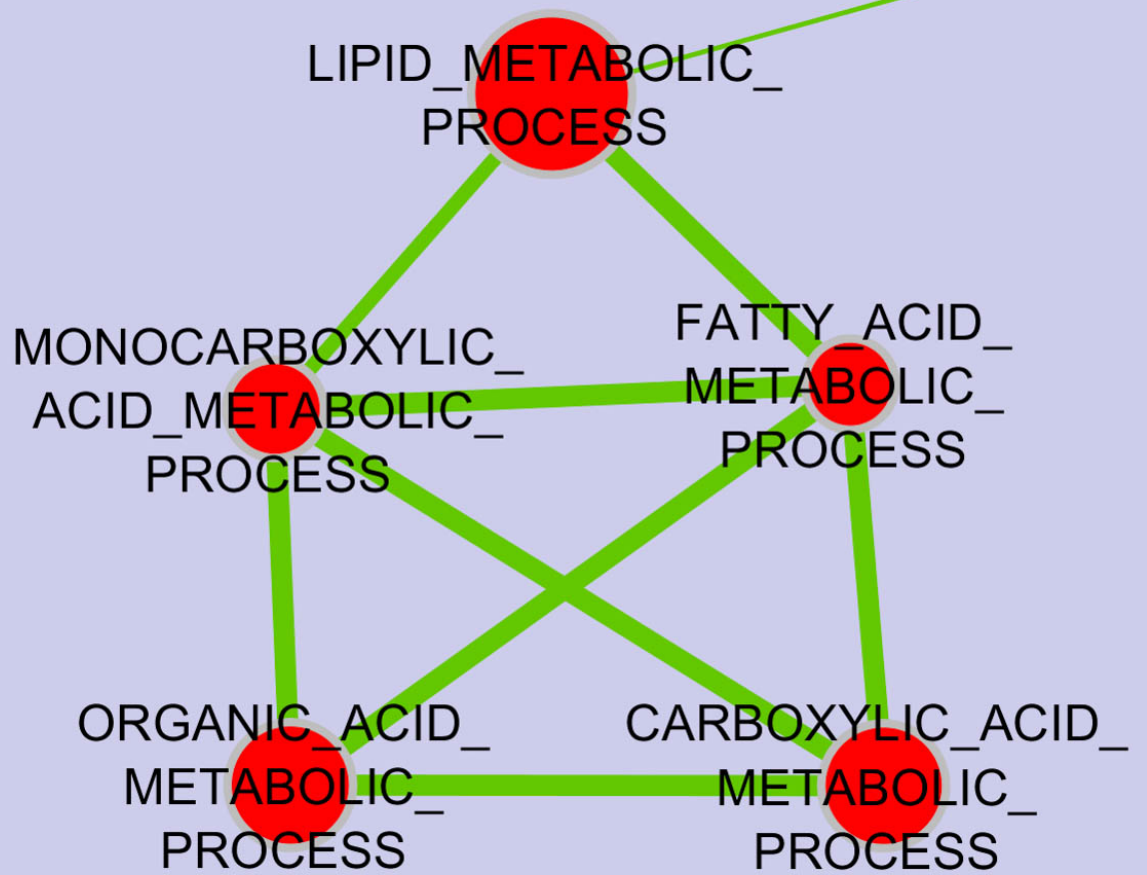
However, clustering did not allow analysis of positive and negative enrichment in gene ontologies or interactions between them. For detailed ontology analysis based on interactions, enrichment map of ontologies was built (figure 17). Positive and negative enrichment in ontologies were calculated based on the number of genes upregulated or downregulated in each ontology and denoted by red or blue colored nodes respectively. Gene ontology interactions (represented as green lines) were calculated based on the number of common genes between them, with thicker lines denoting more common genes. Final output illustrated significant interaction in ten ontology clusters or modules, five of which contained positively enriched ontologies and 5 contained negatively enriched ontologies (figure 17). Out of these, 6 clusters covered more than four individual ontologies, largest being cluster of mitochondria and oxidative respiration related ontologies suggesting that SGBS adipocytes were positively enriched in all these ontologies. Metabolism (especially lipid metabolism) related ontologies formed another cluster of positively enriched ontologies in SGBS adipocytes. Negatively enriched ontology clusters in SGBS adipocytes included (I) transcription and RNA metabolism (II) ECM components and (III) organ and tissue development.

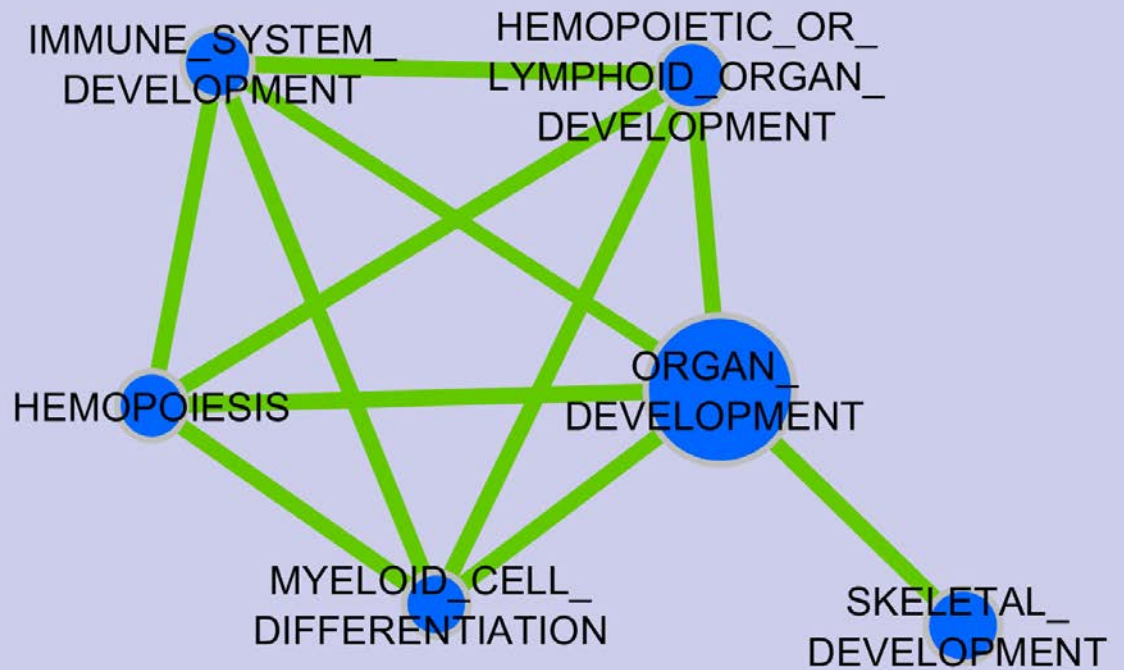


Transcription and RNA metabolism

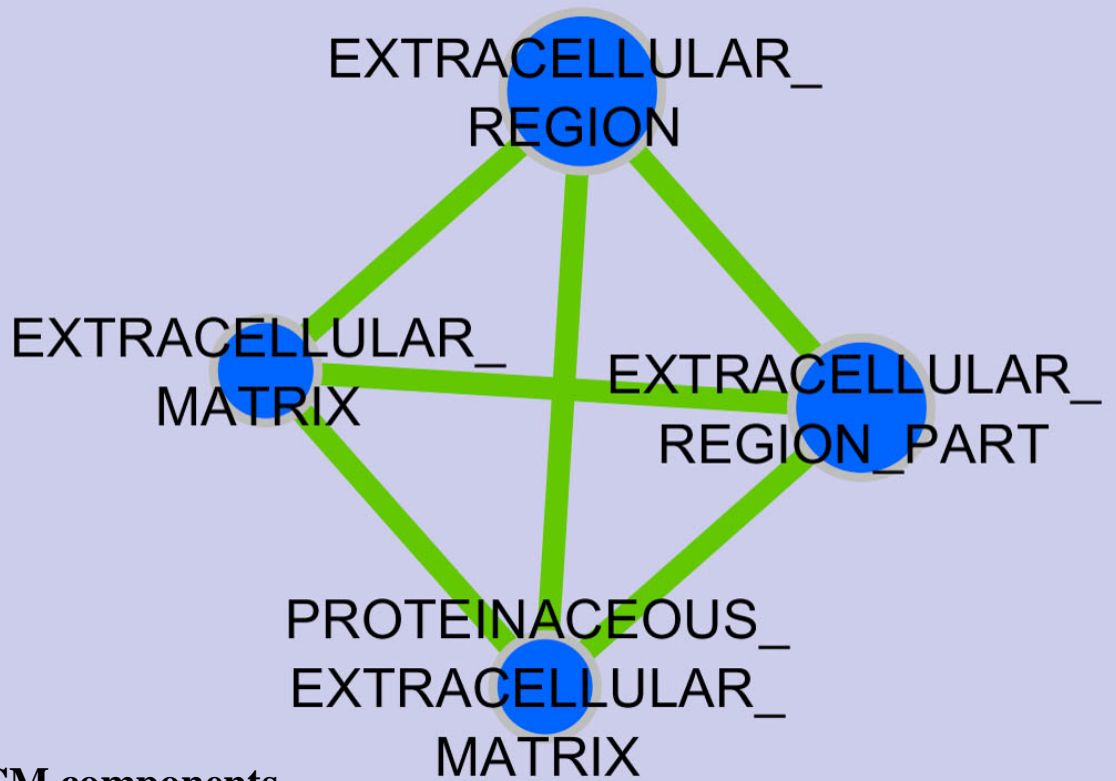


Metabolism





Organ and tissue development



ECM components

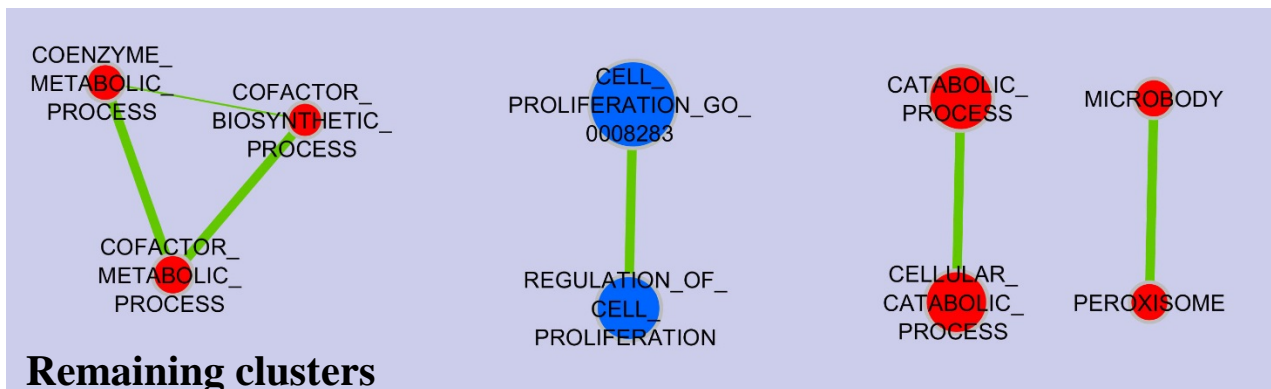
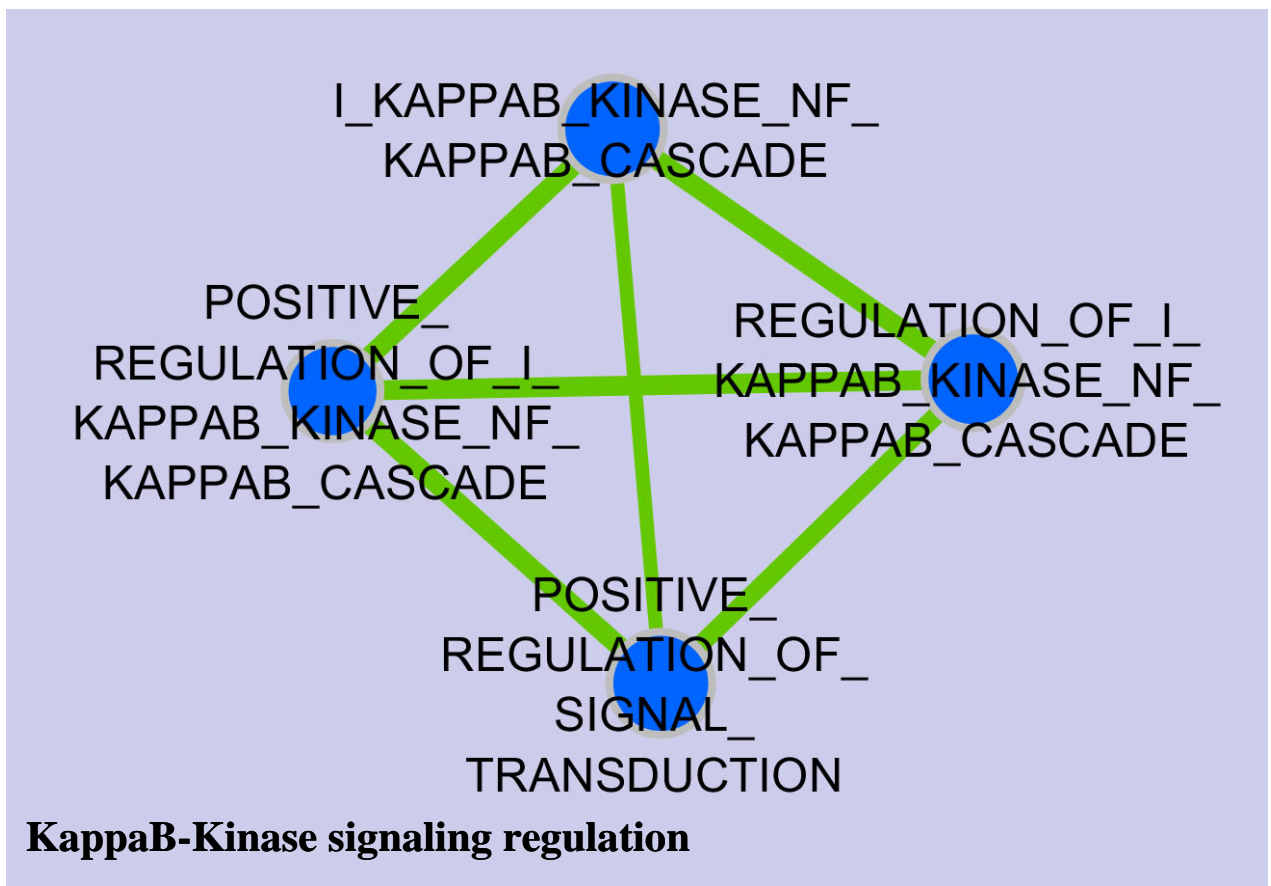


Figure 17: Fully differentiated SGBS and SC adipocytes display distinct ontology clustering.

FPKM values were analyzed in gene set enrichment analysis (GSEA) desktop version [137] and the output was exported in Cytoscape 3.3 (plugin: enrichment map creator) [135] to generate a map of positively and negatively enriched gene ontologies. The size of the node predicts the number of genes in particular ontology and green connecting line represents the number of common genes. Blue and red color denotes down and upregulated ontologies respectively (SGBS vs SC adipocytes). Cut off value for generating enrichment map was capped at conservative (P -value < 0.001, FDR < 0.05). Each cluster is magnified and shown below.

3.3.2 Differentially enriched metabolic pathways in SGBS adipocytes compared to SC adipocytes

iPathwayGuide was used to analyze significantly enriched KEGG biological pathways. More than 20 KEGG biological pathways were enriched in SGBS adipocytes when compared to SC adipocytes (table 12, $P < 0.05$ with Bonferroni correction). Deducing from results obtained in gene ontology analysis, noteworthy among these pathways were ECM-receptor interaction (figure 18), metabolic pathways, fatty acid metabolism (Figure 19), cytokine-cytokine receptor interaction and focal adhesion. Figure 18 and 19 illustrate upregulated (towards red color) and downregulated (towards blue color) genes in respective pathway map. Figure 20 represent up and downregulated genes in ECM-receptor interaction pathway.

Biological Pathways	P-Value (Bonferroni corrected)
ECM-receptor interaction	3.18E-06
Metabolic pathways	3.07E-05
Type I diabetes mellitus	0.000142
Fatty acid metabolism	0.000178
Cytokine-cytokine receptor interaction	0.000256
Calcium signaling pathway	0.000443
Autoimmune thyroid disease	0.001638
PI3K-Akt signaling pathway	0.002073
Neuroactive ligand-receptor interaction	0.003842
Pathways in cancer	0.004007
Hematopoietic cell lineage	0.004051
Graft-versus-host disease	0.005511
Cell adhesion molecules (CAMs)	0.005968
Fatty acid degradation	0.006437
Biosynthesis of unsaturated fatty acids	0.009968

Valine, leucine and isoleucine degradation	0.013166
Focal adhesion	0.016408
Allograft rejection	0.018391
PPAR signaling pathway	0.029223
Glycerolipid metabolism	0.044868

Table 12: Top KEGG biological pathways significantly enriched in SGBS vs SC control adipocytes.

Significance was pegged at $P < 0.05$.

As seen in pathway map as well as bar graph, the majority of genes in ECM receptor interaction pathway were downregulated in SGBS (n = 26 of 31 genes, $\log(\text{FC}) \geq 1$ and $\text{FDR} < 0.05$). Genes in fatty acid metabolism pathway, especially coding for mitochondrial lipolysis enzymes and ER resident proteins catalyzing a reaction for fatty acid elongation from palmitic acid to C22 or C24 free fatty acids were upregulated in SGBS adipocytes.

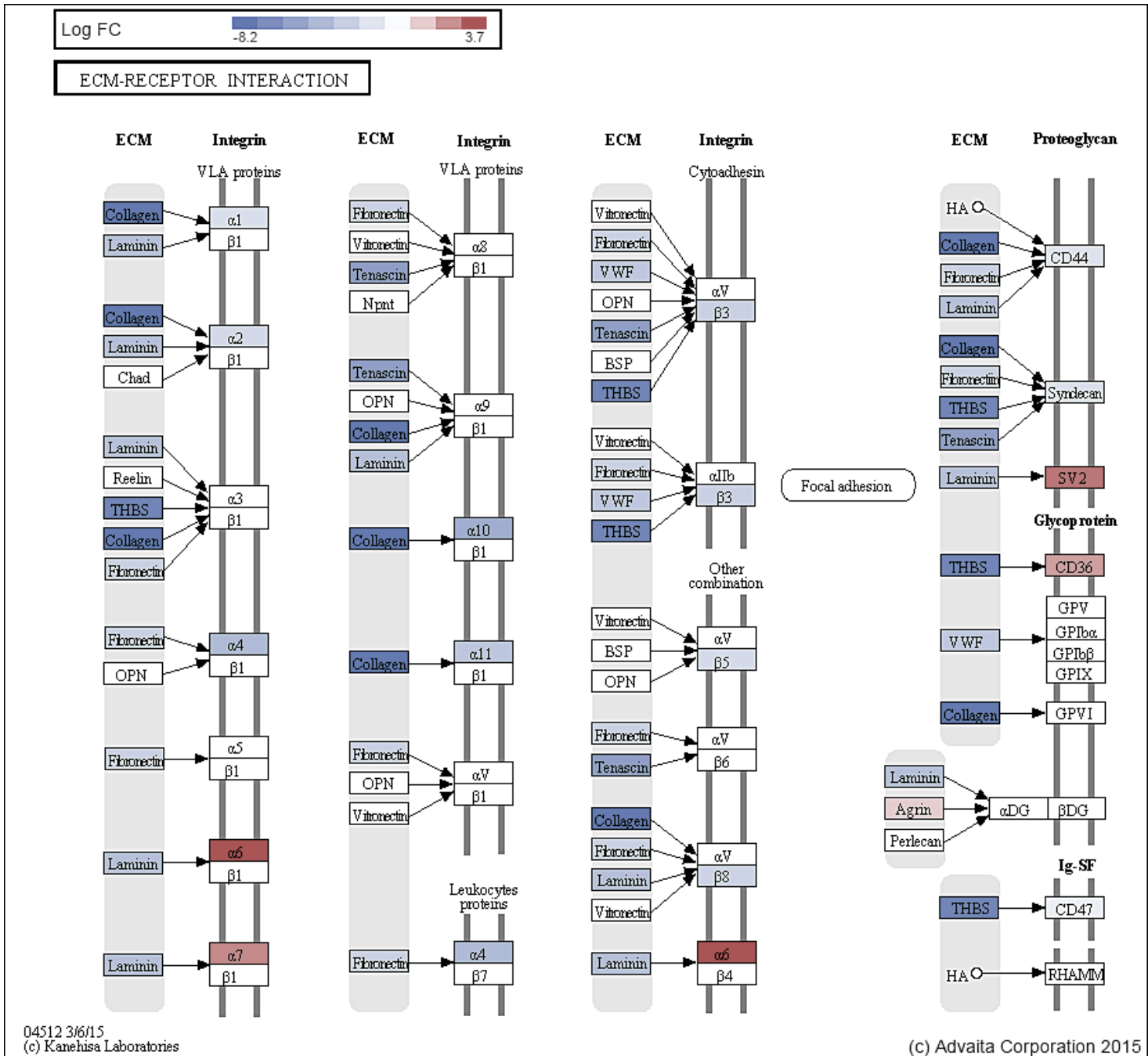


Figure 18: Representation of fold changes in ECM-receptor interaction pathway (SGBS vs SC adipocytes).

Output was generated with the help of iPathwayGuide. Blue and red colors symbolize downregulated and upregulated genes respectively. Significance was pegged at $P < 0.05$.



Fatty acid metabolism

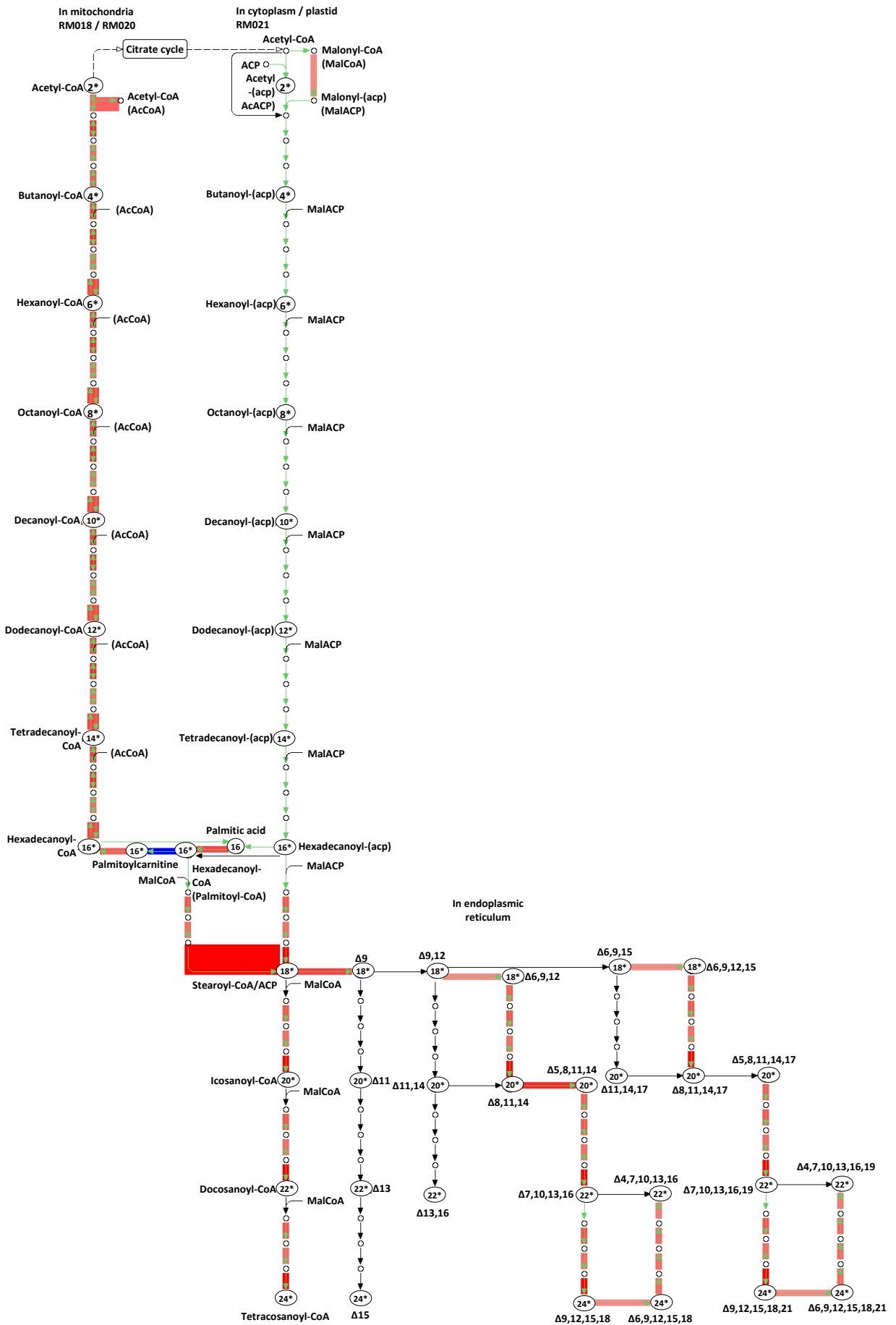


Figure 19: Representation of fold changes in fatty acid metabolism pathway (SGBS vs SC adipocytes).

Output was generated in iPathwayGuide. Blue and red colors symbolize downregulated and upregulated genes respectively. Significance was pegged at $P < 0.05$.

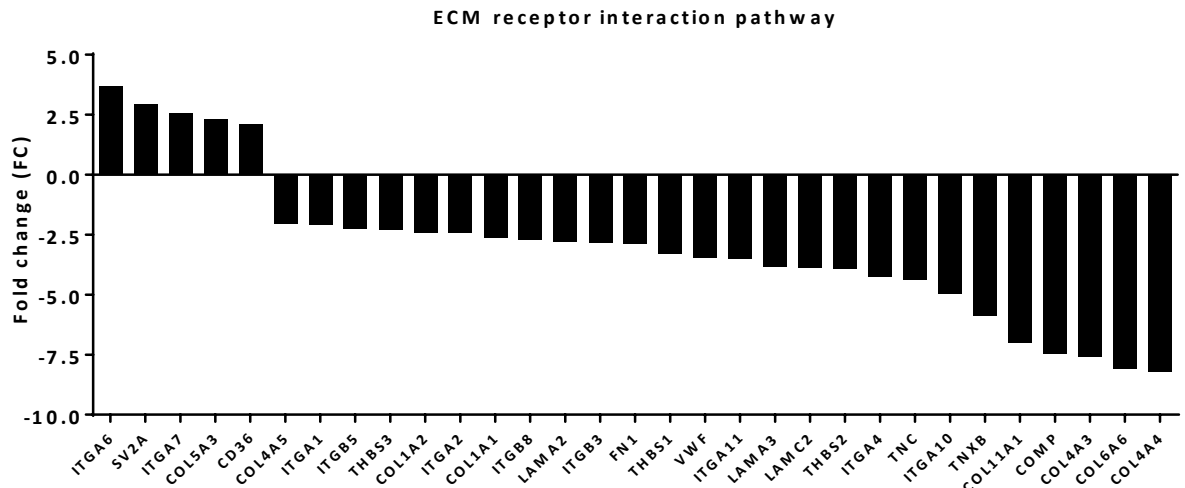


Figure 20: Up and downregulated genes in ECM-receptor interaction pathway (SGBS vs SC adipocytes).

Fold change was capped at ($\log FC \geq \pm 1$ or $FC \geq \pm 2$) with $FDR \leq 0.05$.

3.3.2.1 Significantly up and downregulated metabolic pathways in SGBS adipocytes compared to SC adipocytes

Metabolic pathway (P -value = $3.07E-05$) genes from iPathwayGuide contained a total of 314 genes significantly up or downregulated genes in SGBS adipocytes. To obtain specific metabolism pathways enriched either in upregulated ($n=220$) or downregulated ($n=94$) genes, respective list of genes were input in DAVID bioinformatics tool and enriched KEGG pathways were computed ($P < 0.05$, Bonferroni corrected, table 13). Nineteen pathways were enriched in upregulated set of genes, including oxidative phosphorylation, fatty acid metabolism, glycerolipid metabolism, glycerophospholipid metabolism, TCA or citric acid cycle and pyruvate metabolism. Four pathways were enriched in downregulated set of genes including O-glycan biosynthesis,

sphingolipid metabolism, nicotinate and nicotinamide metabolism and drug metabolism.

Biological Pathways	P-Value (Bonferroni corrected)
Upregulated genes in metabolic pathways	
Oxidative phosphorylation	1E-19
Valine, leucine and isoleucine degradation	2E-19
Parkinson's disease	7E-14
Alzheimer's disease	1E-11
Fatty acid metabolism	6E-11
Huntington's disease	2E-10
Glycerolipid metabolism	9E-08
Butanoate metabolism	3E-07
Propanoate metabolism	2E-06
Citrate cycle (TCA cycle)	2E-05
Terpenoid backbone biosynthesis	7E-05
beta-Alanine metabolism	1E-04
Glycerophospholipid metabolism	2E-04
Glyoxylate and dicarboxylate metabolism	1E-03
Pyruvate metabolism	2E-03
Arginine and proline metabolism	4E-03
Glycolysis / Gluconeogenesis	1E-02
Limonene and pinene degradation	1E-02
Fatty acid elongation in mitochondria	2E-02
Downregulated genes in metabolic pathways	
O-Glycan biosynthesis	4E-04
Sphingolipid metabolism	2E-02
Nicotinate and nicotinamide metabolism	4E-02
Drug metabolism	4E-02

Table 13: Metabolic pathways significantly enriched in SGBS adipocytes compared to SC adipocytes.

Significance was pegged at $P < 0.05$.

Overall, SGBS adipocyte transcriptome indicated downregulated ECM receptor interaction and upregulated fatty acid metabolism (especially mitochondrial lipolysis), pyruvate metabolism, TCA cycle and oxidative phosphorylation, most of which takes place in mitochondria.

3.3.3 Adipogenic and metabolic gene profiling of SGBS and SC adipocytes

To evaluate variances in gene expression profile during adipogenesis, eighteen genes-of-interest vital for differentiation, lipid metabolism, inflammation and browning in adipocytes were quantified at day 0, day 4, day 8 and day 12 of differentiation. SGBS and SC adipocytes were differentiated using respective protocols and gene expression in all samples was compared to day 0 in SC adipocytes. To rule out the possibility that the differences in characteristics seen between the two adipocyte types studied were due to differences in the media used to differentiate them, a series of experiments in which LONZA media was used to differentiate SGBS adipocytes were also performed. The results obtained for the SGBS adipocytes were similar, whether LONZA media or SGBS specific differentiation media was used (results not shown).

Adipogenic markers (PPAR γ , PPAR α , CEBP α , FABP4, adiponectin and leptin) increased in both SGBS and SC adipocytes, but the magnitude was much higher in SGBS adipocytes (except PPAR α) (figure 21A). Differences could be observed starting from day 4 of differentiation and continued until day 8 or 12. In mature state, fold change of adiponectin (~13 fold), CEBP α (FC = 171.05 \pm 83.503 in SC, FC = 1362 \pm 740.98 in SGBS), PPAR γ (FC = 15.98 \pm 7.94 in SC, FC = 35.18 \pm 6.22 in SGBS) and leptin (FC = 40.86 \pm 22.56 in SC, FC = 470.63 \pm 34.002 in SGBS) was greater in SGBS when compared to SC adipocytes, and indicated earlier and better adipogenesis in them. Baseline expression of

adiponectin was significantly higher (~20 fold) in SGBS starting from day 0.

Along with adipogenesis, lipid metabolism genes DGAT1 (~4 fold) and FIT2

(~3 fold) were higher in SGBS (figure 21B).

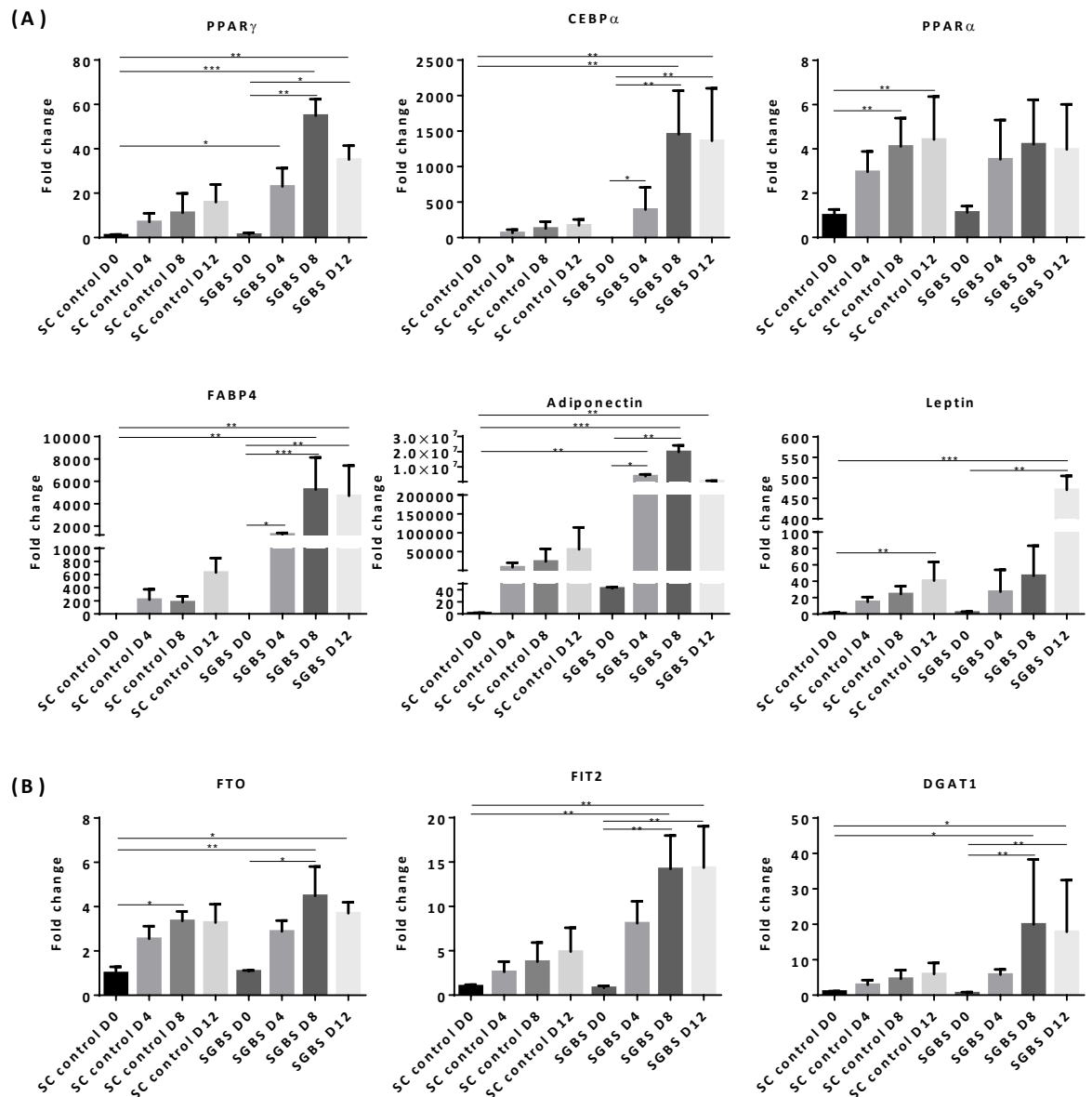


Figure 21: SGBS adipocytes have distinct expression pattern of (A) adipogenic and (B) lipid storage and metabolism genes during adipogenesis

Days of differentiation indicated as D0, D4, D8, and D12 respectively. Data represented as mean \pm SEM obtained from three different donors for SC adipocytes (in duplicates) and three independent trials (in duplicates) for SGBS adipocytes. All data were normalized using SC control D0 samples. * $P < 0.05$, ** $P < 0.005$, *** $P < 0.0001$.

IL18 (~20 fold) and TLR4 (~10 fold) gene expression increased by day 12 of differentiation in SC adipocytes with minimal change in SGBS. On the contrary, IL1 β expression increased (~40 fold) in SGBS adipocytes while minimally changing in SC adipocytes. TNF α and NF κ B1 expression did not change significantly with differentiation in either SC or SGBS adipocytes (figure 22A). However, in mature state, expression of all inflammatory markers was significantly higher in SC adipocytes (except IL1 β).

PGC1 α , PRDM16, DIO2, UCP1 gene expression was analyzed as markers of browning. PGC1 α is an upstream master regulator of mitochondrial biogenesis [138, 139]. At day 0, baseline expression of PGC1 α was significantly higher in SC adipocytes when compared to SGBS adipocytes and continued to be higher (~6 fold at day 12) in SC adipocytes. Similar results were seen for DIO2 gene expression. Unlike PGC1 α and DIO2, UCP1 expression was ~1300 fold higher in mature SGBS adipocytes when compared to SC controls, although baseline expression of UCP1 seemed lower in SGBS adipocytes (figure 22B). PGC1 α is a transcription coactivator for UCP1 gene expression, but we observed an opposing trend in their mRNA expressions in SC adipocytes. This suggested presence of either alternative UCP1 transcription factors in SGBS adipocytes or absence of transcription co-factors of PGC1 α in SC adipocytes but needs further research.

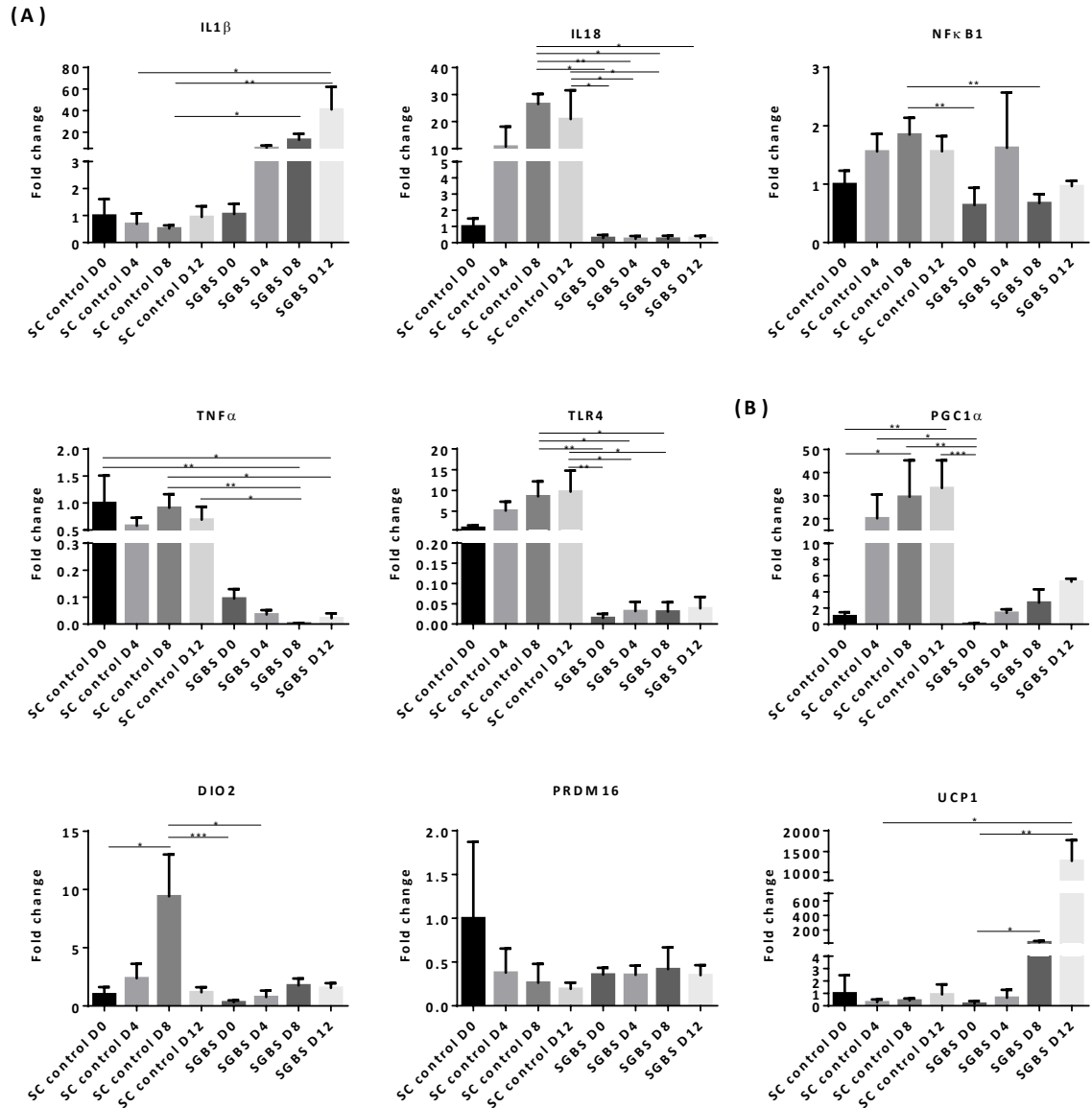


Figure 22: SGBS adipocytes have distinct expression pattern of (A) inflammatory and (B) browning genes during adipogenesis.

Days of differentiation indicated as D0, D4, D8, and D12 respectively. Data represented as mean \pm SEM obtained from three different donors for SC adipocytes (in duplicates) and three independent trials (in duplicates) for SGBS adipocytes. All data were normalized using SC control D0 samples. * $P < 0.05$, ** $P < 0.005$, *** $P < 0.0001$.

Gene expression data in mature adipocytes was used to validate RNAseq data and a strong correlation in log (FC) was observed (linear regression of $r = 0.8289$) ($P < 0.0002$) (figure 23).

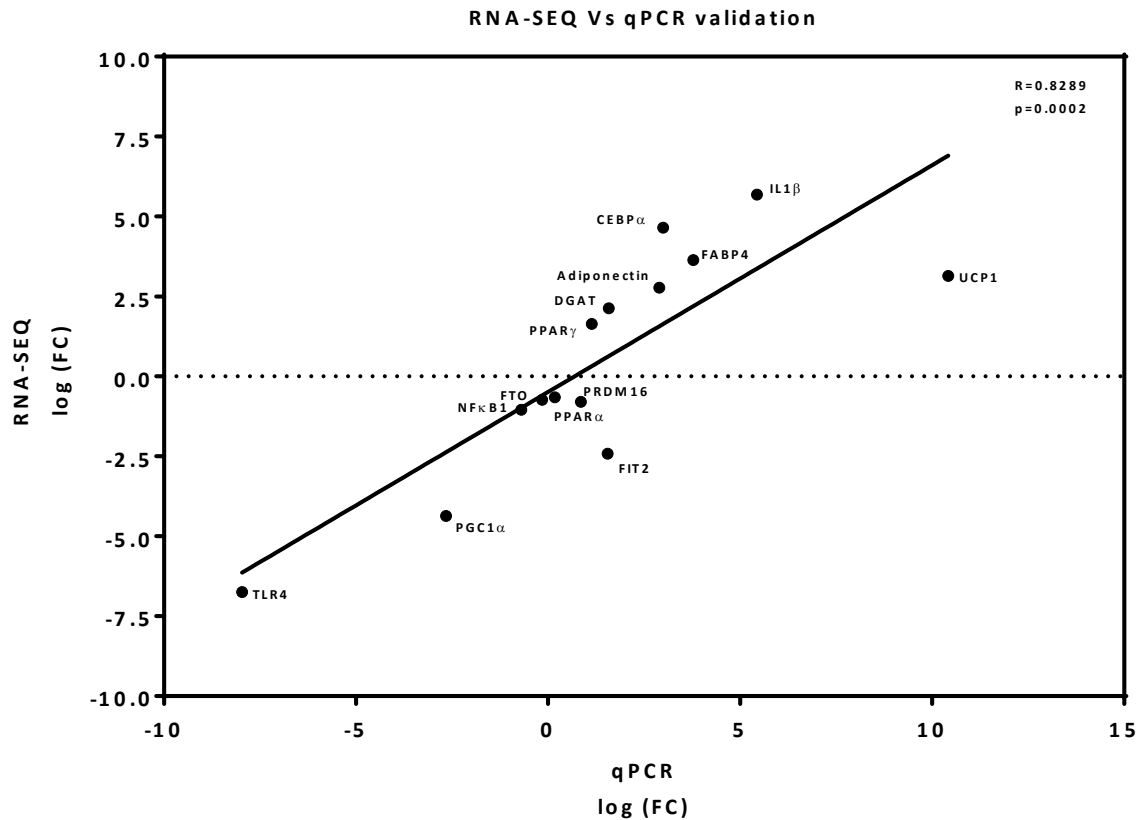


Figure 23: Gene expression data from RNAseq significantly correlated with qPCR data.

Pearson's correlation was used to determine significance among the groups. $P < 0.05$ was considered statistically significant.

3.3.4 SGBS adipocytes have energy dissipating browning phenotype

Ontology, KEGG pathway and UCP1 gene expression pattern in SGBS adipocytes suggest brown or beige adipocyte phenotype. To answer the question if they are brown or beige, we measured UCP1 protein expression, mitochondrial DNA content and respiration in SGBS and SC adipocytes. As beige adipocytes are induced from white adipocytes upon stimulation with PPAR agonist or T3, which are also active components of SGBS differentiation medium; UCP1 protein expression was evaluated before/after depletion of rosiglitazone (PPAR agonist) and T3 from differentiation medium of SGBS adipocytes. Consistent with gene expression, western blot in figure 24A

demonstrated significantly higher UCP1 protein expression in SGBS adipocytes; even after depletion of rosiglitazone or T3.

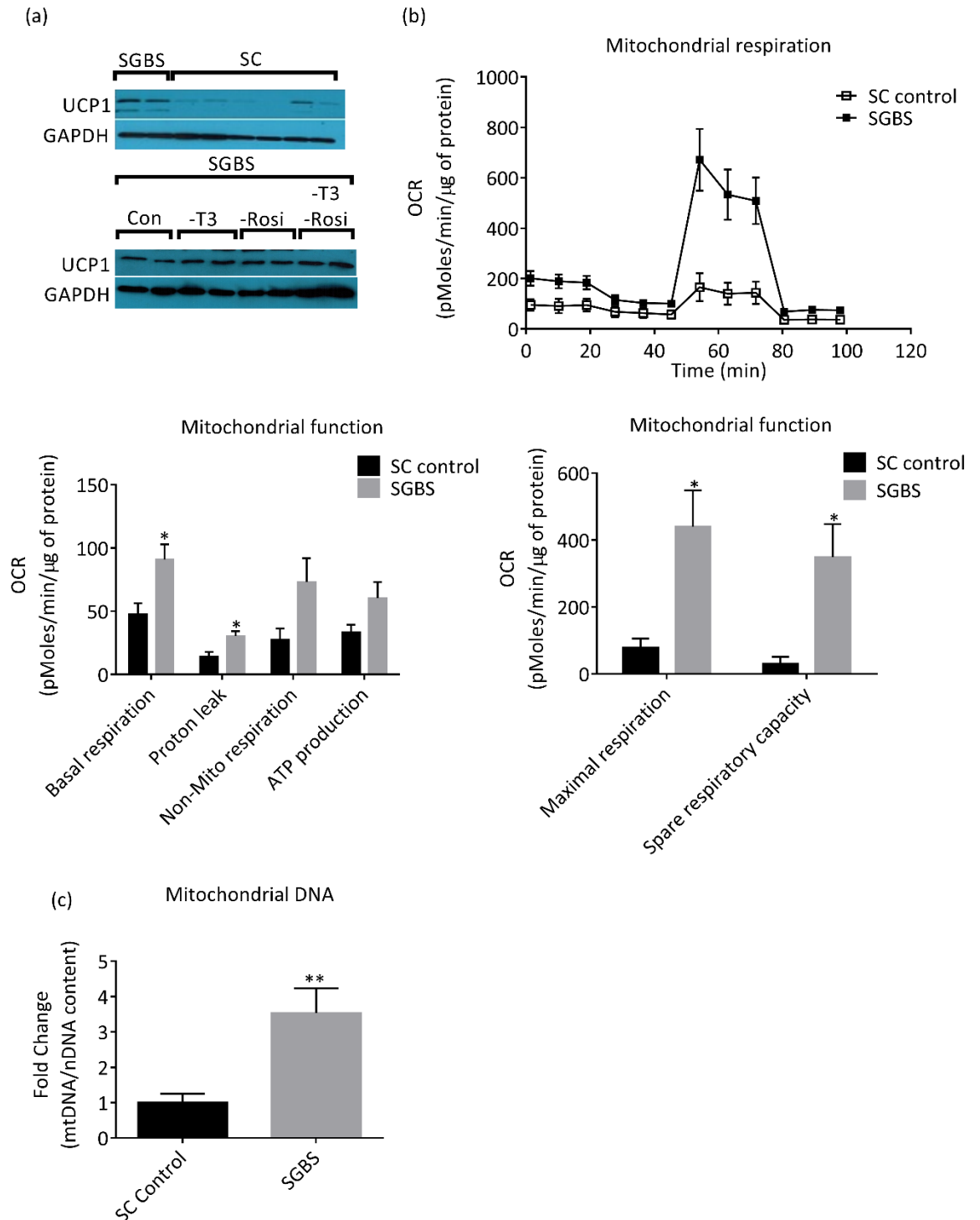


Figure 24: SGBS and its browning phenotype.

(A) UCP1 protein expression in differentiated SGBS and SC adipocytes at basal level and upon depletion of T3 and rosiglitazone (rosi) from differentiation medium. (B) Mitochondrial respiration measured as oxygen consumption rate

*in SGBS and SC adipocytes (detailed protocol discussed in section 2.8 (C) Mitochondrial DNA content measured as a ratio of mitochondrial DNA (mtDNA) by nuclear DNA (nDNA). Data represented as mean \pm SEM obtained from three different donors for SC adipocytes (in duplicates) and three independent trials for SGBS adipocytes. * $P < 0.05$, ** $P < 0.005$.*

Mitochondrial respiration was measured using Seahorse mitochondrial flux analyzer and represented as oxygen consumption rate or OCR (pMoles/min/ μ g of protein). Figure 24B illustrates mitochondrial respiration profile and mitochondrial function. SGBS adipocytes (grey bars) exhibited significantly higher basal respiration (~2 fold), proton leak, maximal respiration (~4 fold) and spare respiratory capacity (~8 fold) when compared to SC adipocytes ($P < 0.05$). Mitochondrial DNA content is an indirect representation a number of mitochondria and was ~3.5 fold higher in SGBS adipocytes ($P = 0.0079$) (figure 24C).

3.3.5 Lipid accumulation and glucose uptake in SGBS adipocytes compared to SC adipocytes

Together with mitochondrial function, we measured lipid accumulation and glucose uptake as functional readouts in both adipocytes. In differentiated state, intracellular lipid droplet accumulation was significantly higher in SGBS adipocytes when compared to SC controls ($P < 0.0001$) (figure 25A). Furthermore, SGBS adipocytes possess higher insulin sensitivity as demonstrated by insulin stimulated glucose uptake ($P < 0.001$, figure 25B).

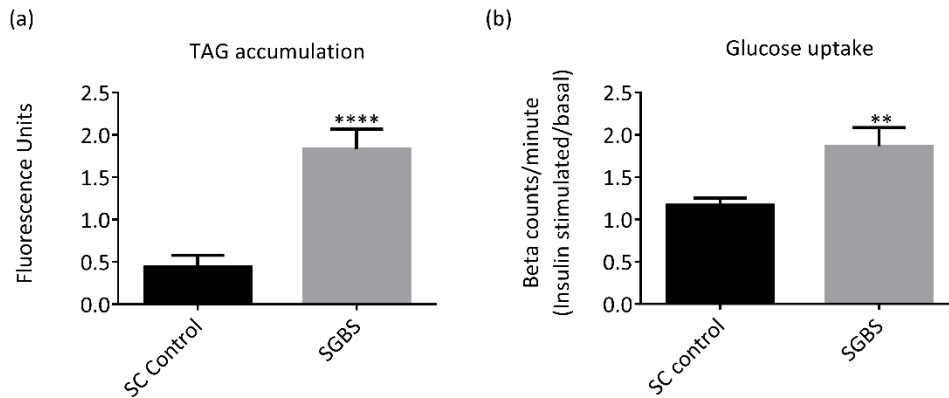


Figure 25: lipid accumulation and insulin-stimulated glucose uptake assay in SGBS vs SC adipocytes.

Data represented as mean \pm SEM obtained from three different donors for SC adipocytes (in duplicates) and three independent trials for SGBS adipocytes. ** $P < 0.005$, **** $P < 0.0001$.

3.3.6 Adipocyte lineage markers in SGBS and SC adipocytes

Results indicated a robust heat producing phenotype in SGBS. To answer the question if lineage of SGBS differed from SC adipocytes, lineage specific markers (pooled from current literature) and their gene expression in SGBS were tabulated (table 14). Lineage markers were divided into 6 categories as brown (BAT), beige, white (WAT), brown and beige, white and beige as well as ubiquitous (found in all types of adipocytes). WAT (white) adipocyte markers ASC-1, NR1H3 and LPL; BAT and beige adipocyte marker PLIN5; and ubiquitous markers CITED1 and adiponectin (ADIPOQ) were upregulated in SGBS. WAT and beige marker PDGFR α and BAT plus beige markers MTUS1 and PGC1 α were downregulated in SGBS. A common marker among beige and brown adipocytes (UCP1) was significantly higher in SGBS adipocytes when compared to SC controls. Overall, SGBS did not match to any lineage per say as we observed up and downregulation of genes specific to all lineages.

Gene Name	Lineage	Fold Change	FDR	Reference
EDNRB	BAT	-5.14	0.00532	Xue and Tseng et al 2015
EBF2	BAT	-4.68	0.00002	Rajakumari, Wu et al 2013
PDK4	BAT	4.57	0.03001	Mottillo et al 2012
PREX1	BAT	5.74	0.00005	Xue and Tseng et al 2015
MYF5	BAT	NA	NA	Seale, Bjork et al 2008
ZIC1	BAT	NA	NA	De Jong and Larsson et al 2015
BMP7	BAT	NA	NA	Tseng et al, 2008
MTUS1	BAT and beige	-61.91	0.00000	Shinoda, Luijten et al 2015
PGC1 α	BAT and beige	-20.66	0.00000	Bostrom, Wu et al 2012
HSPB7	BAT and beige	-5.22	0.00169	Wu, Bostrom et al 2012
EBF3	BAT and beige	-2.18	0.01518	De Jong and Larsson et al 2015
PRDM16	BAT and beige	-1.74	0.44893	Seale et al 2007
KCNK3	BAT and beige	-1.40	0.81898	Shinoda, Luijten et al 2015
SIRT1	BAT and beige	1.90	0.02398	Qiang, Wang et al 2012
UCP1	BAT and beige	8.84	0.03696	Wu, Bostrom et al 2012
PLIN5	BAT and beige	9.50	0.00958	Barneda, Frontini et al 2013
LHX8	BAT and beige	NA	NA	De Jong and Larsson et al 2015
FGF21	BAT and beige	NA	NA	De Jong and Larsson et al 2015

CIDEA	BAT and beige	NA	NA	Barneda, Frontini et al 2013
PAT2	BAT and beige	NA	NA	Ussar, Lee et al 2014
P2RX5	BAT and beige	NA	NA	Ussar, Lee et al 2014
B3AR/ADRB3R	BAT and beige	NA	NA	Lidell et al 2013
CD40	Beige	-6.62	0.00237	Wu, Bostrom et al 2012
EPSTI1	Beige	-4.18	0.01117	De Jong and Larsson et al 2015
SP100	Beige	-2.44	0.00718	Wu, Bostrom et al 2012
EAR2/NR2F6	Beige	1.85	0.00002	Wu, Bostrom et al 2012
SHOX2	Beige	2.03	0.06347	Lidell 2013
SLC27A1	Beige	4.48	0.00017	Wu, Bostrom et al 2012
TBX1	Beige	NA	NA	De Jong and Larsson et al 2015
TNFRSF9/CD137	Beige	NA	NA	De Jong and Larsson et al 2015
TMEM26	Beige	NA	NA	De Jong and Larsson et al 2015
PDGFR α	WAT and Beige	-8.03	0.00001	Yun-Hee Lee 2012
HOXC9	WAT and Beige	-1.68	0.20526	De Jong and Larsson et al 2015
HOXC8	WAT and Beige	-1.27	0.59879	De Jong and Larsson et al 2015
RBL1	WAT	-2.29	0.04992	Scime, Grenier et al 2005
Leptin	WAT	-0.71	0.52992	Ussar, Lee et al 2014
NRIP1/RIP140	WAT	1.09	0.82716	Hallberg, Morganstein et al 2008
RB1	WAT	1.34	0.37996	Hansen, Jorgensen et al 2004

TCF21	WAT	2.94	0.02604	De Jong and Larsson et al 2015
LPL	WAT	13.47	0.00055	Dani, Amri et al 1990
NR1H3/LXR α	WAT	16.32	0.00006	Wang, Zhang et al 2008
ASC-1/SLC7A10	WAT	17.47	0.00009	Ussar, Lee et al 2014
ADIPONECTIN	Ubiquitous in AT	12.44	0.00330	Zhang, Matheny et al 2002
CITED1	Ubiquitous in AT	48.18	0.00000	De Jong and Larsson et al 2015

Table 14: Lineage specific markers in adipocytes and their expression in SGBS and SC control adipocytes. NA: Genes with FPKM < 1 and thus excluded from further analysis. P value < 0.05 and FDR < 0.05 were used as thresholds to select significant genes.

3.4 Discussion

Presence of a distinct transcriptome profiles, robust differentiation, increased oxidative respiration, brown adipocyte like phenotype, higher lipid accumulation and glucose uptake supported our hypothesis that there exists metabolic differences between SGBS adipocytes and primary human subcutaneous adipocytes derived from obese, non-diabetic subjects.

RNA sequencing results showed differences in KEGG biological pathways and gene ontologies. Within these, a number of ECM-receptor interaction genes were differentially down (n=26) and upregulated (n=5) in SGBS when compared to SC controls. Additionally, GSEA output and enrichment map indicated ECM components to be negatively enriched in SGBS adipocytes. Functionally, ECM plays a critical role in maintaining the structural integrity of adipocytes and ECM-receptor interaction is associated with pro-inflammatory changes and dysregulation of adipocyte metabolism; also known to vary with the degree of obesity [140, 141]. Subject to individual protein function, ECM components seem to play a dual role in promoting or inhibiting adipose tissue

expandability. Several reports suggest that excessive ECM deposition in response to obesity-related inflammation reduces adipose tissue expandability which eventually results in adipose tissue dysfunction [15]. However, studies testing the effects of selective macromolecular crowding on adipogenesis and browning suggest beneficial effects. When differentiated with macromolecular crowding, bone marrow derived mesenchymal stem cells undergo improved adipogenesis in the presence of macromolecular crowding. In addition to better adipogenesis, deposition of ECM components such as collagen IV and perlecan (a heparan sulfate proteoglycan) were observed to be significantly higher [16]. Collagen IV cocoon formation around differentiating bone marrow derived mesenchymal stem cells also improved their UCP1 expression and thermogenic capacity [17]. In our dataset, transcripts of subcomponents of collagen IV were differentially expressed in SGBS adipocytes. Some subcomponents were upregulated: COL4A5 (log FC = 2.04), COL4A3 (log FC = 7.57), COL4A4 (log FC = 8.20), whereas other components were downregulated: COL4A1 (log FC = -2.00) and COL4A2 (log FC = -1.77). These observations remain to be verified at the protein expression level, but suggest that subcomponents of collagen IV may have differing activity in terms of whether they are more pro-adipogenic (COL4A5, COL4A3 and COL4A4) or anti-adipogenic (COL4A1 and COL4A2). In addition to ECM-receptor interaction, metabolic pathways in SGBS adipocytes differed from SC adipocytes with 220 genes significantly upregulated and 94 genes significantly downregulated in SGBS. Most of the upregulated genes annotated to oxidative phosphorylation pathway, which is active in brown adipocytes or beige adipocytes upon stimulation. In addition, oxidative respiration and fatty acid oxidation related ontologies were positively

enriched in SGBS. Transcriptome differences were recapitulated in the phenotype of SGBS adipocytes as mitochondrial content, respiration and UCP1 gene as well as protein expression were significantly higher in SGBS adipocytes. Beige adipocytes differ from brown adipocytes in their ability to induce UCP1 expression upon stimulation with cold or PPAR γ which is an active constituent of differentiation medium. SGBS adipocytes were able to maintain UCP1 protein expression even after depletion of PPAR γ agonist. Together, these results were in line with transient brown phenotype in SGBS that has been reported recently [103].

SGBS gene expression profile was unable to fit any specific adipocyte lineage with upregulated and downregulated genes in all of categories although functionally they are similar to brown adipocytes. Resemblance of SGBS to previously documented neonatal white adipocytes is worth considering. Some of the previous reports suggest that neonatal white adipocytes have increased number of mitochondria and browning phenotype when compared to adipocytes derived from adult adipose tissue [142, 143] and function and composition of adipose tissue vary substantially between an early age and adulthood. During infant age, it displays more active thermogenic properties; for example the size, number and structure of its mitochondria are reminiscent to those of BAT [144]. Hence, it is essential to consider the infant origin of SGBS adipocytes (derived from the white adipose tissue of a 3-month-old baby) which could be a key contributing factor to the differences observed [101]. Infant or neonatal origin of SGBS is supported by certain genes. CYP19A1 (also known as aromatase) and ALDH1A1, which are expressed only in adult placental tissue are downregulated in SGBS adipocytes [145, 146]. In addition, ALDH3B2, known

to be minimally expressed in adult adipose tissue [147] is upregulated in SGBS adipocytes. However, studies also found CYP19A1 to be minimally expressed in fully differentiated, lipid-laden adipocytes [148, 149] and McInnes et al. reported similar gene expression of aromatase in SGBS and isolated primary human adipocytes [150]. Inconsistency in our data from previous reports needs further validation, but could be perhaps due to adipocyte differentiation protocol. In our study we limited differentiation of both cell types to 12 days in contrast to 21 days used in previous studies. Moreover, SGBS adipocytes were found to have transient brown phenotype around day 14 of differentiation which changes to white phenotype by day 28. It would be interesting for future studies to fully characterize infant WAT and establish genes differentially expressed in this tissue. It is important to note that reproducibility of this work might be affected by and limited to use of Lonza differentiation medium for primary human subcutaneous adipocytes. Lonza medium provided us with an added advantage of faster and better differentiation within 10 days when compared to homemade differentiation cocktails, which needs 21 days for differentiation.

3.5 Conclusion

Our work demonstrated numerous differences between SGBS and SC adipocytes during 12 days of differentiation. Given their high differentiation capacity and robust viability, SGBS cells remain as a valuable, preliminary, *in vitro* test model for studies relating to human adipocyte metabolism. However, due to the differences observed, we would caution against using SGBS as the only primary human subcutaneous adipocytes in obesity-related studies.

Chapter 4:
Partial deficiency of FIT2 protein
impairs triglyceride storage and insulin
signaling in human adipocytes

4.1 Introduction

Type II Diabetes have prevailed for centuries and due to rapid urbanization and life style modifications, documented cases have soared to nearly 387 million worldwide, with huge financial burden [3]. Historically, onset of diabetes has always been associated with the presence of obesity (defined as Body Mass Index > 30). With advancement in research, the role of different adipose tissue depots in regulating metabolic homeostasis has become increasingly appreciated. Excessive OM adipose tissue and ectopic lipids (fats stored in the liver, kidney, skeletal muscle, cardiac tissue etc.) are known to be more pathogenic compared to SC adipose tissue [22]. However, ectopic lipid deposition is largely implicated to lipid spillover from SC and OM adipose tissue depot due to their impaired lipid storage capacity. The ability of adipose tissue to expand and grow with minimal lipid spillover contributes towards better metabolic health. TAGs within lipid droplets is the most non-toxic form of lipids in adipose tissue and adipocytes [151, 152]. Excess quantities of free fatty acids, diacylglycerols and ceramides are potent toxic lipid species resulting in insulin resistance via activation of inflammation, ER stress and macrophage infiltration [57, 153, 154]. In this context, we studied a recently discovered lipid droplet protein; FIT2 (Fat Storage Inducing Transmembrane 2). The motivation for homing in on studying the FIT2 protein were two fold; (I) RNA-SEQ (discussed in detail in chapter 6) data comparing OM vs SC depot in NT2DM and T2DM subjects revealed that FIT2 protein was one of the lipid storage proteins expressed at significantly lower levels in OM depot from T2DM subjects only (figure 26) (II) FIT2 was recently identified as a GWAS candidate gene associated with T2DM in East Asian population [108].

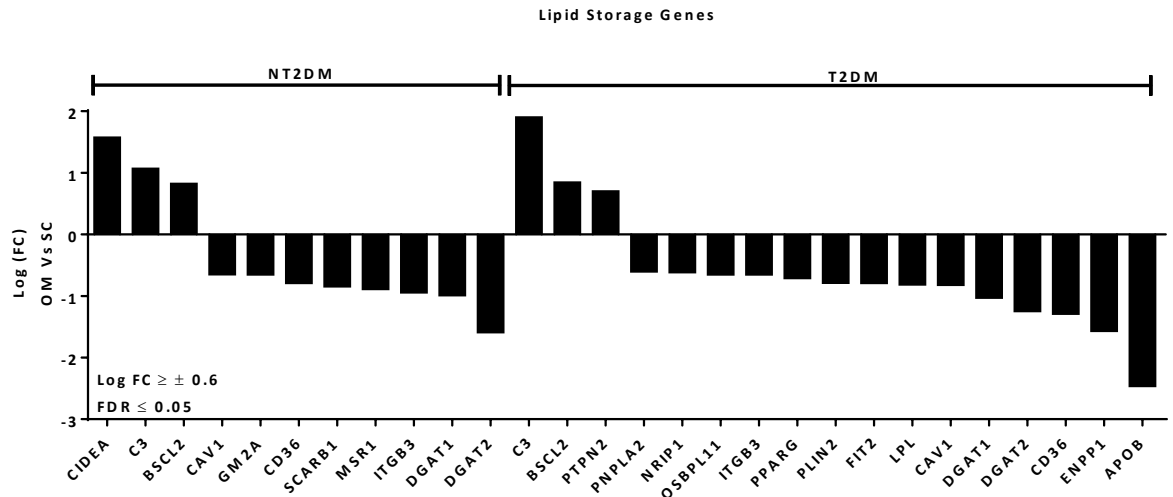


Figure 26: Lipid storage genes in NT2DM and T2DM subjects.

OM depot was compared to SC depot (OM vs SC). Most of the lipid storage genes were downregulated in OM adipose tissue, especially in T2DM subjects. FIT2 was significantly lower in OM depot only in T2DM subjects (FDR < 0.05).

FIT2 is an evolutionarily conserved endoplasmic reticulum (ER) membrane resident protein which plays a role in the partitioning of newly synthesized triacylglycerol (TAG) molecules into lipid droplets [51]. FIT or FITM family of proteins includes FIT1 (292 amino-acids, murine) and FIT2 (262 amino acids, murine) isoforms. In humans, FIT1 is expressed primarily in skeletal muscle tissue whereas FIT2 protein is known to be expressed ubiquitously, being highest in adipose tissue (figure 27) [47, 48]. Both FIT1 and FIT2 proteins have six transmembrane domains with N and C terminus facing the cytosol (figure 28) and specifically binds neutral triglycerides.

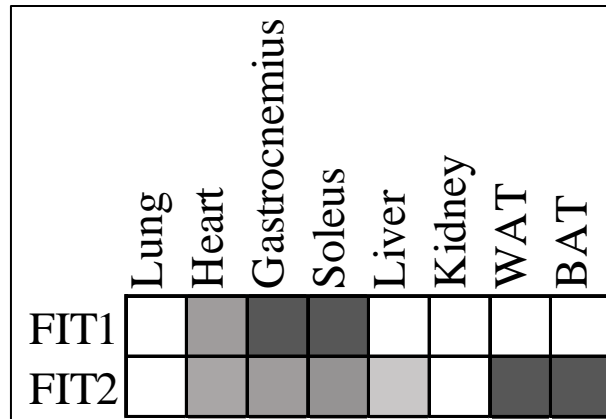


Figure 27: Expression pattern of FIT1 and FIT2 protein.

Analyzed by western blot in various tissues in mice. Figure adapted from Kadereit, B., et al [51]. Darker shade denotes higher protein expression and white boxes indicate zero expression.

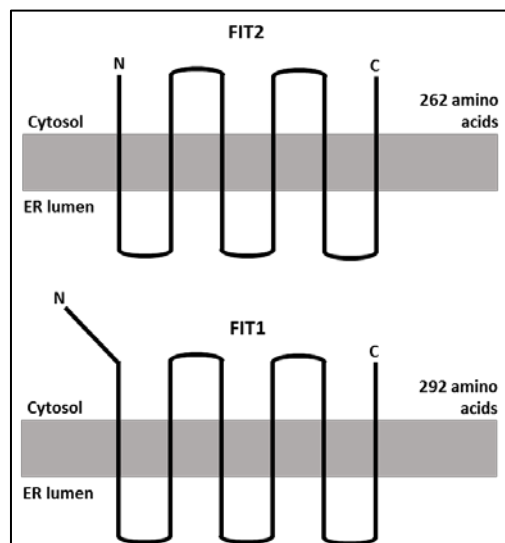


Figure 28: Schematic representation of FIT1 and FIT2 protein structure.

FIT1 contains 292 amino acids and FIT2 protein contains 262 amino acids. FIT1 has 30 extra amino acids at the amino terminus or N-terminus. Adapted from Gross, D.A., et al [47].

Dr. Silver's group showed that FIT2 protein expression increased with differentiation in 3T3-L1 adipocytes and its knockdown led to significant reduction in TAG accumulation, TAG biosynthesis, lipid droplet size and

perilipin protein expression [51]. Overexpression of FIT1 or FIT2 protein in HEK-293T cells increased lipid droplet formation without affecting TAG biosynthesis or lipolysis. However, differentiated adipocytes isolated from adipose tissue specific knockout mice (AF2KO mice) had similar TAG accumulation when compared to differentiated adipocytes from control mice, with significantly larger lipid droplets. These effects were more pronounced upon addition of oleic acid as a high fat challenge [155]. Mice with FIT2 overexpression in skeletal muscle (CFK2 mice) exhibit increased lipid droplets in muscle tissue, reduced body weight, fat mass and lean mass at 6 weeks of age. They also display increased oxygen consumption, glucose excursion rate, energy expenditure and complete protection from diet induced obesity [52]. The beneficial effects of FIT2 overexpression in skeletal muscle in these animals were attributed to re-patterning of muscle tissue metabolism such that glucose is directed towards glycerol-3-phosphate instead of glycolysis. Adipose tissue specific FIT2 knockout mice were lipodystrophic in phenotype with increased macrophage infiltration on high fat diet [155]. In 2012, a GWAS study has identified FIT2 as potential loci (SNP rs6017317) associated with type 2 diabetes in East Asians [108]. To date, the potential role of FIT2 protein in regulating human adipose tissue function has not been investigated. We hypothesized that lack of FIT2 protein in adipocytes would lead to its dysfunction through inflammation and ER stress pathways. Using siRNA mediated FIT2 knockdown in primary human adipocytes, we showed that FIT2 protein was required for efficient TAG storage and its deficiency increased IL6 and IL18 mRNA expression as well as IRE1 α phosphorylation and reduced Akt phosphorylation in primary human adipocytes.

4.2 Materials and Methods

4.2.1 Research design

Subcutaneous (SC) and omental (OM) adipose tissue and primary human adipocytes were obtained from obese non-diabetic (NT2DM) and obese diabetic (T2DM) subjects undergoing bariatric surgery (Table 15). After explaining the nature, purpose, potential and risks of the study, informed consent was obtained from all the subjects. Tissue samples from obese subjects were divided into aliquots for RNA isolation, protein lysate preparation (approx. 250 mg each, snap frozen) and for cell culture. For cell culture, approximately 2 g of the tissue was immersed in HEPES buffer (Gibco, Life Technologies) until isolation of adipocytes (within 4-6 h of obtaining the tissue). Ethics approval was directed by the National Healthcare Group Domain Specific Review Board.

Subjects		BMI	Age	HbA1C	Ethnicity
Obese (Tissue and primary adipocytes)	Diabetic (T2DM) (n=8)	40.7±9.8	43.5±11.3	8.88±1.19*	East Asians
	Non- diabetic (NT2DM) (n=8)	36±2.2	46.6±9.8	5.5±0.38	

Table 15: Characteristics of obese diabetic and obese non-diabetic subjects from whom adipose tissue was derived for FIT2 expression analysis.

* $P < 0.05$ when compared to the non-diabetics

4.2.2 Isolation and culture of adipocytes

Primary human adipocytes were isolated from tissues obtained during bariatric surgery using methods adapted from [156] and standardized in our lab. Briefly, fat tissue was collagenase digested, filtered, centrifuged and stromal vascular fraction (SVF) was used for cell culture. SVF obtained was plated for 3-4 days

in growth medium (DMEM high glucose, 15% fetal bovine serum (FBS), 1% non-essential amino acids (NEAA), 1% penicillin-streptomycin (pen-strep) and 5 ng/ml fibroblast growth factor) for cells to achieve fibroblastic morphology. At confluence, these cells were referred to as preadipocytes. They were either sub-cultured using growth medium or differentiated with help of Lonza differentiation medium for 10 days as recommended by the manufacturer (Lonza Walkersville, Inc.). A detailed protocol is described in section 2.4.1.

4.2.3 Free fatty acid preparation and treatment

Palmitic acid was prepared (section 2.4.3) as a 10 mM soluble conjugate with bovine serum albumin (fatty acid free, Sigma) as previously described [121] and stored at -20°C until use. For treatment with palmitic acid, medium in differentiated adipocytes was replaced with DMEM supplemented with 2% FBS and 1% pen-strep and required volume of conjugated palmitate was added for 24 h. Subsequently, adipocytes were serum starved for 2 h and insulin stimulated (100 nM) for 30 min before RNA or protein isolation.

4.2.4 FIT2 protein knockdown

For knockdown (section 2.5) using SiRNA (5 nM), preadipocytes at 70-80% confluence were transfected either with FIT2 specific (Cat No. SI02825417, Qiagen) or AllStars negative control SiRNA (Cat No.SI03650318) for 6 h in serum free and pen-strep free medium (DMEM, Gibco) using SiTRAN 1.0 transfection reagent (Cat No.TT300002, Origene, Rockville, MD). Transfection medium was replaced by growth medium after 6 h till cells reached full confluence and differentiation was then initiated (considered as day 0). SiRNA transfection was repeated at day 4 of differentiation and replaced with

differentiation medium till day 8. Figure 29 summarizes the key time points in this protocol.

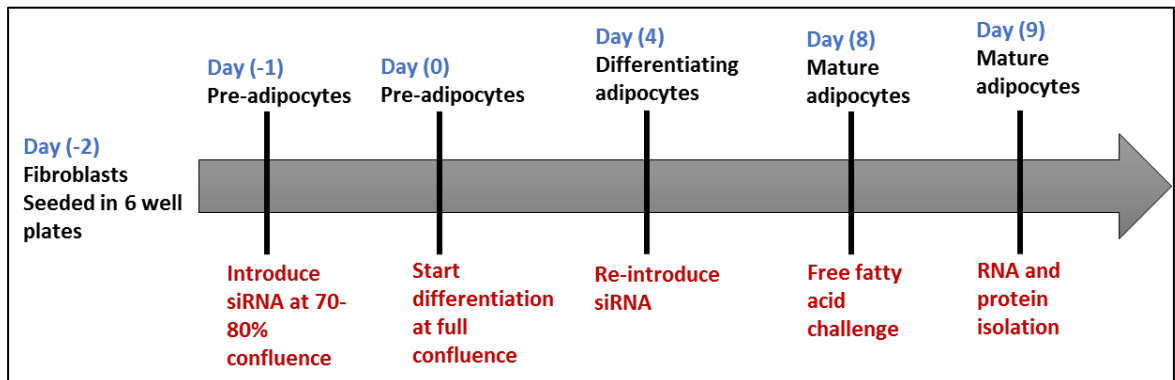


Figure 29: Key time points within protocol for siRNA transfection in primary human adipocytes.

4.2.5 TAG accumulation and lipid droplet size

Triacylglycerol (TAG) accumulation was quantified using AdipoRed kit (Nile red dye, a neutral lipid stain) by protocol suggested (Lonza) (section 2.4.5). Lipid droplet size was measuring by ImageJ (National Institutes of Health) using confocal images from Olympus FluoView FV1000. Nile red (AdipoRed) and Hoechst (cell signaling) were used to fluorescently label and visualize lipid droplets and nucleus respectively.

4.2.6 RNA isolation and Real time PCR

Cellular and Tissue RNA was isolated with Qiagen RNeasy plus mini kit and Qiagen RNeasy lipid tissue mini kit respectively (section 2.1.1 and 2.1.2). High-Capacity cDNA Reverse Transcription Kit (Life Technologies) was used to synthesize cDNA (approx. 300 – 500 ng RNA per sample). QuantiFast SYBR Green PCR Kit (Qiagen) was used to prepare reaction mixtures for quantitative PCR (qPCR) with concentrations suggested by manufacturer. Primers used are enlisted in table 20.

4.2.7 Protein isolation and western blot

Frozen ATs (about 150 mg) were homogenized in 500 μ L RIPA buffer [(supplemented with protease and phosphatase inhibitors (Cat No.78440)] using TissueLyser LT (Qiagen) and centrifuged at 15000 rpm for 40 min. Protein lysates (clear yellow to red layer fluid) were transferred to a new tube, snap frozen-thawed about 5 times in liquid nitrogen followed by centrifugation at 15000 rpm for 25 min to remove any residual lipid and tissue remnants. Lysates were separated using 10% acrylamide gel, transferred to PVDF membrane, blocked with 5% milk (0.1% Tween 20) and incubated with respective antibodies (as instructed by the manufacturer). Following antibodies were used; FIT2 (kind donation from Dr. David Silver, DUKE-NUS, Singapore), BiP, IRE1 α (ER Stress Antibody Sampler Kit #9956, Cell Signaling), p-IRE1 α (PA1-16927, Thermo Scientific), IRS-1 (06-248, Merck Millipore), p-IRS1 (Ser-307, sc-33956, Santa Cruz), p-IRS1 (Tyr-612, #09-432, Millipore), Akt 1/2/3 (sc-8312, Santa Cruz), p-Akt 1/2/3 (sc-7985-R, Santa Cruz), GAPDH (#2118, Cell Signaling). Respective HRP-conjugated secondary antibodies were used to incubate membranes for 2 h and exposed using ECL substrate (WBKLS0500, Merck Millipore). GAPDH was used as a loading control in all experiments. Detailed protocols discussed in section 2.3.

4.2.8 Insulin stimulated glucose uptake assay

Differentiated adipocytes were first incubated in serum-free DMEM supplemented with 0.2% BSA for 6 h prior to the assay (serum starvation). Subsequently, they were washed with PBS to remove glucose completely and were incubated in PBS supplemented with 0.2% BSA for 30 min at 37°C (glucose starvation). Next, cells were insulin stimulated (100 nM) for 15 min

and the assay was initiated by the addition of [³H] 2-deoxyglucose (5 μCi/mL) and deoxyglucose (5 mM). At the end of 20 min incubation, plates were placed on ice immediately and washed thrice with ice cold PBS. Cells were then lysed using RIPA buffer and contents were collected and incubated in ice for another 20 min. Finally, cell-associated radioactivity was determined using a liquid scintillation counter (Perkin Elmer). Detailed protocol discussed in section 2.6.

4.2.9 Statistical analysis

Statistical calculations were performed in GraphPad Prism version 6.00 for Windows (GraphPad Software, San Diego California USA) using non-parametric one-way ANOVA with Holm-Sidak correction for multiple comparisons. Values were expressed as mean ± SEM and P < 0.05 was considered statistically significant.

4.3 Results

4.3.1 FIT2 protein expression in adipose tissue is higher in obese non-diabetics when compared to obese diabetics

FIT2 mRNA and protein expression was quantified in SC and OM depots from obese T2DM and obese NT2DM subjects. Analysis of the results from SC and OM depots from individual subjects were paired to account for baseline variation. As seen in figure 30A, compared to SC depot, mRNA expression of FIT2 was significantly lower in OM depot derived from NT2DM (FC = 0.452 ± 0.094 P < 0.05) and T2DM (FC = 0.430 ± 0.091, P < 0.05) subjects. Protein densitometry (n=8 for all) from western blot (representative blots shown) showed that FIT2 protein expression (figure 30B and 30C) was higher in NT2DM compared to T2DM, in both SC (38.8 ± 14.15 vs 20.37 ± 13.67, non-

significant) and OM (32.75 ± 10.13 vs 11.05 ± 7.06 , $P < 0.05$) depots. Discordance between mRNA expression and protein expression data might be an outcome of regulation of translation level, but we have not explored these mechanisms. There are no known post transcriptional or post translational mechanisms regulating FIT2 protein expression.

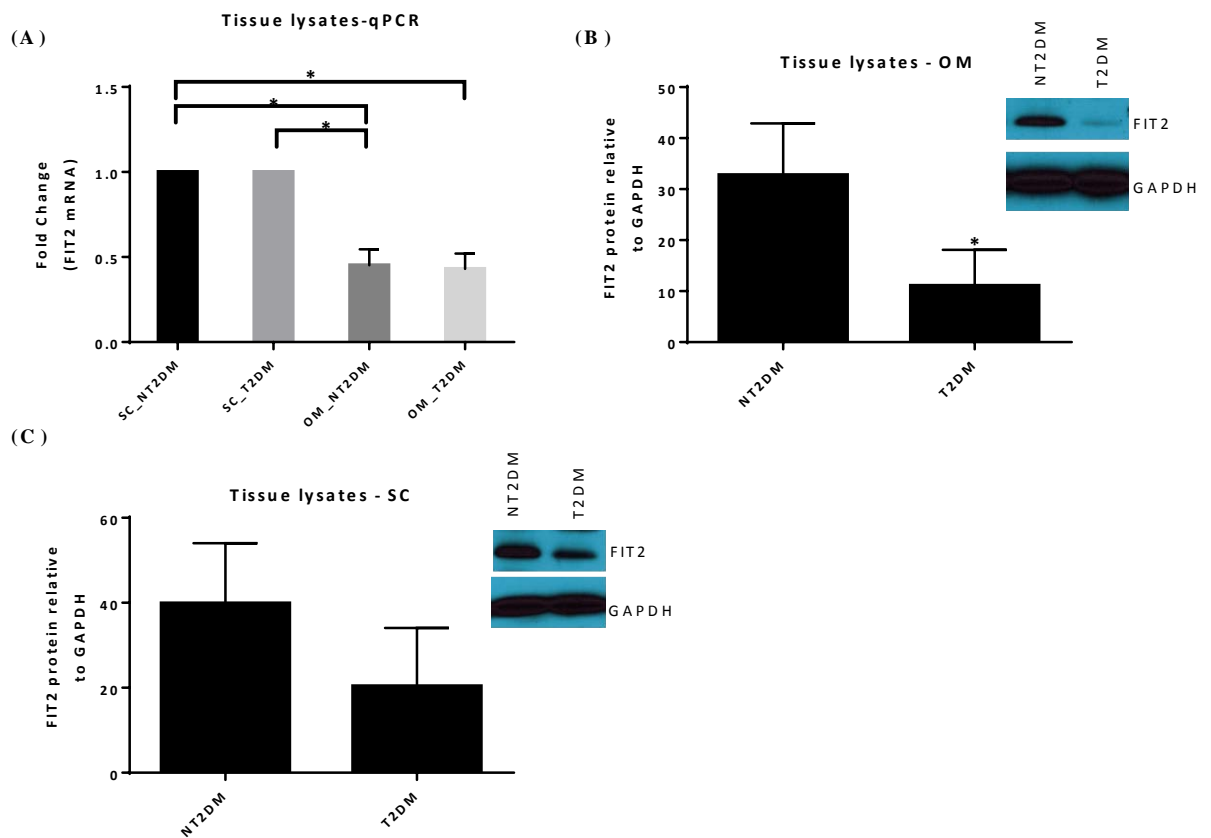


Figure 30: FIT2 protein expression in adipose tissue is higher in non-diabetics when compared to diabetics.

(A) FIT2 mRNA expression (qPCR) in SC and OM adipose tissue from obese subjects (NT2DM and T2DM, $n=5$ per group). SC and OM depots were paired for each subject. (B) and (C) FIT2 protein expression in OM and SC adipose tissue from obese non-diabetics and diabetics ($n=8$ per group). Data was analyzed using non-parametric one-way ANOVA, $*P < 0.05$. Data represented as mean \pm SEM.

4.3.2 FIT2 protein expression is higher in omental adipocytes from non-diabetics as compared to diabetics

Next, we quantified and compared FIT2 mRNA and protein expression in SVF derived primary human adipocytes. FIT2 expression was evaluated in differentiating and mature SC and OM adipocytes. In general, OM adipocytes took a longer time to differentiate and mature during adipogenesis with poorer terminal differentiation capacity at the end of 10 days. Independent of their adipogenic potential; FIT2 mRNA and protein expression was differentiation dependent in both SC and OM adipocytes. As expected, mature OM adipocytes expressed lower FIT2 mRNA ($FC = 0.565 \pm 0.063$, $P < 0.05$) when compared to SC adipocytes (figure 31A) (adipocytes from non-diabetics and diabetics were pooled together for studies comparing mRNA expression in different depots). Measured by densitometry ($n=7$, representative western blot shown), OM adipocytes from NT2DM subjects expressed higher FIT2 protein (39.10 ± 5.5 , $P < 0.05$) when compared to diabetics (22.43 ± 3.09) (figure 31B). Protein expression in SC adipocytes was similar between NT2DM and T2DM subjects. Due to poorer differentiation capacity and technical challenges with maintaining OM adipocytes, SC adipocytes were then used in all subsequent experiments. To verify if adipocytes increased TAG accumulation upon administration of free fatty acids and whether the TAG accumulation was influenced by FIT2 protein concentration, we quantified TAG accumulation before/after palmitic acid treatment in differentiated SC adipocytes. TAG accumulation at baseline, without palmitate treatment, did not correlate with FIT2 protein concentration (data not shown). However, TAG accumulation after 24 h palmitate treatment was directly proportional to FIT2 protein

concentration (quantified by western blots) present at baseline ($R^2 = 0.52$, $P < 0.001$) (figure 31C). These results support a vital role of FIT2 protein in TAG storage in adipocytes during conditions of high fat challenge or free fatty acid overload.

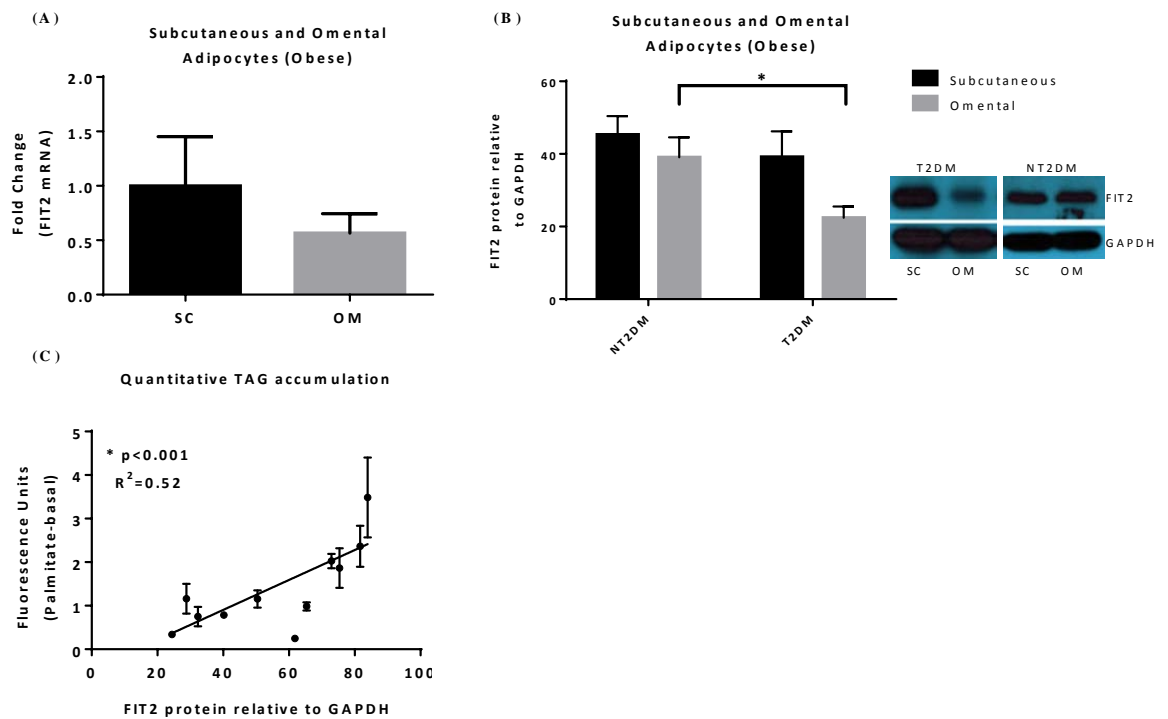


Figure 31: FIT2 protein expression is higher in omental adipocytes from non-diabetics as compared to diabetics.

(A) FIT2 mRNA expression (qPCR) in SC and OM adipocytes from obese subjects (NT2DM and T2DM, $n=6$). (B) FIT2 protein expression in SC and OM adipocytes from obese non-diabetics and diabetics ($n=7$). (C) Correlation of TAG accumulation with FIT2 protein quantity in SC adipocytes from obese non-diabetics and diabetics after palmitate treatment ($500 \mu\text{M}$, $n=10$). Data were analyzed using (A and B) non-parametric independent sample *t*-test and (C) Pearson's correlation, $*P < 0.05$. Data represented as mean \pm SEM.

4.3.3 TAG accumulation after FIT2 knockdown using siRNA

Next, we sought to examine effects of FIT2 protein knockdown in SC adipocytes, particularly on TAG accumulation. Preadipocytes were transfected with 5 nM of FIT2 specific (FIT2 KD adipocytes) or scrambled siRNA (negative control) and differentiated into mature adipocytes. At Day 8,

approximately 50% knockdown was observed in FIT2 mRNA and protein levels (figure 32A). PPAR γ and CEBP α mRNA expression did not differ with either siRNA, which indicated no effect on differentiation in these adipocytes (figure 32B). Next, TAG accumulation was measured before and after palmitate treatment in control and FIT2 KD adipocytes. Lipid droplets were imaged after staining them with AdipoRed. As seen in figure 32C, upon addition of palmitate, TAG accumulation increased significantly in control adipocytes (OD = 2.66 ± 0.298 , $P < 0.05$) and failed to increase significantly in FIT2 KD (OD = 1.36 ± 0.246) adipocytes. Apart from TAG accumulation, size of lipid droplets also determines their metabolic health and enzyme catabolic ability [157]. Previously, reports have observed increased lipid droplet size in adipocytes differentiated from adipose tissue specific FIT2 knockout mice [155] and smaller lipid droplet size after FIT2 knockdown in 3T3-L1 adipocytes [51]. We measured lipid droplet number and size (figure 32D) in images obtained after palmitate treatment in control (blue color) and FIT2 KD (red color) adipocytes using lipid droplet counter (ImageJ plugin) and observed no significant differences between the two groups. It is worth bearing in mind that in these experiments, we achieved ~50% knockdown of FIT2 protein; a higher percentage of FIT2 knockdown in SC adipocytes would be ideal to better appreciate functional effects of FIT2 in adipocytes. Overall, our observations supported the hypothesis that the lack of FIT2 protein in adipocytes would partially reduce the TAG storage capacity in them. Subsequently, we evaluated ER stress and inflammation in control and FIT2 KD adipocytes.

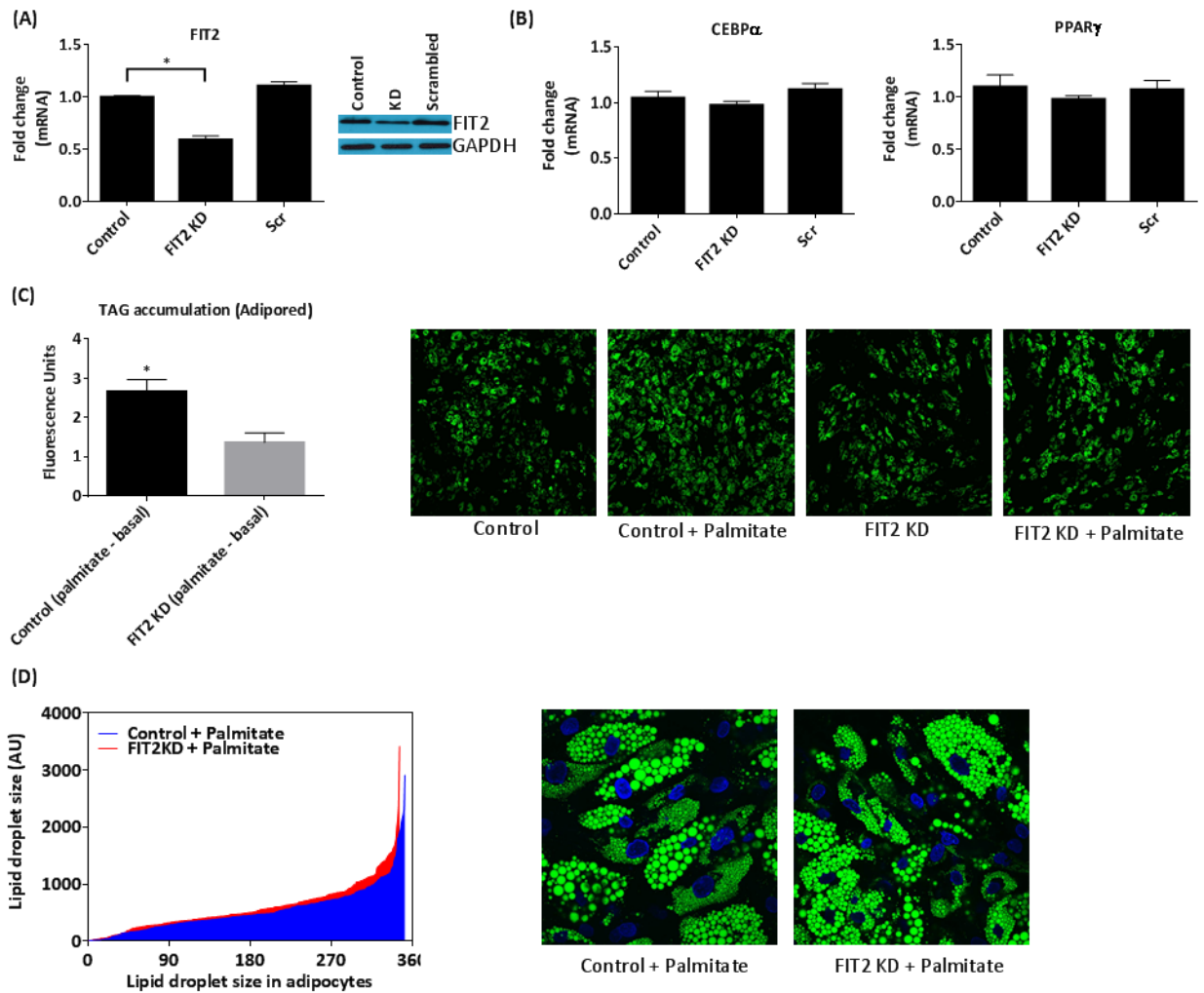


Figure 32: TAG accumulation is reduced after siRNA mediated knockdown of FIT2 protein

(A) mRNA expression (qPCR) and immunoblot of FIT2 in adipocytes transfected with FIT2 specific and scrambled (Scr) siRNA. (B) mRNA expression of differentiation markers PPAR γ and CEBP α in adipocytes after FIT2 KD (n=3). (C) TAG accumulation upon palmitate treatment (500 μ M) in control and FIT2 KD adipocytes with representative images (n=3). (D) Quantification of lipid droplet size (with representative images) in control and FIT2 KD adipocytes after palmitate treatment (500 μ M, n=3). Data were analyzed using non-parametric one-way ANOVA with Holm-Sidak correction for multiple comparisons, * $P < 0.05$ compared to control adipocytes. Data represented as mean \pm SEM.

4.3.4 Effect of palmitic acid on inflammation and ER stress in FIT2 KD adipocyte

We measured gene expression of various markers of inflammation and ER stress in SC adipocytes after FIT2 KD and palmitate treatment for 24 h. Figure 33

shows the relative expression levels of four inflammatory genes measured by qPCR. Pro-inflammatory markers IL18 (FC = 1.29 ± 0.118 , $P < 0.05$) and IL6 (FC = 2.37 ± 0.198 , $P < 0.05$) were upregulated in control adipocytes after addition of palmitic acid which suggests inflammatory response to free fatty acid. However, in FIT2 knockdown adipocytes, IL18 (FC = 1.89 ± 0.054 , $P < 0.05$) and IL6 (FC = 1.35 ± 0.95 , $P < 0.05$) were upregulated even in absence of palmitic acid which indicated low grade inflammation without external free fatty acid challenge. Upon addition of palmitic acid in FIT2 KD adipocytes, IL6 (FC = 2.04 ± 0.113 , $P < 0.05$) mRNA expression increased significantly. TLR4 and IL1 β expression were unchanged either in FIT2 knockdown or palmitate challenged states.

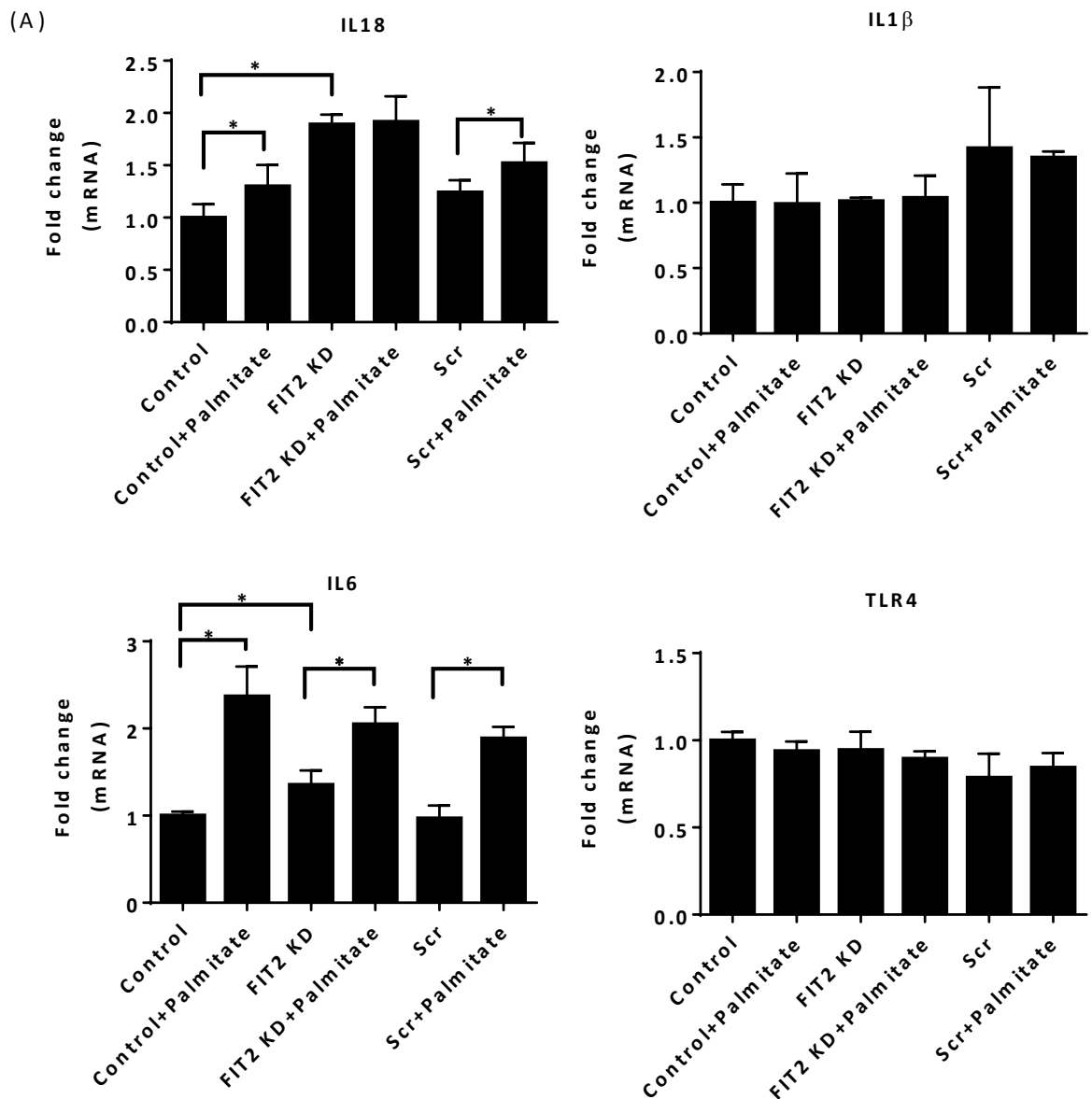


Figure 33: Effect of palmitic acid on inflammation related genes in FIT2 knockdown adipocytes.

(A) mRNA expression of IL18, IL1 β , IL6 and TLR4 in control and FIT2 KD adipocytes ($n=3$). Data were analyzed using non-parametric one-way ANOVA with Holm-Sidak correction for multiple comparisons (Prism 6.0), * $P < 0.05$. Data represented as mean \pm SEM.

Figure 34A and 34B illustrates mRNA and protein expression of ER stress markers. In control adipocytes, mRNA expression of ER stress markers BiP (FC = 1.92 ± 0.039), XBP1s (FC = 2.51 ± 0.256), CHOP (FC = 1.70 ± 0.058), GADD34 (FC = 1.44 ± 0.043) and PERK (FC = 1.35 ± 0.060) increased

significantly after addition of palmitic acid. Conversely, compared to control adipocytes, palmitate induced upregulation of ER stress markers BiP (FC = 1.74 ± 0.018), XBP1s (FC = 1.61 ± 0.030), CHOP (FC = 1.10 ± 0.279), GADD34 (FC = 1.04 ± 0.14) and PERK (FC = 1.17 ± 0.049) was alleviated in FIT2 KD adipocytes. While blotting for proteins (BiP, p-IRE1 α , t-IRE1 α , p-JNK, t-JNK and GAPDH), we included insulin stimulation (every alternate band in blots) as previous reports suggested insulin as an inducer of ER stress in subcutaneous adipose tissue in obese insulin resistant subjects [84]. BiP, t-IRE1 α , p-JNK and t-JNK showed no change in protein expression. However, insulin stimulation increased p-IRE1 α (6th well in blot) in FIT2 KD adipocytes without palmitate treatment and after addition of palmitic acid, p-IRE1 α was upregulated with or without insulin in them. These results indicated activation of IRE1 α arm of ER stress pathway in FIT2 KD adipocytes, especially after treatment with free fatty acid.

PGC1 α (FC = 0.601 \pm 0.027 in control and FC = 0.700 \pm 0.017 in FIT2 KD) and increased mRNA expression of leptin (FC = 1.29 \pm 0.049 and FC = 1.31 \pm 0.025 in FIT2 KD).

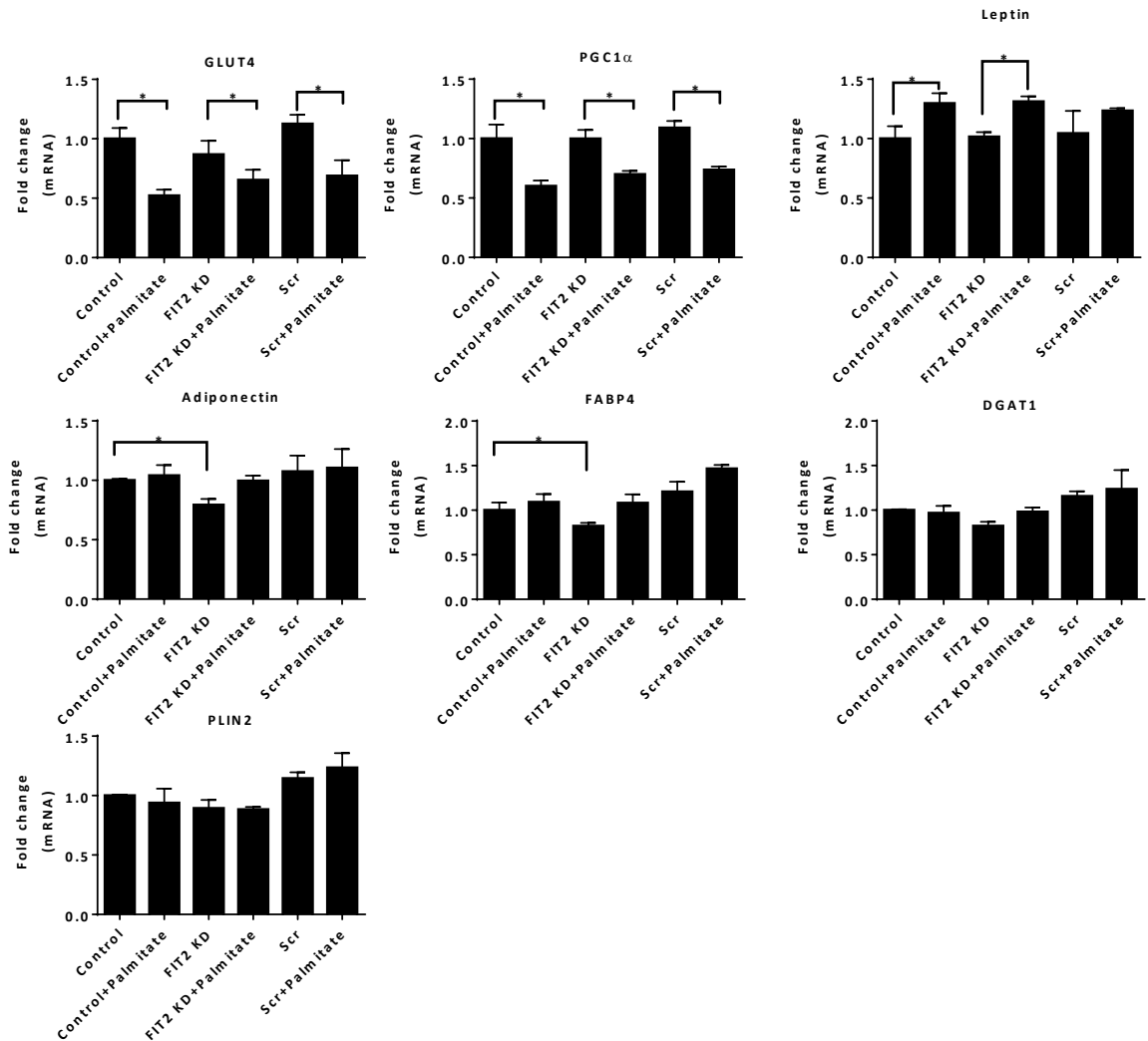


Figure 35: Effect of palmitic acid on adipogenesis related genes in FIT2 knockdown adipocytes.

Markers for various aspects of adipose tissue were chosen. Data was analyzed using non-parametric one-way ANOVA with Holm-Sidak correction for multiple comparisons, * $P < 0.05$. Data represented as mean \pm SEM.

4.3.5 Effect of palmitic acid on insulin signaling pathway proteins and glucose uptake in FIT2 knockdown adipocytes

Insulin signaling pathway proteins are known to be altered *in vitro* in the presence of excess free fatty acids such as palmitate. In our study, we

immunoblotted for p-Akt (Ser-473), t-Akt, p-IRS1 (Ser-312), p-IRS1 (Tyr-612), t-IRS1 and GAPDH in both control and FIT2 KD adipocytes (figure 36A). p-Akt (Ser-473)/ t-Akt was measured by densitometry and represented in bar graph beneath western blots. The left-sided Y-axis denotes ratio from all bands separately (represented as bars in the graph) and right-sided Y-axis (red colored dots) denotes the ratio as insulin stimulated/no insulin for respective conditions. A decrease in pAkt (Ser-473)/ t-Akt ratio after insulin stimulation is representative of insulin resistance. In control adipocytes, phosphorylation of t-Akt (represented as p-Akt (Ser-473)) increased after addition of palmitic acid whereas in FIT2 KD adipocytes, p-Akt (Ser-473) remained high with or without palmitic acid. As seen from red dots in graph, insulin stimulated p-Akt (Ser-473)/ t-Akt ratio was lower in control adipocytes after addition of palmitate which indicated that they were insulin resistant. However, in FIT2 KD adipocytes, this ratio was significantly reduced with and without palmitate treatment indicating insulin resistance even in the absence of external free fatty acid challenge. Compared to control adipocytes, protein expression of t-IRS1, p-IRS1 (Ser-312) and p-IRS1 (Tyr-612) were lower in FIT2 KD adipocytes, which further dropped in the presence of palmitic acid. Near complete disappearance of IRS1 proteins was unexpected. The Probability of cytotoxicity due to knockdown or palmitate treatment cannot be excluded, but is unlikely since other ER stress and insulin signaling proteins did not follow similar expression pattern. Insulin stimulated glucose uptake is shown in figure 36B. Glucose uptake was measured as beta counts/minute and represented on the Y-axis as a ratio of insulin stimulated/no insulin for respective condition. Palmitic acid administration lead to a non-significant reduction in glucose uptake in

control as well as FIT2 KD adipocytes. But glucose uptake was significantly reduced in FIT2 KD adipocytes (1.23 ± 0.062 , $P < 0.05$) at basal state compared to control adipocytes (1.46 ± 0.037) at basal state.

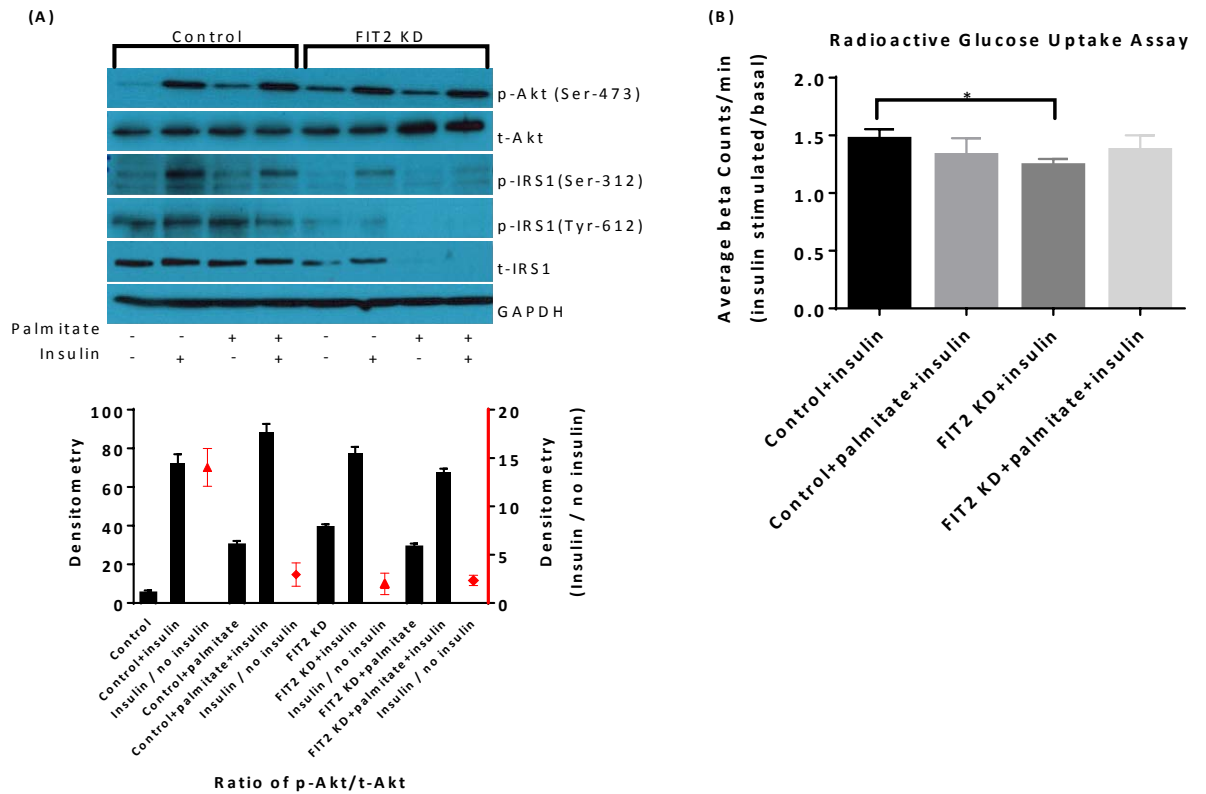


Figure 36: Effect of palmitic acid on insulin signaling pathway proteins and glucose uptake in FIT2 knockdown adipocytes.

(A) Immunoblot of critical proteins involved in insulin signaling pathway [p-Akt (Ser-473), t-Akt, p-IRS1 (Ser-312), p-IRS1 (Tyr-612) and t-IRS1]. Graph represents densitometry for p-Akt/Akt protein and Insulin/no insulin ratio of respective conditions is represented on right y-axis (red symbols and axis). (B) Glucose uptake in mature control and FIT2 KD adipocytes. Data were analyzed using non-parametric one-way ANOVA with Holm-Sidak correction for multiple comparisons, $*P < 0.05$. Data represented as mean \pm SEM.

4.4 Discussion

For the first time, we characterized the role of FIT2 protein in human adipocytes and found that it was important for maintaining healthy adipocyte function. Our results indicated that (1) FIT2 mRNA expression was significantly higher in SC adipose tissue or adipocytes when compared to OM adipose tissue or

adipocytes, (2) FIT2 protein expression was significantly higher in SC and OM adipose tissue samples from NT2DM subjects when compared to T2DM subjects, (3) TAG accumulation after palmitate administration was reduced after FIT2 knockdown in SC adipocytes, (4) basal state mRNA expression of IL18 and IL6 were higher in FIT2 KD adipocytes along with upregulation of p-IRE1 α and (5) Ratio of p-Akt (Ser-473)/t-Akt (insulin stimulated/no insulin) was lower in FIT2 KD adipocytes when compared to control adipocytes. At this stage it would be difficult to conclude that individuals expressing lower FIT2 protein will definitely have reduced lipid storage capacity. But this is supported by the fact that adipose tissue specific FIT2 knockout mice exhibit reduced adipose tissue volume, ectopic lipid deposition, impaired insulin tolerance and increased macrophage infiltration on high fat diet [155].

Previous studies have highlighted the importance of adipose tissue function and appropriate regulation of adipose inflammation in preserving metabolic health [158, 159]. A recent study in humans showed increased visceral adipose tissue (and not subcutaneous adipose tissue) as a crucial predictor for progression of obese non-diabetics to obese diabetics [160]. In particular, IL6 originating from the visceral adipose tissue is thought to be a potential mechanistic link between visceral obesity and systemic inflammation in individuals with abdominal obesity [161] and increased IL6 mRNA expression is also observed in EWAT from adipose tissue specific FIT2 knockout mice on high fat diet [155]. In our study, pro-inflammatory markers IL6 and IL18 were significantly higher at basal state in FIT2 KD adipocytes when compared to control adipocytes. However, only negligible upregulation was observed in IL18 and IL6 mRNA

expression in FIT2 KD adipocytes after palmitate administration which could be due to higher mRNA expression at basal state.

ER stress and UPR mechanisms are known pathogenic pathways especially in metabolically active tissues such as adipose tissue, liver and pancreas [93, 162]. Studies have found upregulated expression of calnexin and p-JNK 1 proteins as well as XBP-1s mRNA in obese individuals [83]. Increased UPR in adipose tissue among obese individuals has also been associated with increased insulin concentration and its protein synthetic or anabolic signal in adipose tissue [84]. Insulin induced UPR was observed in FIT2 KD adipocytes as IRE1 α phosphorylation was higher upon insulin stimulation. On palmitate challenge, p-IRE1 α upregulation was observed even without insulin stimulation in FIT2 KD adipocytes. BiP, XBP1s, CHOP and GADD34 mRNA expression increased significantly and more markedly upon palmitate challenge in control adipocytes when compared to FIT2 KD adipocytes which suggest two possibilities; either FIT2 KD adipocytes have defective UPR sensing mechanisms or they induce and propagate UPR pathways earlier. The Second mechanism seems more plausible since we observed an upregulation of protein expression of p-IRE1 α in FIT2 KD adipocytes.

Insulin signaling pathways involve numerous proteins and we blotted for established markers of insulin resistance after free fatty acid challenge [163-165]. Decreased ratio of p-Akt (Ser-473)/t-Akt before and after insulin stimulation is a direct representation of insulin resistance and was reduced at basal and palmitate challenged states in FIT2 KD adipocyte indicating insulin resistance. Overall, partial absence of FIT2 protein was detrimental to the optimal function of mature human adipocytes as demonstrated by upregulation

of pro-inflammatory markers at basal level, increased phosphorylation of IRE1 α on free fatty acid challenge and reduced glucose uptake.

4.5 Conclusion

Involvement of lipid droplet formation proteins in the pathogenesis of metabolic disorders is a relatively new field of research. Our results demonstrated probable mechanistic links between a GWAS gene candidate (FIT2) and adipose tissue dysfunction in humans.

Chapter 5:

FTO protein knockdown or chemical inhibition of FTO can increase energy expenditure in human adipocytes

5.1 Introduction

Genome Wide Association Studies (GWAS) has been an important approach for identification of gene locus or loci responsible for pathogenesis of multigenic disorders such as Type II diabetes [166]. In 2007, SNPs in first intron of Fat Mass and Obesity (FTO) associated gene was found to be strongly linked to early onset obesity in children and adults of European ancestry [111, 112]. Subsequently, more SNPs in first two introns and second exon of FTO gene were also found to be strongly linked with an increased risk of obesity in both children and adults [167, 168]. To date, FTO locus has showed largest effect size on BMI and obesity risk and is most widely replicated in more than 22 different ethnic populations including Chinese, Malay and Asian-Indian populations in Singapore [169-172]. FTO protein is a member of AlkB related non-haem iron and 2-oxoglutarate-dependent oxygenase superfamily. It was initially identified as single stranded DNA and RNA demethylase or dioxygenase (particularly N6-methyladenosine) [173], and later established to be a transcriptional coactivator of CEBP proteins active in promoting adipogenesis [174]. A second link between FTO and adipogenesis was confirmed by Merkestein, M et al [175]. They showed that FTO leads to alternative splicing of RUNX1T1 mRNA due to demethylation at N6-methyladenosine, which in turn induce mitotic clonal expansion of mice derived pre-adipocytes.

FTO is ubiquitously expressed across multiple tissues, but is most highly expressed in brain, especially the hypothalamus, a region which controls food intake [176]. Human studies suggest that the association between SNPs in FTO and BMI are predominantly driven by increased energy intake and not energy

expenditure [177-179]. For instance, individuals homozygous for the obesity-risk allele present with greater ad libitum food intake [180], particularly consumption of dietary fat [181] along with increased appetite and reduced satiety [182]. Within the arcuate nucleus of the hypothalamus, prolonged exposure to high fat diet increased FTO expression, whereas 48 h fasting reduced FTO expression, [176]. Conversely, alteration of FTO level in the arcuate nucleus also influenced food intake [183]. The presence of FTO SNP (rs1421085 T-to-C) in primary human adipocytes transformed them from an energy expending adipocyte phenotype to a more lipid storing white adipocyte phenotype and correction of this particular SNP reversed them to energy expending phenotype. Detailed studies showed that FTO SNP induced expression IRX3 and IRX5 genes, which in turn drive adipocyte towards white lipid storing phenotype [184].

Recently, several animal studies have shown the effect of FTO on body weight regulation and energy expenditure through peripheral actions of FTO [117, 185]. FTO null mice exhibit a significant reduction in adipose tissue and a decreased propensity towards weight gain on a high-fat diet (HFD), compared with their wild-type littermates. The lean phenotype in these mice developed as a consequence of increased energy expenditure and systemic sympathetic activation, despite decreased physical activity and hyperphagia [117]. Detailed molecular mechanisms by which FTO dioxygenase inhibition regulates energy metabolism in human adipocytes remains to be elucidated. The aim of this research was to characterize the function of FTO in human SGBS adipocyte metabolism using two approaches (I) gene silencing or knockdown and (II) using a novel pharmacologic inhibitor (CA) of FTO catalytic activity. SGBS

adipocytes was a preferred model over SC adipocytes in this instance since our previous results suggest that the SGBS is a human preadipocyte model that has capacity for displaying the bioenergetics characteristics of brown/beige adipocytes.

5.2 Materials and methods

5.2.1 Cell culture and differentiation and drug treatment of SGBS adipocytes

SGBS adipocytes were cultured and differentiated as discussed previously in section 2.4.2. For drug treatment, adipocytes were differentiated for 6 days either in 6-well plates (for RNA and protein expression) or XF^c24-well cell culture microplate (for measuring mitochondrial respiration). Subsequently, drug CA was added at 50 μ M and 100 μ M concentration and incubated for 48 h for all experiments.

5.2.2 Protein knockdown using FTO specific siRNA

SGBS adipocytes were transfected with FTO specific or scrambled siRNA at 5 nM concentration (protocol section 2.5).

5.2.3 Preparation of protein lysates and western blotting

Cell monolayers were washed with cold phosphate buffered saline and lysates were collected in 80 μ L RIPA buffer (Thermo Scientific) using a cell scraper. Detailed protocol of lysate preparation and immunoblotting can be found in section 2.5.

5.2.4 RNA isolation and mRNA expression analysis

RNA was isolated using Qiagen RNeasy plus kits (section 2.1). cDNA was synthesized and used for expression analysis (section 2.2).

5.2.5 Measurement of mitochondrial respiration

Oxygen consumption rate (OCR) was measured in mature SGBS adipocytes. Cells were drug treated for 48 h before performing this experiment (section 2.8). OCR reading was used to compute mitochondrial function parameters.

5.3 Results

5.3.1 FTO knockdown and inhibition increased mRNA expression of PGC1 α and UCP1 in SGBS adipocytes

SGBS and 3T3-L1 adipocytes were transfected with 5 nM of either species specific siRNA against FTO (siRNA_1 and siRNA_2) or scrambled siRNA (negative control). Transfection was performed at preadipocyte stage and maintained throughout differentiation. Drug CA (50 μ M and 100 μ M) and DMSO vehicle control (equivalent to 100 μ M CA volume) were added to partially mature adipocytes at day 6 of differentiation for 48 h. As seen in figure 37A, FTO mRNA and protein was successfully reduced to approximately 50% with two different siRNA transfections, while there was no change with the addition of drug CA, scrambled siRNA and DMSO vehicle control. Differentiation marker, PPAR γ mRNA expression remain unchanged either with siRNA transfection or drug treatment (figure 37B). PGC1 α and UCP1 gene expression increased significantly after FTO knockdown using siRNA_1 (FC = 1.93 ± 0.12 in PGC1 α , FC = 3.02 ± 0.105 in UCP1) and siRNA_2 (FC = 3.26 ± 0.23 in PGC1 α , FC = 3.58 ± 0.523 in UCP1) as well as chemical inhibition using

drug CA at 50 μM ($\text{FC} = 1.83 \pm 0.186$ in $\text{PGC}\alpha$, 1.42 ± 0.24 in UCP1) and 100 μM ($\text{FC} = 2.53 \pm 0.142$ in $\text{PGC}\alpha$, 3.12 ± 0.257 in UCP1) concentration (Figure 37C and 37D).

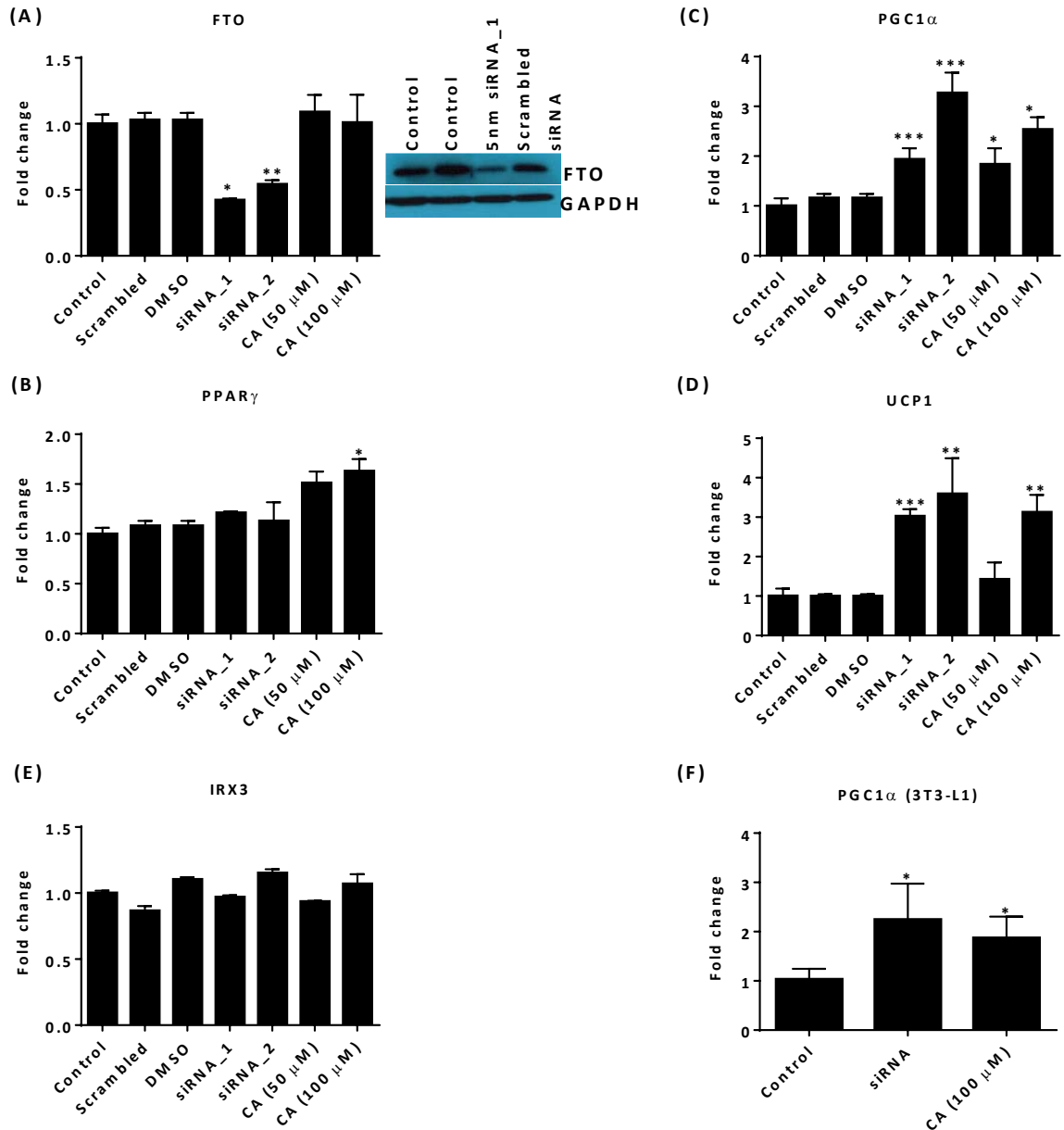


Figure 37: Effect of FTO knockdown and drug inhibition on browning genes in SGBS and 3T3-L1 adipocytes.

(A) FTO mRNA and protein (B), (C), (D) and (E) mRNA expression of PPAR γ , PGC1 α , UCP1 and IRX3 respectively. (F) PGC1 α mRNA expression in 3T3-L1 adipocytes. Fold change as normalized using GAPDH in SGBS and beta actin in 3T3-L1 adipocytes. * $P < 0.05$, ** $P < 0.005$, *** $P < 0.0001$. Data represented

as mean ± SEM. Significance was calculated using Two-Way Anova (with Dunnett's correction for multiple comparisons).

IRX3 mRNA expression remained unchanged in all experimental conditions (figure 37E). Similar to SGBS, FTO knockdown (FC = 2.24 ± 0.22 , $P < 0.05$) and inhibition (100 μ M CA, FC = 1.87 ± 0.13 , $P < 0.05$) increased mRNA expression of PGC1 α in differentiated 3T3-L1 adipocytes as well (figure 37F). Expression of all genes remain unchanged in scrambled siRNA transfected and DMSO vehicle control treated wells.

5.3.2 FTO inhibition using drug CA potentiated spare respiratory capacity and maximal respiration rate

To determine whether upregulation in PGC1 α and UCP1 was functionally relevant, Seahorse mitochondrial flux analyzer was used to measure mitochondrial respiration in SGBS adipocytes treated with 50 μ M or 100 μ M CA or DMSO vehicle control for 48 h. Seahorse flux analyzer uses oligomycin, FCCP and a combination of antimycin A + rotenone sequentially to evaluate mitochondrial activity. FCCP (Carbonyl cyanide 4-(trifluoromethoxy) phenylhydrazone) is an uncoupler of oxidative phosphorylation and allows mitochondria to function at maximal efficiency and oxygen consumption at any stage is representative of mitochondrial activity. Figure 38A and 38B shows mitochondrial respiration as line graph and mitochondrial function parameters as bar graph respectively. Addition of CA did not alter basal respiration (measured before addition of oligomycin), ATP production and proton leak (measured after adding oligomycin). But, compared to control SGBS adipocytes (OCR = 77.8 ± 10.3), maximal respiration rate increased significantly with 50 μ M (OCR = 126.7 ± 10.9 , $P < 0.05$) and 100 μ M (OCR = 97.5 ± 7.2 , $P < 0.05$)

drug CA. Spare respiratory capacity (maximal respiration – basal respiration) also improved significantly at 50 μ M CA (OCR = 80.6 ± 11.4 compared to 40.7 ± 14.7 in controls, $P < 0.05$). Surprisingly, maximal and spare respiratory capacity increased maximally at 50 μ M CA, which suggested an optimum working range of the drug. All the readouts were equivalent in control and DMSO treated SGBS adipocytes. These results confirmed that chemical inhibition of FTO catalytic activity potentiates mitochondrial activity in SGBS adipocytes.

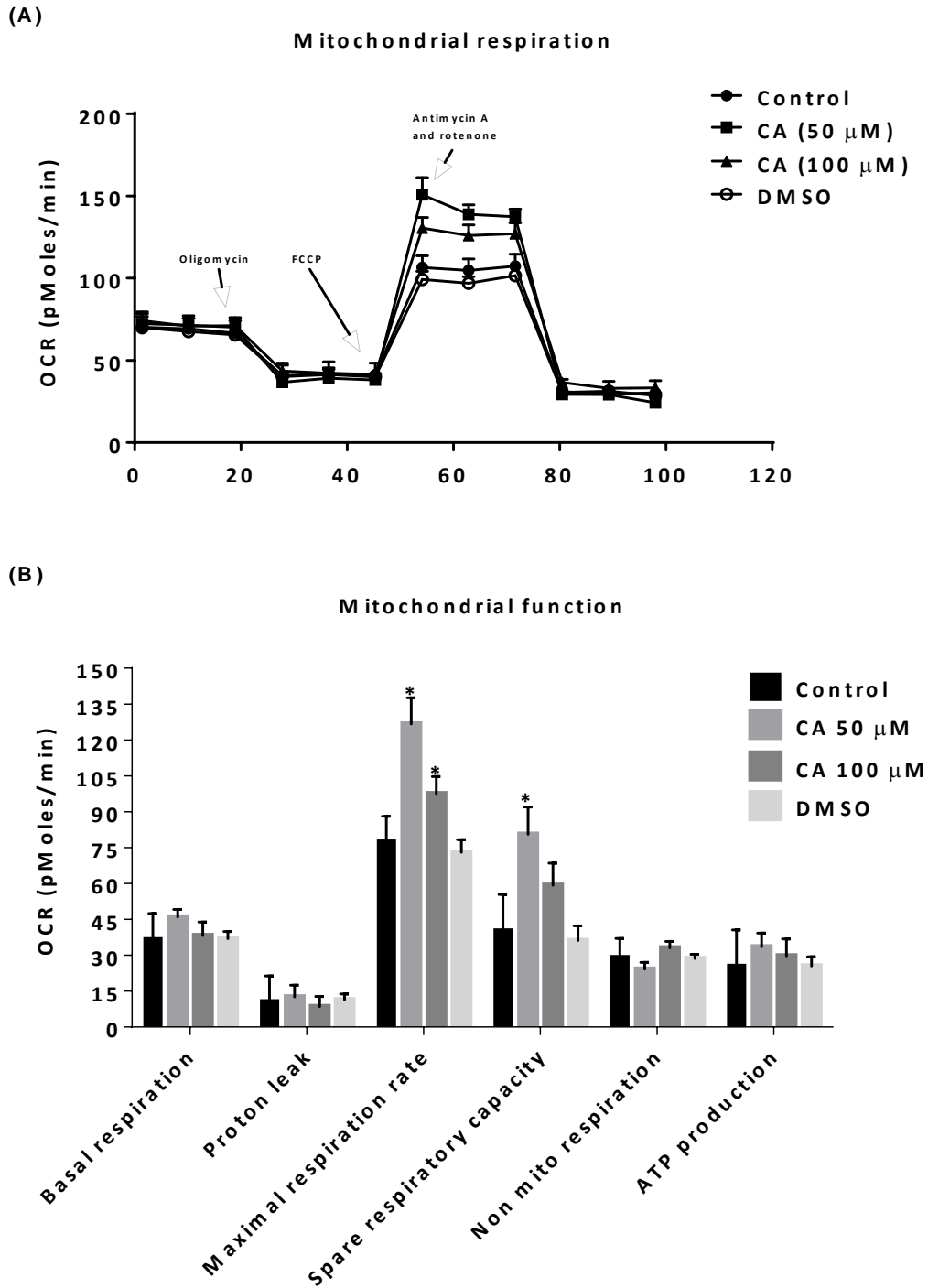


Figure 38: Effects of FTO drug inhibition on mitochondrial respiration and function in SGBS adipocytes.

(A) OCR as measured in Seahorse mitochondrial flux analyzer. (B) Mitochondrial function parameters computed from OCR measurements. * $P < 0.05$ when compared with control adipocytes. Data represented as mean \pm SEM. Significance was calculated using Two-Way Anova (with Dunnett's correction for multiple comparisons).

5.3.3 FTO knockdown and inhibition increased AMPK α phosphorylation

We evaluated t-AMPK α and p-AMPK α protein in SGBS adipocytes with FTO knockdown, CA treatment (50 μ M, 48 h) or both in presence/ absence of insulin. Compared to control adipocytes (figure 39), p-AMPK α increased after FTO protein knockdown and addition of 50 μ M CA for 48 h. Combination of knockdown and CA also elevated p-AMPK α similar to drug only well. p-AMPK α levels reduced after insulin treatment in all conditions. FTO knockdown and inhibition resulted in increased AMPK phosphorylation which might potentially have increased mitochondrial respiration and PGC1 α mRNA expression seen previously, although further research is required to confirm this.

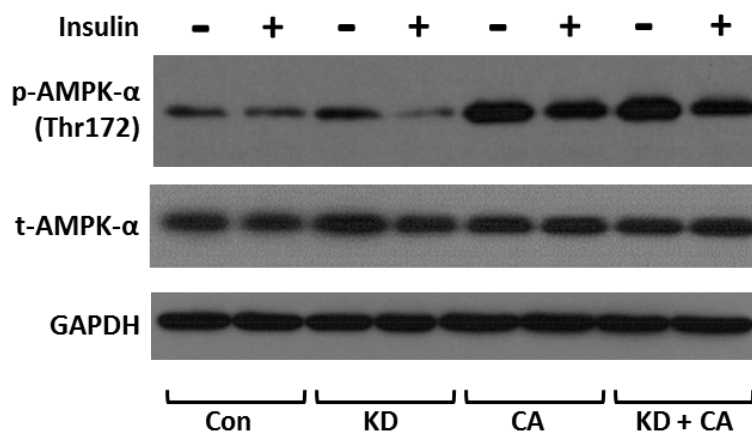


Figure 39: Effect of FTO knockdown and drug inhibition on AMPK α phosphorylation in SGBS adipocytes.

Knockdown was maintained throughout 8 days of differentiation and drug treatment was performed for 48 h starting from day 6.

5.4 Discussion

Single nucleotide polymorphisms (SNPs) in Fat Mass and Obesity Associated gene locus have been the strongest candidate for obesity phenotype across various ethnicities around the world. Studies have identified pathways through which FTO gene locus influences expression or function of FTO, IRX3 and

RPGRIP1L gene expression or protein activity [117, 184, 186-189]. Upon advances in understanding the molecular regulation of energy expenditure, activating energy expending pathways such as oxidative respiration to improve metabolic health of adipocytes and other cell types is being commonly targeted as a potential therapeutic modality to treat obesity. In our study, we tested an inhibitor (drug CA) specific towards dioxygenase or demethylase activity of FTO and evaluated its effect on mitochondrial function in SGBS adipocytes.

In all cell types in humans, mitochondrial biogenesis and adaptive thermogenesis are regulated primarily by upstream transcriptional coactivator PGC1 α in conjunction with NRF1 (nuclear respiratory factor 1) which is strongly activated by cAMP and cytokine pathways [190]. In adipocytes particularly, PGC1 α leads to formation of metabolically active brown (constitutive UCP1 expression) or beige adipocytes (inducible UCP1 expression) possessing inherent capacity for increased mitochondrial respiration, production of heat and free fatty acid oxidation [191-193]. In our data, FTO inhibition and knockdown increased PGC1 α and UCP1 expression which indicated a brown or beige phenotype. Studies suggest that IRX3 and RPGRIP1L are main drivers for activation of energy expending pathways due to presence of obesity associated SNP in FTO gene and not the FTO protein itself. However, the involvement of IRX3 can be excluded in our study since drug inhibition acts directly on FTO protein and no change was observed in IRX3 mRNA expression with either FTO knockdown or drug inhibition. In addition to elevated PGC1 α , maximal respiratory capacity and spare respiratory capacity were significantly increased at 50 μ M drug CA; suggesting an important role for RNA demethylase activity of FTO in forming metabolically

active adipocytes. RNA with N6 methyl-adenosine is shown to be a substrate of FTO [173, 194] and studies show that FTO overexpression enhances adipogenesis in mice derived pre-adipocytes via alternative splicing of pro-adipogenic gene RUNX1T1 [175]. AMPK pathway is actively involved in regulation of mitochondrial function at both transcriptional and post-translational levels [195] and it also influences coactivator function of PGC1 α with help of SIRT1. FTO knockdown and inhibition increased phosphorylation of AMPK α which might may explain the increased mitochondrial function but needs further validation. Though, recently, IOX3, an inhibitor of HIF prolyl hydroxylases (also known to inhibit FTO) was found to increase FTO protein expression, AMPK α phosphorylation and mitochondrial respiration in C2C12 cells [196], drug treatment in our study did not influence FTO mRNA or protein expression. These differences in results could be due to (I) cellular model used (C2C12 myotubes used previously versus SGBS adipocytes used in our study) and (II) broad specificity of IOX3 unlike CA which is highly specific for FTO protein. Altogether, we confirmed the involvement of FTO protein in influencing PGC1 α expression and successfully tested the ability of an FTO inhibitor to increase mitochondrial respiration.

5.5 Conclusion

Our results show that inhibiting demethylase activity of FTO by drug CA led to increased UCP1 and PGC1 α mRNA expression along with elevated mitochondrial respiration in SGBS adipocytes; a phenotype similar to FTO protein knockdown. Collectively, these findings support plausible utility of pharmacological FTO inhibition as anti-obesity drugs

Chapter 6:

Transcriptomic analysis reveals a role for extracellular matrix and fibrosis pathways in maintaining healthy human adipose tissue function in obese non-diabetics

6.1 Introduction

White adipose tissue (WAT) distribution in different depots (SC or OM) and anatomical regions (central vs peripheral) of the body is an important determinant of metabolic homeostasis [197]. Even in lean individuals, a higher proportion of central to peripheral adipose tissue mass can increase the risk of insulin resistance in them [198]. Adipocytes within different depots are distinct in their metabolic capacity, adipokine secretion and proliferation pattern which eventually affects their lipid storage capacity and inflammation process [29, 199, 200]. The OM depot in particular is more susceptible to macrophage infiltration when compared to SC depot. The differences in macrophage infiltration within the adipose tissue depots are further exaggerated by the presence of central obesity, which itself is strongly linked with elevated inflammation, macrophage infiltration and adverse metabolic outcomes [201-203].

Genome and transcriptome analysis between the adipose from different depots under different metabolic disease status can be informative to delineate the complex networks of genes and signaling pathways that may contribute to dysregulation of metabolic homeostasis. Significant variation has been described in more than 500 genes between human mesenteric, SC and OM depots as well as preadipocytes, most of them being developmental regulators [204, 205]. The role of ECM and its components in adipose tissue expandability and insulin resistance has been characterized recently [41]. Structural proteins like collagens, adherent proteins such as fibronectins, laminins and integrins are vital ECM components for adipose tissue remodeling, but in excess certain collagens and integrins have known detrimental effects [41, 206, 207].

During the development of obesity, an aberrant increase in interstitial fibrosis in adipose tissue impairs adipose tissue flexibility and reduces its plasticity and leads to adipocyte dysfunction [45]. On a high fat diet, fibrosis events precede inflammation and begins shortly after high fat diet challenge [44]. Additionally, the macrophages also contribute to fibrosis by producing soluble factors like TGF β 1 and PDGF and direct activation of fibroblasts [208]. Analogous to weight gain, ECM alters along with weight loss as well. Comparing transcriptomes of adipose tissue from obese subjects before and after undergoing bariatric surgery suggested increased interstitial fibrosis in WAT of obese [209]. Specifically, increased ECM constituents and members of integrin family play an important role in mediating interactions between inflammation and alteration of metabolism in WAT [209]. Accumulated ECM components signal via integrin receptors and contribute to pathogenic environment. In 3T3-L1 adipocytes, accumulation of ECM during differentiation leads to metabolically unfavorable environment via impaired insulin signaling and increased secretion of MCP1 and NF κ B [210].

Our objective was to address differences in transcriptomic signatures in adipose tissue from obese diabetics compared to obese non-diabetics with a particular focus on KEGG biological pathways and gene ontologies related to ECM constituents, integrins and fibrosis and evaluate transcripts involved in maintaining healthy adipose tissue function in obese non-diabetics.

6.2 Materials and methods

6.2.1 Characteristics of subject

	NT2DM (n=8)	T2DM (n=8)
Age (years)	46.6 ± 9.8	43.5 ± 11.3
BMI (kg/m ²)	36 ± 2.2	40.7 ± 9.8
HBA1C (mmol/L)	5.5 ± 0.38	8.88 ± 1.19 *
Ethnicity	(Chinese=2, Malay=4, Indian=2)	(Chinese=3, Malay=4, Indian=1)
Tissue types	SC and OM	SC and OM

Table 16: Characteristics of obese diabetic and obese non-diabetic subjects from which adipose tissue was derived for RNA sequencing analysis.

*Frozen subcutaneous and omental adipose tissue were used for RNA isolation. *P < 0.05, significance calculated using non-parametric Independent sample t-test.*

SC and OM adipose tissue samples were selected from age and BMI matched obese non-diabetic (n=8) and obese diabetic (n=8) subjects of South Asian ethnicity. Subjects on medication that can affect adipose tissue function and/or metabolic homeostasis (such as corticosteroids and thiazolidinediones) were excluded. Glycated hemoglobin or HBA1C was used to define presence of diabetes and was significantly higher in the diabetic subjects when compared to non-diabetic subjects (table 16).

6.2.2 Tissue RNA isolation

Approximately 250 mg of frozen tissue was used to extract total RNA using Qiagen RNeasy lipid tissue mini kit. Protocol was followed as discussed in section 2.1.2.

6.2.3 RNA sequencing and data analysis

Detailed RNA-SEQ experimental protocol is written in section 2.7. RNA sample from omental adipose tissue from one diabetic subject was of poor quality and hence excluded from analysis resulting in n=7 for this group. We analyzed both disease specific (T2DM vs NT2DM) and depot specific (OM vs SC) differences (figure 40). In the depot specific analysis, we paired expression in OM and SC depots from each subject in order to eliminate baseline intra-individual variation. This method involved normalization of each gene in OM depot to a respective gene in SC depot for an individual subject and then grouping them into T2DM and NT2DM. Due to pairing of data for depot specific analysis, FPKM values for SC depot for all genes was normalized to one and hence not used for depot specific transcriptome analysis. FPKM values were used for disease specific enrichment analysis into pathways and ontologies. The following groups were finally used for analysis:

1. OM vs SC depot (NT2DM, paired data).
2. OM vs SC depot (T2DM, paired data).
3. T2DM vs NT2DM (SC depot).
4. T2DM vs NT2DM (OM depot).

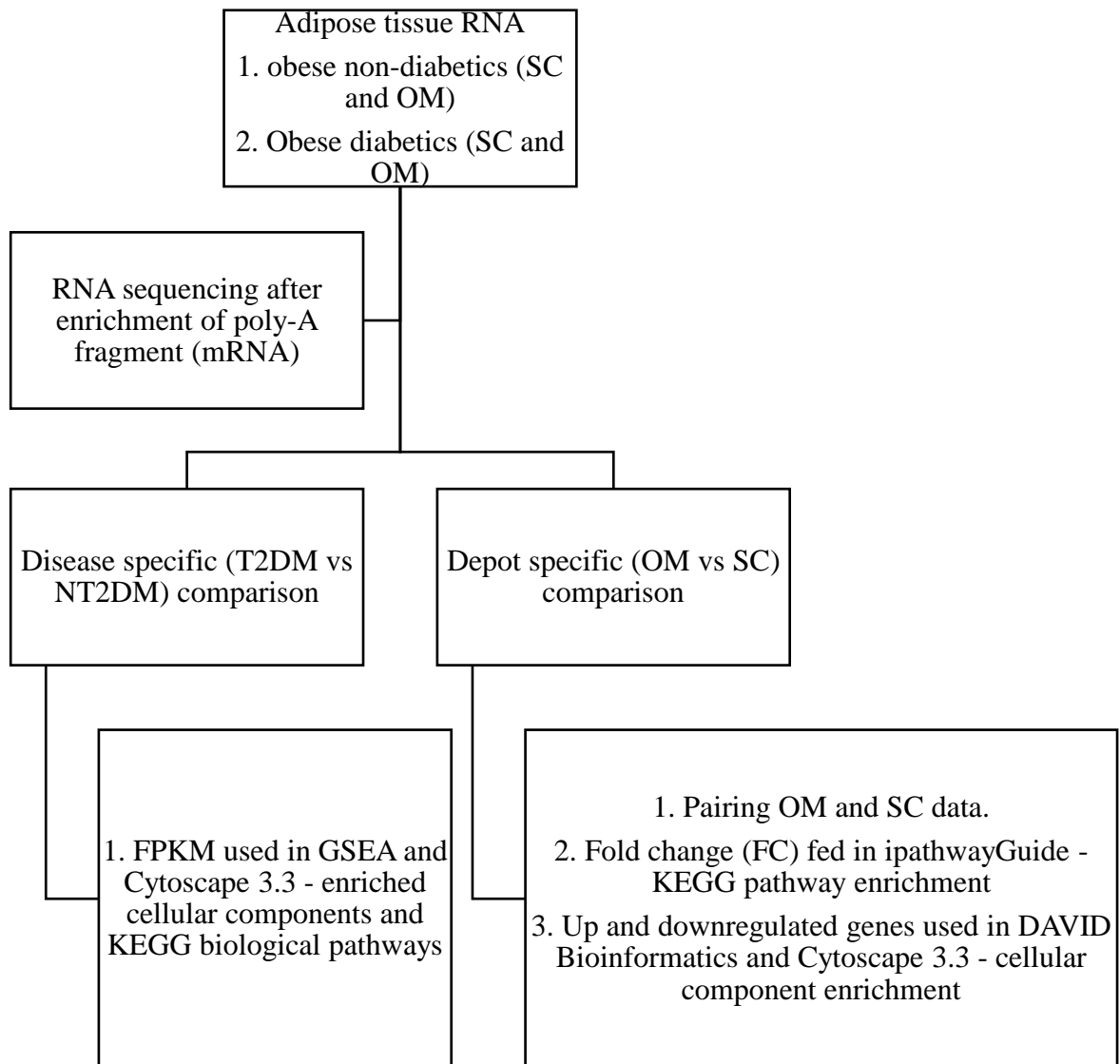


Figure 40: Workflow for RNA-SEQ data analysis for comparing adipose tissue depots.

Disease specific and depot specific differences in gene ontologies and KEGG biological pathways were analyzed using iPathwayGuide or GSEA in conjunction with enrichment map creator.

6.3 Results

6.3.1 Depot specific and disease specific differences in transcriptomes

6.3.1.1 Sample – to – sample distance

Data obtained from RNA sequencing was used to visualize sample – to – sample distance by means of Euclidean distance heatmap (figure 41) and principle

component analysis (PCA) (figure 42) using R package. In the heatmap, all subject characteristics (SC/OM and NT2DM/T2DM) are denoted on X and Y axis and compared to every other sample. Each square represents a comparison between two intersecting samples and the darker shades of blue denote increasing similarity between the two samples. As seen in the heatmap, SC and OM samples clustered distinctly, suggesting considerable variance between them, whereas NT2DM and T2DM samples were distributed randomly, suggesting less variation between these comparator groups.

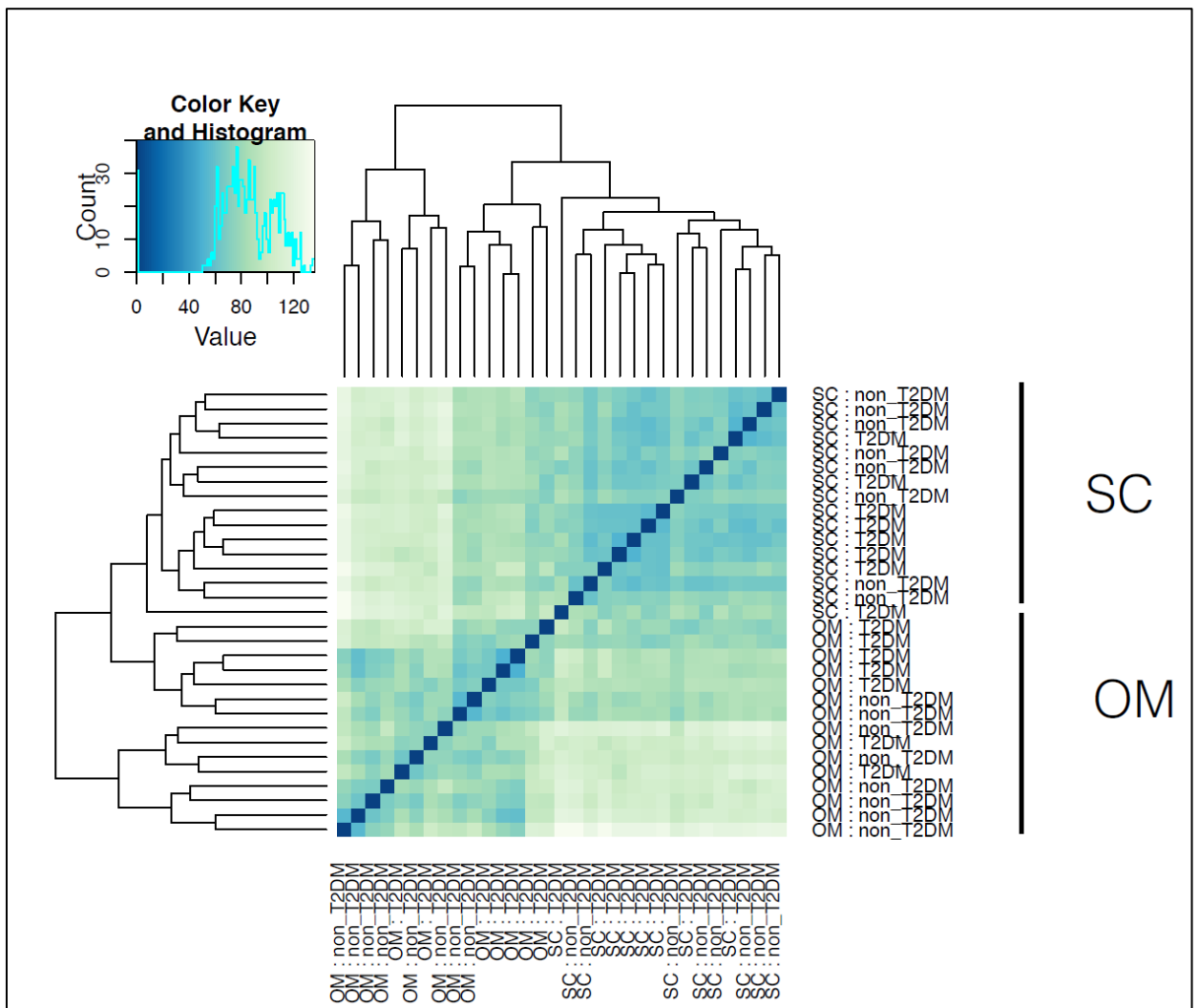


Figure 41: Euclidean distance (sample – to – sample distance) heatmap of all tissue RNA-SEQ data.

Tissue samples are individually arranged on X and Y axis with each sample being compared to the other. Darker shades of blue denote decreased distance

or increased similarity between the compared samples. As seen, all SC samples clustered together and distinctly from OM samples. This suggests considerable transcriptome variation among the SC and OM tissue samples.

In principle component analysis, samples were distributed in two directions or principle components (PC1 and PC2) and results indicated that different adipose depots (OM or SC) resulted in 61% (principle component 1/PC1) variance among the samples. Disease state (being T2DM or NT2DM) resulted in 10% (principle component 2/PC2) variation.

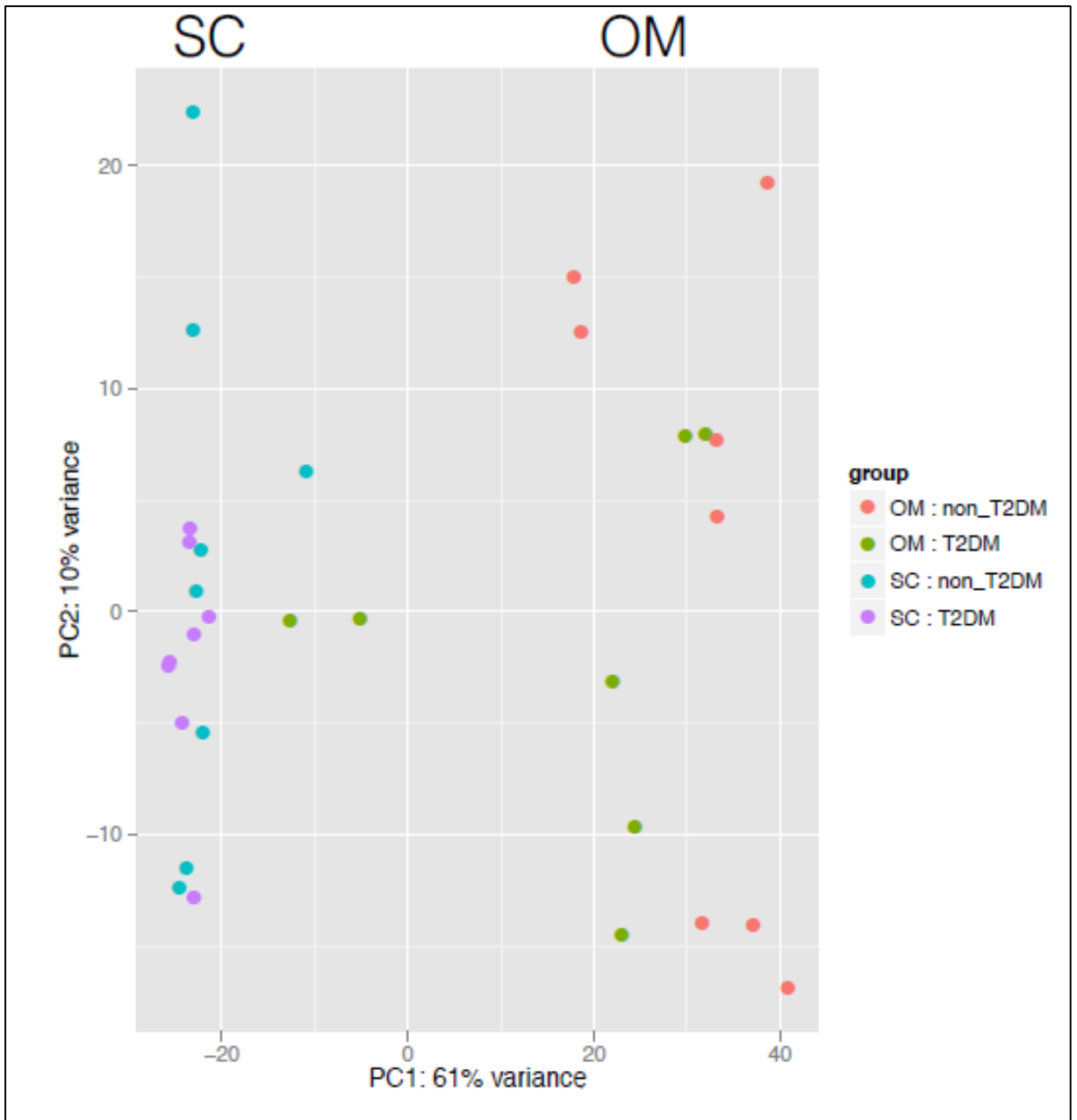


Figure 42: Principle component analysis of RNA-SEQ data.

Each sample from RNA-SEQ is represented as a circle, orange: OM (non_T2DM or NT2DM), green: OM (T2DM), blue: SC (non_T2DM or NT2DM), purple: SC (T2DM). Samples were distributed into two components (PC1 and PC2) to identify differences among them.

6.3.1.2 Up and downregulated genes

About 15000 genes were finally read and annotated in the RNA-SEQ results.

Figure 43 shows Venn diagram and bar graph for the number of differentially expressed genes (DEGs) in OM depot compared to SC depot. 3063 and 1944

(FC $\geq \pm 1.5$, FDR < 0.05) genes were differentially up or downregulated in OM depot from T2DM and NT2DM respectively. Of these, 1850 genes were upregulated and 1213 genes were downregulated in T2DM whereas 1149 genes upregulated and 795 genes downregulated in NT2DM. As shown in the Venn diagram, 1547 DEGs in OM depot were common between NT2DM and T2DM group while 398 genes were exclusive to T2DM.

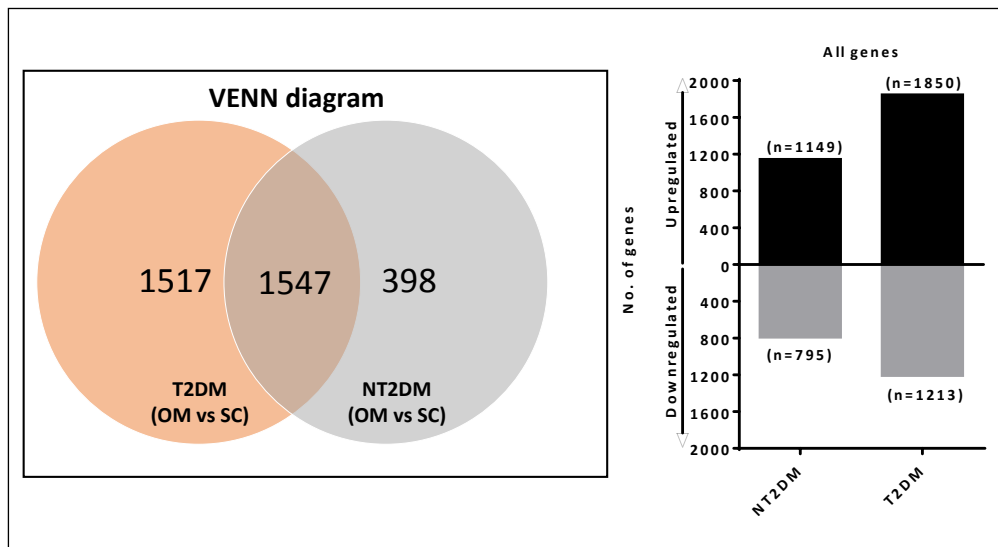


Figure 43: Illustration of the number of differentially expressed genes by depot specific comparisons.

Numbers in Venn diagram on the left represents number of DEGs in T2DM or NT2DM or common in both. Bar graph on the right denotes number of up and downregulated genes either in T2DM or NT2DM subjects. Inclusion: $\log FC \geq \pm 0.6$ and FDR < 0.05.

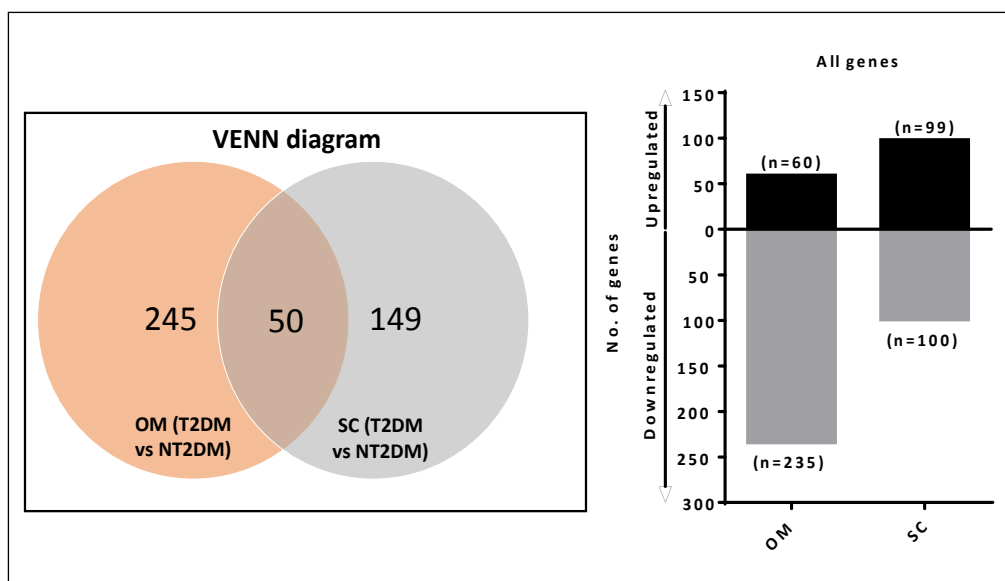


Figure 44: Illustration of the number of differentially expressed genes by disease specific comparisons.

Numbers in Venn diagram on the left represents number DEGs in OM or SC depot or common in both depots. Bar graph on the right denotes the number of up and downregulated genes either in OM or SC depots. Inclusion: $\log FC \geq \pm 0.6$ and $FDR < 0.05$.

Compared to the respective depots from NT2DM, 199 genes (n = 100 downregulated, n = 99 upregulated) were differentially expressed in SC depot from T2DM and 295 genes (n = 235 downregulated and n = 60 upregulated) were differentially expressed in the OM depot from T2DM (figure 44).

6.3.2 Enriched KEGG biological pathways in OM depot compared to SC depot

We identified KEGG pathways significantly enriched in OM depot when compared to SC depot and looked for any notable differences between NT2DM and T2DM subjects. Fold changes ($\log FC \geq \pm 0.6$, $FDR < 0.05$) obtained from paired data were analyzed via iPathwayGuide to identify significantly enriched KEGG biological pathways based on overrepresentation and impact analysis [122]. Compared to SC depot, 6 pathways were significantly enriched in OM depot of NT2DM ($P < 0.05$, Bonferroni corrected) and 18 pathways were

significantly enriched in OM depot of T2DM (table 17). Pathways exclusive to T2DM are highlighted in red text and common pathways between both groups are highlighted in blue text.

	P Value (Bonferroni) (OM vs. SC T2DM)	P Value (Bonferroni) (OM vs. SC NT2DM)
Protein digestion and absorption	9.26E-07	7.58E-08
Basal cell carcinoma	0.000219	0.233382
Arrhythmogenic right ventricular cardiomyopathy (ARVC)	0.000653	0.04904
Cytokine-cytokine receptor interaction	0.001519	0.085594
ECM-receptor interaction	0.00156	0.002171
Cell adhesion molecules (CAMs)	0.001938	0.020796
PI3K-Akt signaling pathway	0.002497	0.076626
Hippo signaling pathway	0.002605	0.051186
Complement and coagulation cascades	0.003442	1
Neuroactive ligand-receptor interaction	0.004274	0.063844
Pathways in cancer	0.011087	1
Retinol metabolism	0.017137	0.016105
Focal adhesion	0.018516	0.006296
Steroid hormone biosynthesis	0.025695	0.184109
Melanogenesis	0.037103	1
Hypertrophic cardiomyopathy (HCM)	0.041311	1
Dilated cardiomyopathy	0.041905	1
Proteoglycans in cancer	0.049116	0.77726

Table 17: Significantly enriched biological pathways in NT2DM and T2DM subjects (OM vs SC).

Output was generated in iPathwayGuide. Significance was pegged at $P \leq 0.05$ with Bonferroni correction to minimize false positive results.

6.3.2.1 PI3K-Akt signaling pathway

Cytokine-cytokine receptor interaction and PI3K-Akt signaling pathways were exclusively enriched in OM depot from T2DM. In the PI3K-Akt signaling pathway, 91 genes were differentially expressed (43 upregulated and 48 downregulated). The top 10 most up and downregulated genes in T2DM are shown in the bar graph (figure 45) and pathway map with up (pink to red colored rectangles) and downregulated genes (blue colored rectangles) illustrated in figure 46. As seen in pathway map, PI3K-Akt signaling pathway is influenced by growth factors (GF), cytokines, extra cellular matrix (ECM) components, chemokines, hormones and neurotransmitters. As shown in green boxes, thirteen of the top 20 DEGs in PI3K-Akt signaling pathway were upstream genes such as growth factors (FGF1, NGF, FGF9, ANGPT4), extracellular matrix components (TNC, COL5A3, VWF, TNN, SPP1, LAMB3, COL4A5, ITGB8) and cytokines (CSF3). Among the intermediates in PI3K-Akt signaling pathway, PPP2R2C (Protein Phosphatase 2, Regulatory Subunit B, Gamma, log FC = 2.06) and PPP2R2B (Protein Phosphatase 2, Regulatory Subunit B, Beta, log FC = 1.38) were significantly upregulated in OM depot (when compared to SC depot). Differential expressions of upstream genes indicated a potential link between ECM and PI3K-Akt signaling pathway in our data.

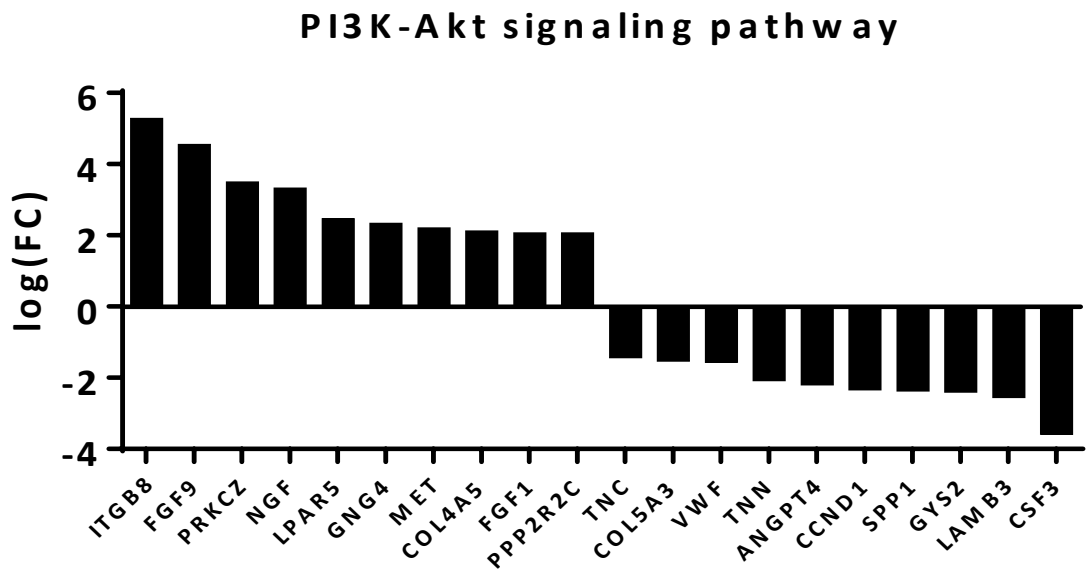


Figure 45: Top 10 up and downregulated genes in PI3K-Akt signaling pathway in T2DM subjects (OM vs SC).

All genes were significant with $FDR \leq 0.05$.

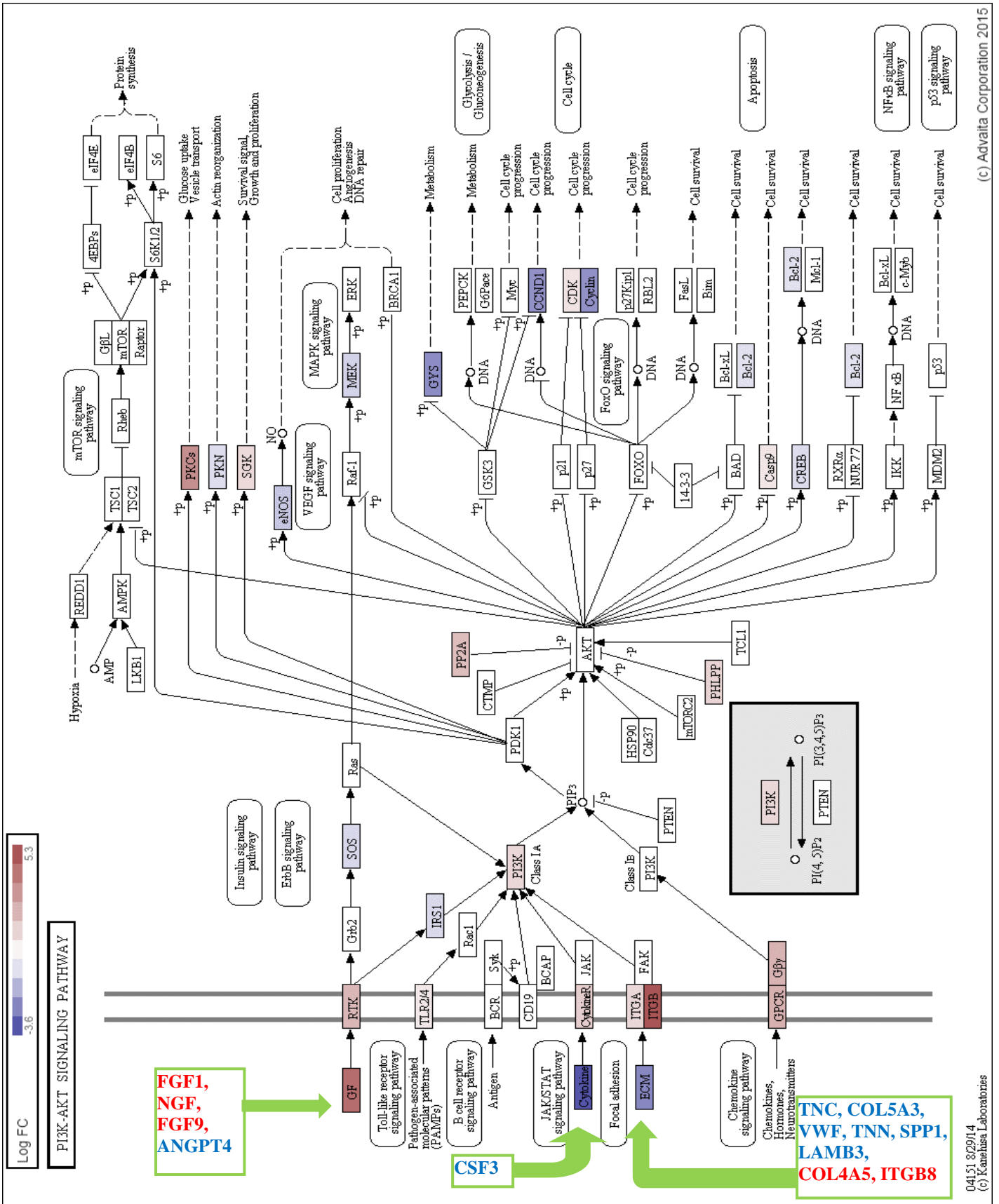


Figure 46: Representation of fold change of genes in PI3K-Akt signaling pathway in T2DM subjects.

Fold changes in genes are represented by colors (upregulation – towards red and downregulation – towards blue). Green text boxes represent genes in GF (growth factor), cytokine and ECM within PI3K-Akt signaling pathway.

6.3.2.2 ECM receptor interaction pathway

ECM receptor interaction, cell adhesion molecules (CAMs) and focal adhesion were enriched in OM depot (compared to SC depot) from both NT2DM and T2DM. Figure 47 shows DEGs in ECM receptor interaction pathway in both groups. Collagens COL24A1 (log FC = -1.24), COL11A1 (log FC = -2.82), COL6A2 (log FC = -0.78), COL6A1 (log FC = -0.80), COL5A1 (log FC = -0.75), COL4A4 (log FC = -1.17) were downregulated and COL6A6 (log FC = 0.96) was upregulated in OM depot (compared to SC depot) from NT2DM only. COL5A3 (log FC = -1.23 in NT2DM and log FC = -1.54 in T2DM) and COL4A5 (log FC = 1.73 in NT2DM and log FC = 2.12 in T2DM) were differentially expressed in OM depot (compared to SC depot) from both NT2DM and T2DM.

Integrins ITGA11 (log FC = -1.38), ITGA10 (log FC = -0.62), ITGB5 (log FC = -0.64), ITGB1 (log FC = -0.95), ITGA1 (log FC = -1.02) were downregulated and ITGA3 (log FC = 1.21) as well as ITGA2 (log FC = 0.79) were upregulated in OM depot (compared to SC depot) from T2DM only. ITGB8 was upregulated in both T2DM (log FC = 5.28) and NT2DM (log FC = 3.99). Additional DEGs in ECM receptor interaction pathway were THBS4 (log FC = -0.84 in T2DM), VWF (log FC = -1.57 in T2DM) and TNN (log FC = -1.13 in NT2DM and log FC = -2.08, T2DM). Next, we analyzed enriched cellular components to study ECM components in detail.

ECM receptor interaction pathway

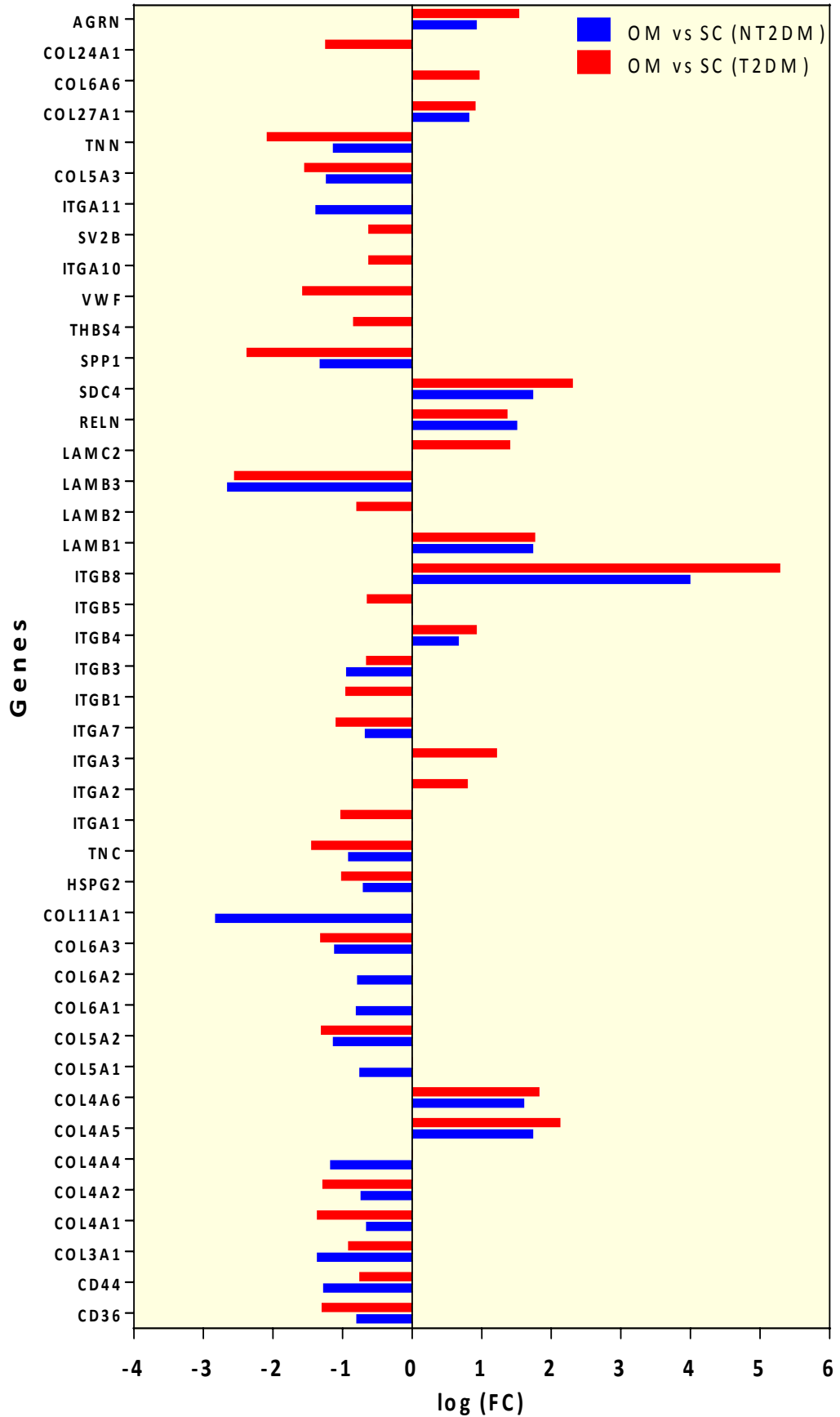


Figure 47: ECM receptor interaction pathway genes in NT2DM and T2DM subjects.

Log (FC) for all the genes were plotted ($\text{Log FC} \geq \pm 0.6$ and $\text{FDR} < 0.05$). Genes below the cut off values in either NT2DM or T2DM are indicated as empty bar spaces.

6.3.3 Enriched cellular components in OM depot compared to SC depot

The cellular component ontology describes locations, at the levels of subcellular structures and macromolecular complexes. Table 18 illustrates enriched cellular components (GO_CC) in OM depot compared to SC depot in NT2DM and T2DM subjects.

GO_CC	P Value (Bonferroni) (OM vs. SC T2DM)	P Value (Bonferroni) (OM vs. SC NT2DM)
Extracellular space	1.00E-24	3.38E-20
Extracellular region	1.00E-24	1.00E-24
Membrane part	1.00E-24	1.32E-19
Integral component of membrane	1.00E-24	2.20E-20
Plasma membrane part	1.00E-24	3.23E-21
Integral component of plasma membrane	1.00E-24	1.03E-15
Intrinsic component of plasma membrane	1.00E-24	1.76E-16
Extracellular matrix	1.00E-24	1.00E-24
Intrinsic component of membrane	1.00E-24	1.10E-22
Plasma membrane	1.00E-24	1.00E-24
Cell periphery	1.00E-24	1.00E-24
Membrane	7.60E-23	0.000044774
Proteinaceous extracellular matrix	1.50E-21	3.20E-23
Cell surface	9.74E-15	3.1562E-06
Plasma membrane region	1.15E-13	1.25E-07
Extracellular region part	9.74E-13	3.23E-14

Cell-cell junction	4.87E-11	0.00020552
Cell projection	1.15E-10	0.0044774
Neuron part	2.39E-10	1.69E-07
Cell junction	3.63E-10	0.0071932
Anchored component of membrane	1.15E-08	0.00063124
Membrane region	2.66E-08	0.02569
Apical plasma membrane	2.66E-08	0.000001835
Apical part of cell	4.69E-08	2.20E-07
Ion channel complex	1.06E-07	0.0019084
Receptor complex	1.59E-07	0.44774
Extracellular matrix part	5.40E-07	3.82E-09
Synapse	6.37E-07	0.12478
Collagen trimer	0.000001062	0.000016148
Transmembrane transporter complex	0.000001062	0.0041838
Transporter complex	0.000005133	0.010276
External side of plasma membrane	6.6375E-06	1
Somatodendritic compartment	0.000008496	0.00023488
Neuron projection	0.000036285	0.00016882
Cation channel complex	0.00004956	0.06239
Golgi lumen	0.000071685	8.81E-07
Basolateral plasma membrane	0.00007611	0.0027892
Neuronal cell body	0.00011505	0.000008808
Cell projection part	0.0001239	0.16148
Cell body	0.000177	0.000013212
Membrane raft	0.00018585	1
Axon	0.0002655	0.0034498
Basement membrane	0.0003894	0.00019084
Intermediate filament	0.0025665	0.0013946
Axon part	0.0057525	0.0027158
Keratin filament	0.0076995	0.027158
Sodium channel complex	0.0076995	1
Anchored component of plasma membrane	0.01416	1

Side of membrane	0.020355	1
Synaptic membrane	0.025665	1
Junctional sarcoplasmic reticulum membrane	0.02832	1
Cornified envelope	0.02832	0.019084
Myelin sheath	0.02832	1
Sarcolemma	0.029205	0.016882
Postsynaptic membrane	0.03186	1
Main axon	0.03363	1
Secretory granule	0.04071	1

Table 18: Enriched GO_CC in OM depot compared to SC depot in both NT2DM and T2DM subjects.

Output was generated in iPathwayGuide. Significance was pegged at $P \leq 0.05$ with Bonferroni correction to minimize false positive results.

Both positively and negatively enriched cellular components (OM vs SC) from NT2DM and T2DM were used to build enrichment maps using Cytoscape 3.3 (enrichment map creator plugin). Only interacting clusters are shown here (interaction defined by $FDR < 0.05$). As seen in blue discontinuous circles, upregulated genes formed two ontology clusters or modules and downregulated genes formed one ontology cluster or module in both NT2DM (figure 48 and 50) and T2DM (figure 49 and 51). Significant interactions were observed within clusters or modules and contained membrane proteins and ECM or extracellular matrix components related ontologies, with a different set of genes in NT2DM and T2DM subjects.

Figure 48: Positively enriched cellular components in NT2DM (OM vs SC).

Upregulated genes were analyzed using DAVID bioinformatics and the “functional annotation chart” output was exported in Cytoscape 3.3 (plugin: enrichment map creator) [135] to generate a map of enriched GO_CC. Size of the node predicts the number of genes in particular ontology with green connecting line representing the number of common genes. Cut off value for generating enrichment map was capped at conservative (P -value < 0.001 , FDR < 0.05).

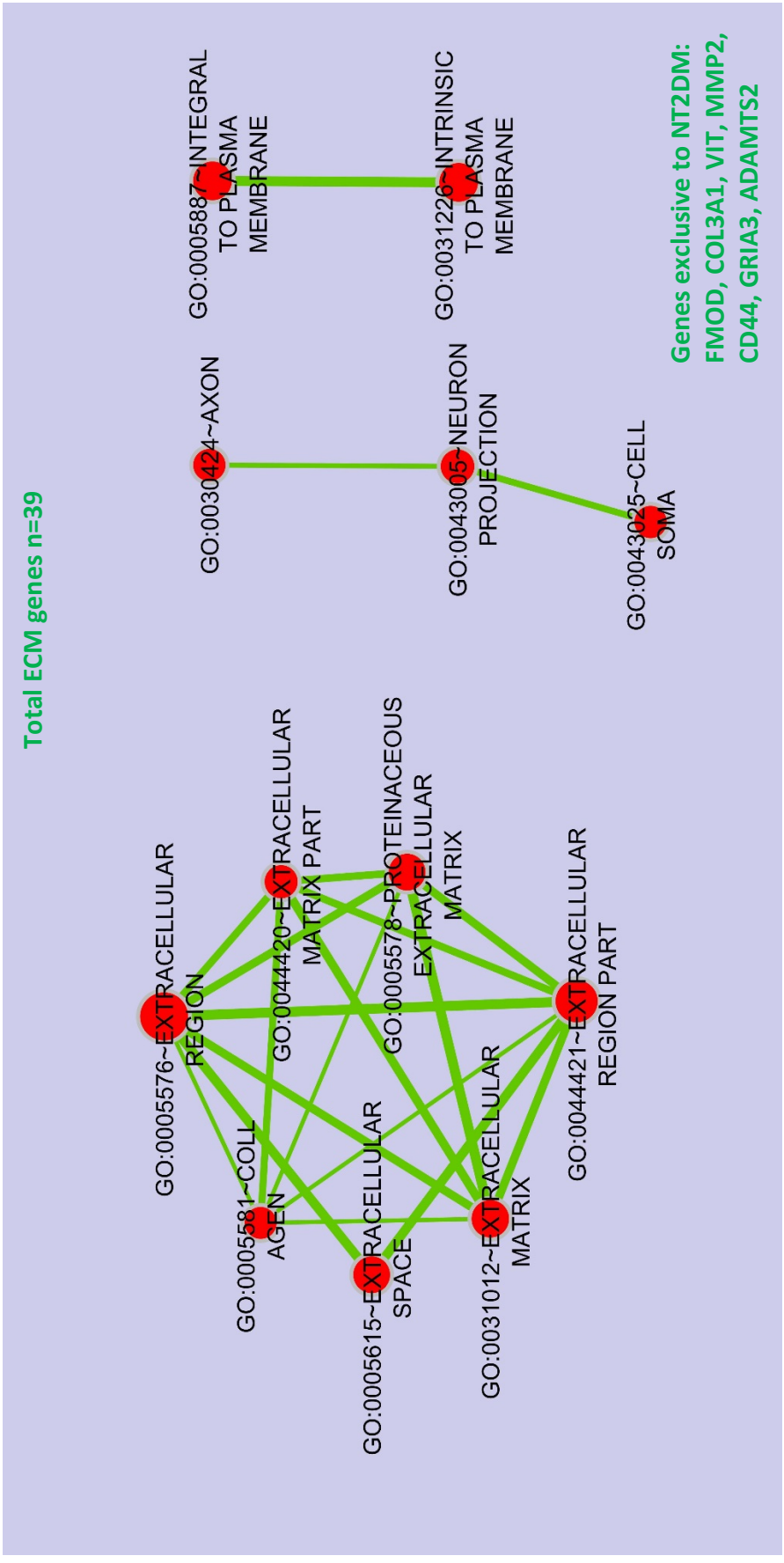
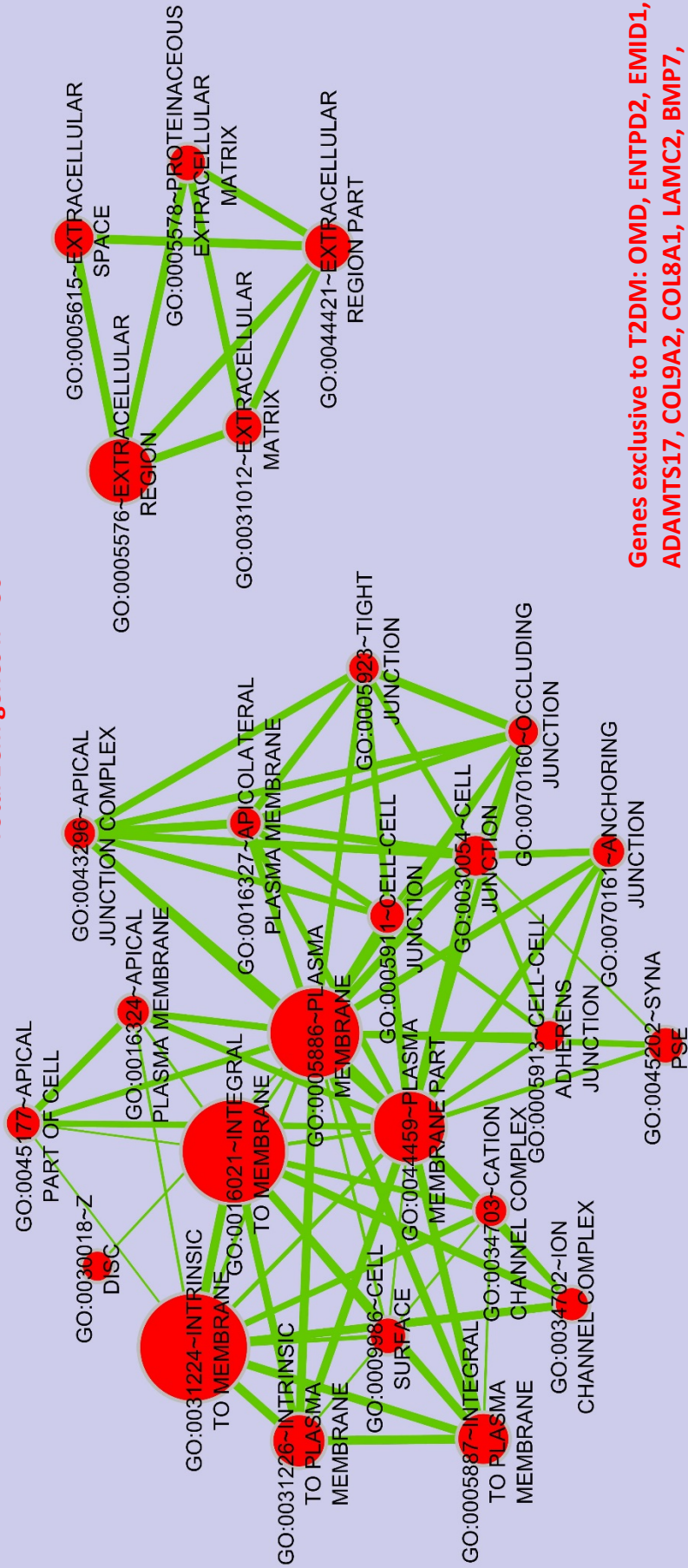


Figure 49: Negatively enriched cellular components in NT2DM (OM vs SC).

Downregulated genes were analyzed using DAVID bioinformatics and the “functional annotation chart” output was exported in Cytoscape 3.3 (plugin: enrichment map creator) [135] to generate a map of enriched GO_CC. Size of the node predicts the number of genes in particular ontology with green connecting line representing number of common genes. Cut off value for generating enrichment map was capped at conservative (P -value < 0.001 , FDR < 0.05).

Total ECM genes n = 50

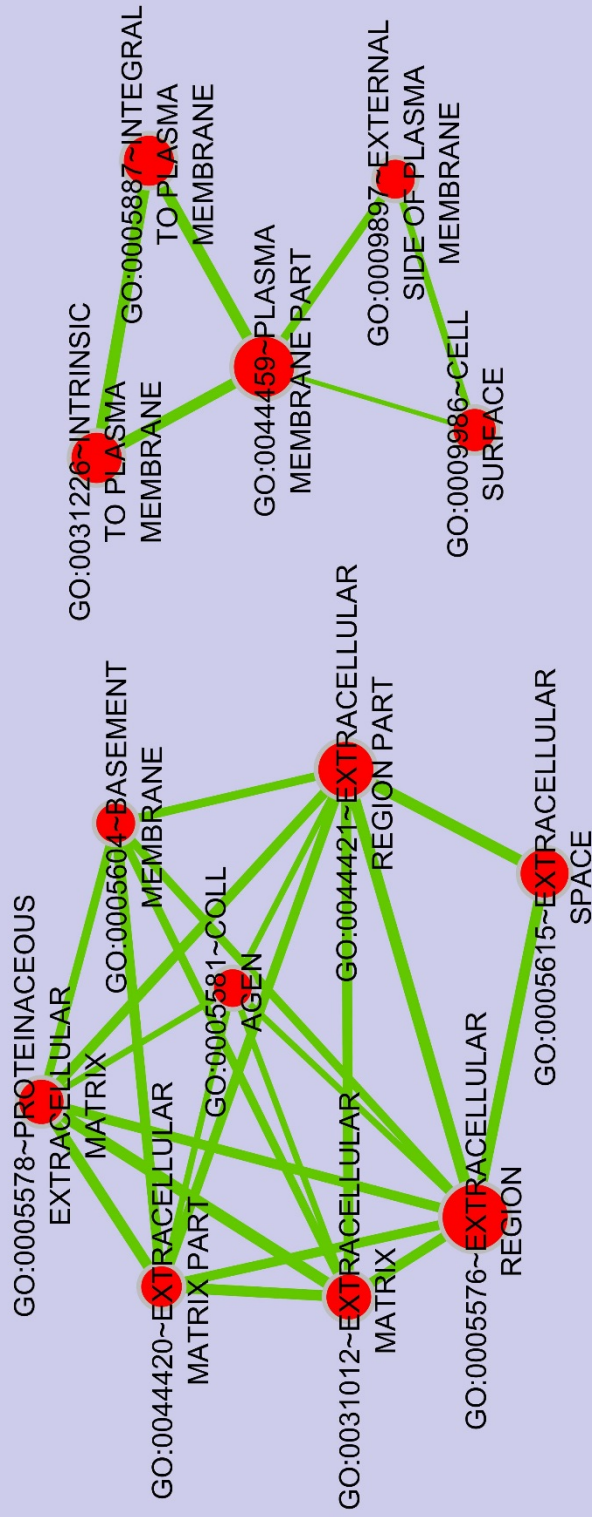


Genes exclusive to T2DM: OMD, ENTPD2, EMID1, ADAMTS17, COL9A2, COL8A1, LAMC2, BMP7, ADAMTS3, ARGN, BMP4, EMILIN3, WNT9A, COL17A1, PRSS12, TGFB2, WNT4, WNT3, TGFB3, WNT5B

Figure 50: Positively enriched cellular components in T2DM (OM vs SC).

Upregulated genes were analyzed using DAVID bioinformatics and the “functional annotation chart” output was exported in Cytoscape 3.3 (plugin: enrichment map creator) [135] to generate a map of enriched GO_CC. Size of the node predicts the number of genes in particular ontology with green connecting line representing number of common genes. Cut off value for generating enrichment map was capped at conservative (P -value < 0.001 , FDR < 0.05).

Total ECM genes n=41



Genes exclusive to T2DM: HSPG2, NID, COL16A1, MMRN2, VWF, COL12A1, FREM1, VWA1, COL24A1, TNC, COL4A2 COL4A1

Figure 51: Negatively enriched cellular components in T2DM (OM vs SC).

Downregulated genes were analyzed using DAVID bioinformatics and the “functional annotation chart” output was exported in Cytoscape 3.3 (plugin: enrichment map creator) [135] to generate a map of enriched GO_CC. Size of the node predicts the number of genes in particular ontology with green connecting line representing number of common genes. Cut off value for generating enrichment map was capped at conservative (P -value < 0.001 , FDR < 0.05).

Gene symbols written in red or green text in each figure denote ECM genes exclusive to that group. Compared to SC depot, 2 genes (LTBP4, VEGF) were upregulated and 7 genes (FMOD, COL3A1, VIT, MMP2, CD44, GRIA3, ADAMTS2) were downregulated in OM depot from NT2DM exclusively. On the other hand, 20 genes (OMD, ENTPD2, EMID1, ADAMTS17, COL9A2, COL8A1, LAMC2, BMP7, ADAMTS3, ARGN, BMP4, EMILIN3, WNT9A, COL17A1, PRSS12, TGFB2, WNT4, WNT3, TGFB3, WNT5B) were upregulated and 12 genes (HSPG2, NID, COL16A1, MMRN2, VWF, COL12A1, FREM1, VWA1, COL24A1, TNC, COL4A2, COL4A1) were downregulated in OM tissue from T2DM exclusively.

6.3.4 Enriched KEGG pathways in T2DM compared to NT2DM

To evaluate disease specific differences in KEGG pathways, we used FPKM values and Gene Set Enrichment Analysis (GSEA) which empowered us to visualize positively and negatively enriched ontologies based on enrichment score (ES). ES score obtained from GSEA reflects the degree to which a gene set is overrepresented at the top or bottom of a ranked list of genes. A positive ES indicates gene set enrichment at the top of the ranked list and a negative ES indicates gene set enrichment at the bottom of the ranked list. Bar graphs show the percentage of gene coverage (GC) in particular cellular component (ratio of

genes in database/ total number of genes in the ontology) and blue and red color signify negative and positive enrichment in respective ontologies (figure 52).

Total 160 gene sets or KEGG pathways were analyzed. Compared to SC depot in NT2DM, 25 gene sets ($P < 0.05$) were upregulated and 19 gene sets ($P < 0.05$) were downregulated in SC depot from T2DM (table 21). Compared to OM depot from NT2DM, 3 gene sets ($P < 0.05$) were upregulated and 19 gene sets ($P < 0.05$) were downregulated in OM depot from T2DM subjects (table 22). Pathways with significant interactions are shown here and detailed list is tabulated in the appendix. Three metabolic pathways including butanoate metabolism (FDR = 0.041), propanoate metabolism (FDR = 0.012) as well as valine, leucine and isoleucine degradation (FDR = 0.01) were negatively enriched in SC depot (shown in blue bars) from T2DM subjects compared to SC depot from NT2DM subjects. Gene coverage was highest in butanoate metabolism (54%) followed by propanoate metabolism (52%) and valine, leucine and isoleucine degradation (43%).

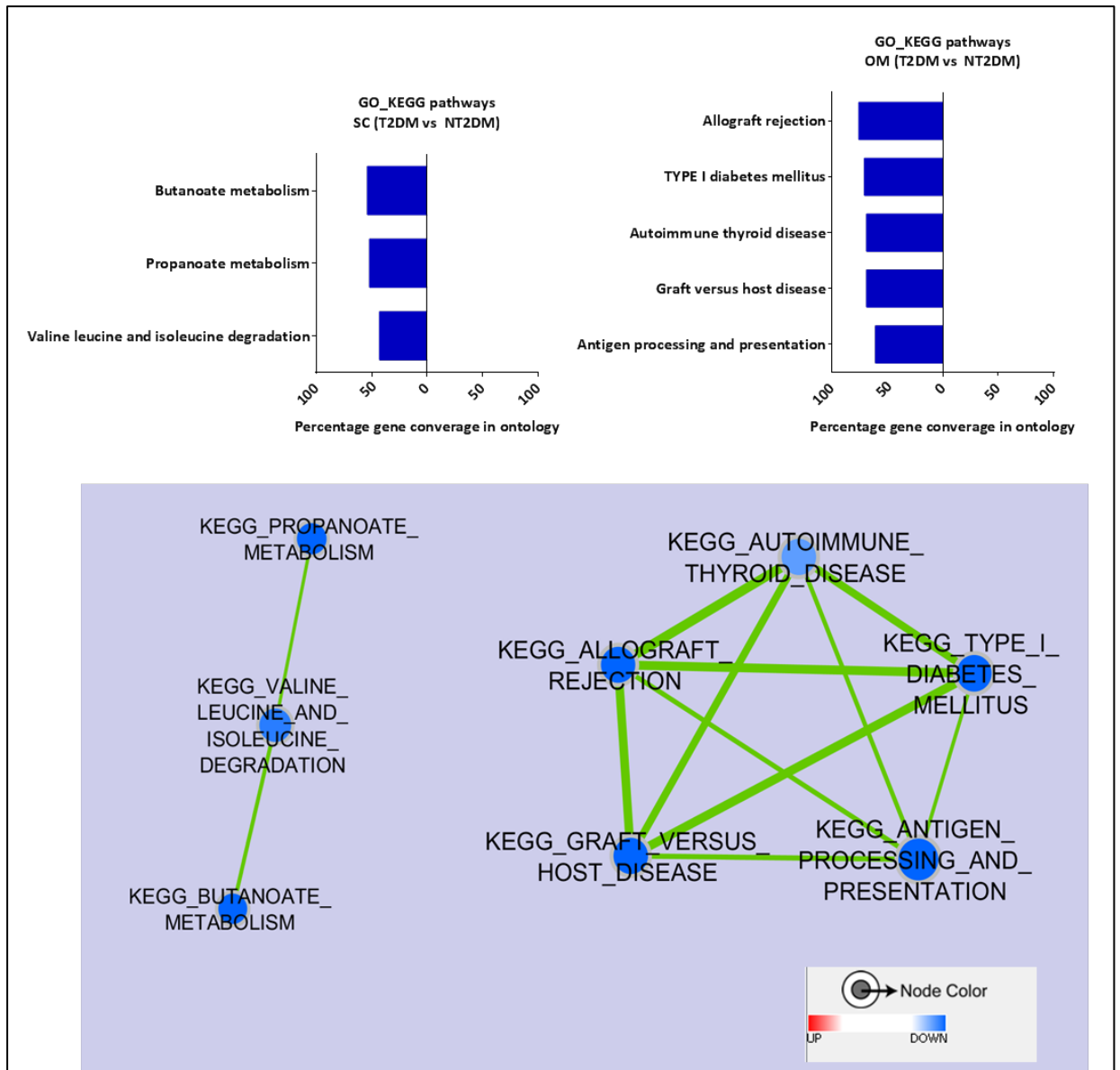


Figure 52: KEGG pathway enrichment and their interaction map illustrating transcriptomic signatures in T2DM compared to NT2DM subjects.

FPKM values were analyzed in gene set enrichment analysis (GSEA) desktop version [165] and the output was exported in Cytoscape 3.3 (plugin: enrichment map creator) [163] to generate a map of positively and negatively enriched gene ontologies. Inner node represents enrichment in SC depot (left cluster) and OM depot (right cluster). The size of the node predicts the number of genes in particular ontology with green connecting line representing number of common genes or interaction. Blue and red color denote significant negative and positive enrichment respectively. Cut off value for generating enrichment map was capped at permissive (P -value < 0.05 , $FDR < 0.25$).

In addition to these, cytokine-cytokine receptor interaction ($FDR = 0.016$) and chemokine signaling ($FDR = 0.038$) (not present in interaction maps) pathways

were positively enriched in SC depot from T2DM subjects compared to SC depot from NT2DM subjects. In OM depot, allograft rejection (FDR = 0.006), type 1 diabetes mellitus (FDR = 0.008), autoimmune thyroid disease (FDR = 0.02), graft versus host disease (0.006) and antigen processing and presentation (FDR = 0.03) were negatively enriched. 6.3.5 Enriched cellular components in T2DM compared to NT2DM

GSEA and Cytoscape 3.3 were used to identify enriched ontologies and build interaction maps using FPKM values as an input (figure 53). Common cellular components were present in both datasets and hence enrichment maps have been combined for easier visualization. Inner node denotes enrichment in SC depot (T2DM vs NT2DM) and outer border denotes enrichment in OM depot (T2DM vs NT2DM), with red color representing significant positive enrichment and white color representing non-significant enrichment. Bar graph depicts the percentage of gene coverage (GC) in particular cellular component (ratio of genes in database/ total number of genes in the ontology).

Total 138 gene sets or GO_CC were analyzed. Compared to SC depot from NT2DM, 19 gene sets ($P < 0.05$) were upregulated and 1 gene set ($P < 0.05$) was downregulated (table 23) in SC depot from T2DM. Compared to OM depot from NT2DM, 17 gene sets ($P < 0.05$) were upregulated ($P < 0.05$) (table 24) in OM depot from T2DM. No gene sets were significantly downregulated in OM depot from T2DM.

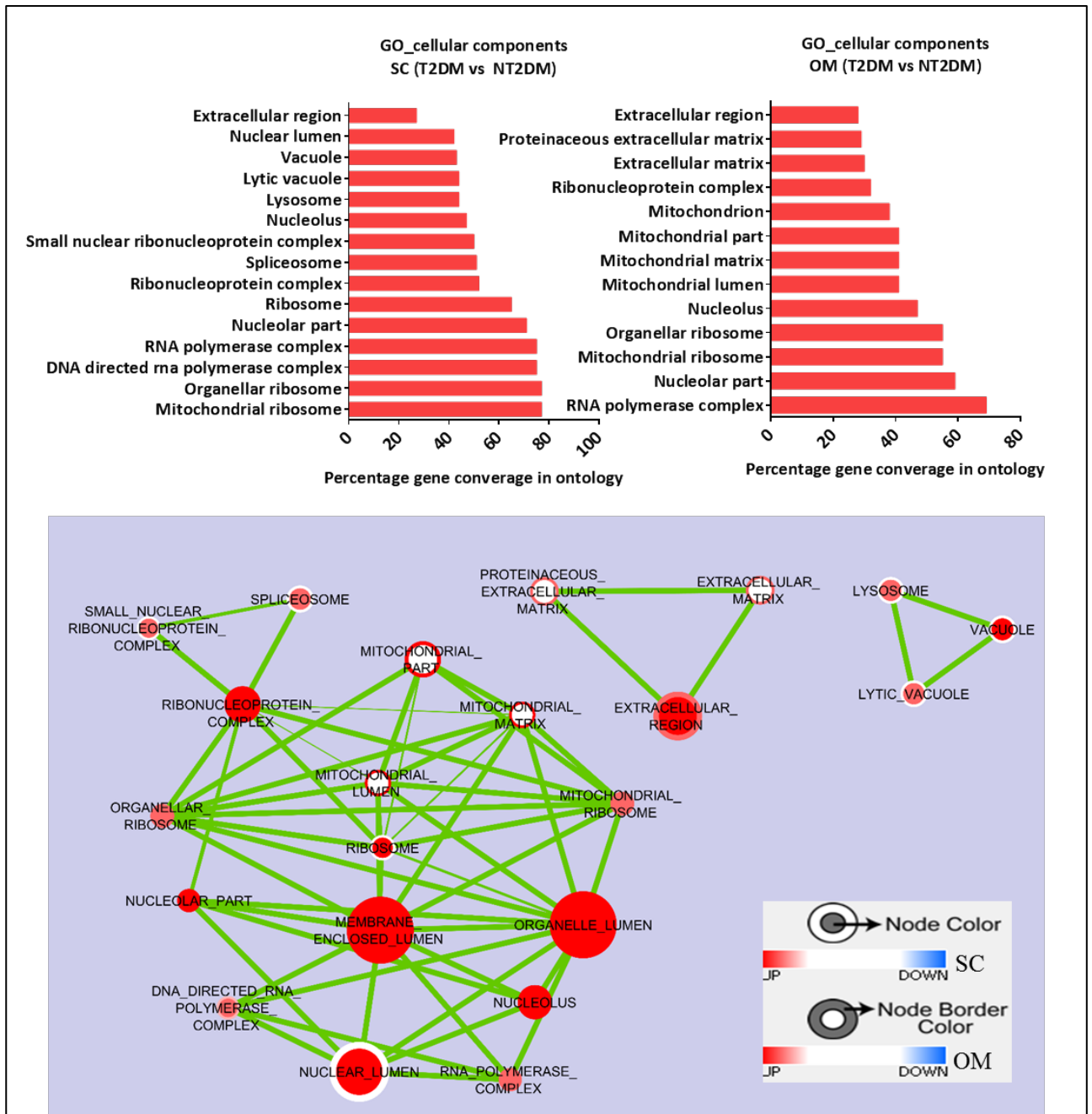


Figure 53: GO cellular component enrichment and their interaction map illustrating transcriptomic signatures in T2DM compared to NT2DM subjects.

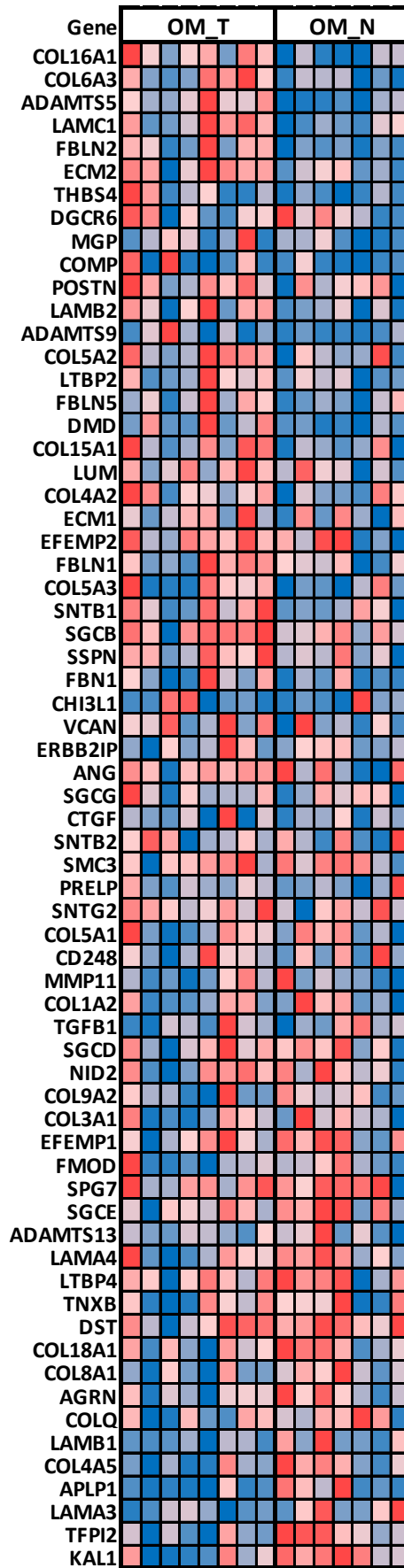
FPKM values were input into gene set enrichment analysis (GSEA) desktop version [165] and the output was exported in Cytoscape 3.3 (plugin: enrichment map creator) [163] to generate a map of positively and negatively enriched gene ontologies. Inner node represents enrichment in SC depot and outer border in node represents enrichment in OM depot. Size of the node predicts the number of genes in the particular ontology with green connecting line representing the number of common genes or interaction. Blue and red color denote significant negative and positive enrichment respectively. Cut off value

for generating enrichment map was capped at permissive (P -value < 0.05 , FDR < 0.25).

Pathways with significant interactions are shown here. ECM components including extracellular region (GC = 27% in SC depot and 28% in OM depot), extracellular matrix (GC = 30%) and proteinaceous extracellular matrix (GC = 29%) formed a cluster, with later 2 ontologies being significantly positively enriched only in OM depot (T2DM vs NT2DM). Next, we analyzed the ECM and fibrosis components respectively in details.

6.3.5.1 ECM and fibrosis components

Heatmap (figure 54) represents ranked FPKM values of ECM genes in OM depot from T2DM and NT2DM subjects and enrichment plot shows density of overrepresented genes in up or downregulated genes. ECM comprised of 67 genes in total and the top 20 genes in heatmap contributed the most towards positive enrichment (ES score = 0.354). As seen from the figure, upregulated genes included collagens (COL16A1, COL6A3, COL4A2, COL5A2, COL5A3 and COL15A1), laminins (LAMC1 and LAMB2), metallopeptidases (ADAMTS5 and ADAMTS9) and fibulins (FBLN1 and FBLN2).



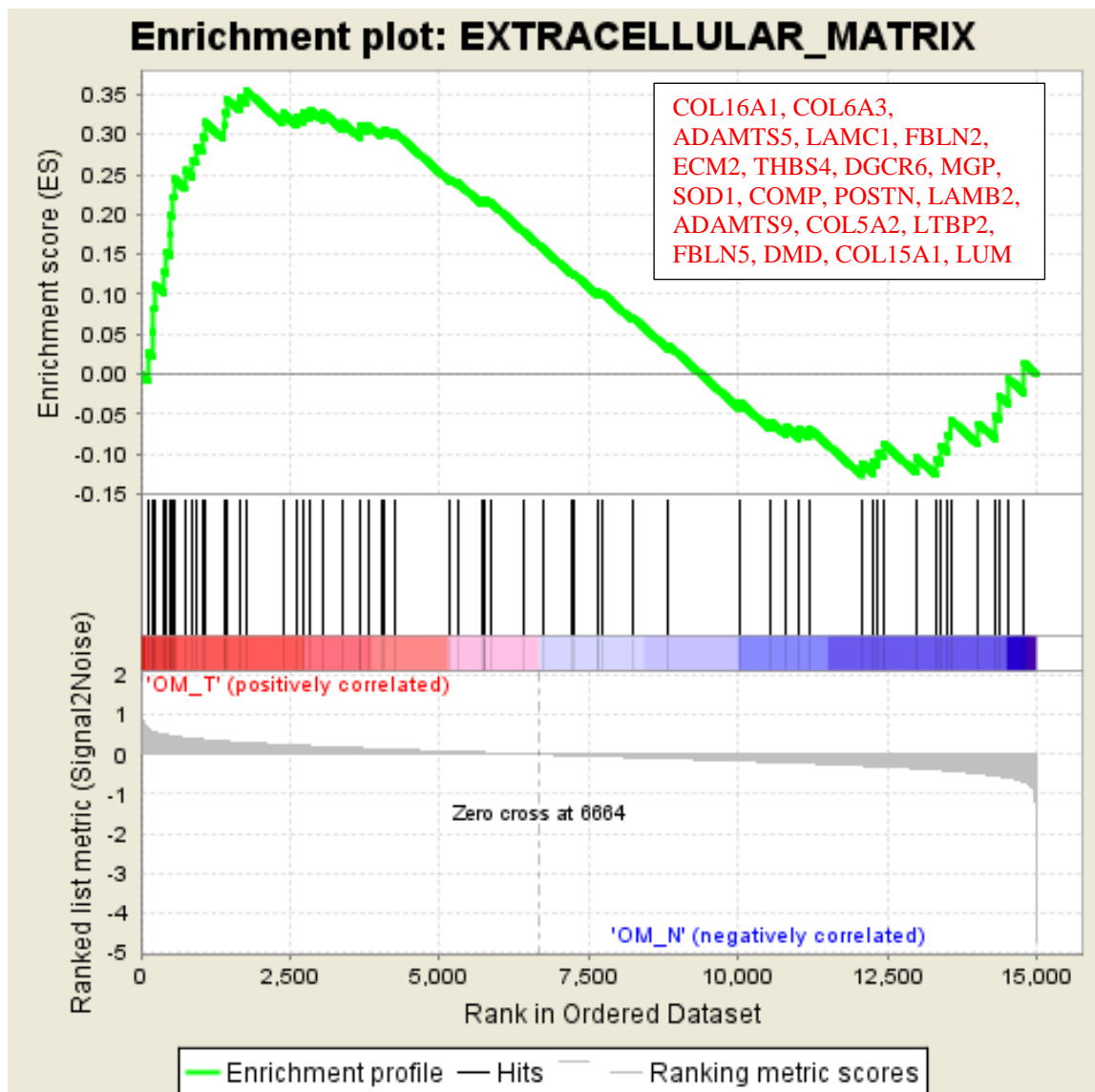
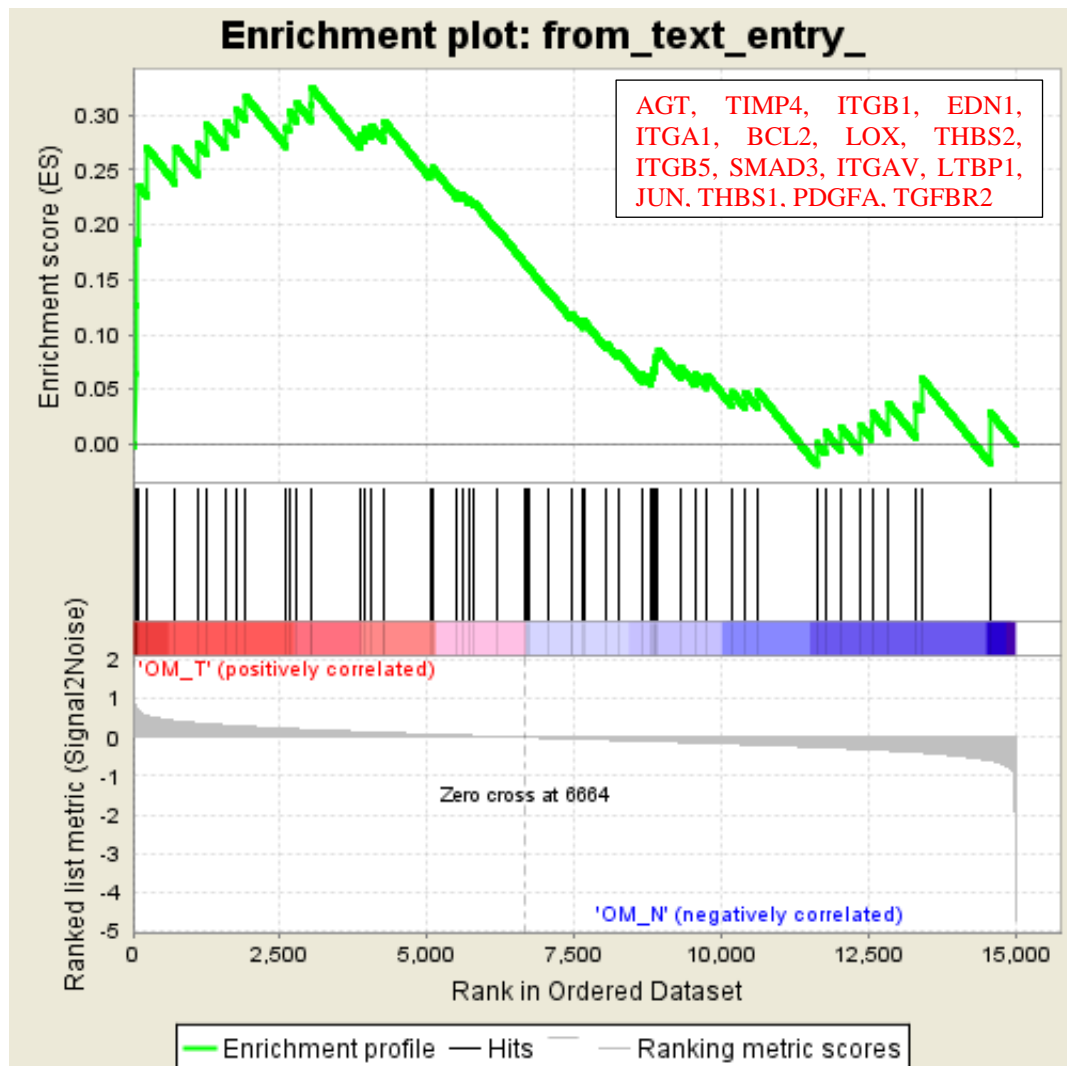


Figure 54: Heat map and enrichment plots of ECM genes in OM depot (T2DM vs NT2DM).

Each black vertical line in enrichment plot denotes one gene and color bar represents gene rank within list of genes. Output was generated in GSEA and significance was capped at $P < 0.05$.

Fibrosis is deposition of excess connective tissue including extracellular matrix proteins such as collagens. We analyzed list of 59 genes responsible for fibrosis in T2DM compared to NT2DM subjects in both SC and OM depots (figure 55). Fibrosis genes were positively enriched (ES = 0.324) in OM depot from T2DM (compared to NT2DM) whereas enrichment was non-significant in SC depot indicating increased fibrosis in OM from T2DM subjects. 16 genes (AGT,

TIMP4, ITGB1, EDN1, ITGA1, BCL2, LOX, THBS2, ITGB5, SMAD3, ITGAV, LTBP1, JUN, THBS1, PDGFA, TGFBR2) contributed significantly towards positive enrichment. Altogether, ECM and fibrosis genes were positively enriched in T2DM, especially in OM depot indicating the role of ECM in maintaining adipose tissue health.



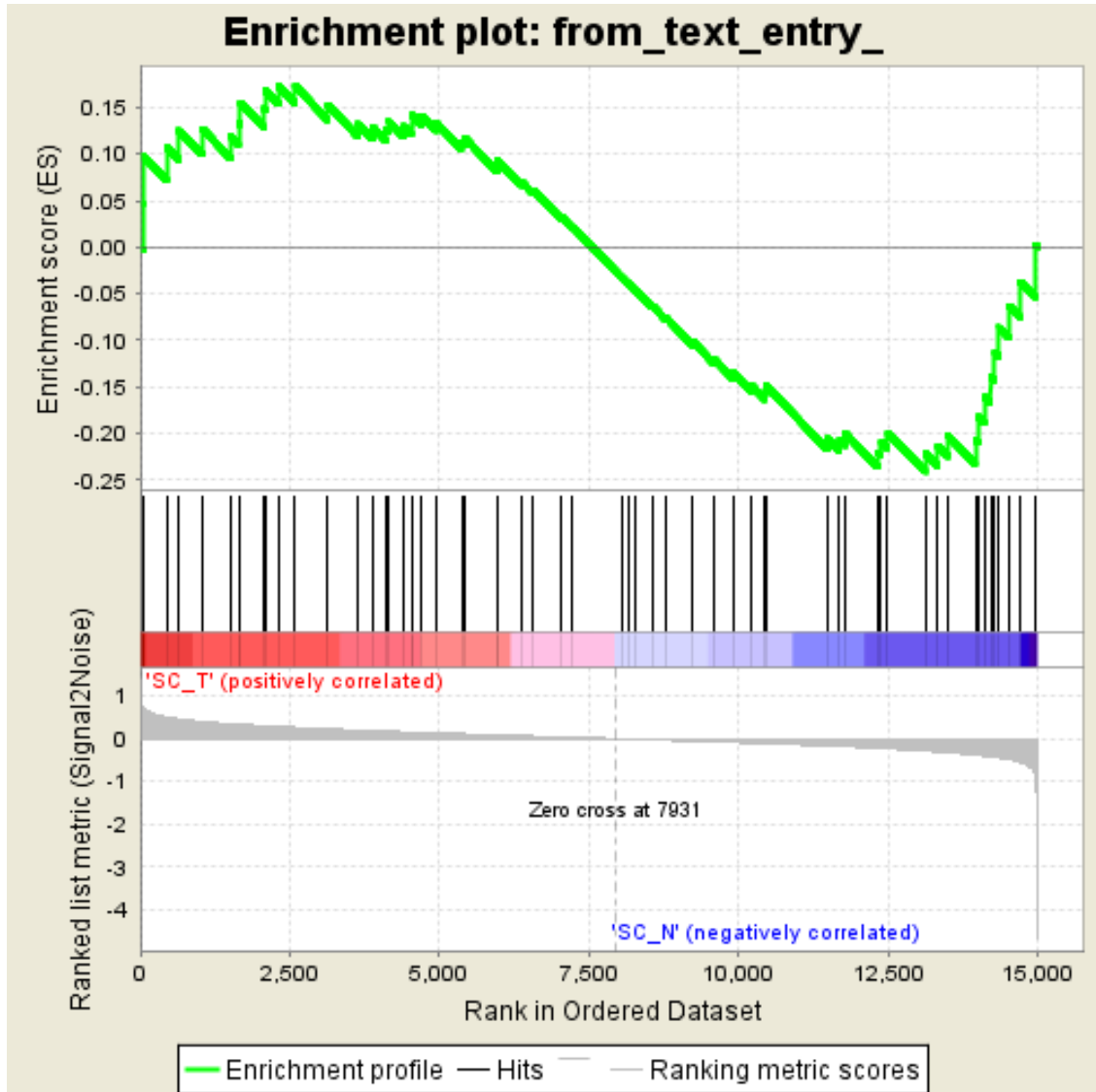


Figure 55: Enrichment analysis of fibrosis genes in T2DM compared to NT2DM (SC and OM depots).

Each black vertical line in enrichment plot denotes one gene and color bar represents gene rank within list of genes. Output was generated by analyzing genes of interest using GSEA and significance was capped at $P < 0.05$.

6.4 Discussion

Adipose tissue function and expandability is an important determinant of metabolic homeostasis [211] and failure to remodel ECM during obesity results in adipose dysfunction and onset of T2DM [37]. Although, several secretory and functional variances among OM and SC depot are now understood, transcriptomic differences between adipose from obese non-diabetics

(metabolically healthy obese) and obese diabetics have not been explored previously. In the present study, we performed detailed KEGG pathway and GO_cellular component enrichment as well as interaction analysis of transcripts between (I) OM depot compared to SC depot in both T2DM and NT2DM subjects and (II) T2DM compared to NT2DM in both SC and OM depots. This strategy enabled us to elaborate on both the depot specific and the disease specific differences occurring in obese diabetics compared to obese non-diabetics.

Sample-to-sample distance calculation and principle component analysis showed that OM and SC depot have very distinct transcriptome signatures, whereas there is less variation between T2DM and NT2DM samples. This is also confirmed by number of differentially expressed genes (DEGs) in OM depot compared to SC depot in both T2DM (n = 3063) and NT2DM (n = 1944) subjects in contrast to DEGs in T2DM compared to NT2DM subjects in SC (n = 199) and OM (n = 295) depot. Raw data was paired subject-wise (OM normalized to SC in each subject) when comparing OM with SC depot in order to reduce baseline biological variation and hence, the functional annotation of DEGs to KEGG biological pathways and gene ontologies was performed using fold change in this case. The Ranked FPKM was used for comparing unpaired data sets between T2DM and NT2DM subjects with the help of gene set enrichment analysis tool or GSEA.

KEGG pathways and cellular components of interest in OM compared to SC depot

Cytokine-cytokine receptor interaction ($P = 0.0015$) and PI3K-Akt signaling pathway were exclusively enriched in the omental depot from T2DM subjects ($P = 0.002$). PI3K-Akt signaling pathway was of an interest owing to its direct link to insulin signaling pathway, growth stimuli, activation of transcription, translation, proliferation, growth and survival. The majority of DEGs (total DEGs = 91) were positioned upstream in this pathway and contained genes common with the ECM-receptor interaction pathway (COL5A3, COL4A5, LAMB3, ITGB8, TNC, VWF, TNN and SPP1, figure 46). Compared to SC depot, COL5A3 was downregulated in the OM depot in both T2DM ($\log FC = -1.54$) and NT2DM ($\log FC = -1.23$) subjects. COL5A3 deficient mice exhibit lipodystrophy like phenotype with reduced dermal fat, resistance to diet induced weight gain, glucose intolerance and insulin resistance [212]. Hence downregulation of COL5A3 in OM depot compared to SC depot may indicate a pathogenic role of COL5A3 in the OM depot specifically. Several other members of collagen family including COL9A2, COL8A1 and COL17A1 were upregulated in OM depot whereas COL16A1, COL12A1, COL24A1 and COL4A2 were downregulated in OM depot exclusively in T2DM subjects but their functions are not fully understood yet. VEGF is an angiogenesis promoter [37] and compared to SC, was upregulated in OM depot from NT2DM only. Angiogenesis is a vital process to maintain growing adipose tissue in a non-hypoxic environment and multiple studies have linked impaired angiogenesis and increased hypoxia to metabolic dysregulation [18, 20, 27, 41, 42, 88, 213, 214].

Apart from several collagens, detailed analysis of GO_CC revealed upregulation in Wnt signaling genes; WNT5B, WNT11, WNT9A, WNT3 and WNT4 in OM depot exclusively in T2DM subjects (figure 50). Wnt signaling glycoproteins are part of the canonical pathway which signals growth, proliferation, cell fate specification and cell migration. Among the members of Wnt signaling pathway, TCF7L2 and WNT5B mutations have been previously implicated to increased T2DM ($\chi^2 = 15.6$, $P = 00008$; odds ratio = 1.74; 95% confidence interval = 1.32–2.29) susceptibility in humans. WNT5B overexpression improves adipogenesis and also plays a role in the pathogenesis of T2DM through regulation of adipocyte function through adipokine production [215-218]. WNT4 promotes adipogenesis and WNT3A inhibits adipogenesis in 3T3-L1 adipocytes [219, 220]. Due to opposing effects of Wnt members, our results remain inconclusive, but dysregulated expression in numerous members of this pathway supported the role of Wnt signaling pathway in the pathogenesis of insulin resistance, partly because of OM depot related pathogenic mechanisms.

KEGG pathways and cellular components of interest in T2DM compared to NT2DM subjects

In the SC depot, three metabolic pathways including butanoate metabolism, propanoate metabolism as well as valine, leucine and iso-leucine (branched chain amino acids or BCAA) degradation were negatively enriched and showed significant interactions. Increased BCAA are associated with obesity, insulin resistance and T2DM [221, 222] and casual mechanisms involves activation of mTORC pathway and uncoupling of IRS1 from insulin receptor, thus inhibiting insulin signaling pathway. Reduced transcripts of BCAA in our dataset might

indicate a propensity towards increased cellular BCAA, but needs further quantitative validation. The role of butanoate and propanoate metabolism in adipose tissue associated pathogenesis of insulin resistance is not well studied yet. Mice supplemented with butanoate or butyric acid exhibit increased PGC1 α and UCP1 gene expression in brown adipose tissue and skeletal muscle and are protected from diet induced obesity and insulin resistance [223]. Compared to NT2DM subjects, insulin signaling pathway was negatively enriched (ES = -0.30, P = 0.40) in SC depot from T2DM. PPP1R3C, PRKAR2B, IRS2, PHK2 and PRKAG2 genes contributed to negative enrichment. IRS2 is an upstream signaling molecule in insulin signaling pathway and its disruption in mice is known to result in hepatic as well as skeletal muscle insulin resistance and onset of type 2 diabetes [224].

Amid ECM genes (T2DM compared to NT2DM); structural proteins such as collagens (COL16A1, COL6A3, COL5A2, COL4A2 and COL5A3), laminins (LAMC1 and LAMB2) and fibulins (FBLN2 and FBLN5) were upregulated in OM depot and contributed to core enrichment in ECM in this subject group. Among fibrosis genes; integrins (ITGAV, ITGB1, ITGB5 and ITGA1), glycoproteins (THBS1 and THBS2) and enzymes (LOX and TIMP4) were upregulated in OM depot (T2DM compared to NT2DM subjects). Previously, Collagen I, III and VI were observed to be particularly abundant in SC and OM depot from obese individuals when compared to lean individuals [225]. Our results suggest that these are differentially expressed amongst the diabetics and non-diabetics at same BMI. Collagen VI is one of the highly enriched collagen in adipose tissue and upon its deletion in adipose tissue results in uninhibited expansion capacity in conjunction with improved energy homeostasis; both in

HFD and *ob/ob* background. A recent study linked expression of collagen VI, alpha 3 (COL6A3) to paracrine effects of leptin secreted from adipose tissue [226]; where leptin resulted in the dose dependent decrease in gene expression of COL6A3.

Pathogenic contribution of ECM and fibrosis components in obese diabetics is partially understood, and our analysis showed upregulation of transcripts annotated to ECM and fibrosis components in OM depot from T2DM compared to OM depot from NT2DM subjects, which highlights their importance in healthy adipose tissue expandability in obese non-diabetics compared to obese diabetics. However, it is important to consider possible discordance between expression at transcript level and protein level and selected genes might need further validation.

6.5 Conclusion

RNA sequencing showed that there are more distinguishing features between the OM and SC adipose depots than there are between adipose from T2DM vs NT2DM, even when variability due to inter individual differences are accounted for. RNA sequencing analyses interestingly revealed that pathways involved in ECM and fibrosis to be different in OM depot between T2DM and NT2DM subjects, supporting the concept that healthy adipose expansion in obesity is required for maintenance of metabolic homeostasis.

7. Summary and future work

Adipose tissue health is determined by its ability to expand and (I) store excess nutrients inside lipid droplets without spill over to visceral organs such as liver, skeletal muscle and heart (II) maintain adipokine secretion and inflammation (III) balance lipogenesis and lipolysis according to fed or fasting state and (IV) remodel ECM and angiogenesis [58, 199]. We studied three aspects of adipose tissue biology which included lipid storage via FIT2 protein, mitochondrial function via FTO protein and the relevance of extracellular matrix components.

Re-evaluating the use of SGBS adipocytes as a representative model of human adipocytes, by comparison with primary human subcutaneous adipocytes

Transcriptome and functional analysis suggested that SGBS adipocytes retained a UCP1 expressing brown adipocyte like phenotype when compared to stromal vascular fraction derived primary human adipocytes. Moreover, results obtained from RNA sequencing indicated positive enrichment of transcripts belonging to mitochondria and oxidative phosphorylation gene ontologies. This is further validated and confirmed by elevated UCP1 mRNA and protein expression as well as significantly increased mitochondrial spare respiratory capacity and maximal respiratory capacity in them. SGBS adipocytes also have elevated radioactive glucose uptake and lipid accumulation. Overall, even with existing differences, SGBS are a valid and robust model for preliminary studies in adipocyte metabolism. But, it is still unclear if phenotypic variances are due to neonatal origin or mutations in SGBS adipocytes and needs further studies.

Partial deficiency of FIT2 protein impairs triglyceride storage and insulin signaling in human adipocytes

Deficiency of lipid storage protein FIT2 leads to dysfunctional primary human adipocytes at basal and free fatty acid challenged state. FIT2 protein expression was higher in SC and OM adipose tissue depot from non-diabetics compared respective depots from diabetics. We used palmitic acid, one of the most abundant and pathogenic saturated free fatty acid to induce insulin resistance in adipocytes derived from the stromal vascular fraction of adipose tissue. In SC adipocytes, palmitate induced lipid accumulation was directly proportional to FIT2 protein expression. Its Knockdown resulted in reduced TAG accumulation, significantly increased IL6 and IL18 mRNA expression as well as palmitate induced IRE1 α phosphorylation. Akt phosphorylation at Ser-473 amino acid was observed to be lower in FIT2 knockdown adipocytes along with decreased radioactive glucose uptake.

Next, we aim to:

- **Investigate effect of oleic acid in FIT2 deficient SC adipocytes.** Oleic acid is a relatively low toxicity monounsaturated free fatty acid [165]. This experiment will enable us to mimic the free fatty acid milieu more accurately.

FTO protein knockdown or chemical inhibition of FTO can increase energy expenditure in human adipocytes

FTO protein knockdown and drug inhibition resulted in increased PGC1 α and UCP1 mRNA expression. In addition, FTO inhibition by drug CA at 50 μ M concentration increased mitochondrial spare respiratory capacity and maximal

respiration capacity in SGBS adipocytes. Also, FTO knockdown or drug inhibition or a combination of both augmented AMPK α phosphorylation indicating possible role of AMPK pathway in FTO induced mitochondrial function. AMPK pathway contributes to adipose health through suppression of inflammation and regulation of adipogenesis as well as carbohydrate and lipid metabolism pathways [227]. In recent years, AMPK pathway proteins have become lucrative drug targets to combat insulin resistance and type 2 diabetes [228] and we validated an FTO inhibitor with potential for further elaborate studies and therapeutic use.

Next we aim to:

- **Examine the role of AMPK pathway in FTO mediated upregulation of mitochondrial function.** Normally, AMPK pathway is activated by cAMP in response to stimuli such as glucose deprivation or lack of ATP. In conjunction with drug CA, we aim to use cAMP inhibitors in SGBS adipocytes to study FTO biology in more detail.

In future, we also hope to relate our work to studies in animal models that establish causality. It will be of tremendous clinical interest to determine if the FTO inhibitor could bring about similar beneficial metabolic effects in animal models. It would also be interesting to map out the mRNAs targeted by FTO demethylase activity in order to give rise to the obesity phenotypes and better understand the biological pathways that may be regulated by FTO.

Transcriptomic analysis reveals a role for extracellular matrix and fibrosis pathways in maintaining healthy human adipose tissue function in obese non-diabetics

Transcriptome analysis by RNA sequencing displayed significant enrichment in numerous KEGG biological pathways and gene ontologies in OM depot compared to SC depot in both diabetics and non-diabetics. PI3K-Akt signaling pathway was enriched in OM depot compared to SC depot in T2DM subjects. Extracellular matrix and fibrosis components were positively enriched in OM depot from diabetics when compared to OM depot from non-diabetics. Increased fibrosis and extracellular matrix are known to be detrimental to adipose tissue expandability [45]. Hence, our data suggest that increased ECM and fibrosis could potentially contribute to adipose tissue dysfunction and pathogenesis of type 2 diabetes in obese individuals.

Future directions:

- Currently, our analysis is limited to gene expression obtained from RNA sequencing. Our next step would be to validate differences in expression of selected genes at the protein level.
- Novel genes identified from this study can be functionally validated and characterized in human derived cell lines to better understand processes driving insulin sensitivity in the metabolically healthy obese. In particular, genes contributing significantly to positive enrichment in ECM and fibrosis components in T2DM subjects can be investigated further either by inhibiting over-accumulation of ECM or fibrosis

components or by targeting certain proteins via pharmacological intervention

8. References

1. Gardner DG, S.D., *Greenspan's Basic & Clinical Endocrinology*. Chapter 1. Hormones and Hormone Action, ed. A.M. Gardner DG, Nissenson RA. Vol. 9e. 2011, New York, NY: McGraw-Hill.
2. *Diabetes Fact sheet N°312*. January 2015; Available from: <http://www.who.int/mediacentre/factsheets/fs312/en/>.
3. *International Diabetes Federation in IDF Diabetes Atlas*. 2013, International Diabetes Federation: Brussels, Belgium.
4. Haldar, S., S.C. Chia, and C.J. Henry, *Body Composition in Asians and Caucasians: Comparative Analyses and Influences on Cardiometabolic Outcomes*. Adv Food Nutr Res, 2015. **75**: p. 97-154.
5. Ramachandran, A., et al., *Obesity in Asia – is it different from rest of the world*. Diabetes/Metabolism Research and Reviews, 2012. **28**: p. 47-51.
6. Ramachandran, A., R.C. Ma, and C. Snehalatha, *Diabetes in Asia*. Lancet, 2010. **375**(9712): p. 408-18.
7. Cohen, P. and B.M. Spiegelman, *Brown and Beige Fat: Molecular Parts of a Thermogenic Machine*. Diabetes, 2015.
8. Betz, M.J. and S. Enerbäck, *Human Brown Adipose Tissue: What We Have Learned So Far*. Diabetes, 2015.
9. Virtanen, K.A., et al., *Functional Brown Adipose Tissue in Healthy Adults*. New England Journal of Medicine, 2009. **360**(15): p. 1518-1525.
10. Wu, J., et al., *Beige adipocytes are a distinct type of thermogenic fat cell in mouse and human*. Cell, 2012. **150**(2): p. 366-76.
11. Thomas, E.L., et al., *The missing risk: MRI and MRS phenotyping of abdominal adiposity and ectopic fat*. Obesity (Silver Spring), 2012. **20**(1): p. 76-87.
12. Thorne, A., et al., *A pilot study of long-term effects of a novel obesity treatment: omentectomy in connection with adjustable gastric banding*. Int J Obes Relat Metab Disord, 2002. **26**(2): p. 193-9.
13. Motoshima, H., et al., *Differential regulation of adiponectin secretion from cultured human omental and subcutaneous adipocytes: effects of insulin and rosiglitazone*. J Clin Endocrinol Metab, 2002. **87**(12): p. 5662-7.
14. Fisher, F.M., et al., *Differences in adiponectin protein expression: effect of fat depots and type 2 diabetic status*. Horm Metab Res, 2002. **34**(11-12): p. 650-4.
15. Zhang, Y.Y., et al., *Positional Cloning of the Mouse Obese Gene and Its Human Homolog*. Nature, 1994. **372**(6505): p. 425-432.
16. Halaas, J.L., et al., *Weight-Reducing Effects of the Plasma-Protein Encoded by the Obese Gene*. Science, 1995. **269**(5223): p. 543-546.
17. Scherer, P.E., et al., *A novel serum protein similar to C1q, produced exclusively in adipocytes*. J Biol Chem, 1995. **270**(45): p. 26746-9.
18. Rupnick, M.A., et al., *Adipose tissue mass can be regulated through the vasculature*. Proc Natl Acad Sci U S A, 2002. **99**(16): p. 10730-5.
19. Hotamisligil, G.S., N.S. Shargill, and B.M. Spiegelman, *Adipose expression of tumor necrosis factor-alpha: direct role in obesity-linked insulin resistance*. Science, 1993. **259**(5091): p. 87-91.
20. Trayhurn, P., *Hypoxia and Adipose Tissue Function and Dysfunction in Obesity*. Physiological Reviews, 2013. **93**(1): p. 1-21.

21. Virtue, S. and A. Vidal-Puig, *It's Not How Fat You Are, It's What You Do with It That Counts*. PLoS Biol, 2008. **6**(9): p. e237.
22. Virtue, S. and A. Vidal-Puig, *Adipose tissue expandability, lipotoxicity and the Metabolic Syndrome--an allostatic perspective*. Biochim Biophys Acta, 2010. **1801**(3): p. 338-49.
23. Karelis, A.D., M. Brochu, and R. Rabasa-Lhoret, *Can we identify metabolically healthy but obese individuals (MHO)?* Diabetes & Metabolism, 2004. **30**(6): p. 569-572.
24. Karelis, A.D., et al., *The metabolically healthy but obese individual presents a favorable inflammation profile*. J Clin Endocrinol Metab, 2005. **90**(7): p. 4145-50.
25. Barroso, I., et al., *Dominant negative mutations in human PPARgamma associated with severe insulin resistance, diabetes mellitus and hypertension*. Nature, 1999. **402**(6764): p. 880-3.
26. Nichols, G.A. and A. Gomez-Camirero, *Weight changes following the initiation of new anti-hyperglycaemic therapies*. Diabetes Obes Metab, 2007. **9**(1): p. 96-102.
27. Trayhurn, P. and I.S. Wood, *Adipokines: inflammation and the pleiotropic role of white adipose tissue*. Br J Nutr, 2004. **92**(3): p. 347-55.
28. Kim, J.-Y., et al., *Obesity-associated improvements in metabolic profile through expansion of adipose tissue*. The Journal of Clinical Investigation, 2007. **117**(9): p. 2621-2637.
29. McLaughlin, T., et al., *Preferential fat deposition in subcutaneous versus visceral depots is associated with insulin sensitivity*. J Clin Endocrinol Metab, 2011. **96**(11): p. E1756-60.
30. Gavrilova, O., et al., *Surgical implantation of adipose tissue reverses diabetes in lipoatrophic mice*. J Clin Invest, 2000. **105**(3): p. 271-8.
31. Rosen, E.D. and B.M. Spiegelman, *What we talk about when we talk about fat*. Cell, 2014. **156**(1-2): p. 20-44.
32. Krotkiewski, M., et al., *Impact of obesity on metabolism in men and women. Importance of regional adipose tissue distribution*. J Clin Invest, 1983. **72**(3): p. 1150-62.
33. Veilleux, A., et al., *Visceral Adipocyte Hypertrophy is Associated With Dyslipidemia Independent of Body Composition and Fat Distribution in Women*. Diabetes, 2011. **60**(5): p. 1504-1511.
34. DiGirolamo, M., et al., *Qualitative regional differences in adipose tissue growth and cellularity in male Wistar rats fed ad libitum*. Am J Physiol, 1998. **274**(5 Pt 2): p. R1460-7.
35. Spalding, K.L., et al., *Dynamics of fat cell turnover in humans*. Nature, 2008. **453**(7196): p. 783-7.
36. Kral, J.G., et al., *Body composition and adipose tissue cellularity before and after jejuno-ileostomy in severely obese subjects*. Eur J Clin Invest, 1977. **7**(5): p. 413-9.
37. Lee, M.J., Y. Wu, and S.K. Fried, *Adipose tissue remodeling in pathophysiology of obesity*. Curr Opin Clin Nutr Metab Care, 2010. **13**(4): p. 371-6.
38. Bourlier, V., et al., *Remodeling phenotype of human subcutaneous adipose tissue macrophages*. Circulation, 2008. **117**(6): p. 806-15.

39. Frantz, C., K.M. Stewart, and V.M. Weaver, *The extracellular matrix at a glance*. *Journal of Cell Science*, 2010. **123**(24): p. 4195-4200.
40. Corvera, S. and O. Gealekman, *Adipose tissue angiogenesis: impact on obesity and type-2 diabetes*. *Biochim Biophys Acta*, 2014. **1842**(3): p. 463-72.
41. Spencer, M., et al., *Adipose tissue extracellular matrix and vascular abnormalities in obesity and insulin resistance*. *J Clin Endocrinol Metab*, 2011. **96**(12): p. E1990-8.
42. Nishimura, S., et al., *Adipogenesis in Obesity Requires Close Interplay Between Differentiating Adipocytes, Stromal Cells, and Blood Vessels*. *Diabetes*, 2007. **56**(6): p. 1517-1526.
43. Hosogai, N., et al., *Adipose Tissue Hypoxia in Obesity and Its Impact on Adipocytokine Dysregulation*. *Diabetes*, 2007. **56**(4): p. 901-911.
44. Halberg, N., et al., *Hypoxia-inducible factor 1alpha induces fibrosis and insulin resistance in white adipose tissue*. *Mol Cell Biol*, 2009. **29**(16): p. 4467-83.
45. Sun, K., et al., *Fibrosis and adipose tissue dysfunction*. *Cell Metab*, 2013. **18**(4): p. 470-7.
46. Brasaemle, D.L., *Thematic review series: adipocyte biology. The perilipin family of structural lipid droplet proteins: stabilization of lipid droplets and control of lipolysis*. *J Lipid Res*, 2007. **48**(12): p. 2547-59.
47. Gross, D.A., E.L. Snapp, and D.L. Silver, *Structural insights into triglyceride storage mediated by fat storage-inducing transmembrane (FIT) protein 2*. *PLoS One*, 2010. **5**(5): p. e10796.
48. Gross, D.A., C. Zhan, and D.L. Silver, *Direct binding of triglyceride to fat storage-inducing transmembrane proteins 1 and 2 is important for lipid droplet formation*. *Proc Natl Acad Sci U S A*, 2011. **108**(49): p. 19581-6.
49. Qiu, W., et al., *Suppression of Adipogenesis by Pathogenic Seipin Mutant Is Associated with Inflammatory Response*. *PLoS ONE*, 2013. **8**(3): p. e57874.
50. Szymanski, K.M., et al., *The lipodystrophy protein seipin is found at endoplasmic reticulum lipid droplet junctions and is important for droplet morphology*. *Proceedings of the National Academy of Sciences*, 2007. **104**(52): p. 20890-20895.
51. Kadereit, B., et al., *Evolutionarily conserved gene family important for fat storage*. *Proc Natl Acad Sci U S A*, 2008. **105**(1): p. 94-9.
52. Miranda, D.A., et al., *Re-patterning of skeletal muscle energy metabolism by fat storage-inducing transmembrane protein 2*. *J Biol Chem*, 2011. **286**(49): p. 42188-99.
53. Fei, W., et al., *Molecular characterization of seipin and its mutants: implications for seipin in triacylglycerol synthesis*. *J Lipid Res*, 2011. **52**(12): p. 2136-47.
54. Boden, G., et al., *Excessive caloric intake acutely causes oxidative stress, GLUT4 carbonylation, and insulin resistance in healthy men*. *Sci Transl Med*, 2015. **7**(304): p. 304re7.
55. Griffin, M.E., et al., *Free fatty acid-induced insulin resistance is associated with activation of protein kinase C theta and alterations in the insulin signaling cascade*. *Diabetes*, 1999. **48**(6): p. 1270-4.

56. Szendroedi, J., et al., *Role of diacylglycerol activation of PKC θ in lipid-induced muscle insulin resistance in humans*. Proc Natl Acad Sci U S A, 2014. **111**(26): p. 9597-602.
57. Kawasaki, N., et al., *Obesity-induced endoplasmic reticulum stress causes chronic inflammation in adipose tissue*. Sci Rep, 2012. **2**: p. 799.
58. Shulman, G.I., *Ectopic fat in insulin resistance, dyslipidemia, and cardiometabolic disease*. N Engl J Med, 2014. **371**(12): p. 1131-41.
59. Liu, L., et al., *Upregulation of myocellular DGAT1 augments triglyceride synthesis in skeletal muscle and protects against fat-induced insulin resistance*. J Clin Invest, 2007. **117**(6): p. 1679-89.
60. Dresner, A., et al., *Effects of free fatty acids on glucose transport and IRS-1-associated phosphatidylinositol 3-kinase activity*. J Clin Invest, 1999. **103**(2): p. 253-9.
61. Yu, C., et al., *Mechanism by which fatty acids inhibit insulin activation of insulin receptor substrate-1 (IRS-1)-associated phosphatidylinositol 3-kinase activity in muscle*. J Biol Chem, 2002. **277**(52): p. 50230-6.
62. Itani, S.I., et al., *Lipid-induced insulin resistance in human muscle is associated with changes in diacylglycerol, protein kinase C, and I κ B α* . Diabetes, 2002. **51**(7): p. 2005-11.
63. Hotamisligil, G.S., *Inflammation and metabolic disorders*. Nature, 2006. **444**(7121): p. 860-7.
64. Pal, D., et al., *Fetuin-A acts as an endogenous ligand of TLR4 to promote lipid-induced insulin resistance*. Nat Med, 2012.
65. Shi, H., et al., *TLR4 links innate immunity and fatty acid-induced insulin resistance*. J Clin Invest, 2006. **116**(11): p. 3015-25.
66. Hellman, B., S. Larsson, and S. Westman, *Mast Cell Content and Fatty Acid Metabolism in the Epididymal Fat Pad of Obese Mice*. Acta Physiologica Scandinavica, 1963. **58**(2-3): p. 255-262.
67. Hotamisligil, G.S., et al., *IRS-1-mediated inhibition of insulin receptor tyrosine kinase activity in TNF- α - and obesity-induced insulin resistance*. Science, 1996. **271**(5249): p. 665-8.
68. Fischer-Posovszky, P., et al., *Targeted deletion of adipocytes by apoptosis leads to adipose tissue recruitment of alternatively activated M2 macrophages*. Endocrinology, 2011. **152**(8): p. 3074-81.
69. Oh, D.Y., et al., *Increased macrophage migration into adipose tissue in obese mice*. Diabetes, 2012. **61**(2): p. 346-54.
70. Weisberg, S.P., et al., *Obesity is associated with macrophage accumulation in adipose tissue*. J Clin Invest, 2003. **112**(12): p. 1796-808.
71. Xu, H., et al., *Chronic inflammation in fat plays a crucial role in the development of obesity-related insulin resistance*. J Clin Invest, 2003. **112**(12): p. 1821-30.
72. Ouchi, N., et al., *Adipokines in inflammation and metabolic disease*. Nat Rev Immunol, 2011. **11**(2): p. 85-97.
73. Wernstedt Asterholm, I., et al., *Adipocyte Inflammation Is Essential for Healthy Adipose Tissue Expansion and Remodeling*. Cell Metabolism, 2014. **20**(1): p. 103-118.
74. Kiortsis, D.N., et al., *Effects of infliximab treatment on insulin resistance in patients with rheumatoid arthritis and ankylosing spondylitis*. Ann Rheum Dis, 2005. **64**(5): p. 765-6.

75. Gonzalez-Gay, M.A., et al., *Anti-tumor necrosis factor-alpha blockade improves insulin resistance in patients with rheumatoid arthritis*. Clin Exp Rheumatol, 2006. **24**(1): p. 83-6.
76. Nguyen, K.D., et al., *Alternatively activated macrophages produce catecholamines to sustain adaptive thermogenesis*. Nature, 2011. **480**(7375): p. 104-8.
77. Oyadomari, S., et al., *Nitric oxide-induced apoptosis in pancreatic beta cells is mediated by the endoplasmic reticulum stress pathway*. Proc Natl Acad Sci U S A, 2001. **98**(19): p. 10845-50.
78. Wang, H., G. Kouri, and C.B. Wollheim, *ER stress and SREBP-1 activation are implicated in beta-cell glucolipotoxicity*. J Cell Sci, 2005. **118**(Pt 17): p. 3905-15.
79. Schroder, M. and R.J. Kaufman, *ER stress and the unfolded protein response*. Mutat Res, 2005. **569**(1-2): p. 29-63.
80. Kaneto, H., et al., *Oxidative stress, ER stress, and the JNK pathway in type 2 diabetes*. J Mol Med (Berl), 2005. **83**(6): p. 429-39.
81. Tabas, I., *Macrophage apoptosis in atherosclerosis: consequences on plaque progression and the role of endoplasmic reticulum stress*. Antioxid Redox Signal, 2009. **11**(9): p. 2333-9.
82. Sharma, N.K., et al., *Endoplasmic Reticulum Stress Markers Are Associated with Obesity in Nondiabetic Subjects*. Journal of Clinical Endocrinology & Metabolism, 2008. **93**(11): p. 4532-4541.
83. Boden, G. and S. Merali, *Measurement of the increase in endoplasmic reticulum stress-related proteins and genes in adipose tissue of obese, insulin-resistant individuals*. Methods Enzymol, 2011. **489**: p. 67-82.
84. Boden, G., et al., *Insulin regulates the unfolded protein response (UPR) in human adipose tissue*. Diabetes, 2013.
85. Gregor, M.F., et al., *Endoplasmic reticulum stress is reduced in tissues of obese subjects after weight loss*. Diabetes, 2009. **58**(3): p. 693-700.
86. Hotamisligil, G.S. and E. Erbay, *Nutrient sensing and inflammation in metabolic diseases*. Nat Rev Immunol, 2008. **8**(12): p. 923-34.
87. Ye, R., et al., *Grp78 heterozygosity promotes adaptive unfolded protein response and attenuates diet-induced obesity and insulin resistance*. Diabetes, 2010. **59**(1): p. 6-16.
88. Doroudgar, S., et al., *Ischemia activates the ATF6 branch of the endoplasmic reticulum stress response*. J Biol Chem, 2009. **284**(43): p. 29735-45.
89. Rao, R.V., H.M. Ellerby, and D.E. Bredesen, *Coupling endoplasmic reticulum stress to the cell death program*. Cell Death Differ, 2004. **11**(4): p. 372-80.
90. Zhou, J., et al., *Activation of the unfolded protein response occurs at all stages of atherosclerotic lesion development in apolipoprotein E-deficient mice*. Circulation, 2005. **111**(14): p. 1814-21.
91. Sokka, A.L., et al., *Endoplasmic reticulum stress inhibition protects against excitotoxic neuronal injury in the rat brain*. Journal of Neuroscience, 2007. **27**(4): p. 901-908.
92. Tanaka, Y., et al., *A role for glutathione peroxidase in protecting pancreatic beta cells against oxidative stress in a model of glucose toxicity*. Proc Natl Acad Sci U S A, 2002. **99**(19): p. 12363-8.

93. Robertson, R.P., et al., *Glucose toxicity in beta-cells: type 2 diabetes, good radicals gone bad, and the glutathione connection*. Diabetes, 2003. **52**(3): p. 581-7.
94. Brownlee, M., *Biochemistry and molecular cell biology of diabetic complications*. Nature, 2001. **414**(6865): p. 813-20.
95. Matsuoka, T., et al., *Glycation-dependent, reactive oxygen species-mediated suppression of the insulin gene promoter activity in HIT cells*. J Clin Invest, 1997. **99**(1): p. 144-50.
96. Poitout, V. and R.P. Robertson, *Minireview: Secondary beta-cell failure in type 2 diabetes--a convergence of glucotoxicity and lipotoxicity*. Endocrinology, 2002. **143**(2): p. 339-42.
97. Zhang, X., et al., *Hypothalamic IKKbeta/NF-kappaB and ER stress link overnutrition to energy imbalance and obesity*. Cell, 2008. **135**(1): p. 61-73.
98. Uehara, T., et al., *S-nitrosylated protein-disulphide isomerase links protein misfolding to neurodegeneration*. Nature, 2006. **441**(7092): p. 513-7.
99. Toth, A., et al., *Endoplasmic reticulum stress as a novel therapeutic target in heart diseases*. Cardiovasc Hematol Disord Drug Targets, 2007. **7**(3): p. 205-18.
100. Isodono, K., et al., *PARM-1 is an endoplasmic reticulum molecule involved in endoplasmic reticulum stress-induced apoptosis in rat cardiac myocytes*. PLoS One, 2010. **5**(3): p. e9746.
101. Wabitsch, M., et al., *Characterization of a human preadipocyte cell strain with high capacity for adipose differentiation*. Int J Obes Relat Metab Disord, 2001. **25**(1): p. 8-15.
102. Schlottmann, I., et al., *Calcium-dependent release of adipocyte fatty acid binding protein from human adipocytes*. Int J Obes (Lond), 2014. **38**(9): p. 1221-7.
103. Guennoun, A., et al., *Comprehensive molecular characterization of human adipocytes reveals a transient brown phenotype*. J Transl Med, 2015. **13**: p. 135.
104. Green, H. and M. Meuth, *An established pre-adipose cell line and its differentiation in culture*. Cell, 1974. **3**(2): p. 127-33.
105. Todaro, G.J. and H. Green, *Quantitative studies of the growth of mouse embryo cells in culture and their development into established lines*. J Cell Biol, 1963. **17**: p. 299-313.
106. Negrel, R., P. Grimaldi, and G. Ailhaud, *Establishment of preadipocyte clonal line from epididymal fat pad of ob/ob mouse that responds to insulin and to lipolytic hormones*. Proc Natl Acad Sci U S A, 1978. **75**(12): p. 6054-8.
107. Sugihara, H., et al., *Primary cultures of unilocular fat cells: characteristics of growth in vitro and changes in differentiation properties*. Differentiation, 1986. **31**(1): p. 42-9.
108. Cho, Y.S., et al., *Meta-analysis of genome-wide association studies identifies eight new loci for type 2 diabetes in east Asians*. Nat Genet, 2012. **44**(1): p. 67-72.
109. Stunkard, A.J., T.T. Foch, and Z. Hrubec, *A twin study of human obesity*. Jama, 1986. **256**(1): p. 51-4.

110. Bouchard, C., et al., *The response to long-term overfeeding in identical twins*. N Engl J Med, 1990. **322**(21): p. 1477-82.
111. Frayling, T.M., et al., *A common variant in the FTO gene is associated with body mass index and predisposes to childhood and adult obesity*. Science, 2007.
112. Dina, C., et al., *Variation in FTO contributes to childhood obesity and severe adult obesity*. Nat Genet, 2007. **39**(6): p. 724-6.
113. Loos, R.J.F. and C. Bouchard, *FTO: the first gene contributing to common forms of human obesity*. Obesity reviews, 2008.
114. Hunt, S.C., et al., *Association of the FTO gene with BMI*. ..., 2008.
115. Tan, J.T., et al., *FTO variants are associated with obesity in the Chinese and Malay populations in Singapore*. Diabetes, 2008.
116. Speliotes, E.K., et al., *Association analyses of 249,796 individuals reveal 18 new loci associated with body mass index*. Nat Genet, 2010. **42**(11): p. 937-48.
117. Fischer, J., et al., *Inactivation of the Fto gene protects from obesity*. Nature, 2009. **458**(7240): p. 894-8.
118. Karaderi, T., A.W. Drong, and C.M. Lindgren, *Insights into the Genetic Susceptibility to Type 2 Diabetes from Genome-Wide Association Studies of Obesity-Related Traits*. Curr Diab Rep, 2015. **15**(10): p. 83.
119. Bai, R.-K., et al., *Quantitative PCR Analysis of Mitochondrial DNA Content in Patients with Mitochondrial Disease*. Annals of the New York Academy of Sciences, 2004. **1011**(1): p. 304-309.
120. Fischer-Posovszky, P., et al., *Human SGBS Cells – a Unique Tool for Studies of Human Fat Cell Biology*. Obesity Facts, 2008. **1**(4): p. 184-189.
121. Jeffrey, K.D., et al., *Carboxypeptidase E mediates palmitate-induced β -cell ER stress and apoptosis*. Proceedings of the National Academy of Sciences, 2008. **105**(24): p. 8452-8457.
122. Draghici, S., et al., *A systems biology approach for pathway level analysis*. Genome Research, 2007. **17**(10): p. 1537-1545.
123. Tarca, A.L., et al., *A novel signaling pathway impact analysis*. Bioinformatics, 2009. **25**(1): p. 75-82.
124. Da Wei, H., T.S. Brad, and A.L. Richard, *Systematic and integrative analysis of large gene lists using DAVID bioinformatics resources*. Nature Protocols, 2008. **4**(1): p. 44-57.
125. Huang da, W., B.T. Sherman, and R.A. Lempicki, *Systematic and integrative analysis of large gene lists using DAVID bioinformatics resources*. Nat Protoc, 2009. **4**(1): p. 44-57.
126. Capurro, M.I., et al., *Glypican-3 inhibits Hedgehog signaling during development by competing with patched for Hedgehog binding*. Dev Cell, 2008. **14**(5): p. 700-11.
127. Young, E.L., R. Wishnow, and M.A. Nigro, *Expanding the clinical picture of Simpson-Golabi-Behmel syndrome*. Pediatr Neurol, 2006. **34**(2): p. 139-42.
128. Pilia, G., et al., *Mutations in GPC3, a glypican gene, cause the Simpson-Golabi-Behmel overgrowth syndrome*. Nat Genet, 1996. **12**(3): p. 241-7.
129. DeBaun, M.R., J. Ess, and S. Saunders, *Simpson Golabi Behmel syndrome: progress toward understanding the molecular basis for*

- overgrowth, malformation, and cancer predisposition.* Mol Genet Metab, 2001. **72**(4): p. 279-86.
130. Hughes-Benzie, R.M., et al., *Simpson-Golabi-Behmel syndrome: genotype/phenotype analysis of 18 affected males from 7 unrelated families.* Am J Med Genet, 1996. **66**(2): p. 227-34.
 131. Allott, E.H., et al., *The SGBS cell strain as a model for the in vitro study of obesity and cancer.* Clin Transl Oncol, 2012. **14**(10): p. 774-82.
 132. Murholm, M., et al., *Retinoic acid has different effects on UCP1 expression in mouse and human adipocytes.* BMC Cell Biol, 2013. **14**: p. 41.
 133. Tews, D., et al., *FTO deficiency induces UCP-1 expression and mitochondrial uncoupling in adipocytes.* Endocrinology, 2013. **154**(9): p. 3141-51.
 134. Subramanian, A., et al., *Gene set enrichment analysis: A knowledge-based approach for interpreting genome-wide expression profiles.* Proceedings of the National Academy of Sciences, 2005. **102**(43): p. 15545-15550.
 135. Merico, D., et al., *Enrichment map: a network-based method for gene-set enrichment visualization and interpretation.* PLoS One, 2010. **5**(11): p. e13984.
 136. Alexander, C.Z., et al., *GO-Elite: a flexible solution for pathway and ontology over-representation.* Bioinformatics, 2012. **28**(16): p. 2209-2210.
 137. Mootha, V.K., et al., *PGC-1alpha-responsive genes involved in oxidative phosphorylation are coordinately downregulated in human diabetes.* Nat Genet, 2003. **34**(3): p. 267-73.
 138. Harms, M. and P. Seale, *Brown and beige fat: development, function and therapeutic potential.* Nat Med, 2013. **19**(10): p. 1252-63.
 139. Liang, H. and W.F. Ward, *PGC-1alpha: a key regulator of energy metabolism.* Adv Physiol Educ, 2006. **30**(4): p. 145-51.
 140. Henegar, C., et al., *Adipose tissue transcriptomic signature highlights the pathological relevance of extracellular matrix in human obesity.* Genome Biol, 2008. **9**(1): p. R14.
 141. Huang, G. and D.S. Greenspan, *ECM roles in the function of metabolic tissues.* Trends Endocrinol Metab, 2012. **23**(1): p. 16-22.
 142. Rylander, E.V.A., H. PŘilbylovÁ, and J. Lind, *A THERMOGRAPHIC STUDY OF INFANTS EXPOSED TO COLD.* Acta Pædiatrica, 1972. **61**(1): p. 42-48.
 143. Mrosovsky, N. and U. Rowlatt, *Changes in the Microstructure of Brown Fat at Birth in the Human Infant.* Neonatology, 1968. **13**(3-4): p. 230-252.
 144. Novak, M., et al., *The role of carnitine in subcutaneous white adipose tissue from newborn infants.* Biol Neonate, 1973. **23**(1): p. 11-8.
 145. Petryszak, R., et al., *Expression Atlas update—a database of gene and transcript expression from microarray- and sequencing-based functional genomics experiments.* Nucleic Acids Research, 2014. **42**(D1): p. D926-D932.
 146. Kapushesky, M., et al., *Gene Expression Atlas update—a value-added database of microarray and sequencing-based functional genomics experiments.* Nucleic Acids Research, 2012. **40**(D1): p. D1077-D1081.

147. Kitamura, T., et al., *Mouse aldehyde dehydrogenase ALDH3B2 is localized to lipid droplets via two C-terminal tryptophan residues and lipid modification*. *Biochem J*, 2015. **465**(1): p. 79-87.
148. Zhao, Y., et al., *Aromatase P450 gene expression in human adipose tissue. Role of a Jak/STAT pathway in regulation of the adipose-specific promoter*. *J Biol Chem*, 1995. **270**(27): p. 16449-57.
149. Clyne, C.D., et al., *Liver receptor homologue-1 (LRH-1) regulates expression of aromatase in preadipocytes*. *J Biol Chem*, 2002. **277**(23): p. 20591-7.
150. McInnes, K.J., et al., *Characterisation of aromatase expression in the human adipocyte cell line SGBS*. *Breast Cancer Res Treat*, 2008. **112**(3): p. 429-35.
151. Rydén, M., et al., *Adipocyte triglyceride turnover and lipolysis in lean and overweight subjects*. *Journal of Lipid Research*, 2013. **54**(10): p. 2909-2913.
152. Ahmadian, M., et al., *Adipose overexpression of desnutrin promotes fatty acid use and attenuates diet-induced obesity*. *Diabetes*, 2009. **58**(4): p. 855-66.
153. Gu, X., et al., *Bip overexpression, but not CHOP inhibition, attenuates fatty-acid-induced endoplasmic reticulum stress and apoptosis in HepG2 liver cells*. *Life Sci*, 2010. **87**(23-26): p. 724-32.
154. Das, S.K., et al., *Effect of pioglitazone treatment on endoplasmic reticulum stress response in human adipose and in palmitate-induced stress in human liver and adipose cell lines*. *Am J Physiol Endocrinol Metab*, 2008. **295**(2): p. E393-400.
155. Miranda, D.A., et al., *Fat storage-inducing transmembrane protein 2 is required for normal fat storage in adipose tissue*. *J Biol Chem*, 2014. **289**(14): p. 9560-72.
156. Carswell, K., M.-J. Lee, and S. Fried, *Culture of Isolated Human Adipocytes and Isolated Adipose Tissue*, in *Human Cell Culture Protocols*, R.R. Mitry and R.D. Hughes, Editors. 2012, Humana Press. p. 203-214.
157. Yang, H., et al., *Controlling the size of lipid droplets: lipid and protein factors*. *Current Opinion in Cell Biology*, 2012. **24**(4): p. 509-516.
158. Denis, G.V. and M.S. Obin, *'Metabolically healthy obesity': origins and implications*. *Mol Aspects Med*, 2013. **34**(1): p. 59-70.
159. Olefsky, J.M. and C.K. Glass, *Macrophages, inflammation, and insulin resistance*. *Annu Rev Physiol*, 2010. **72**: p. 219-46.
160. Hwang, Y.C., et al., *Visceral abdominal fat accumulation predicts the conversion of metabolically healthy obese subjects to an unhealthy phenotype*. *Int J Obes*, 2015.
161. Fontana, L., et al., *Visceral fat adipokine secretion is associated with systemic inflammation in obese humans*. *Diabetes*, 2007. **56**(4): p. 1010-3.
162. Araki, E., S. Oyadomari, and M. Mori, *Impact of endoplasmic reticulum stress pathway on pancreatic beta-cells and diabetes mellitus*. *Exp Biol Med (Maywood)*, 2003. **228**(10): p. 1213-7.
163. Guo, W., et al., *Palmitate modulates intracellular signaling, induces endoplasmic reticulum stress, and causes apoptosis in mouse 3T3-L1*

- and rat primary preadipocytes.* Am J Physiol Endocrinol Metab, 2007. **293**(2): p. E576-86.
164. Karaskov, E., et al., *Chronic palmitate but not oleate exposure induces endoplasmic reticulum stress, which may contribute to INS-1 pancreatic beta-cell apoptosis.* Endocrinology, 2006. **147**(7): p. 3398-407.
 165. Talbot, N.A., C.P. Wheeler-Jones, and M.E. Cleasby, *Palmitoleic acid prevents palmitic acid-induced macrophage activation and consequent p38 MAPK-mediated skeletal muscle insulin resistance.* Molecular and Cellular Endocrinology, 2014. **393**(1-2): p. 129-142.
 166. Hara, K., T. Kadowaki, and M. Odawara, *Genes associated with diabetes: potential for novel therapeutic targets?* Expert Opin Ther Targets, 2015: p. 1-13.
 167. Frayling, T.M., et al., *A common variant in the FTO gene is associated with body mass index and predisposes to childhood and adult obesity.* Science, 2007. **316**(5826): p. 889-94.
 168. Scuteri, A., et al., *Genome-wide association scan shows genetic variants in the FTO gene are associated with obesity-related traits.* PLoS Genet, 2007. **3**(7): p. e115.
 169. Lu, Y. and R.J. Loos, *Obesity genomics: assessing the transferability of susceptibility loci across diverse populations.* Genome Med, 2013. **5**(6): p. 55.
 170. Tan, J.T., et al., *FTO variants are associated with obesity in the Chinese and Malay populations in Singapore.* Diabetes, 2008. **57**(10): p. 2851-7.
 171. Yajnik, C.S., et al., *FTO gene variants are strongly associated with type 2 diabetes in South Asian Indians.* Diabetologia, 2009. **52**(2): p. 247-52.
 172. Liu, Y., et al., *Meta-analysis added power to identify variants in FTO associated with type 2 diabetes and obesity in the Asian population.* Obesity (Silver Spring), 2010. **18**(8): p. 1619-24.
 173. Jia, G., et al., *Oxidative demethylation of 3-methylthymine and 3-methyluracil in single-stranded DNA and RNA by mouse and human FTO.* FEBS letters, 2008.
 174. Wu, Q., et al., *The obesity-associated Fto gene is a transcriptional coactivator.* Biochem Biophys Res Commun, 2010. **401**(3): p. 390-5.
 175. Merkestein, M., et al., *FTO influences adipogenesis by regulating mitotic clonal expansion.* Nat Commun, 2015. **6**: p. 6792.
 176. Gerken, T., et al., *The obesity-associated FTO gene encodes a 2-oxoglutarate-dependent nucleic acid demethylase.* Science, 2007. **318**(5855): p. 1469-72.
 177. Do, R., et al., *Genetic variants of FTO influence adiposity, insulin sensitivity, leptin levels, and resting metabolic rate in the Quebec Family Study.* Diabetes, 2008. **57**(4): p. 1147-50.
 178. Speakman, J.R., K.A. Rance, and A.M. Johnstone, *Polymorphisms of the FTO gene are associated with variation in energy intake, but not energy expenditure.* Obesity (Silver Spring), 2008. **16**(8): p. 1961-5.
 179. Haupt, A., et al., *Variation in the FTO gene influences food intake but not energy expenditure.* Exp Clin Endocrinol Diabetes, 2009. **117**(4): p. 194-7.
 180. Cecil, J.E., et al., *An obesity-associated FTO gene variant and increased energy intake in children.* N Engl J Med, 2008. **359**(24): p. 2558-66.

181. Park, S.L., et al., *Association of the FTO obesity risk variant rs8050136 with percentage of energy intake from fat in multiple racial/ethnic populations: the PAGE study*. Am J Epidemiol, 2013. **178**(5): p. 780-90.
182. Wardle, J., et al., *Obesity associated genetic variation in FTO is associated with diminished satiety*. J Clin Endocrinol Metab, 2008. **93**(9): p. 3640-3.
183. Tung, Y.C., et al., *Hypothalamic-specific manipulation of Fto, the ortholog of the human obesity gene FTO, affects food intake in rats*. PLoS One, 2010. **5**(1): p. e8771.
184. Claussnitzer, M., et al., *FTO Obesity Variant Circuitry and Adipocyte Browning in Humans*. N Engl J Med, 2015.
185. Church, C., et al., *A mouse model for the metabolic effects of the human fat mass and obesity associated FTO gene*. PLoS Genet, 2009. **5**(8): p. e1000599.
186. Stratigopoulos, G., et al., *Hypomorphism for RPGRIP1L, a ciliary gene vicinal to the FTO locus, causes increased adiposity in mice*. Cell Metab, 2014. **19**(5): p. 767-79.
187. Smemo, S., et al., *Obesity-associated variants within FTO form long-range functional connections with IRX3*. Nature, 2014. **507**(7492): p. 371-5.
188. Ragvin, A., et al., *Long-range gene regulation links genomic type 2 diabetes and obesity risk regions to HHEX, SOX4, and IRX3*. Proc Natl Acad Sci U S A, 2010. **107**(2): p. 775-80.
189. Church, C., et al., *Overexpression of Fto leads to increased food intake and results in obesity*. Nature ..., 2010.
190. Puigserver, P. and B.M. Spiegelman, *Peroxisome proliferator-activated receptor-gamma coactivator 1 alpha (PGC-1 alpha): transcriptional coactivator and metabolic regulator*. Endocr Rev, 2003. **24**(1): p. 78-90.
191. Park, A., W.K. Kim, and K.H. Bae, *Distinction of white, beige and brown adipocytes derived from mesenchymal stem cells*. World J Stem Cells, 2014. **6**(1): p. 33-42.
192. Nascimento, E.B., M.R. Boon, and W.D. van Marken Lichtenbelt, *Fat cells gain new identities*. Sci Transl Med, 2014. **6**(247): p. 247fs29.
193. Bartelt, A. and J. Heeren, *Adipose tissue browning and metabolic health*. Nat Rev Endocrinol, 2014. **10**(1): p. 24-36.
194. Jia, G., et al., *N6-methyladenosine in nuclear RNA is a major substrate of the obesity-associated FTO*. Nat Chem Biol, 2011. **7**(12): p. 885-7.
195. Sanders, M.J., et al., *Investigating the mechanism for AMP activation of the AMP-activated protein kinase cascade*. Biochem J, 2007. **403**(1): p. 139-48.
196. McMurray, F., et al., *Pharmacological Inhibition of FTO*. PLoS One, 2015. **10**(4): p. e0121829.
197. Tchkonina, T., et al., *Mechanisms and metabolic implications of regional differences among fat depots*. Cell Metab, 2013. **17**(5): p. 644-56.
198. Kahn, S.E., et al., *Obesity, body fat distribution, insulin sensitivity and Islet beta-cell function as explanations for metabolic diversity*. J Nutr, 2001. **131**(2): p. 354S-60S.

199. Alligier, M., et al., *Visceral fat accumulation during lipid overfeeding is related to subcutaneous adipose tissue characteristics in healthy men.* J Clin Endocrinol Metab, 2013. **98**(2): p. 802-10.
200. Le, K.A., et al., *Subcutaneous Adipose Tissue Macrophage Infiltration Is Associated With Hepatic and Visceral Fat Deposition, Hyperinsulinemia, and Stimulation of NF- κ B Stress Pathway.* Diabetes, 2011. **60**(11): p. 2802-9.
201. Malin, A., et al., *The Human Visceral Fat Depot Has a Unique Inflammatory Profile.* Obesity, 2010. **18**(5): p. 879-883.
202. Ibrahim, M.M., *Subcutaneous and visceral adipose tissue: structural and functional differences.* Obes Rev, 2010. **11**(1): p. 11-8.
203. Harman-Boehm, I., et al., *Macrophage infiltration into omental versus subcutaneous fat across different populations: effect of regional adiposity and the comorbidities of obesity.* J Clin Endocrinol Metab, 2007. **92**(6): p. 2240-7.
204. Karastergiou, K., et al., *Distinct developmental signatures of human abdominal and gluteal subcutaneous adipose tissue depots.* J Clin Endocrinol Metab, 2013. **98**(1): p. 362-71.
205. Tchkonina, T., et al., *Identification of depot-specific human fat cell progenitors through distinct expression profiles and developmental gene patterns.* Am J Physiol Endocrinol Metab, 2007. **292**(1): p. E298-307.
206. Khan, T., et al., *Metabolic dysregulation and adipose tissue fibrosis: role of collagen VI.* Mol Cell Biol, 2009. **29**(6): p. 1575-91.
207. Hyun-Jeong, L., et al., *Comparative Transcriptome Analysis of Adipose Tissues Reveals that ECM-Receptor Interaction Is Involved in the Depot-Specific Adipogenesis in Cattle.* PLoS ONE, 2013. **8**(6).
208. Gonzalez, A.D., et al., *OCI-5/GPC3, a glypican encoded by a gene that is mutated in the Simpson-Golabi-Behmel overgrowth syndrome, induces apoptosis in a cell line-specific manner.* J Cell Biol, 1998. **141**(6): p. 1407-14.
209. Henegar, C., et al., *Adipose tissue transcriptomic signature highlights the pathological relevance of extracellular matrix in human obesity.* Genome Biology, 2008. **9**(1): p. R14.
210. Li, Q., et al., *The density of extracellular matrix proteins regulates inflammation and insulin signaling in adipocytes.* FEBS Letters, 2010. **584**(19): p. 4145-4150.
211. Kim, J.Y., et al., *Obesity-associated improvements in metabolic profile through expansion of adipose tissue.* J Clin Invest, 2007. **117**(9): p. 2621-37.
212. Huang, G., et al., *α 3(V) collagen is critical for glucose homeostasis in mice due to effects in pancreatic islets and peripheral tissues.* J Clin Invest, 2011. **121**(2): p. 769-83.
213. Brakenhielm, E., et al., *Angiogenesis inhibitor, TNP-470, prevents diet-induced and genetic obesity in mice.* Circ Res, 2004. **94**(12): p. 1579-88.
214. Leiberer, A., et al., *Hypoxia induces a HIF-1 α dependent signaling cascade to make a complex metabolic switch in SGBS-adipocytes.* Mol Cell Endocrinol, 2014. **383**(1-2): p. 21-31.

215. Grant, S.F., et al., *Variant of transcription factor 7-like 2 (TCF7L2) gene confers risk of type 2 diabetes*. Nat Genet, 2006. **38**(3): p. 320-3.
216. Bordonaro, M., *Role of Wnt signaling in the development of type 2 diabetes*. Vitam Horm, 2009. **80**: p. 563-81.
217. Liu, C.C., et al., *Deficiency in LRP6-Mediated Wnt Signaling Contributes to Synaptic Abnormalities and Amyloid Pathology in Alzheimer's Disease*. Neuron, 2014. **84**(1): p. 63-77.
218. Kanazawa, A., et al., *Association of the Gene Encoding Wingless-Type Mammary Tumor Virus Integration-Site Family Member 5B (WNT5B) with Type 2 Diabetes*. The American Journal of Human Genetics, 2004. **75**(5): p. 832-843.
219. Nishizuka, M., et al., *Wnt4 and Wnt5a promote adipocyte differentiation*. FEBS Lett, 2008. **582**(21-22): p. 3201-5.
220. Kanazawa, A., et al., *Wnt5b partially inhibits canonical Wnt/beta-catenin signaling pathway and promotes adipogenesis in 3T3-L1 preadipocytes*. Biochem Biophys Res Commun, 2005. **330**(2): p. 505-10.
221. Adeva, M.M., et al., *Insulin resistance and the metabolism of branched-chain amino acids in humans*. Amino Acids, 2012. **43**(1): p. 171-81.
222. Lynch, C.J. and S.H. Adams, *Branched-chain amino acids in metabolic signalling and insulin resistance*. Nat Rev Endocrinol, 2014. **10**(12): p. 723-36.
223. Gao, Z., et al., *Butyrate Improves Insulin Sensitivity and Increases Energy Expenditure in Mice*. Diabetes, 2009. **58**(7): p. 1509-1517.
224. Withers, D.J., et al., *Disruption of IRS-2 causes type 2 diabetes in mice*. Nature, 1998. **391**(6670): p. 900-904.
225. Divoux, A., et al., *Fibrosis in human adipose tissue: composition, distribution, and link with lipid metabolism and fat mass loss*. Diabetes, 2010. **59**(11): p. 2817-25.
226. McCulloch, L.J., et al., *COL6A3 is regulated by leptin in human adipose tissue and reduced in obesity*. Endocrinology, 2015. **156**(1): p. 134-46.
227. Bijland, S., Sarah J. Mancini, and Ian P. Salt, *Role of AMP-activated protein kinase in adipose tissue metabolism and inflammation*. Clinical Science, 2013. **124**(8): p. 491-507.
228. Zhang, B.B., G.C. Zhou, and C. Li, *AMPK: An Emerging Drug Target for Diabetes and the Metabolic Syndrome*. Cell Metabolism, 2009. **9**(5): p. 407-416.

9. Appendix

I. List of SYBR green primers used for real-time qPCR.

Gene	Primer sequence (5' – 3')
Human specific primers	
FIT2	FP: CTGCCTTTCATTGCCCTCA RP: CTGCTTGCTCTGGTGTTCCTT
PPAR γ	FP: AGACATTCAAGACAACCTGCTACAA RP: GGAGCAGCTTGCAAACAG
PPAR α	FP: CGATCTAGAGAGCCCGTTATCTGA RP: TGTCCCCGCAGATTCTACATT
CEBP α	FP: GAGGGACCGGAGTTATGACAAG RP: CGCACATTCACATTGCACAA
IL18	FP: ATCGCTTCCTCTCGCAACAA RP: ATCGCTTCCTCTCGCAACAA
IL1 β	FP: TGAGCTCGCCAGTGAAATGA RP: AGATTTCGTAGCTGGATGCCG
IL6	FP: CAATAACCACCCCTGACCCA RP: TCTGAGGTGCCCATGCTACA
TLR4	FP: AGCGAGCCACGCATTCAC RP: GCCATGGCTGGGATCAGA
TNF α	FP: TCCCCTGCCCAATCC RP: CCAATTCTCTTTTGGAGCCAGAA
NF κ B1	FP: GGCTACACCGAAGCAATTGAA RP: CAGCGAGTGGGCCTGAGA
BiP	FP: GGCCGCACGTGGAATG RP: AACCACCTTGAACGGCAAGA
CHOP/DDIT3	FP: CATCACCACACCTGAAAGCAGA RP: CCTCATACCAGGCTTCCAGC
IRE1 α	FP: ATGTGGAAGAGCCTGCCTTTC RP: GGATGCCTGCACCAATTCTG

GADD34	FP: GAAGCTAGGACTCCTCTGGCAA RP: GCTTCAGGAAGGGAAGCTGCTG
PERK	FP: CGATGTCCGAGATAGGCTGTC RP: GGAGCTCCCAAGAAGGCAAG
GLUT4	FP: TTCTTTCATCTTCGCCGCC RP: TCCCCATCTTCGGAGCCTA
PGC1 α	FP: GGTCTCTCCTTGCAGCACAAG RP: CTGGGATGACCGAAGTGCTT
Leptin	FP: CGGAGAGTACAGTGAGCCAAGA RP: CGGAATCTCGCTCTGTCATCA
DIO2	FP: TTTTCTCCAAGTGCCTCTTCCT RP: CATGCGCCGCCACTCT
PRDM16	FP: GCTCCTTCAGCATCTCTTCGA RP: GCTGGTCCCCAGGTGGTT
UCP1	FP: GGCTTCAGCGGCAAATCA RP: GAACTCCTGGACCGTGTCGTA
FTO	FP: CATGCCAGGTGCCAGTCA RP: GGCATCGAAGCATCATCCTT
ADIPOQ	FP: TGCCCAAAGAGGAGAGAGGAA RP: TCAGAAACAGGCACACAACTCA
FABP4	FP: CATAAAGAGAAAACGAGAGGATGATAAA RP: CCCTTGGCTTATGCTCTCTCA
DGAT1	FP: ACCTCATCTGGCTCATCTTCTTCTA RP: CCCGGTCTCCAAACTGCAT
PLIN2	FP: CCTGCTCTTCGCCTTTTCG RP: TGCAACGGATGCCATTTTT
IRX3	FP: GATCGCTGTAGTGCCTTGGAA RP: GTCCAGATGGTTCTGGGGC
PRDM16	FP: AGACACCTGAGGACGCACACT RP: GCTGGTCCCCAGGTGGTT
GAPDH	FP: GCCCCCGGTTTCTATAAATTG RP: GTCGAACAGGAGGAGCAGAGA

Mouse specific primers	
Mouse PGC1 α	FP: GATGACCCTCCTCACACCAA RP: AGTTGTGGGAGGAGTTAGGC
Mouse FTO	FP: CCCTGGGTCTCCATAATCGC RP: TCTAGAAAGTGCTGCTGGGACG
Mouse Beta Actin	FP: ATGCCCTGAGGCTCTTTTCC RP: AATGCCTGGGTACATGGTGG

Table 19: List of SYBR green primers for Real-time qPCR.

2. List of primers and probes used for quantification of mitochondrial DNA content.

Gene	Sequence (5' – 3')	Modification
Mitochondrial DNA	Primers FP: CACCCAAGAACAGGGTTTGT RP: TGGCCATGGGTATGTTGTAA Probe TTACCGGGCTCTGCCATCT	Probe 5' – FAM 3' - TAMRA
Nuclear DNA (18s rRNA)	Primers FP: TAGAGGGACAAGTGGCGTTC RP: CGCTGAGCCAGTCAGTGT Probe AGCAATAACAGGTCTGTGATG	Probe 5' – FAM 3' - TAMRA

Table 20: List of primers and TaqMan probes for quantification of mitochondrial DNA.

3. Table of KEGG biological pathways enriched in SC depot from diabetics compared to SC depot from non-diabetics.

Gene Set	Number of genes annotated	Enrichment score	P-value
KEGG_RIBOSOME	83	0.721	0
KEGG_SPLICEOSOME	124	0.498	0
KEGG_PROTEASOME	40	0.603	0
KEGG_LEISHMANIA_INFECTION	61	0.518	0
KEGG_ANTIGEN_PROCESSING_AND_PRESENTATION	54	0.514	0
KEGG_SYSTEMIC_LUPUS_ERYTHEMATOSUS	68	0.487	0
KEGG_NOD_LIKE_RECEPTOR_SIGNALING_PATHWAY	55	0.496	0
KEGG_PRIMARY_IMMUNODEFICIENCY	24	0.595	0
KEGG_CYTOKINE_CYTOKINE_RECEPTOR_INTERACTION	152	0.384	0
KEGG_HEMATOPOIETIC_CELL_LINEAGE	63	0.439	0
KEGG_BUTANOATE_METABOLISM	24	-0.616	0
KEGG_PROPANOATE_METABOLISM	29	-0.641	0
KEGG_CHEMOKINE_SIGNALING_PATHWAY	147	0.358	0.002
KEGG_NATURAL_KILLER_CELL_MEDIATED_CYTOTOXICITY	91	0.405	0.002
KEGG_VALINE_LEUCINE_AND_ISOLEUCINE_DEGRADATION	42	-0.574	0.002
KEGG_TGF_BETA_SIGNALING_PATHWAY	68	-0.451	0.002
KEGG_ALZHEIMERS_DISEASE	134	-0.329	0.004

KEGG_LYSOSOME	112	0.352	0.006
KEGG_DRUG_METABOLISM_OTHER_ENZYMES	22	0.562	0.006
KEGG_CITRATE_CYCLE_TCA_CYCLE	28	-0.54	0.007
KEGG_PYRUVATE_METABOLISM	33	-0.507	0.007
KEGG_TOLL_LIKE_RECEPTOR_SIGNALING_PATHWAY	83	0.366	0.011
KEGG_INOSITOL_PHOSPHATE_METABOLISM	49	-0.45	0.013
KEGG_VASCULAR_SMOOTH_MUSCLE_CONTRACTION	83	-0.378	0.015
KEGG_CYTOSOLIC_DNA_SENSING_PATHWAY	40	0.446	0.016
KEGG_GRAFT_VERSUS_HOST_DISEASE	26	0.472	0.018
KEGG_COMPLEMENT_AND_COAGULATION_CASCADES	41	0.428	0.018
KEGG_B_CELL_RECEPTOR_SIGNALING_PATHWAY	69	0.375	0.019
KEGG_OXIDATIVE_PHOSPHORYLATION	104	-0.339	0.019
KEGG_OLFACTORY_TRANSDUCTION	21	0.537	0.02
KEGG_AMYOTROPHIC_LATERAL_SCLEROSIS_ALS	37	0.422	0.022
KEGG_VASOPRESSIN_REGULATED_WATER_REABSORPTION	39	-0.439	0.022
KEGG_FATTY_ACID_METABOLISM	36	-0.474	0.023
KEGG_PATHOGENIC_ESCHERICHIA_COLI_INFECTION	45	0.404	0.027
KEGG_PARKINSONS_DISEASE	101	-0.345	0.028
KEGG_INTESTINAL_IMMUNE_NETWORK_FOR_IGA_PRODUCTION	29	0.443	0.03

KEGG_PHOSPHATIDYLINOSITOL_SIGNALING_SYSTEM	65	-0.394	0.033
KEGG_ALANINE_ASPARTATE_AND_GLUTAMATE_METABOLISM	26	-0.467	0.035
KEGG_GLYCINE_SERINE_AND_THREONINE_METABOLISM	22	-0.485	0.038
KEGG_INSULIN_SIGNALING_PATHWAY	119	-0.303	0.04
KEGG_FC_GAMMA_R_MEDIATED_PHAGOCYTOSIS	91	0.321	0.04
KEGG_PPAR_SIGNALING_PATHWAY	50	-0.389	0.041
KEGG_RNA_POLYMERASE	29	0.43	0.044
KEGG_PROXIMAL_TUBULE_BICARBONATE_RECLAMATION	15	-0.553	0.048

Table 21: KEGG biological pathways enriched in SC depot from diabetics when compared to SC depot from non-diabetics.

FPKM values were fed in gene set enrichment analysis (GSEA) desktop version [165] and positively and negatively enriched KEGG pathways (as denoted by enrichment score) were analyzed. Significance was pegged at P-value < 0.05).

4. Table of KEGG biological pathways enriched in OM depot from diabetics compared to OM depot from non-diabetics.

Gene Set	Number of genes annotated	Enrichment score	P-value
KEGG_ANTIGEN_PROCESSING_AND_PRESENTATION	54	-0.524	0
KEGG_GRAFT_VERSUS_HOST_DISEASE	26	-0.657	0
KEGG_ALLOGRAFT_REJECTION	25	-0.674	0
KEGG_TYPE_I_DIABETES_MELLITUS	28	-0.675	0
KEGG_BASAL_CELL_CARCINOMA	32	-0.605	0.002
KEGG_ASTHMA	16	-0.645	0.002
KEGG_PROTEIN_EXPORT	23	0.511	0.003
KEGG_RNA_POLYMERASE	29	0.533	0.003
KEGG_AUTOIMMUNE_THYROID_DISEASE	26	-0.6	0.005
KEGG_AXON_GUIDANCE	101	-0.387	0.007
KEGG_OXIDATIVE_PHOSPHORYLATION	104	-0.386	0.008
KEGG_CELL_ADHESION_MOLECULES_CAMS	95	-0.385	0.01
KEGG_PROTEASOME	40	0.398	0.014
KEGG_LYSOSOME	112	-0.356	0.015
KEGG_APOPTOSIS	78	-0.38	0.029
KEGG_PARKINSONS_DISEASE	101	-0.353	0.033
KEGG_ENDOMETRIAL_CANCER	47	-0.415	0.036
KEGG_ENDOCYTOSIS	161	-0.31	0.037
KEGG_VIRAL_MYOCARDITIS	55	-0.406	0.038

KEGG_ALZHEIMERS_DISEASE	134	-0.314	0.043
KEGG_HEDGEHOG_SIGNALING_PATHWAY	29	-0.458	0.045
KEGG_CARDIAC_MUSCLE_CONTRACTION	43	-0.422	0.046
KEGG_FC_EPSILON_RI_SIGNALING_PATHWAY	64	-0.379	0.05

Table 22: KEGG biological pathways enriched in OM depot from diabetics when compared to OM depot from non-diabetics.

FPKM values were fed in gene set enrichment analysis (GSEA) desktop version [165] and positively and negatively enriched KEGG pathways (as denoted by enrichment score) were analyzed. Significance was pegged at P-value < 0.05.

5. Table of GO_cellular components enriched in SC depot from diabetics compared to SC depot from non-diabetics.

Gene Set	Number of genes annotated	Enrichment score	P-value
NUCLEOLUS	116	0.506	0
RIBONUCLEOPROTEIN_COMPLEX	136	0.491	0
RIBOSOME	37	0.534	0
NUCLEAR_LUMEN	350	0.317	0
MEMBRANE_ENCLOSED_LUMEN	414	0.295	0
ORGANELLE_LUMEN	414	0.295	0
VACUOLE	56	0.409	0.002
EXTRACELLULAR_REGION	248	0.298	0.004
NUCLEOLAR_PART	17	0.613	0.004
PROTEASOME_COMPLEX	23	0.536	0.004
SPLICEOSOME	51	0.44	0.006
GOLGI_APPARATUS_PART	90	-0.372	0.013
LYSOSOME	48	0.411	0.015
LYTIC_VACUOLE	48	0.411	0.02
SMALL_NUCLEAR_RIBONUCLEOPROTEIN_COMPLEX	22	0.534	0.021
RNA_POLYMERASE_COMPLEX	16	0.528	0.025
DNA_DIRECTED_RNA_POLYMERASE_COMPLEX	16	0.528	0.026
ORGANELLAR_RIBOSOME	22	0.484	0.027
MITOCHONDRIAL_RIBOSOME	22	0.484	0.027

EXTRACELLULAR_SPACE	127	0.297	0.035
NUCLEAR_DNA_DIRECTED_RNA_POLYMERASE_COMPLEX	16	0.528	0.05

Table 23: GO_cellular components enriched in SC depot from diabetics when compared to SC depot from non-diabetics.

FPKM values were fed in gene set enrichment analysis (GSEA) desktop version [165] and positively and negatively enriched KEGG pathways (as denoted by enrichment score) were analyzed. Significance was pegged at P-value < 0.05).

6. Table of GO_cellular components enriched in OM depot from diabetics compared to OM depot from non-diabetics.

Gene Set	Number of genes annotated	Enrichment score	P-value
PROTEASOME_COMPLEX	23	0.611	0
MITOCHONDRIAL_LUMEN	44	0.466	0
MITOCHONDRIAL_MATRIX	44	0.466	0
NUCLEOLUS	116	0.382	0
MITOCHONDRIAL_PART	135	0.314	0
RIBONUCLEOPROTEIN_COMPLEX	136	0.307	0
EXTRACELLULAR_REGION_PART	189	0.252	0
MEMBRANE_ENCLOSED_LUMEN	414	0.223	0
ORGANELLE_LUMEN	414	0.223	0
NUCLEOLAR_PART	17	0.654	0.003
MITOCHONDRION	318	0.223	0.011
MITOCHONDRIAL_RIBOSOME	22	0.489	0.011
EXTRACELLULAR_MATRIX	67	0.355	0.012
PROTEINACEOUS_EXTRACELLULAR_MATRIX	66	0.342	0.016
ORGANELLAR_RIBOSOME	22	0.489	0.017
RNA_POLYMERASE_COMPLEX	16	0.488	0.037
EXTRACELLULAR_REGION	248	0.219	0.045
RIBONUCLEOPROTEIN_COMPLEX	136	0.491	0
RIBOSOME	37	0.534	0

NUCLEAR_LUMEN	350	0.317	0
MEMBRANE_ENCLOSED_LUMEN	414	0.295	0
ORGANELLE_LUMEN	414	0.295	0
VACUOLE	56	0.409	0.002
EXTRACELLULAR_REGION	248	0.298	0.004
NUCLEOLAR_PART	17	0.613	0.004
PROTEASOME_COMPLEX	23	0.536	0.004
SPLICEOSOME	51	0.44	0.006
GOLGI_APPARATUS_PART	90	-0.372	0.013
LYSOSOME	48	0.411	0.015
LYTIC_VACUOLE	48	0.411	0.02
SMALL_NUCLEAR_RIBONUCLEOPROTEIN_COMPLEX	22	0.534	0.021
RNA_POLYMERASE_COMPLEX	16	0.528	0.025
DNA_DIRECTED_RNA_POLYMERASE_COMPLEX	16	0.528	0.026
ORGANELLAR_RIBOSOME	22	0.484	0.027
MITOCHONDRIAL_RIBOSOME	22	0.484	0.027
EXTRACELLULAR_SPACE	127	0.297	0.035
NUCLEAR_DNA_DIRECTED_RNA_POLYMERASE_COMPLEX	16	0.528	0.05

Table 24: GO_cellular components enriched in OM depot from diabetics when compared to OM depot from non-diabetics.

FPKM values were fed in gene set enrichment analysis (GSEA) desktop version [165] and positively and negatively enriched KEGG pathways (as denoted by enrichment score) were analyzed. Significance was pegged at P-value < 0.05).

Response to examiners comments

Examiner 1:

1. *Figures (e.g. Fig 6, 8, 9, 10), if cited from literature, should include the statement such as “adopted from [reference and #]”*

- Amendments have been made to figure legends for figure 6, 8 and 10. The signal transduction pathway in figure 9 was built in
Pathway Builder Tool

(<http://www.proteinlounge.com/PathwayBuilder.aspx>) based on literature review and this has been indicated as well.

- **Figure 6: Mechanism of lipid induced insulin resistance.**

Elevated DAGs and free fatty acids activate PKC θ (protein kinase C θ) which blocks IRS1 signaling by serine phosphorylation of IRS1. Eventually, insulin stimulated GLUT4 translocation is compromised. Adopted from Shulman et al [58].

- **Figure 8: Modulation of adipose tissue inflammation during weight gain or metabolic dysfunction.**

An imbalance between inflammation, metabolic control and vascular function occurs in obese individuals. Along with increasing inflammation, adipocytes secrete pro-inflammatory adipokines such as leptin, resistin and RBP4 in increasing amounts. Macrophage phenotype changes from M2 to M1, which further contributes to inflammation. Adopted from Ouchi, N. et al [72].

- **Figure 10: The unfolded protein response, nutrient sensing and inflammation.**

UPR is induced in response to ER stress inducers and can result in altered metabolic and inflammatory responses and thus metabolic disease. Adopted from Hotamisligil, G.S. et al [86].

2. *p51, SGBS line was reported in 2001, not 2011*

- Corrected in the thesis.
- **Revised text**

In 2001, investigators isolated preadipocytes from an infant derived adipose tissue [2] which could grow up to 50 passages while maintaining growth and differentiation capacity. SGBS adipocytes were derived from a 3 year old infant suffering from Simpson Golabi Behmel syndrome or SGBS. Since isolation, they have been widely distributed around the world and reported as a representative adipocyte model for primary human adipocytes.

3. *What does 'NA' mean in Table 14? Simply did not examine?*

- NA (not applicable) refers to all the genes with FPKM < 1 and thus were not included in our analysis. Have updated the figure legend accordingly.
- **Revised Legend:**

Table 14: Lineage specific markers in adipocytes and their expression in SGBS and SC control adipocytes. NA: Genes with FPKM < 1 and thus excluded from further analysis. P value <

0.05 and $FDR < 0.05$ were used as thresholds to select significant genes.

4. *What is the future plan for the project #4 (Transcriptome analysis of fat depots)?*

- A description of future plans have since been added in the thesis as well.
- Currently, our analysis is limited to gene expression obtained from RNA sequencing. Our next step would be to validate differences in expression of selected genes at the protein level.
- Novel genes identified from this study can be functionally validated and characterized in human derived cell lines to better understand processes driving insulin sensitivity in the metabolically healthy obese. In particular, genes contributing significantly to positive enrichment in ECM and fibrosis components in T2DM subjects can be investigated further either by inhibiting over-accumulation of ECM or fibrosis components or by targeting certain proteins via pharmacological intervention

Examiner 2:

1. *The abstract is weak: it merely recites results, but does not state the background, the research question, and the final outcome of the work; this needs to be completely rewritten, this is not an abstract for a publication, this is the essence of your PhD work!*

- **Revised abstract**

Adipose tissue (AT) functions as an active endocrine organ and an energy reserve compartment for storing lipids. It's now well accepted that adipose tissue expandability, remodelling and effective storage of excess lipids in the form of triglycerides (TAGs) play an important role in maintaining metabolic homeostasis. To understand healthy AT expansion and function, we used human derived in-vitro adipocyte models to interrogate pathways of interest, as well as Next Generation Sequencing methods. We first sought to validate and functionally characterize two GWAS candidate genes involved in lipid metabolism and expressed in adipose; FIT2 (Fat Storage Inducing Transmembrane Protein 2) and FTO (Fat Mass and Obesity Associated). The FIT2 gene is associated with type 2 diabetes in the East Asian population and plays a role in transporting TAGs from ER to lipid droplets. On the other hand, FTO is an obesity associated gene in multiple ethnicities and regulates mitochondrial energy expenditure through central and peripheral mechanisms. Our observations suggest that improved TAG storage via FIT2 protein as well as improved mitochondrial

oxidative capacity via FTO protein can promote insulin sensitivity in primary human adipocytes. Next, using RNA sequencing data from AT, we observed positive enrichment in the extracellular matrix (ECM) and fibrosis components in omental AT depots from T2DM when compared to NT2DM subjects. Excessive ECM and fibrosis components have been shown to inhibit obesity associated adipose tissue expansion and inflammation in the obese, but the differences identified in the OM depot among obese T2DM and obese NT2DM subjects are novel. Overall, our work contributes insights into the molecular and transcriptomic determinants of adipocyte and adipose tissue function as well as their potential role in health and disease.

2. *A hypothesis is needed, along with a clear research question. The expandability hypothesis is mentioned, it is a general hypothesis (who put it forth the first time?), but what is the candidate's own hypothesis and what are the specific aims of this work, and what was the strategy behind this. Where relevant, each chapter discussing data sets should reiterate what the specific aim was. Chapter 1.9 does at least some work here.*

- The adipose tissue expandability hypothesis was put forth for the first time by Dr. Tony Vidal-Puig [3] and this is described in the introduction section 1.4, as outlined below.

- **Adipose tissue expandability hypothesis:**

“The adipose tissue expandability hypothesis states that the capacity of an individual to expand their fat mass to store lipid is a more important determinant of obesity-associated metabolic problems than the absolute amount of AT an individual possesses” [3, 4]. In a situation where an individual fails to maintain AT functions due to impaired expansion, usually due to excessive obesity, ectopic lipids begin to accumulate in tissues such as liver, heart and skeletal muscle which accelerates development of metabolic syndrome.

- Updated the hypothesis (section 1.9)

Revised aims and hypothesis of the study

In the studies presented here, we have leveraged on current knowledge on adipose tissue expandability hypothesis [3], with the aim of furthering insights into novel adipose tissue related mechanisms leading to the development of insulin resistance or T2DM.

We first sought to characterize human adipocyte cell models, to better understand the strengths and limitations of the SGBS human adipocyte cell line. SGBS adipocytes were derived from a child with an overgrowth syndrome [2, 5] and are widely used as a representative human adipocyte model. More recently SGBS adipocytes were observed to also exhibit a transient browning phenotype mid-way during their course of differentiation [6]. To date, any potential transcriptomic and

functional phenotypic differences between SGBS and primary human subcutaneous adipocytes have not been examined. We hypothesized that while there are overlapping characteristics, there may be distinct metabolic signatures involving adipogenesis, lipid metabolism, browning and mitochondrial capacity between the two cell types. A better understanding of these similarities and differences would assist in their appropriate usage in our studies or other studies in the future.

Following this, we leveraged on the use of these adipocytes as human derived in vitro models and investigated the role of two GWAS gene candidates that are associated with type 2 diabetes and expressed in adipose; namely FIT2 and FTO. Both these proteins are known to be involved in lipid metabolism pathways in adipocytes but its role and function in human adipose have yet to be validated and the mechanistic links to the development of type 2 diabetes are incompletely understood.

FIT2 is an ER membrane associated lipid droplet protein, responsible for transferring newly synthesized TAGs into lipid droplets and a GWAS gene candidate for T2DM in the East Asian population [7]. Adipose tissue specific FIT2 protein knockout mice show a lipodystrophic phenotype with smaller adipose tissue depots accompanied by peripheral insulin resistance [8]. The potential role of FIT2 protein in human derived adipocytes or adipose tissue has not been established. We hypothesized that even partial deficiency of FIT2 protein would lead to reduced

triglyceride storage, accumulation of free fatty acids and defective insulin signalling in the adipocytes. Here, we used primary human adipocytes to test this hypothesis.

In contrast to the lipid storage function of FIT2 protein, data from human adipocytes and animal models suggest a role of FTO protein in regulating energy expenditure through central and peripheral mechanisms [9-11]. Along with FTO protein knockdown, we tested the effects of a novel chemical inhibitor of dioxygenase activity of FTO protein in SGBS adipocytes [12]. We hypothesized that chemical inhibition of FTO protein would mimic increase in mitochondrial energy expenditure as observed after FTO protein knockdown in SGBS adipocytes [13] and thus may potentially be developed as an anti-obesity drug. Since FTO protein influences mitochondrial energy expenditure and SGBS adipocytes showed higher mitochondrial oxidative capacity in our initial experiments, SGBS were initially used for studies related to FTO protein.

The fourth chapter focusses on studying transcriptomic signatures that may differ between obese diabetics and obese non-diabetics. Insulin resistance is associated with obesity and Type 2 Diabetes, and comparing obese diabetics vs obese non-diabetics would enable us to tease out which signals are unique to diabetes. We were interested to examine whether FIT2 and/or FTO expression may differ between these two groups we also aimed to identify other adipose tissue related pathways that may

be relevant to the development of insulin resistance and type 2 diabetes. Specifically, contributions of extracellular matrix (ECM) components in obesity and inflammation associated adipose tissue dysfunction have been suggested widely [14], but potential differences amongst obese diabetics and obese non-diabetics have not been systematically examined. We compared transcriptomes of subcutaneous and omental adipose tissue from obese diabetics and obese non-diabetics to address the question whether ECM components are involved in adipose tissue dysfunction in obese diabetics.

3. *The rationale for using SGBS cells is not clear. Genetic databases do not reveal a connection of mutations in the SBGS locus, or specifically in glypican 3, an extracellular matrix component. The candidate needs to build a case using literature and then extract a research quest(ion) from it that guided him through the thesis work. References are cited copiously, but the candidate's own thinking on what is driving his work remains obscure.*

- The possibility of a mutation (not characterized yet) in GPC3 or OFD1 driving the phenotype in SGBS cannot be excluded and remains a limitation of using SGBS adipocytes.
- SGBS and stromal vascular fraction (SVF) derived pre-adipocytes are the most commonly used primary human adipocyte cell model. Despite both being primary adipocytes in origin, SGBS adipocytes can grow up to a passage number 30 with better differentiation capacity when compared to SVF

derived adipocytes from adults. These properties give SGBS adipocytes a significant advantage over SC adipocytes especially in experiments involving sub-culturing multiple times. However, our preliminary data showed that SGBS adipocytes differentiate into brown or beige adipocytes with a higher number of active mitochondria and UCP1 protein expression when compared to SC adipocytes, and thus we initiated studies for characterizing them in detail. SGBS adipocytes were especially useful in preliminary studies on FTO protein due to its role in regulating mitochondrial energy expenditure. Overall, both SGBS and SC adipocytes have its advantages and drawbacks, and our argument is that understanding their characteristics in greater depth allows for more appropriate choice of the adipocyte model to be used.

4. *If the extracellular matrix is seen as important in terms of adipogenesis, the candidate might want to refer to and cite Ang et al 2014 in Tissue Engineering, highlighting differentiation of MSCs into adipocytes which is improved under improved matrix deposition.*

- Have updated this in the discussion of SGBS chapter in section 3.4.
- **Discussion added**

Subject to individual protein function, ECM components seem to play a dual role in promoting or inhibiting adipose tissue expandability. Several reports suggest that excessive ECM deposition in response to obesity-related inflammation reduces

adipose tissue expandability which eventually results in adipose tissue dysfunction [15]. However, studies testing the effects of selective macromolecular crowding on adipogenesis and browning suggest beneficial effects. When differentiated with macromolecular crowding, bone marrow derived mesenchymal stem cells undergo improved adipogenesis in the presence of macromolecular crowding. In addition to better adipogenesis, deposition of ECM components such as collagen IV and perlecan (a heparan sulfate proteoglycan) were observed to be significantly higher [16]. Collagen IV cocoon formation around differentiating bone marrow derived mesenchymal stem cells also improved their UCP1 expression and thermogenic capacity [17]. In our dataset, transcripts of subcomponents of collagen IV were differentially expressed in SGBS adipocytes. Some subcomponents were upregulated: COL4A5 (log FC = 2.04), COL4A3 (log FC = 7.57), COL4A4 (log FC = 8.20), whereas other components were downregulated: COL4A1 (log FC = -2.00) and COL4A2 (log FC = -1.77). These observations remain to be verified at the protein expression level, but suggest that subcomponents of collagen IV may have differing activity in terms of whether they are more pro-adipogenic (COL4A5, COL4A3 and COL4A4) or anti-adipogenic (COL4A1 and COL4A2).

5. *1.4 mentioning the lipodystrophy syndrome actually makes a point on free TAGs as in the lipotoxicity hypothesis by Vidal-Puig. It is not clear what you wish to tell the reader in this paragraph that bears the heading “Adipose tissue expandability hypothesis”. It’s not clear what case you are building here. At the end, isn’t the expandability hypothesis intertwined with lipotoxicity? Do you wish to demonstrate expandability and what can be done to promote it? The motivation is not always clear.*

- AT Expandability hypothesis is closely intertwined with lipotoxicity. Three contrasting examples have been stated here to demonstrate the importance of healthy AT expansion. Lipodystrophy syndrome exemplifies a group of lean patients who have insulin resistance due to inability to store lipids in the AT. In contrast, metabolically healthy obese subjects represent a condition where individuals have excess AT, which is able to expand and maintain metabolic homeostasis and insulin sensitivity. They were used to support the overall AT expandability hypothesis which is the basis of all our studies.

6. *I am not sure whether it is acceptable in scientific work to use an adipocyte different ion medium provided by a manufacturer, which ingredients are not fully disclosed. How can people reproduce your work with non-LONZA medium, or will your work forever be specific for Lonza medium-cultivated cells. At least this should be stressed in the results and discussion section that the universality of your data is strictly limited to this culture medium. Why was it not possible, as many other labs to make your own differentiation medium? FBS is variable enough*

as an additive, so at least the concentration of components of the other ingredients should be clear.

- Primary human adipocytes can be differentiated with either in-house reconstituted adipogenic medium or commercially available (such as Lonza) adipogenic medium. In our experience, Lonza medium induces better and faster adipogenesis in SC adipocytes within 10 days without any need for replacing fresh differentiation medium. Maturation of these subcutaneous adipocytes takes approximately 21 days while using in-house formulated differentiation medium.
- During initial validation experiments in our study, SGBS adipocytes were differentiated with both Lonza and SGBS differentiation medium. Phenotype and gene expression pattern was similar in SGBS adipocytes differentiated with either adipogenic medium. However, SC adipocytes did not differentiate well when subjected to SGBS differentiation medium due to the absence of FBS in it. Thus, we eventually used their respective ‘optimal’ differentiation medium for both cells types due to following reasons:
 - To standardize differentiation timeline to 10 - 12 days in both adipocyte models. (For near complete differentiation, Lonza differentiation medium in SC adipocytes and SGBS differentiation medium for SGBS adipocytes).

- To mimic most widely used and published differentiation conditions for SGBS adipocytes since we were trying to characterize both the adipocyte models using the most commonly used protocols [18].
- Results of this study will be best replicated when primary adipocytes are differentiated using Lonza differentiation medium and SGBS adipocytes will be differentiated using recommended in-house or Lonza differentiation medium.

7. *It is stated the SGBS went brown while SVF went white after differentiation. However, you added rosiglitazone and T3 to SGBS and not to SVF so of course they did not go white, what happened if you gave the rosiglitazone, and T3-containing protocol to SVF, while exposing SGBS to LONZA medium? Was there underlying knowledge and rationale why you gave SGBS only the brown and the primary adipocytes only the white treatment? So it is no wonder you get different gene expressions. So what was the goal, to find a difference between human brown and white expression or of different cell sources. You could have used a white and a brown protocol on the same cell type and seen the gene expression differences. At the moment this thesis compares a normal and a mutated subcutaneous cell source not in one protocol but with two different differentiation protocols. Thus the comparison appears to make little sense. The observed differences could merely be caused by the different differentiation media. For example the intrinsic brown potential in SGBS, might have been visible already in a white differentiation setting? Please explain.*

- Motives to use their respective differentiation medium have been discussed in the previous section.
- Rosiglitazone and T3 (triiodothyronine) are known inducers of browning *in-vitro*. Thus, in addition to complete adipogenic medium, we also differentiated SGBS adipocytes in medium depleted with either T3 or rosiglitazone individually or in combination. UCP1 protein expression remained similar in all the above mentioned conditions. These results are discussed in section 3.3.4. This suggests that browning potential observed in SGBS adipocytes is an inherent capacity, which might be due to either (1) underlying mutation in GPC3 or OFD1 gene (not characterized yet) or (2) the fact that they originate from the subcutaneous white AT of a 3 month old infant. White AT from infants is known to be metabolically very active with a greater number of mitochondria [5].
- Irrespective of certain limitations, SGBS serves as a valid adipocyte model especially when one needs to evaluate and compare phenotype in both white and brown adipocytes.

8. *RNA-seq and PCR validation correlation, UCP-1 and inflammation markers do not seem to correlate that much, what role did leptin as maturation marker play here; it seems to be missing from Fig 23.*

- Leptin was not significantly different between SGBS and SC adipocytes in RNA-seq data ($P > 0.05$) and thus not included in this analysis.

- Fold changes (SGBS vs SC control adipocytes) in the expression of UCP-1 and inflammation genes were marginally higher when analysed with qPCR when compared to RNA sequencing data. Due to these differences in expression pattern, a shift in Pearson's co-relation coefficient may arise.

9. *Not clear how brown and white are defined in your study. UCP-1 for brown is clear; however, what was your criterion for white – simply absence of UCP-1? What role did you assign to leptin in your differentiation system, a white or maturation marker?*

- Presence of UCP-1 protein was used as a definitive marker of browning in all our studies. White adipocytes were defined by; (1) absence of UCP-1 protein expression and (2) decreased mitochondrial number and mitochondrial respiration in them.
- Lipid storage capacity was not used as a marker for white or brown adipocytes.
- Leptin was used as a marker of maturation in adipocytes.

10. *Genes up and down. As long as you do not know the protein expression levels you will not know how significant these data are. The ECM genes for example show some discordance between mRNA and protein levels. It is conceivable that after ample deposition of a certain collagen for example, like type IV, mRNA levels will drop in response to that as in a negative feed-back loop. In this case, an mRNA analysis would suggest “reduced expression” while in reality a lot of the protein is around (see Ang et al 2014 on collagen IV).*

- Strength of RNA sequencing is limited to analysis of transcript expression. It allows visualization of the whole transcriptome and pathway interactions within the transcriptome. As suggested by the examiner, discordance between mRNA and protein expression is expected and we have updated this as a limitation of our study in the discussion of the chapter (section 6.4).
- **Revised text:**

Pathogenic contribution of ECM and fibrosis components in obese and in diabetics is being understood progressively. Our analysis showed upregulation of transcripts annotated to ECM and fibrosis components in OM depot from T2DM compared to OM depot from NT2DM subjects. However, it is important to consider possible discordance between expression at transcript level and protein level and selected genes will need further validation.

11. Define “healthy adipocyte function”

- In our understanding, healthy adipocyte function can be defined as a state where adipocytes are able to maintain their physiological functions such as lipid storage, lipid utilization, adipokine secretion and expandability even in the presence of stress inducers such as excess nutrients. Overloading of adipocytes with excess free fatty acids, glucose and certain amino acids is known to disrupt its functions and the insulin signalling pathway and lead to dysfunctional adipocytes.

12. Numbering of chapters skips jumps from 6 to 8 and omits.

- Corrected in thesis.

13. Figure 5: ECM, laminins do not form fibers, I would prefer the term *supramolecular assemblies to macromolecules, as these assemblies are made from macromolecules.*

- Corrected in the thesis.

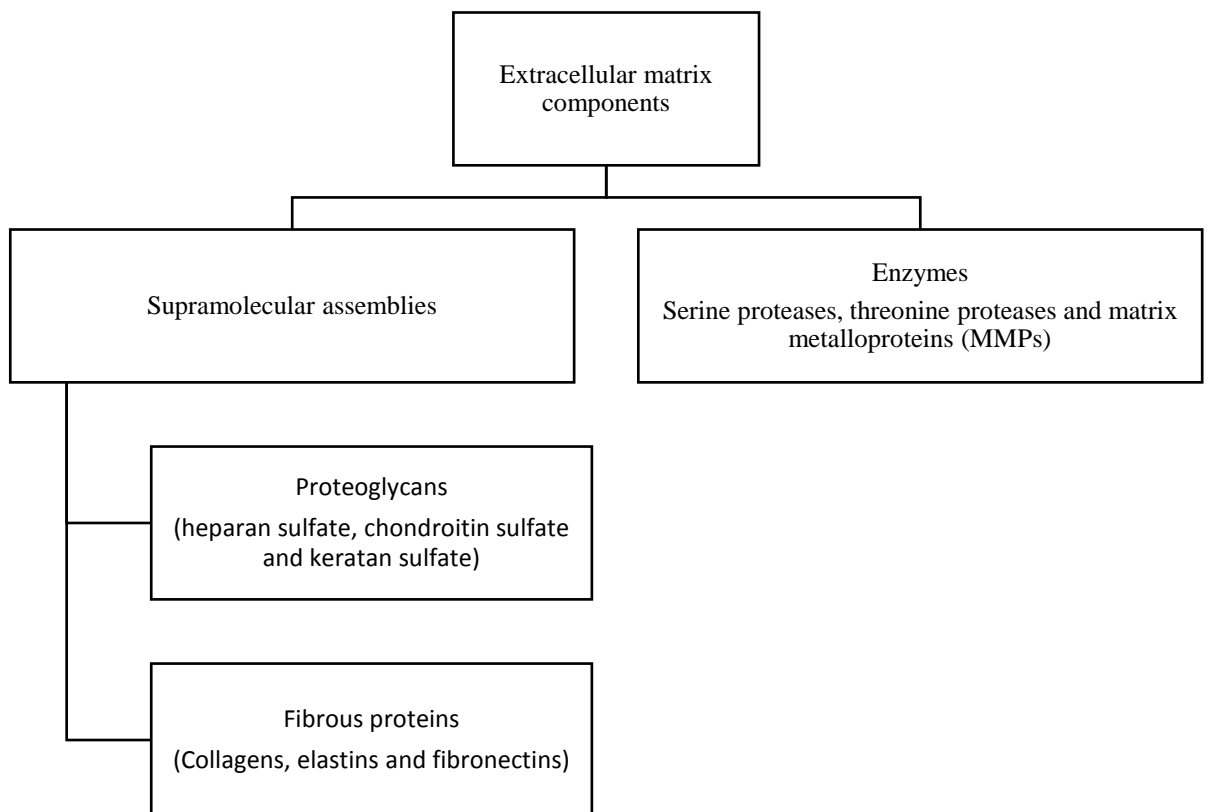


Figure 1: Basic components of ECM. ECM composition is tissue specific and varies with obesity and age in AT. Macromolecules including fibrous proteins and proteoglycans support internal cellular components and enzymes such as MMPs which are usually involved in degeneration of ECM, particularly important for a process like bone resorption, migration and tissue remodeling.

14. P 6 spell out TAG here, it's the first you use the abbreviation.

- Corrected in the thesis.

15. Resolution of images (At least in my copy of the thesis) is often substandard. When lifted from pdf documents enlarge at least to 400% before you snapshot them and paste them. Figures 15, 17-19, 41, 46 -55 etc are in the softcopy not legible at all, and a lot of other figures look pixelated and annoy the reader.

- Have changed the figures with higher resolution images or have added magnified images of individual sub-components for easier reading.

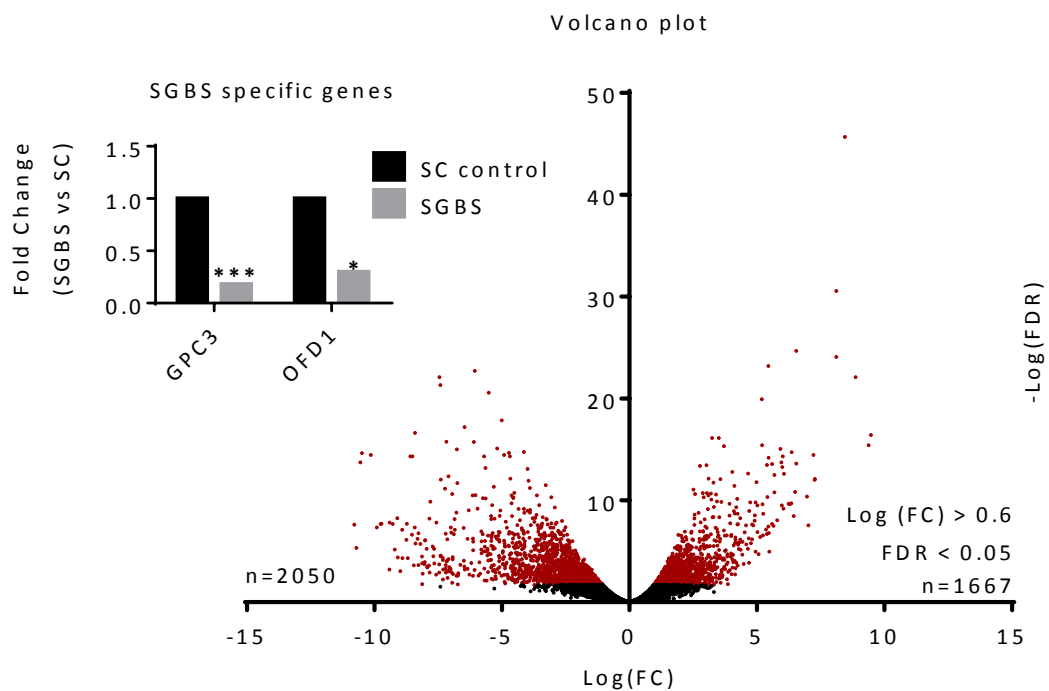
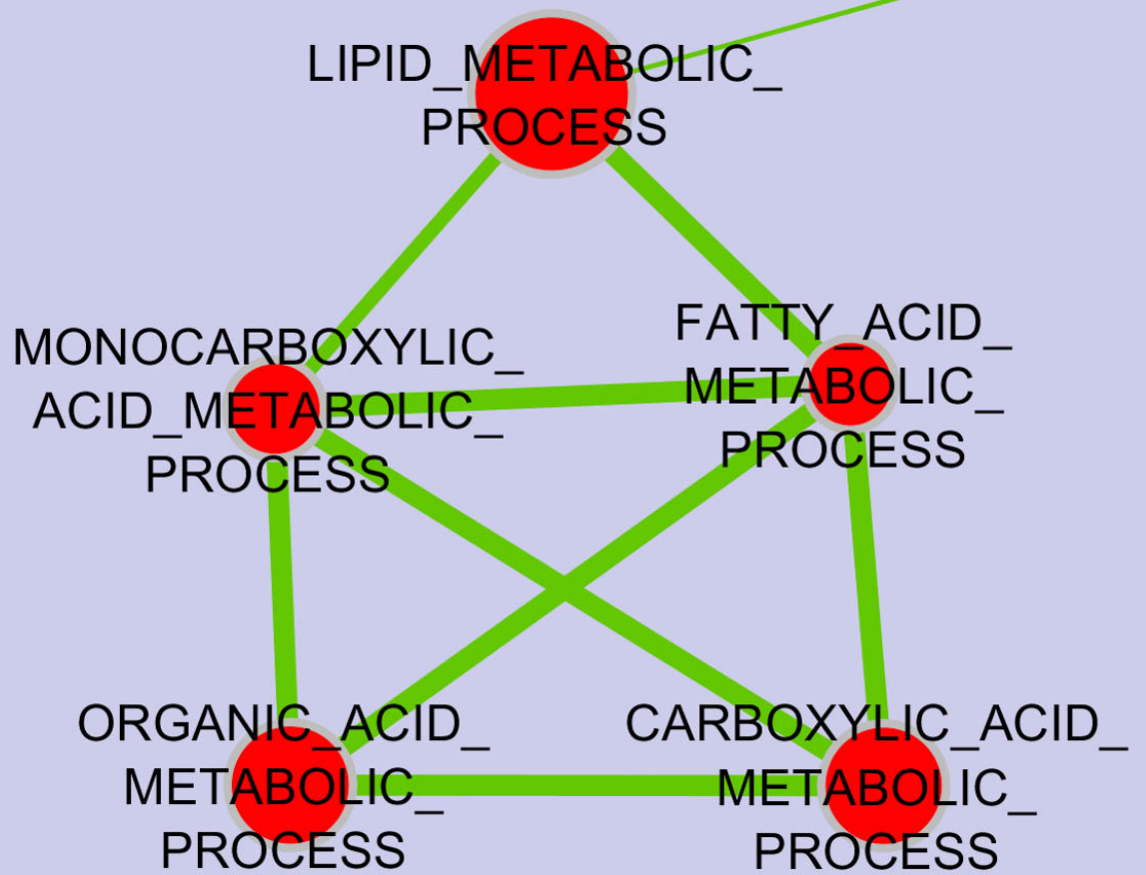
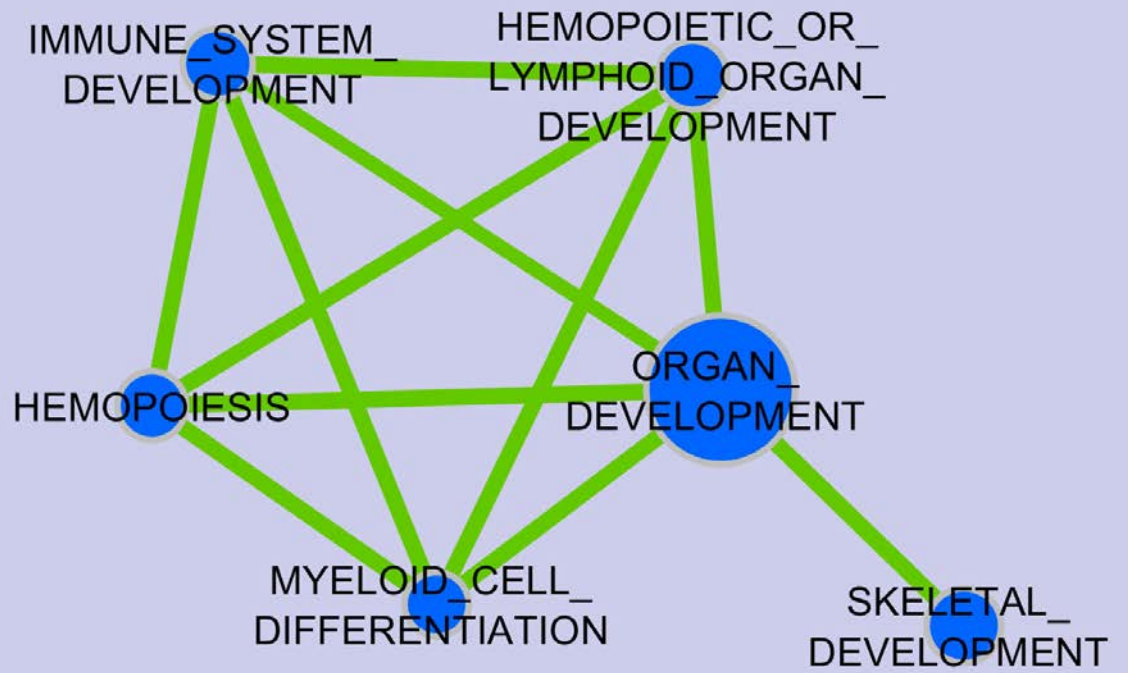


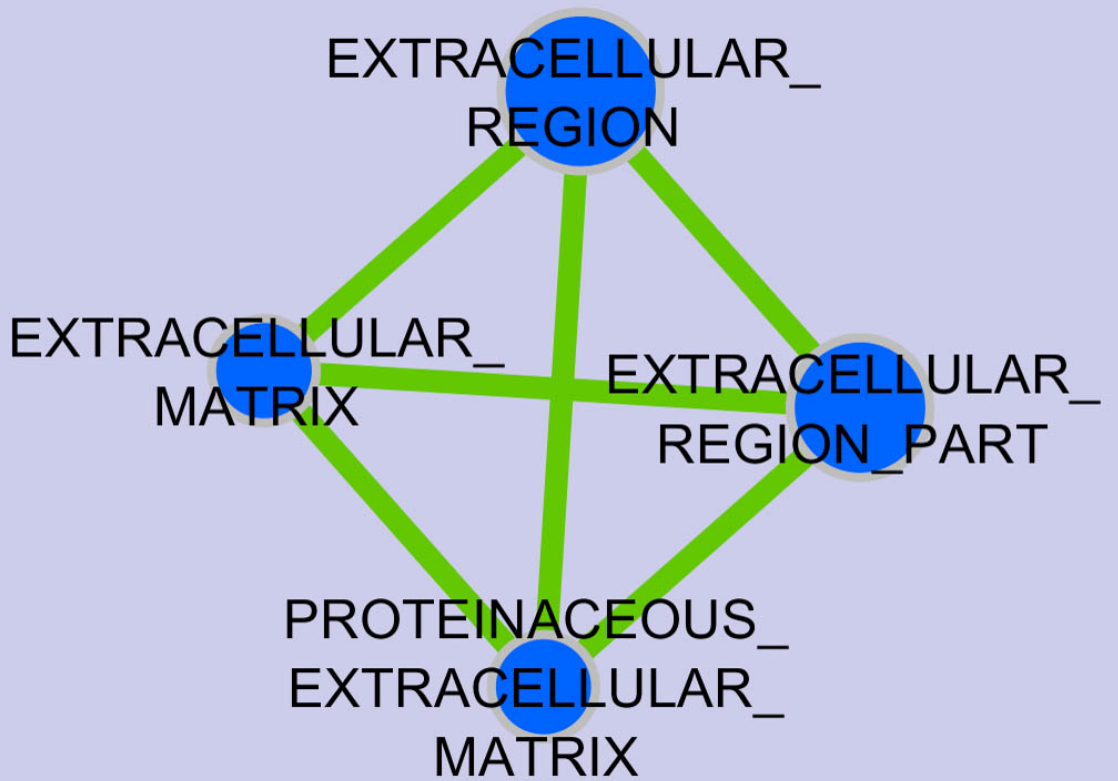
Figure 2: Global transcriptome profiling of SGBS and SC adipocytes (volcano plot). Volcano plots displaying number of differentially expressed genes in SGBS adipocytes compared to SC adipocytes. Red dots denote statistically significant genes. Genes with $FDR < 0.05$ and $\log(FC) > 0.60$ were included. For the experiments involving SC adipocytes, experiments were performed in cells derived from 4 different donors (SC_1 to SC_4). For SGBS adipocytes, experiments were performed in duplicates (SGBS_1 and SGBS_2) from the same SGBS adipocyte.

Metabolism





Organ and tissue development



ECM components

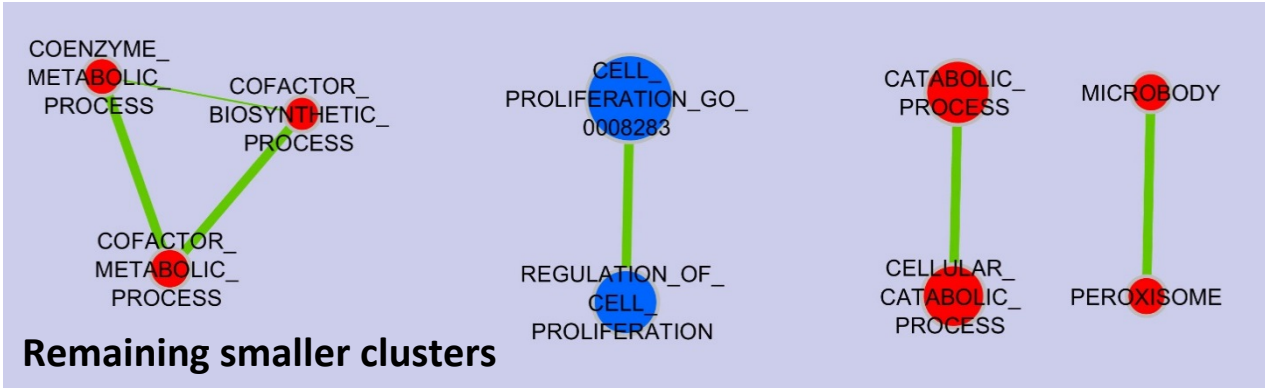
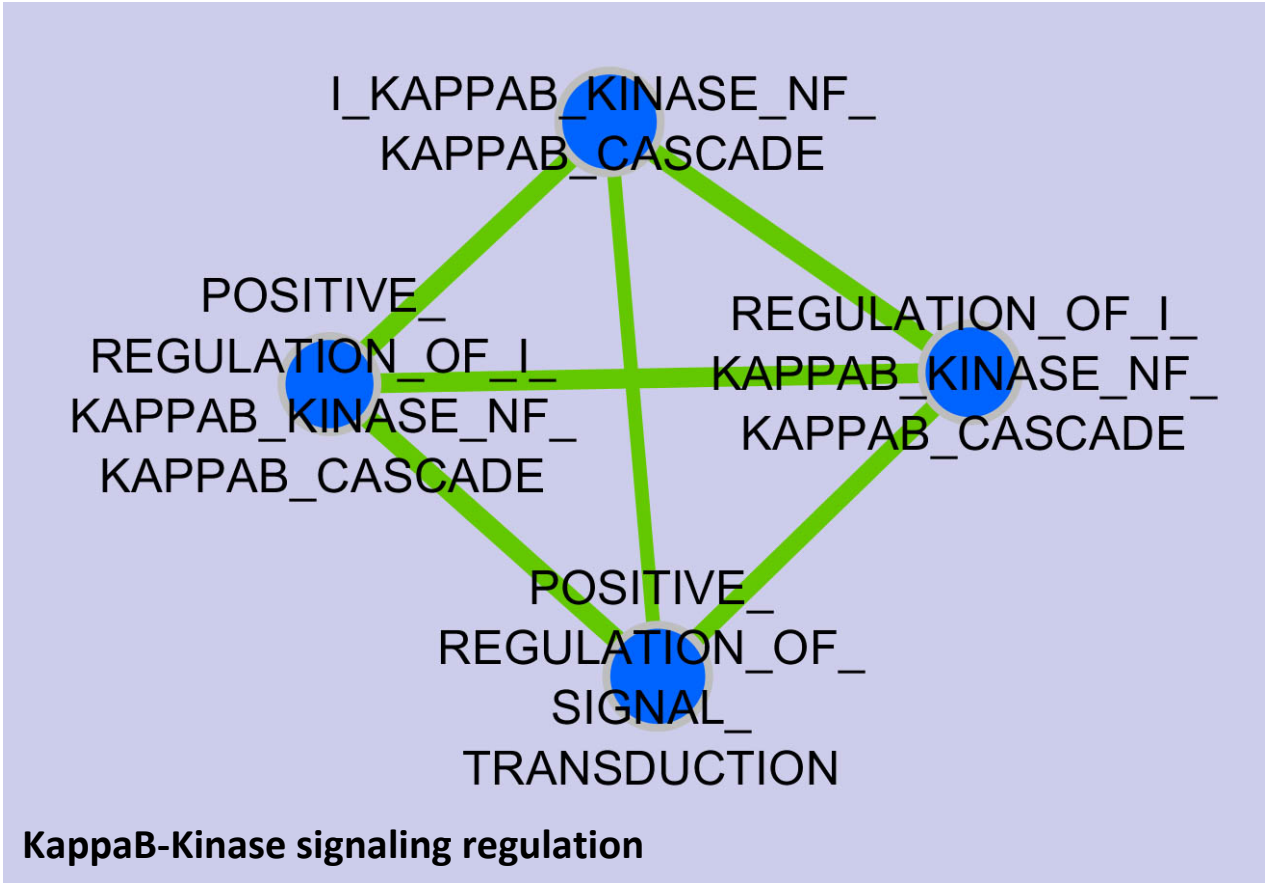


Figure 17: Fully differentiated SGBS and SC adipocytes display distinct ontology clustering. FPKM values were analyzed in gene set enrichment analysis (GSEA) desktop version [6] and the output was exported in Cytoscape 3.3 (plugin: enrichment map creator) [7] to generate a map of positively and negatively enriched gene ontologies. Size of the node predicts the number of genes in particular ontology and green connecting line represents number of common genes. Blue and red color denotes down and upregulated ontologies respectively (SGBS vs SC adipocytes). Cut off value for generating

enrichment map was capped at conservative (P-value < 0.001, FDR < 0.05).

Each cluster is magnified and shown separately.

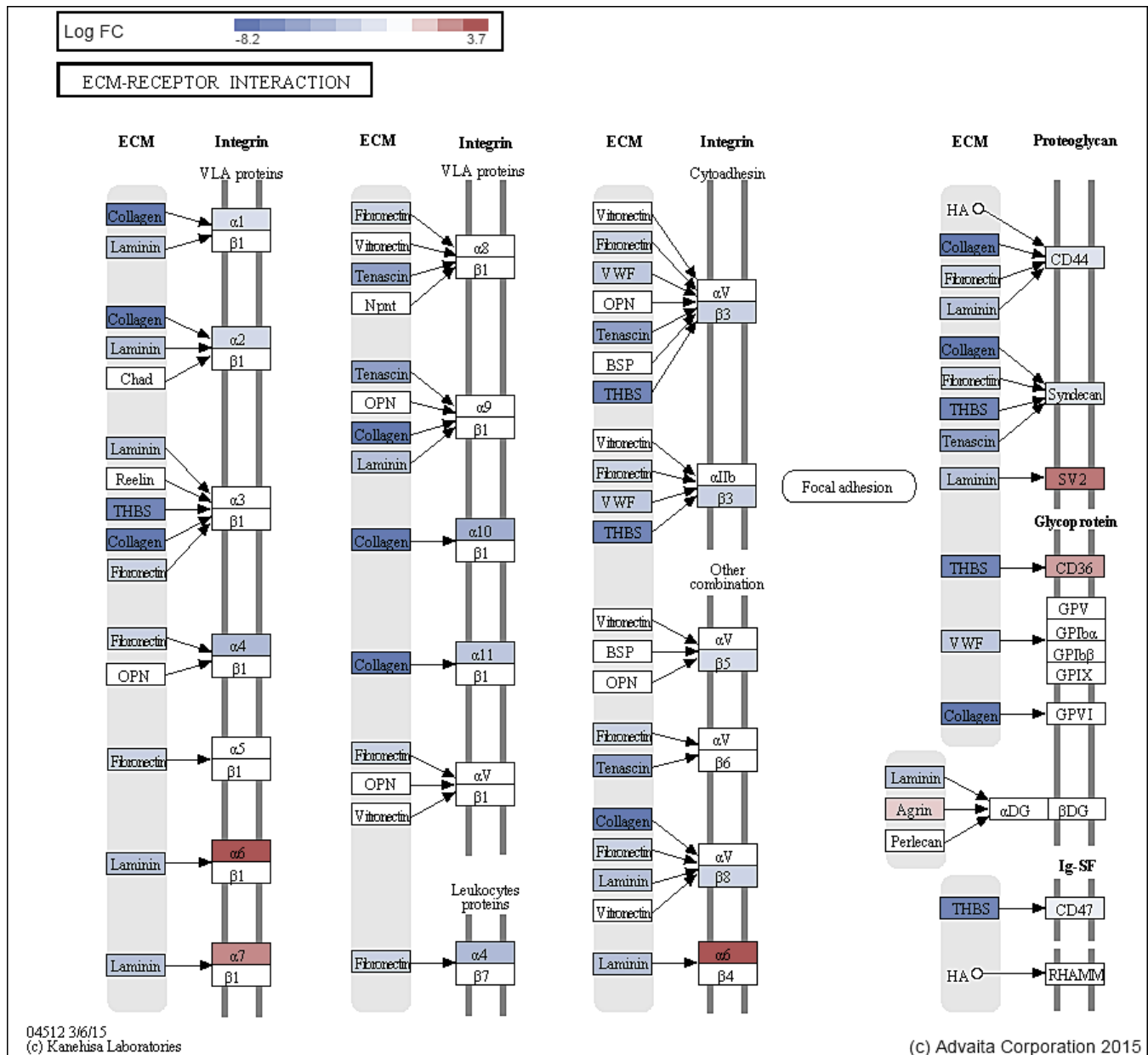


Figure 18: Representation of fold changes in ECM-receptor interaction pathway (SGBS vs SC adipocytes). Output was generated with help of iPathwayGuide. Blue and red colors symbolize downregulated and upregulated genes respectively. Significance was pegged at P < 0.05.

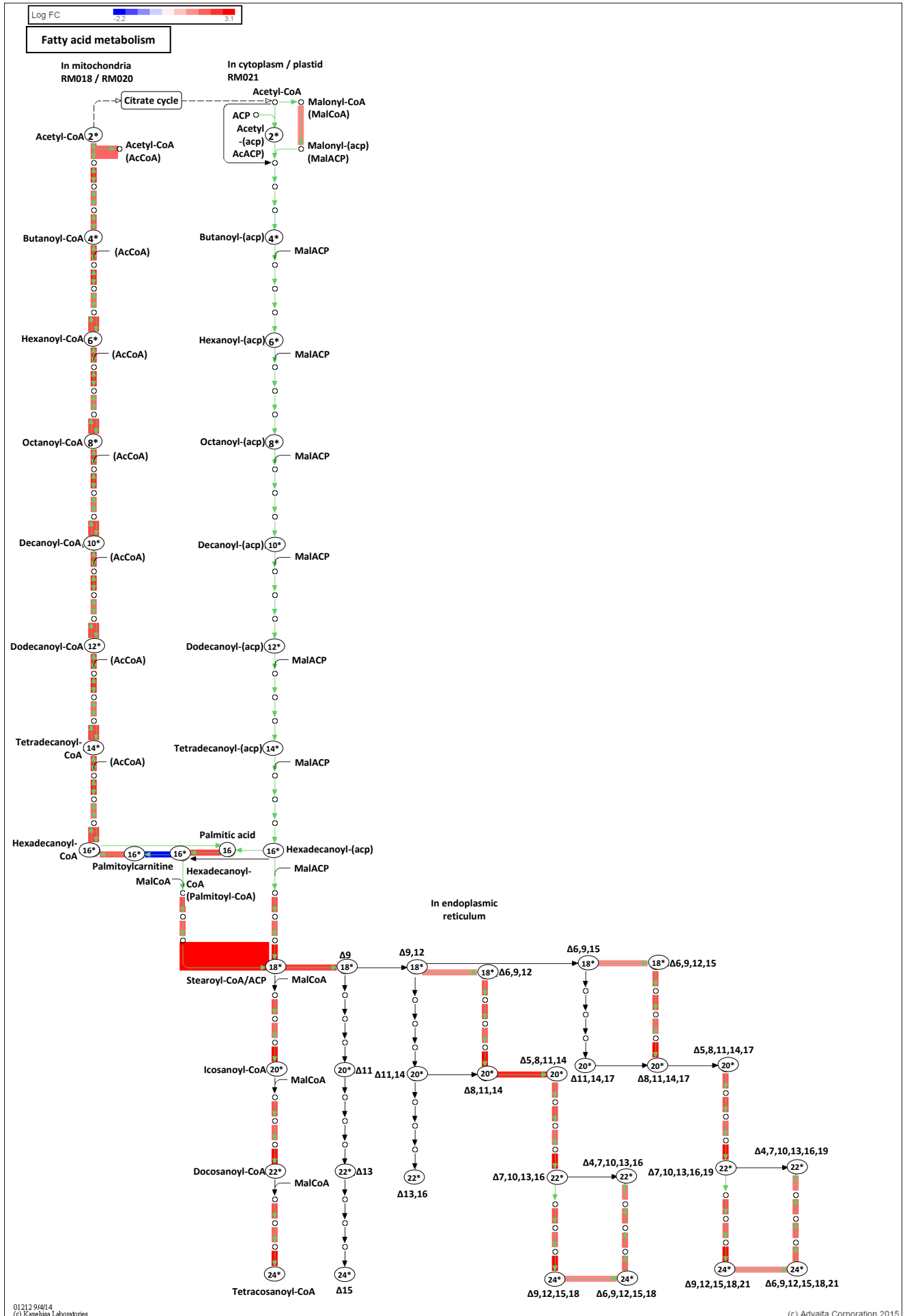


Figure 19: Representation of fold changes in fatty acid metabolism pathway (SGBS vs SC adipocytes). Output was generated in iPathwayGuide. Blue and red colors symbolize downregulated and upregulated genes respectively. Significance was pegged at $P < 0.05$.

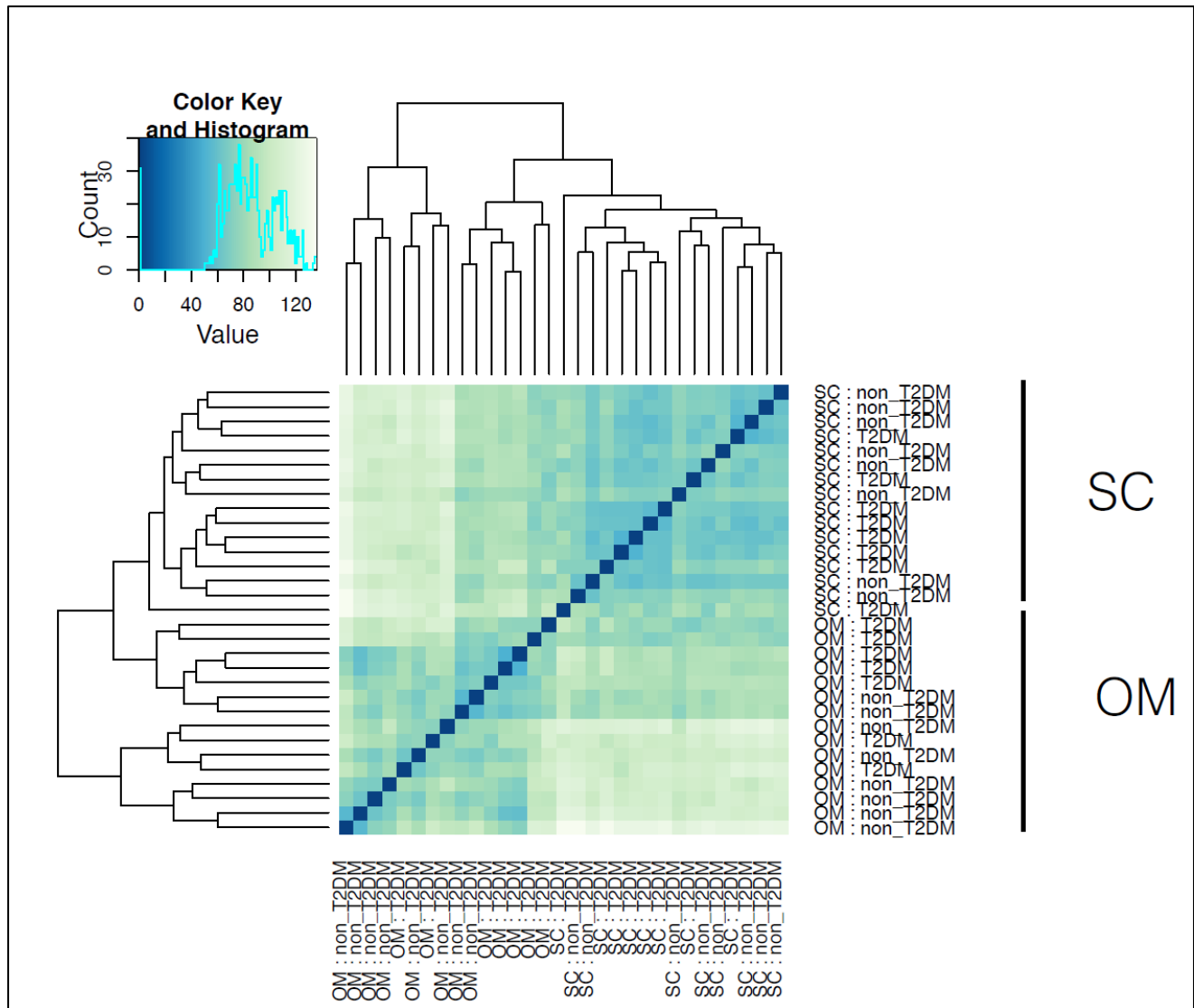


Figure 3: Euclidean distance (sample – to – sample distance) heatmap of all tissue RNA-SEQ data. Tissue samples are individually arranged on X and Y axis with each sample being compared to the other. Darker shades of blue denote decreased distance or increased similarity between the compared samples. As seen, all SC samples clustered together and distinctly from OM samples. This suggests considerable transcriptome variation among the SC and OM tissue samples.

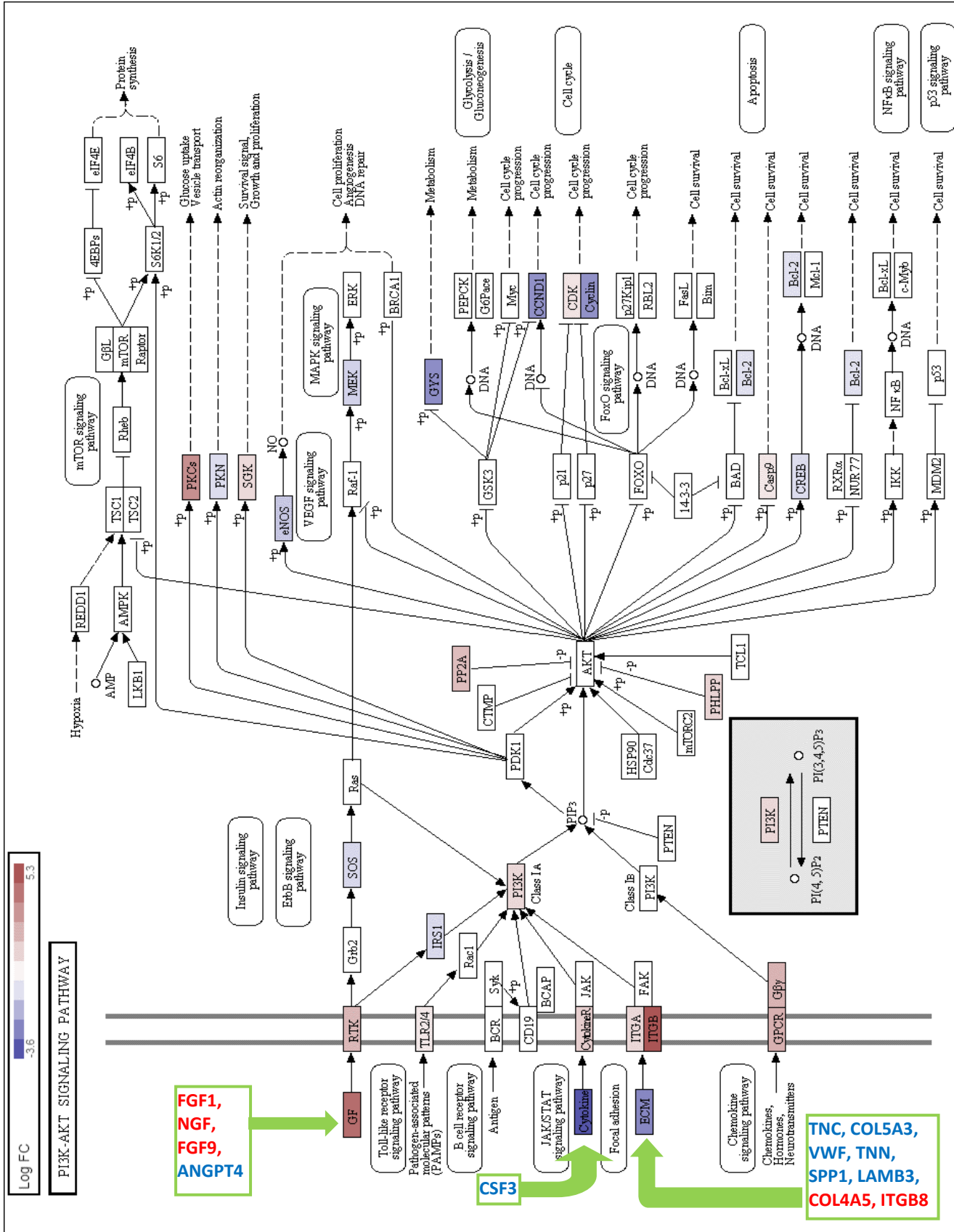


Figure 4: Representation of fold change of genes in PI3K-Akt signaling pathway in T2DM subjects. Fold changes in genes are represented by colors (upregulation – towards red and downregulation – towards blue). Green text boxes represent genes in GF (growth factor), cytokine and ECM within PI3K-Akt signaling pathway.

ECM receptor interaction pathway

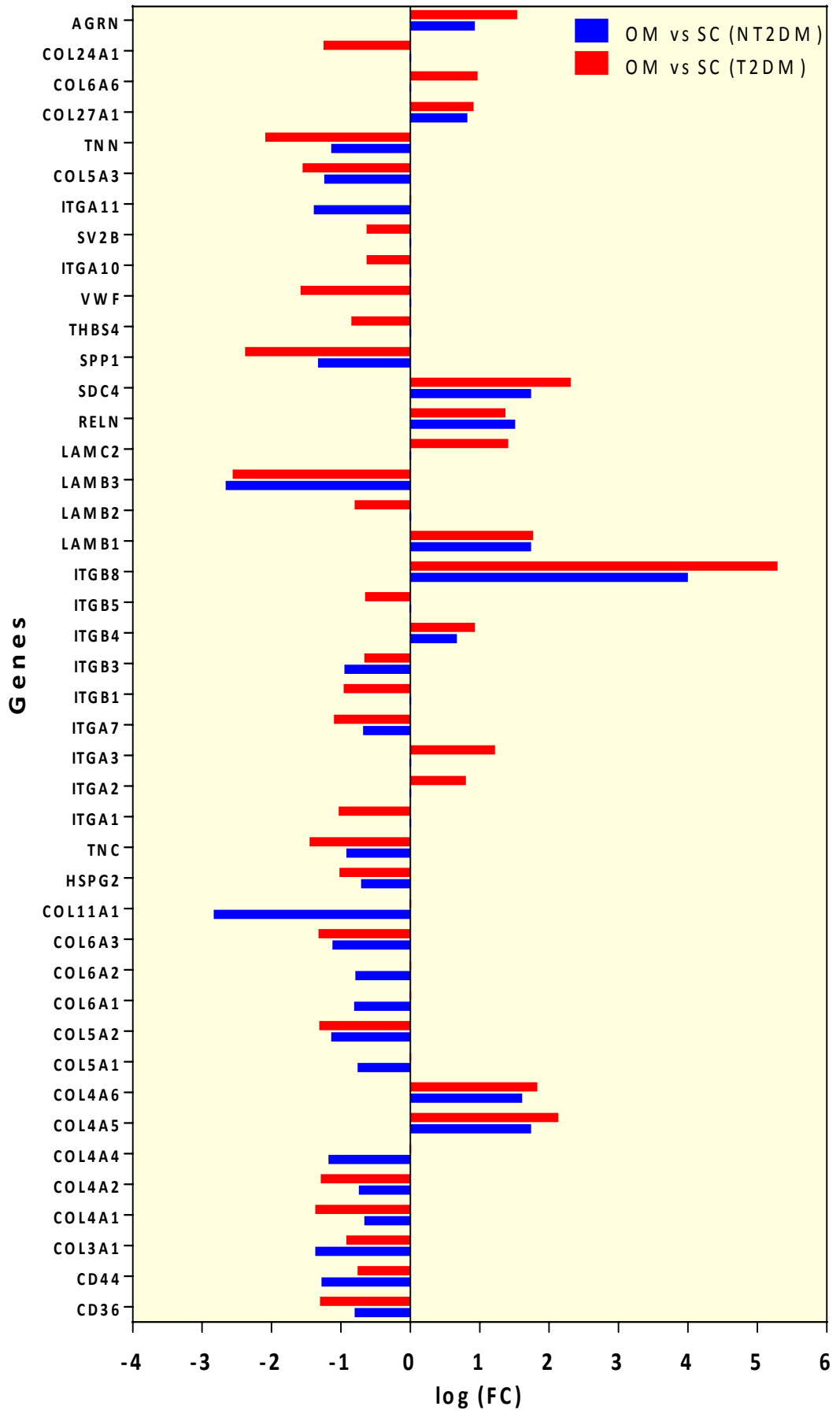
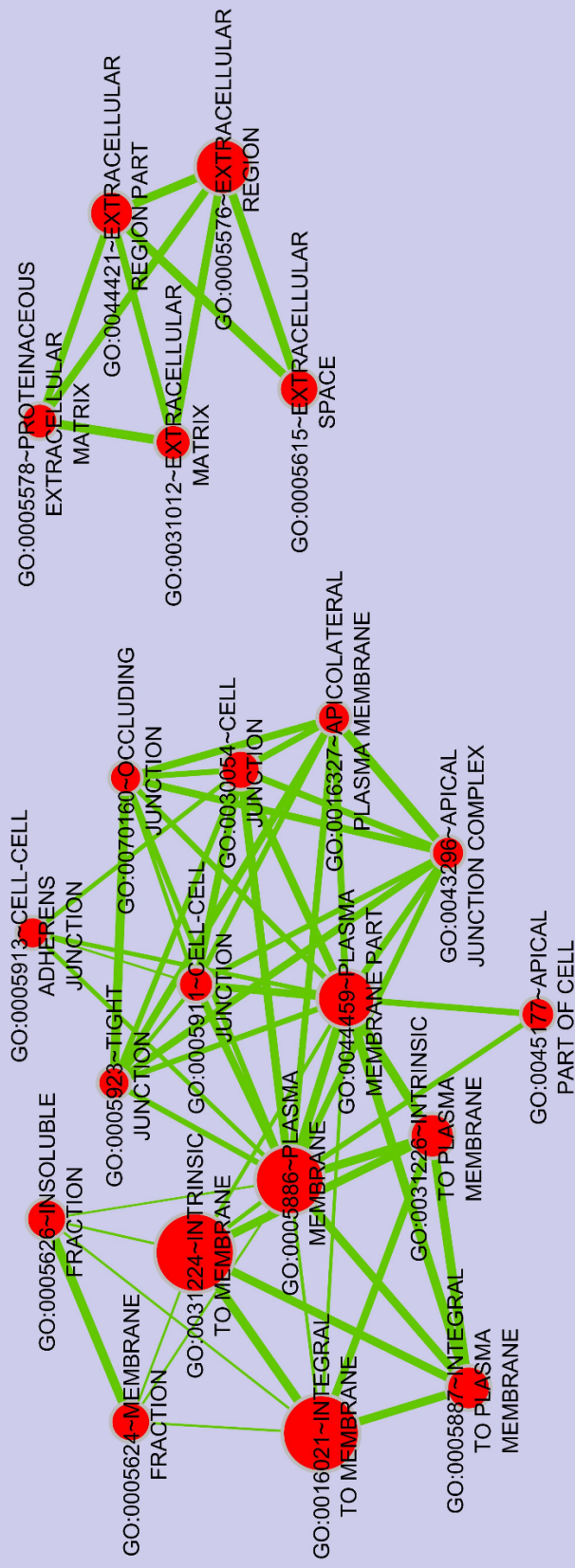


Figure 5: ECM receptor interaction pathway genes in NT2DM and T2DM subjects. Log (FC) for all the genes were plotted ($\text{Log FC} \geq \pm 0.6$ and $\text{FDR} < 0.05$). Genes below the cut off values in either NT2DM or T2DM are indicated as empty bar spaces.

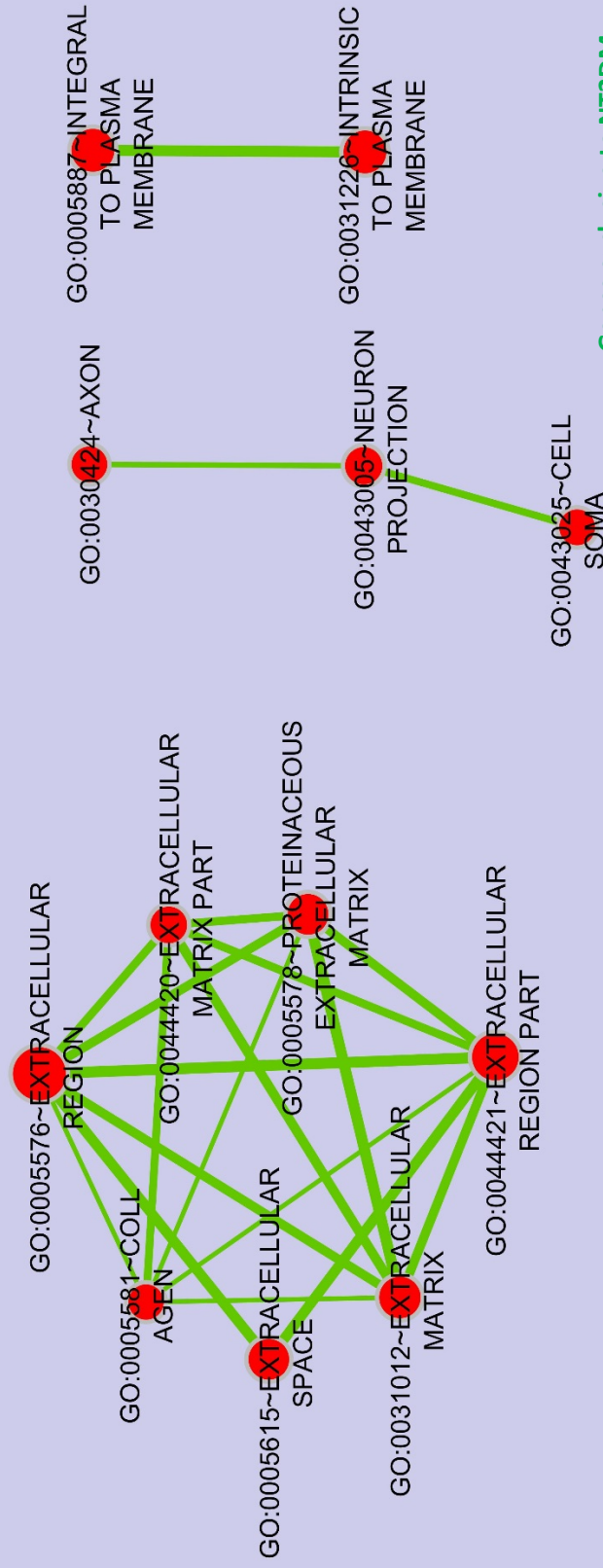
Total ECM genes n=32



Genes exclusive to
NT2DM: LTBP4, VEGF

Figure 6: Positively enriched cellular components in NT2DM (OM vs SC). Upregulated genes were analyzed using DAVID bioinformatics and the “functional annotation chart” output was exported in Cytoscape 3.3 (plugin: enrichment map creator) [7] to generate a map of enriched GO_CC. Size of the node predicts the number of genes in particular ontology with green connecting line representing number of common genes. Cut off value for generating enrichment map was capped at conservative (P-value < 0.001, FDR < 0.05).

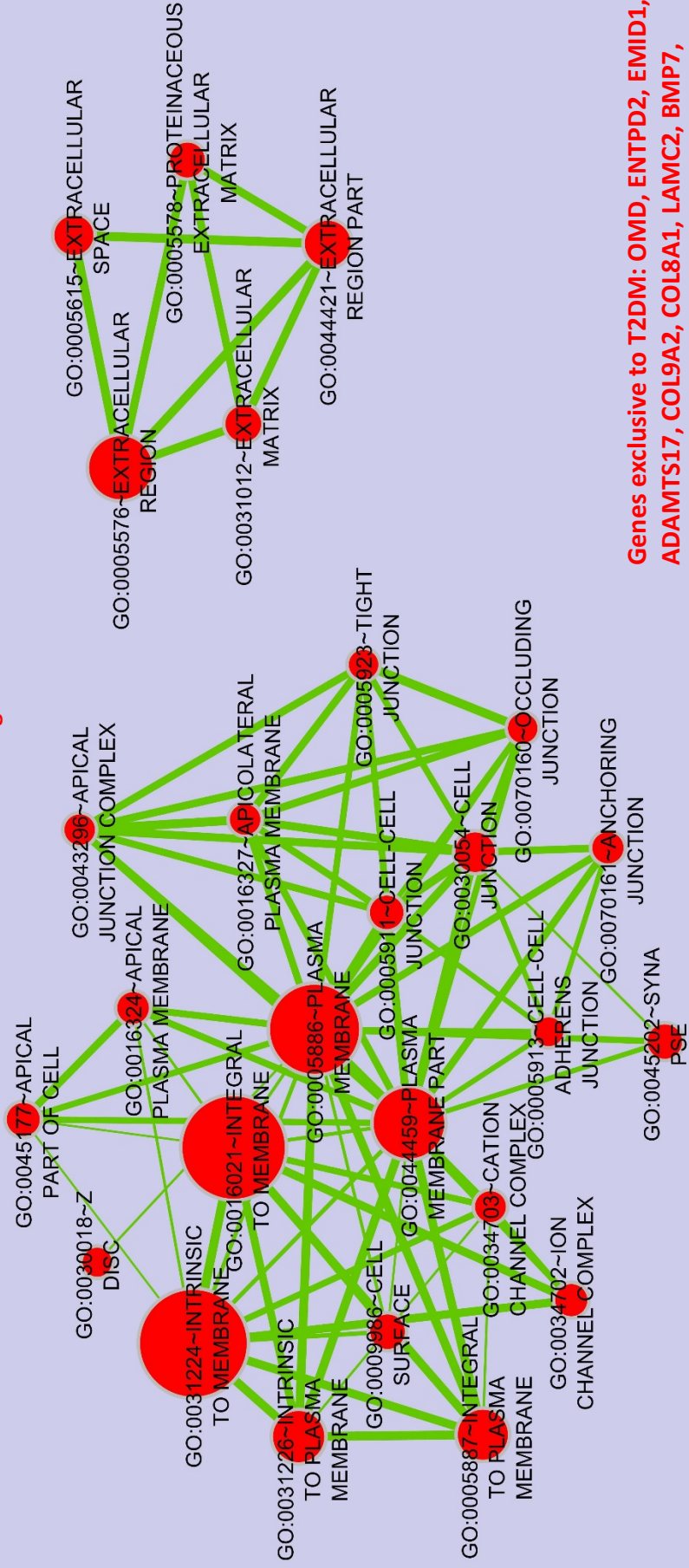
Total ECM genes n=39



Genes exclusive to NT2DM:
FMOD, COL3A1, VIT, MMP2,
CD44, GRIA3, ADAMTS2

Figure 7: Negatively enriched cellular components in NT2DM (OM vs SC). Downregulated genes were analyzed using DAVID bioinformatics and the “functional annotation chart” output was exported in Cytoscape 3.3 (plugin: enrichment map creator) [7] to generate a map of enriched GO_CC. Size of the node predicts the number of genes in particular ontology with green connecting line representing number of common genes. Cut off value for generating enrichment map was capped at conservative (P-value < 0.001, FDR < 0.05).

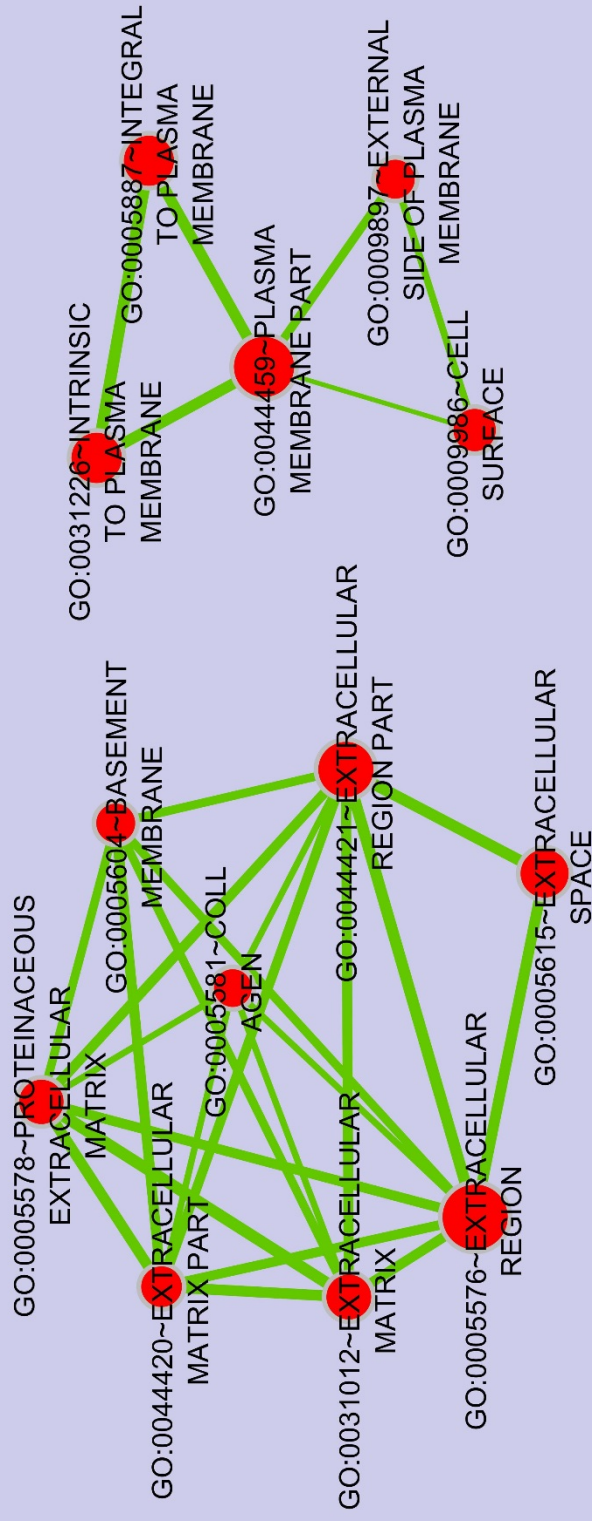
Total ECM genes n = 50



Genes exclusive to T2DM: OMD, ENTPD2, EMID1, ADAMTS17, COL9A2, COL8A1, LAMC2, BMP7, ADAMTS3, ARGN, BMP4, EMILIN3, WNT9A, COL17A1, PRSS12, TGFB2, WNT4, WNT3, TGFB3, WNT5B

Figure 8: Positively enriched cellular components in T2DM (OM vs SC). Upregulated genes were analyzed using DAVID bioinformatics and the “functional annotation chart” output was exported in Cytoscape 3.3 (plugin: enrichment map creator) [7] to generate a map of enriched GO_CC. Size of the node predicts the number of genes in particular ontology with green connecting line representing number of common genes. Cut off value for generating enrichment map was capped at conservative (P-value < 0.001, FDR < 0.05).

Total ECM genes n=41



Genes exclusive to T2DM: HSPG2, NID, COL16A1, MMRN2, VWF, COL12A1, FREM1, VWA1, COL24A1, TNC, COL4A2 COL4A1

Figure 9: Negatively enriched cellular components in T2DM (OM vs SC). Downregulated genes were analyzed using DAVID bioinformatics and the “functional annotation chart” output was exported in Cytoscape 3.3 (plugin: enrichment map creator) [7] to generate a map of enriched GO_CC. Size of the node predicts the number of genes in particular ontology with green connecting line representing number of common genes. Cut off value for generating enrichment map was capped at conservative (P-value < 0.001, FDR < 0.05).

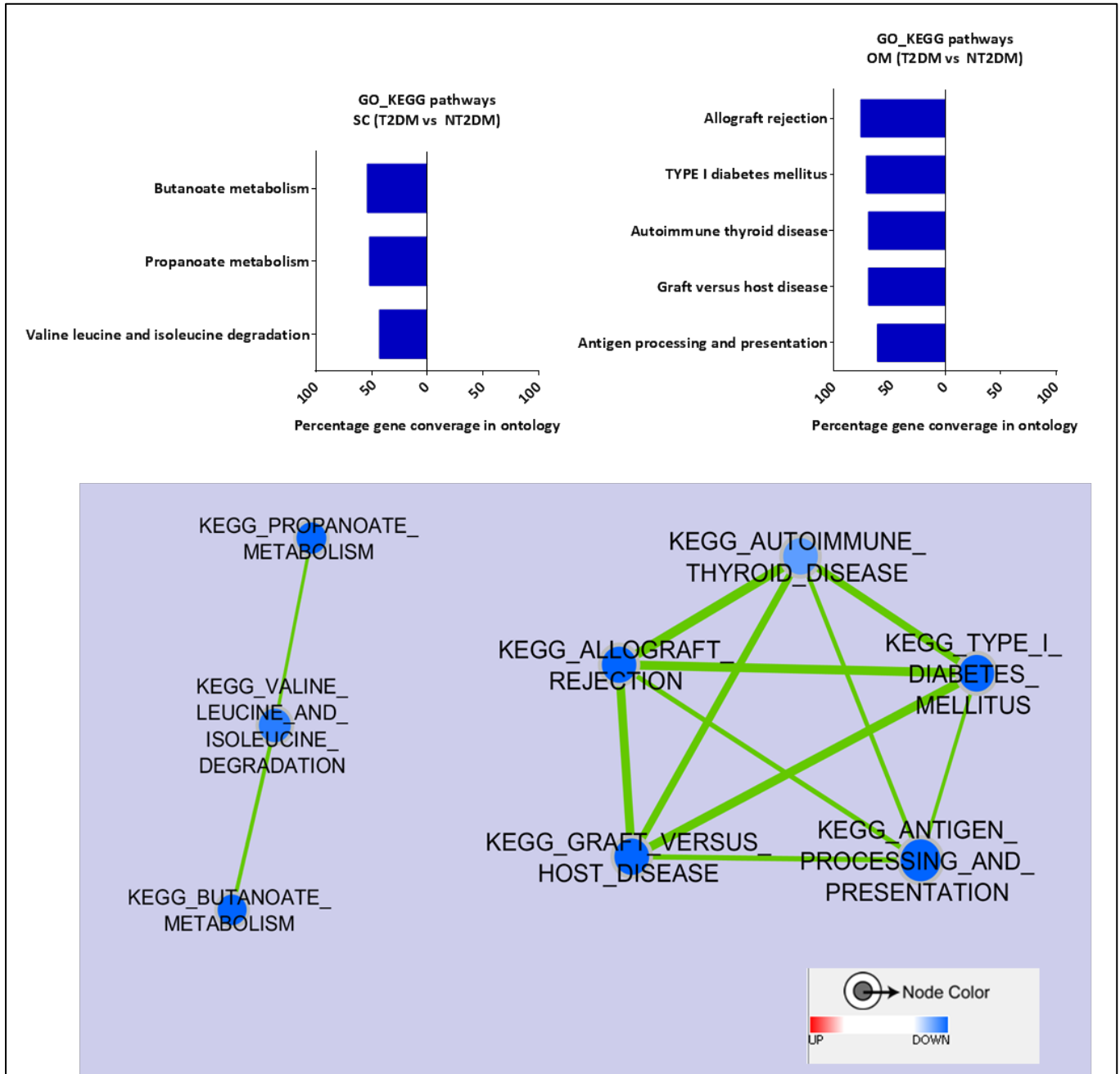


Figure 10: KEGG pathway enrichment and their interaction map illustrating transcriptomic signatures in T2DM compared to NT2DM subjects. FPKM values were analyzed in gene set enrichment analysis (GSEA) desktop version [165] and the output was exported in Cytoscape 3.3 (plugin: enrichment map creator) [163] to generate

a map of positively and negatively enriched gene ontologies. Inner node represents enrichment in SC depot (left cluster) and OM depot (right cluster). Size of the node predicts the number of genes in particular ontology with green connecting line representing number of common genes or interaction. Blue and red color denotes significant negative and positive enrichment respectively. Cut off value for generating enrichment map was capped at permissive (P-value < 0.05, FDR < 0.25).

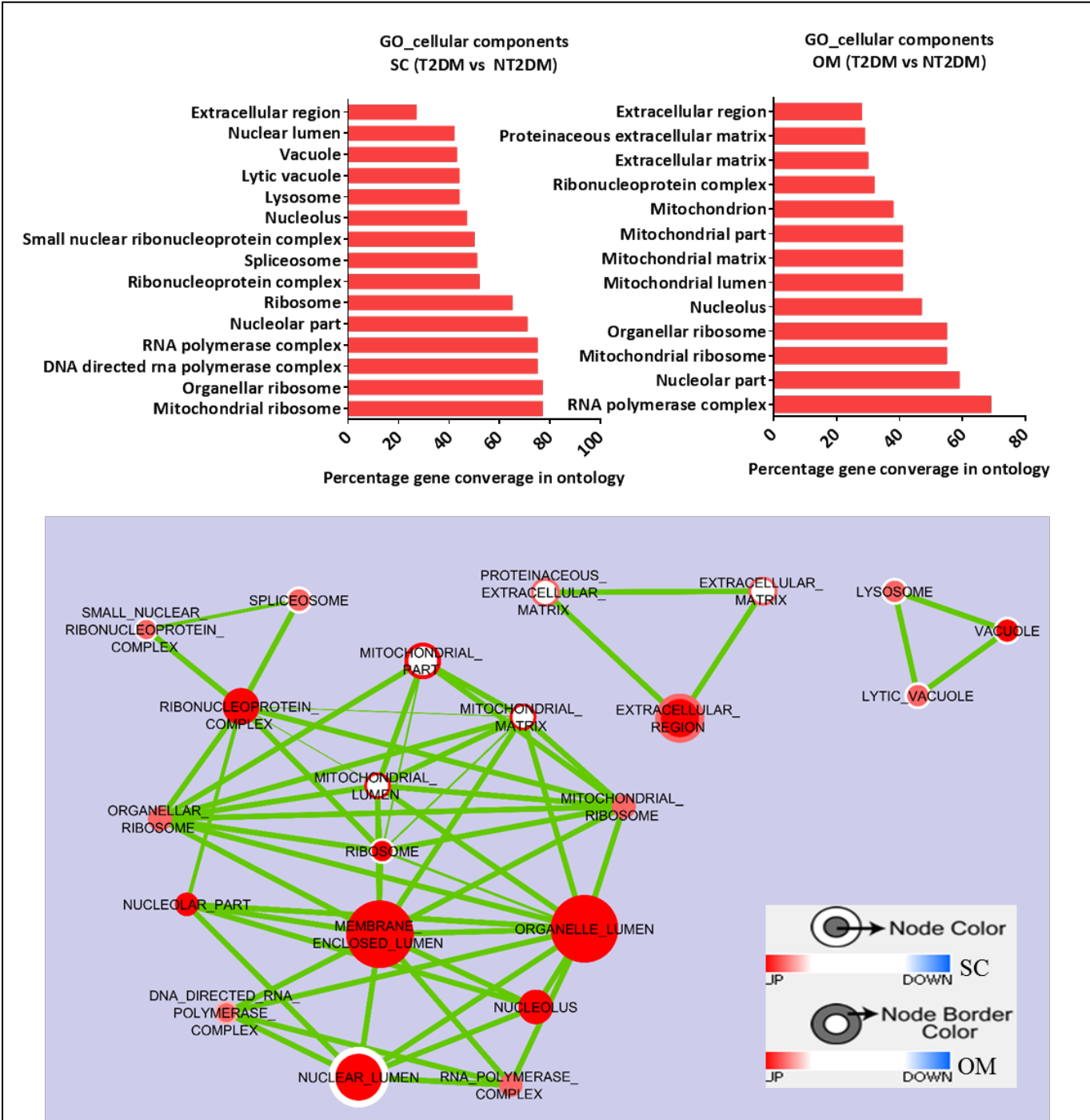


Figure 11: GO cellular component enrichment and their interaction map illustrating transcriptomic signatures in T2DM compared to NT2DM subjects. FPKM values were input into gene set enrichment analysis (GSEA) desktop version [165] and the output was exported in Cytoscape 3.3 (plugin: enrichment map creator) [163] to generate a map of positively and negatively enriched gene ontologies. Inner node represents enrichment in SC depot and outer border in node represents enrichment in OM depot. Size of the node predicts the number of genes in particular ontology with green connecting line representing number of common genes or interaction. Blue and red color denotes significant negative and positive enrichment respectively. Cut off value for generating enrichment map was capped at permissive (P-value < 0.05, FDR < 0.25).

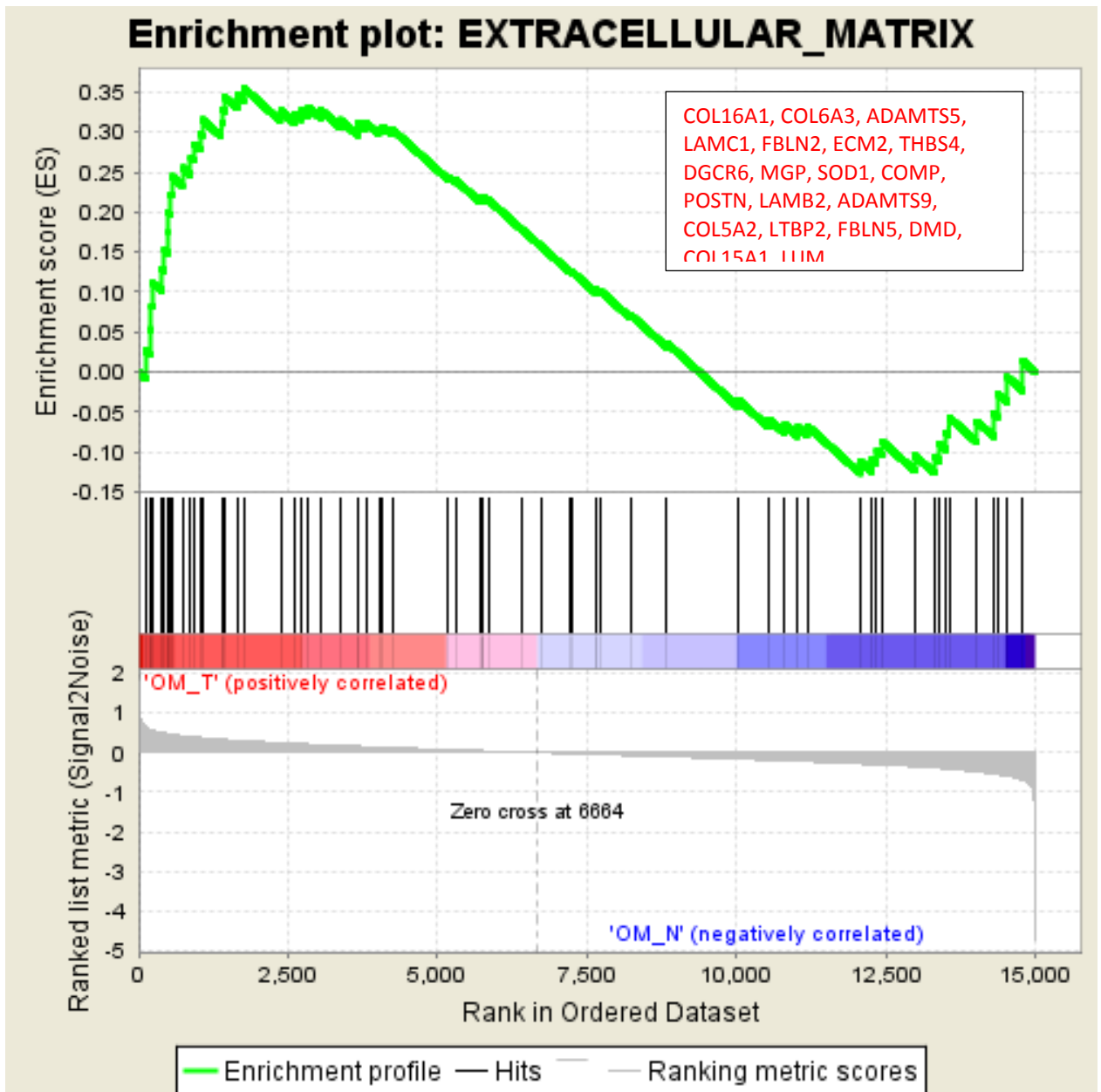
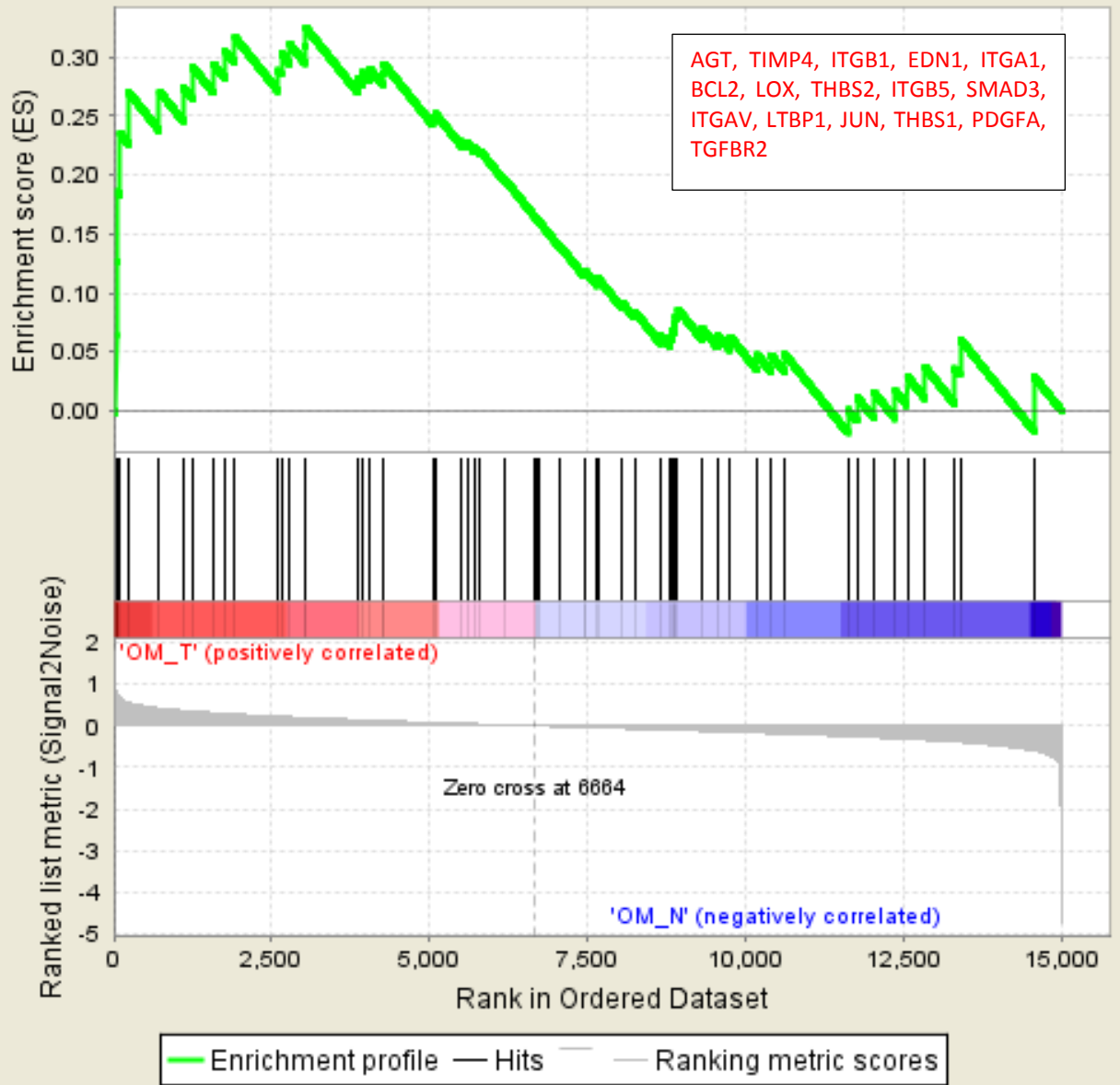


Figure 12: Heat map and enrichment plots of ECM genes in OM depot (T2DM vs NT2DM). Each black vertical line in enrichment plot denotes one gene and color bar represents gene rank within list of genes. Output was generated in GSEA and significance was capped at $P < 0.05$.

Enrichment plot: from_text_entry_



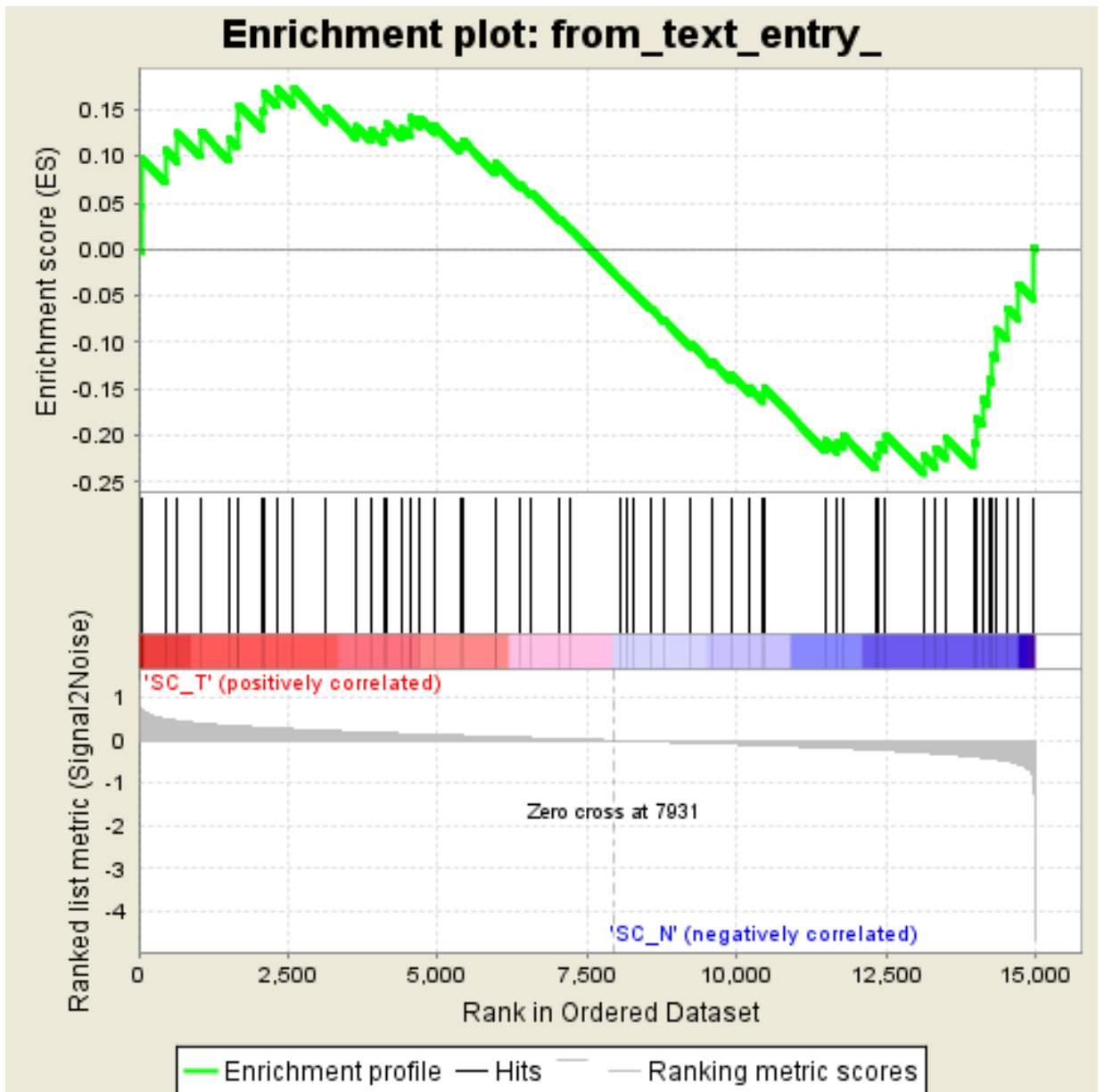


Figure 13: Enrichment analysis of fibrosis genes in T2DM compared to NT2DM (SC and OM depots). Each black vertical line in enrichment plot denotes one gene and color bar represents gene rank within list of genes. Output was generated by analyzing genes of interest using GSEA and significance was capped at $P < 0.05$.

16. Table 2: mouse cells should be shown as a group separate from human cells, and not in mixed order. The point is that that much knowledge in human cells does not exist; most of the work in adipocyte biology is mouse-heavy.

- Order of cells revised.
- New table

Cell line/model	Origin	Reference
Adipocytes from rodent models		
3T3-L1 adipocytes	Mouse 3T3-L1 fibroblasts	[8, 9]
3T3-F442A adipocytes	Mouse 3T3-L1 fibroblasts	[9]
Ob17 adipocytes	Epididymal fat pad of C57BL/6J ob/ob mouse	[10]
Adipocytes from human derived adipose depot		
Human or animal preadipocytes	Mature adipocytes from adipose tissue depot from humans or rats – also called ceiling culture	[11]
Simpson-Golabi Behmel Syndrome or SGBS adipocytes	3 month old infant suffering from SGBS	[2]

Table 1: Adipocyte models used for research.

17. 3.2.4 “GAPDH (Cell Signalling)” in Western Blotting is not used for cell signalling but as a housekeeping protein analogously to a housekeeping gene

- Cell signalling is the name of the company where antibody was bought from. Have correct it to GAPDH (Cell Signalling, MA, USA) for better understanding.

Examiner 3

Introduction.

1. Page 6. *It is remarkable that the main function of adipose tissue, storage of fuel is not included.*

- Have updated the introduction section in the thesis accordingly.
- **Revised part:**

Conventionally, AT was considered as merely a storage organ for excess nutrients in the form of lipid droplets which could be utilized during periods of fasting/starvation via lipolysis. Over the years, more complex functions of fat (mentioned below) were slowly understood. Figure 4 summarizes known functions of AT. AT functions include:

1. Endocrine function: secretion of hormones such as leptin [12, 13] and adiponectin [14] which regulate food intake and fuel utilization.
2. Regulation of angiogenesis to support adipocyte growth within the tissue [15].
3. Regulation of inflammation and macrophage infiltration [16].
4. Metabolic functions including lipogenesis, lipid storage and lipolysis.

In healthy individuals, the degree of lipid storage or breakdown is controlled primarily by insulin and glucagon hormones. During the fed state, insulin promotes the storage of dietary lipids in AT. After being absorbed, free fatty acids

are converted to TAGs (triacylglycerol/triglycerides) in the liver and transported to the AT after being packaged inside lipoproteins. Inside adipose, lipase enzyme in the plasma membrane of adipocytes breaks these TAGs to free fatty acids which eventually enter inside ER as fatty acyl-CoA. In ER, these fatty acyl-CoA are converted back to TAGs (re-esterification) and stored in lipid droplets. Adipocytes also synthesize free fatty acids such as palmitic acid from acetyl-CoA by the process of *de novo* lipogenesis.

During fasting state, glucagon hormone is secreted from pancreatic alpha cells, which in turn activates lipolysis of stored TAGs in adipocytes. Free fatty acids released upon lipolysis are distributed to energy deficient tissues such as skeletal muscle. Here, these free fatty acids are oxidized into acetyl-CoA in mitochondria via β -oxidation pathway to generate energy in the form of ATP.

2. *Page 7. It is important not to confuse de novo lipogenesis with fatty acid reesterification. The text should indicate where the fatty acids released by AT go e.g. muscle, to synthesise ATP in their mitochondria.*
 - Have updated the introduction section 1.3 in the thesis (also mentioned in comment 1 by examiner 3).

Chapter 3 Comparison of experimental models: SGBS vs primary subcutaneous adipocytes.

3. *Figure 16: could be labelled more intuitively easier and independent of the main text. Identification of clusters should be clearer.*

- Updated the figure legend and also added figures with magnified view.

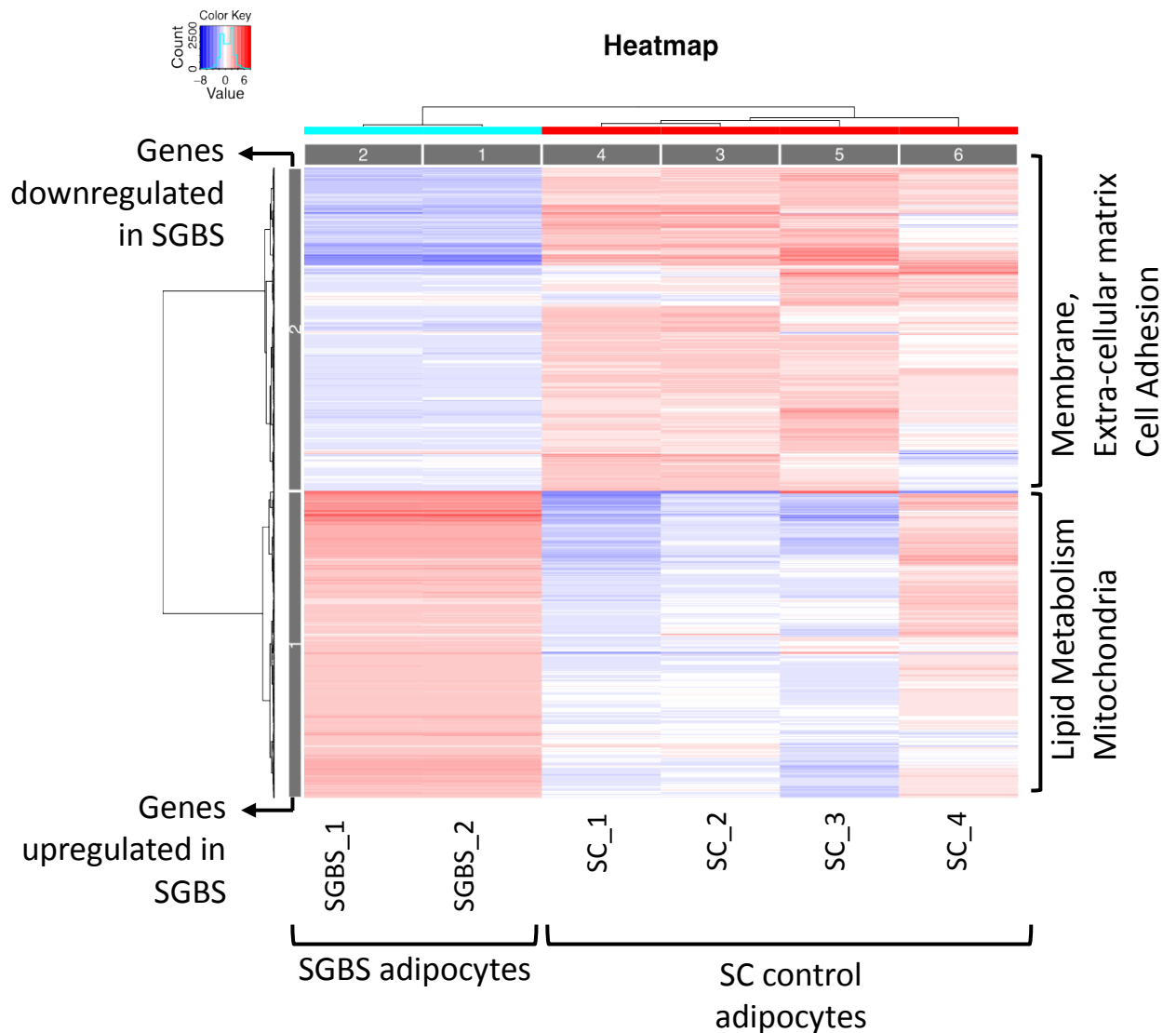


Figure 16: Transcriptome profiling of top 1000 differentially expressed genes in SGBS adipocytes. Heat map clustering (unsupervised) top 1000 significantly upregulated (red) or downregulated (blue) genes in SGBS ($n = 2$) when compared to SC ($n = 4$) adipocytes. Enriched genes ontologies in up (lipid metabolism) or downregulated (membrane, extra-cellular matrix) set of genes in SGBS adipocytes are denoted on the right side of the figure. For the experiments involving SC adipocytes, experiments were performed in cells derived from 4 different donors (SC_1 to SC_4). For SGBS

adipocytes, experiments were performed in duplicates (SGBS_1 and SGBS_2) from the same SGBS adipocyte.

4. *Figure 17 does not permit reading the content of the enrichment map of gene ontologies. It is too small.*

- Have added magnified view of each ontology clusters for better understanding. Figure included in previous comments.

5. *Figure 18 it is difficult to read. Dark blue colours not appropriate to read inside boxes.*

- Have improved the contrast in the figure. Included in previous comments.

6. *Figure 19. Too small font*

- Have magnified the figure and made text sharper for better visualization. Included in previous comments.

7. *Page 67. PGC1 α is not a transcription factor. It is a coactivator of several transcription factors.*

- Have corrected this in text in section 5.4
- **Revised text**

In all cell types in humans, mitochondrial biogenesis and adaptive thermogenesis are regulated primarily by upstream transcriptional coactivator PGC1 α in conjunction with NRF1 (nuclear respiratory factor 1) which is strongly activated by cAMP and cytokine pathways [17].

8. *Figure 24 B. It is unclear how this experiment was performed. The graph should include information on the specific treatments. Also, some indication of increased mitochondria per/cell would have been helpful.*

- Have updated in the protocol section 2.8.

- **Updated version**

XF Cell Mito Stress test kit (Seahorse Bioscience) was used to measure mitochondrial function in adipocytes in a 24 well plate format. Data were reported as pmoles of oxygen consumed per minute or oxygen consumption rate. Cellular respiration parameters calculated are basal respiration, ATP production, proton leak, maximal respiration and spare respiratory capacity. As suggested by the manufacturer, 5 replicates of control, treatment conditions and negative controls were used. Oligomycin inhibits ATP synthase (complex V) and the decrease in OCR following injection of oligomycin correlates to the mitochondrial respiration associated with cellular ATP production. Carbonyl cyanide-4 (trifluoromethoxy) phenylhydrazone (FCCP) is an uncoupling agent that collapses the proton gradient and disrupts the mitochondrial membrane potential. As a result, electron flow through the ETC is uninhibited and oxygen is maximally consumed by complex IV. The FCCP-stimulated OCR can then be used to calculate spare respiratory capacity, defined as the difference between maximal respiration and basal respiration. Spare respiratory capacity is a measure of the ability of the cell to respond to increased energy demand. The third injection is a mix of rotenone, a complex I inhibitor, and antimycin A, a complex III inhibitor. This combination shuts down mitochondrial respiration and enables

the calculation of non-mitochondrial respiration driven by processes outside the mitochondria.

- We have used relative quantification of mitochondrial DNA as a surrogate marker of mitochondrial content. The results are presented in figure 24 C.

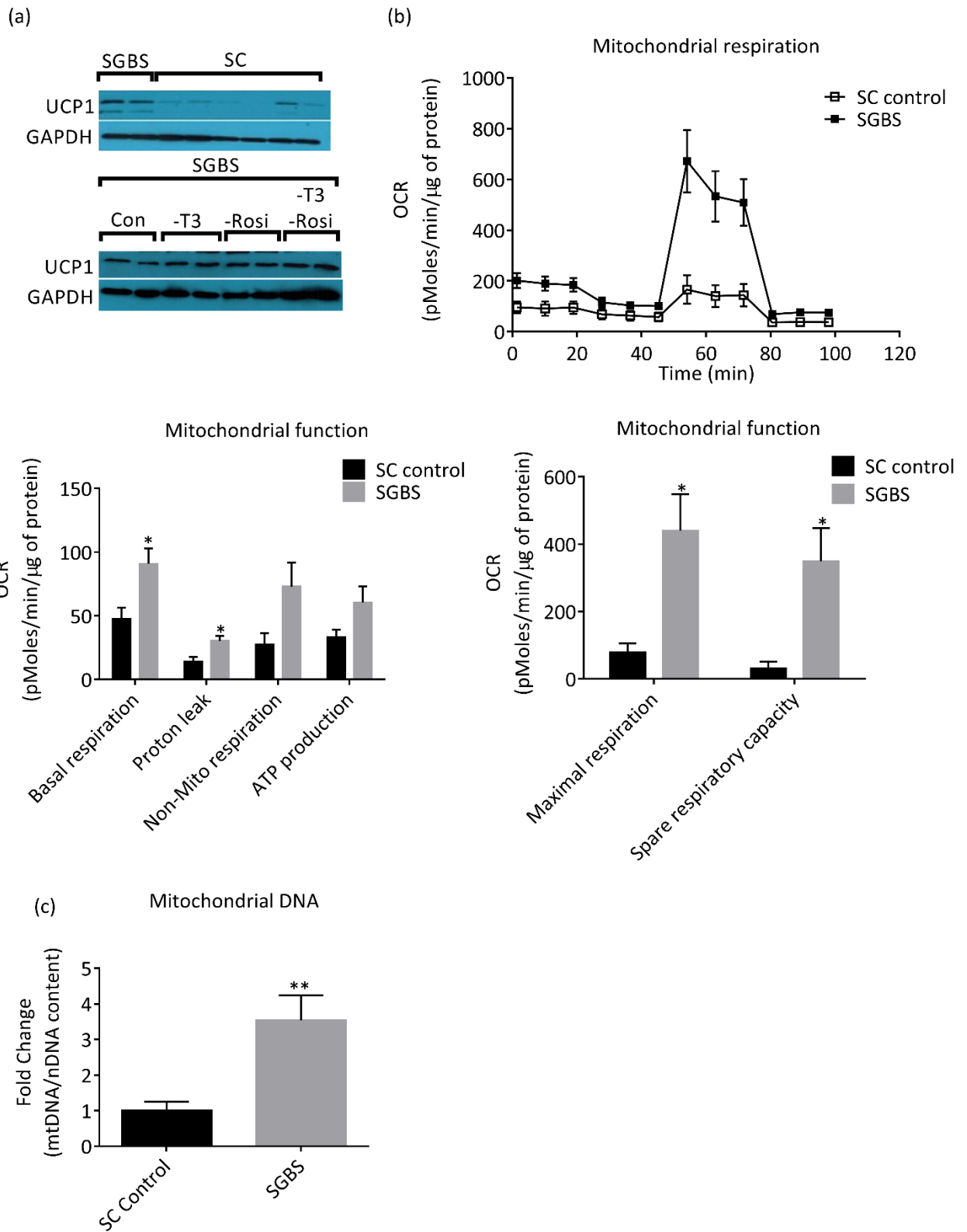


Figure 24: SGBS and its browning phenotype. (A) UCP1 protein expression in differentiated SGBS and SC adipocytes at basal level and upon depletion of T3 and rosiglitazone (rosi) from differentiation medium. (B) Mitochondrial respiration measured as oxygen consumption rate in SGBS and SC adipocytes (detailed protocol

discussed in section 2.8 (C) Mitochondrial DNA content measured the ratio of mitochondrial DNA (mtDNA) by nuclear DNA (nDNA). Data represented as mean \pm SEM obtained from three different donors for SC adipocytes (in duplicates) and three independent trials for SGBS adipocytes.*P < 0.05, **P < 0.005.

9. *This differential differentiation occurred with a cocktail targeted for white or brown differentiation?*

- SGBS adipocytes show a high level of UCP1 mRNA and protein expression irrespective of the differentiation medium used (discussed in previous comments). On the other hand, in our experience, SC adipocytes show a minimal increase in UCP1 expression when differentiated with the conventional adipogenic medium. Studies have observed moderate upregulation in UCP1 expression after adding BMP4 to adipogenic cocktail [18], but does not equate with approximately 1500 higher fold induction of UCP1 in SGBS adipocytes. Thus, differential differentiation of SC towards white phenotype and SGBS towards brown phenotype seemed to be an inherent property, and not influenced by differentiation medium composition.

10. *How do you reconcile the increase in oxidative capacity and the increase in triglyceride deposition? Any insights of de novo lipogenesis?*

- RNA-sequencing data shows that key genes involved in various lipid metabolism genes are expressed higher in SGBS adipocytes when compared to SC adipocytes. These pathways include de-novo lipogenesis (Figure 19), triglyceride biosynthesis as well as lipolysis. Based on these readouts, we cannot explain higher amount of TAG accumulation in SGBS adipocytes. Most

importantly, RNA sequencing data is unable to predict information about the hormonal and post-translational regulation of lipid metabolism. However, higher TAG accumulation coupled with increased mitochondrial oxidative capacity suggests that SGBS adipocytes may have suppressed lipolysis which allows TAGs to accumulate inside the adipocytes.

11. Is the increased browning of the SGBS cells relevant for the phenotype of the patient?

- SGBS patients suffer from growth abnormalities, with no reported brown or beige phenotype in their AT.

Chapter 4 Deficiency of FIT2 protein impairs triglyceride storage and insulin signalling in adipocytes.

12. Figure 26. Shows that genes in OM are less expressed than in SC in both Non-Diabetics and Diabetics. However, this figure does not tell whether the Diabetic patients had lower level in absolute terms in comparison to non-Diabetics.

- FIT2 mRNA expression is lower in OM depot when compared to SC depot in both NT2DM and T2DM subjects. In absolute terms, mRNA expression in SC and OM depot from NT2DM subjects is similar to respective SC and OM depot from T2DM subjects. The expression trends differ more at the protein level. Compared to NT2DM subjects, T2DM subjects tend to have lower FIT2 expression in both OM ($P < 0.05$) as well as SC depot (non-significant).

13. *FIT2 is highly expressed in Brown AT. The role of this gene in BAT may also be relevant for the browning of the white AT as well as for the size of the lipid droplets and mobilisation of lipids required for thermogenesis.*

- Based on our results after FIT2 knockdown in adipocytes, it is unlikely that FIT2 protein will independently drive browning or differentiation (PPAR γ and CEBP α remain unchanged upon FIT2 knockdown). In BAT, role of FIT2 protein would probably be similar to WAT i.e. TAG distribution and lipid droplet size determination. Absence of FIT2 protein drives the formation of larger lipid droplets as observed in adipocytes from AT specific knockout mice [19]. Typically, smaller lipid droplets undergo more efficient lipolysis and thus contribute towards maintaining adipocyte health [19].

14. *Figure 30: There seems to be a difference between the effect at mRNA and protein level. Is there any evidence for regulation at the level of protein degradation?*

- To our knowledge, there are no known post transcriptional or post translational modifications of FIT2. The difference between mRNA and protein expression may be implicated to the longer half-life of FIT2 protein.

15. *Any information about the promoters of FIT1 and FIT2? Their comparative analysis may help to understand their regulation and the possibility that may be regulated by insulin.*

- PPAR γ is a known transcriptional regulator of FIT2 gene expression during adipogenesis [20]. In-silico predicted transcription factors of FIT2 gene include PPAR α , PPAR γ 1, PPAR γ 2, CREB, Δ CREB, FOXC1, FOXO3a, FOXO3b, FOXF2 and FOXO3. (Predicted by SABiosciences' Text Mining Application, http://www.sabiosciences.com/chipqpcrsearch.php?species_id=0&factor=Over+200+TF&gene=FITM2&nfactor=n&ninfo=n&ngene=n&B2=Search). Their role in-vitro or in-vivo has not been examined yet.
- Predicted transcription factors for FIT1 include TBP, AML1 α , TFIID, GATA-2, FOXF2, STAT5A and SREBP1C. (Predicted by SABiosciences' Text Mining Application http://www.sabiosciences.com/chipqpcrsearch.php?species_id=0&nfactor=n&ninfo=n&ngene=n&B2=Search&src=genecard&factor=Over+200+TF&gene=FITM1). Based on these details about transcription factors, FIT1 and FIT2 genes seem to have distinct transcriptional control.
- In our experiments, FIT2 protein expression was unchanged upon 30 minute insulin stimulation.

16. *Any information about expression in FIT2 in macrophages?*

- FIT2 mRNA is expressed is very low in the macrophages. However, its protein expression has not been investigated in blood borne and plasma cells.

Chapter 5: FTO protein knock down or chemical inhibition of FTO can increase energy expenditure in human adipocytes

17. Page 107: *It would be nice to explain well how these treatments (FCCP, rotenone, antimycin etc) work.*

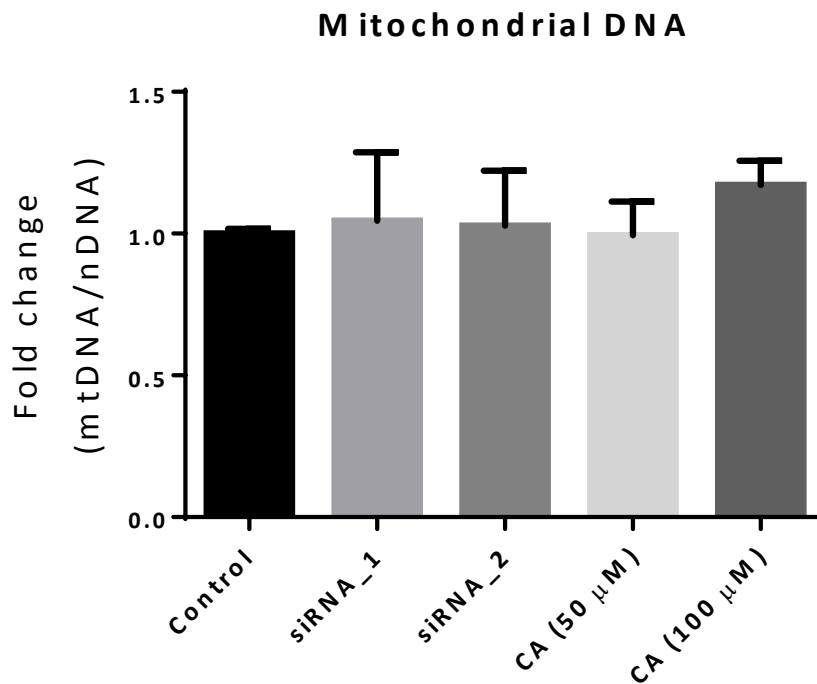
- Have updated in the protocol section 2.8.
- **Updated version**

XF Cell Mito Stress test kit (Seahorse Bioscience) was used to measure mitochondrial function in adipocytes in a 24 well plate format. Data were reported as pmoles of oxygen consumed per minute or oxygen consumption rate. Cellular respiration parameters calculated are basal respiration, ATP production, proton leak, maximal respiration and spare respiratory capacity. As suggested by the manufacturer, 5 replicates of control, treatment conditions and negative controls were used. Oligomycin inhibits ATP synthase (complex V) and the decrease in OCR following injection of oligomycin correlates to the mitochondrial respiration associated with cellular ATP production. Carbonyl cyanide-4 (trifluoromethoxy) phenylhydrazone (FCCP) is an uncoupling agent that collapses the proton gradient and disrupts the mitochondrial membrane potential. As a result, electron flow through the ETC is uninhibited and oxygen is maximally consumed by complex IV. The FCCP-stimulated OCR can then be used to calculate spare respiratory capacity, defined as the difference between maximal respiration and basal respiration. Spare respiratory capacity is a

measure of the ability of the cell to respond to increased energy demand. The third injection is a mix of rotenone, a complex I inhibitor, and antimycin A, a complex III inhibitor. This combination shuts down mitochondrial respiration and enables the calculation of non-mitochondrial respiration driven by processes outside the mitochondria.

18. Any evidence of changes in the number of mitochondria? Results of Oxygen consumption after FCCP is compatible with increased number of mitochondria

- We have evaluated mitochondrial DNA content and expressed it as a ratio of mitochondrial DNA: nuclear DNA (figure below). This serves as a surrogate marker for a number of mitochondria and remained unchanged with either FTO knock-down or inhibition suggesting the influence of FTO protein on mitochondrial function and not quantity. Figure attached.



Chapter 6: Transcriptomic Analysis reveals a role for extracellular matrix and fibrosis pathways in maintaining healthy human adipose tissue function in obese non diabetics.

19. *Fig 41 may benefit from a more clear explanation in the legend independent from the main text.*

- Included more comprehensive explanation in the figure legend.
Figure included in previous comments.

20. *To what extent the difference could be explained by different in macrophage concentration?*

- Transcriptomic data does not enable us to predict the contribution of macrophage infiltration. Examiner's concern is justified as ECM components are secreted mostly by preadipocytes during maturation and onsite macrophages [21, 22]. Our aim was to investigate transcriptomic signatures using

the whole tissue, and in future, we can perform tissue sectioning and imaging to study the probable influence of macrophage infiltration.

21. Figure 46: may benefit from increased font that could make it easier to read.

- Have enlarged figure and improved colour contrast for easier reading and understanding. Figure included in previous comments.

1. Shulman, G.I., *Ectopic fat in insulin resistance, dyslipidemia, and cardiometabolic disease*. N Engl J Med, 2014. **371**(12): p. 1131-41.
2. Wabitsch, M., et al., *Characterization of a human preadipocyte cell strain with high capacity for adipose differentiation*. Int J Obes Relat Metab Disord, 2001. **25**(1): p. 8-15.
3. Sethi, J.K. and A.J. Vidal-Puig, *Thematic review series: adipocyte biology. Adipose tissue function and plasticity orchestrate nutritional adaptation*. J Lipid Res, 2007. **48**(6): p. 1253-62.
4. Virtue, S. and A. Vidal-Puig, *It's Not How Fat You Are, It's What You Do with It That Counts*. PLoS Biol, 2008. **6**(9): p. e237.
5. Hahn, P. and M. Novak, *Development of brown and white adipose tissue*. J Lipid Res, 1975. **16**(2): p. 79-91.
6. Mootha, V.K., et al., *PGC-1alpha-responsive genes involved in oxidative phosphorylation are coordinately downregulated in human diabetes*. Nat Genet, 2003. **34**(3): p. 267-73.
7. Merico, D., et al., *Enrichment map: a network-based method for gene-set enrichment visualization and interpretation*. PLoS One, 2010. **5**(11): p. e13984.
8. Green, H. and M. Meuth, *An established pre-adipose cell line and its differentiation in culture*. Cell, 1974. **3**(2): p. 127-33.
9. Todaro, G.J. and H. Green, *Quantitative studies of the growth of mouse embryo cells in culture and their development into established lines*. J Cell Biol, 1963. **17**: p. 299-313.
10. Negrel, R., P. Grimaldi, and G. Ailhaud, *Establishment of preadipocyte clonal line from epididymal fat pad of ob/ob mouse that responds to insulin and to lipolytic hormones*. Proc Natl Acad Sci U S A, 1978. **75**(12): p. 6054-8.
11. Sugihara, H., et al., *Primary cultures of unilocular fat cells: characteristics of growth in vitro and changes in differentiation properties*. Differentiation, 1986. **31**(1): p. 42-9.
12. Zhang, Y.Y., et al., *Positional Cloning of the Mouse Obese Gene and Its Human Homolog*. Nature, 1994. **372**(6505): p. 425-432.
13. Halaas, J.L., et al., *Weight-Reducing Effects of the Plasma-Protein Encoded by the Obese Gene*. Science, 1995. **269**(5223): p. 543-546.
14. Scherer, P.E., et al., *A novel serum protein similar to C1q, produced exclusively in adipocytes*. J Biol Chem, 1995. **270**(45): p. 26746-9.
15. Rupnick, M.A., et al., *Adipose tissue mass can be regulated through the vasculature*. Proc Natl Acad Sci U S A, 2002. **99**(16): p. 10730-5.
16. Hotamisligil, G.S., N.S. Shargill, and B.M. Spiegelman, *Adipose expression of tumor necrosis factor-alpha: direct role in obesity-linked insulin resistance*. Science, 1993. **259**(5091): p. 87-91.
17. Puigserver, P. and B.M. Spiegelman, *Peroxisome proliferator-activated receptor-gamma coactivator 1 alpha (PGC-1 alpha): transcriptional coactivator and metabolic regulator*. Endocr Rev, 2003. **24**(1): p. 78-90.
18. Park, A., W.K. Kim, and K.H. Bae, *Distinction of white, beige and brown adipocytes derived from mesenchymal stem cells*. World J Stem Cells, 2014. **6**(1): p. 33-42.
19. Miranda, D.A., et al., *Fat storage-inducing transmembrane protein 2 is required for normal fat storage in adipose tissue*. J Biol Chem, 2014. **289**(14): p. 9560-72.
20. Kadereit, B., et al., *Evolutionarily conserved gene family important for fat storage*. Proc Natl Acad Sci U S A, 2008. **105**(1): p. 94-9.

21. Trayhurn, P., *Hypoxia and Adipose Tissue Function and Dysfunction in Obesity*. *Physiological Reviews*, 2013. **93**(1): p. 1-21.
22. Sun, K., et al., *Fibrosis and adipose tissue dysfunction*. *Cell Metab*, 2013. **18**(4): p. 470-7.